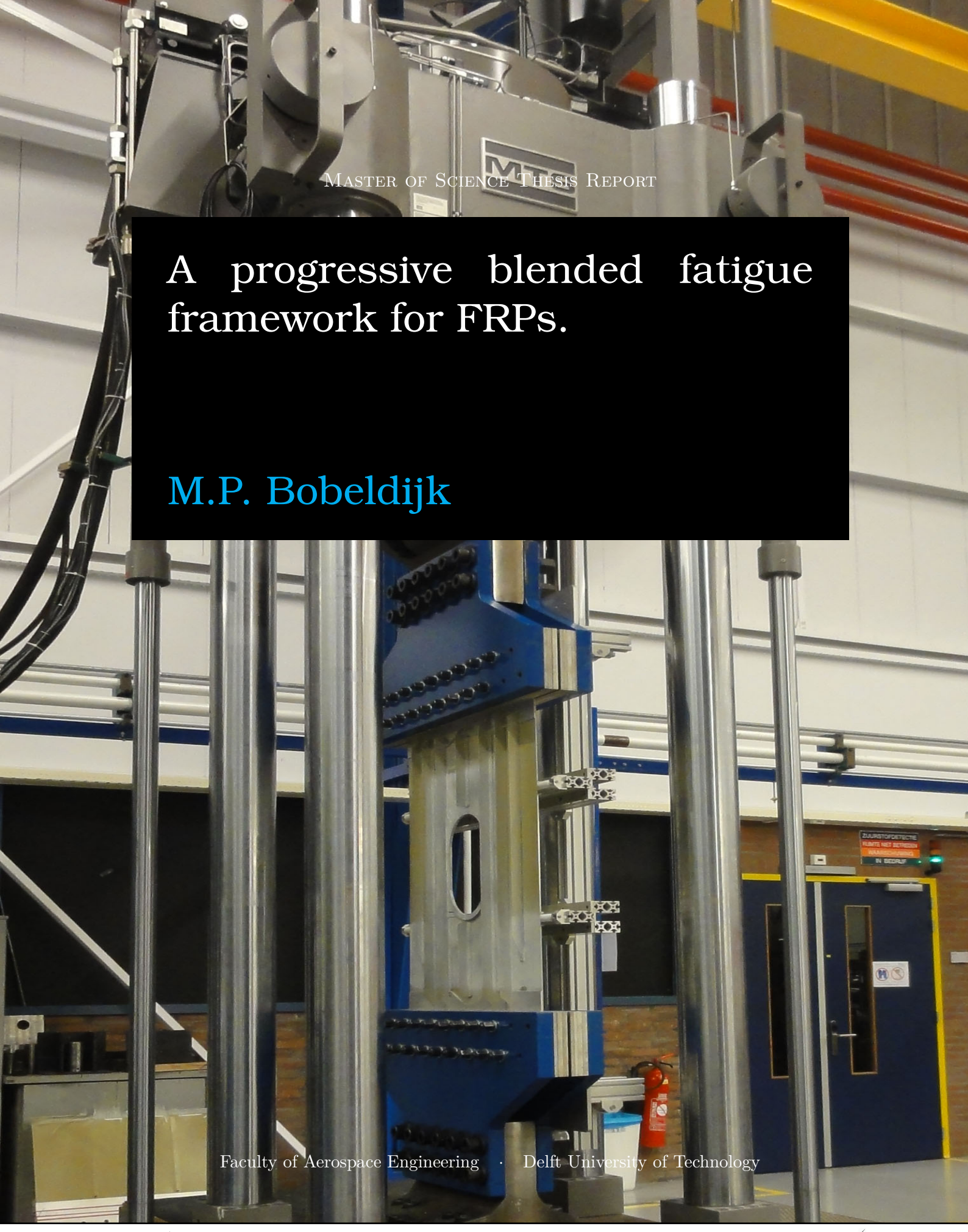

Master of Science Thesis Report

A progressive blended fatigue framework for FRPs.

M.P. Bobeldijk

Faculty of Aerospace Engineering · Delft University of Technology

TU Delft Delft University of Technology

A progressive blended fatigue framework for FRPs.

Master of Science Thesis Report

M.P. Bobeldijk

13 July 2018

Faculty of Aerospace Engineering · Delft University of Technology

Delft University of Technology
Faculty of Aerospace Engineering
Department of Aerospace Structures and Materials

GRADUATION COMMITTEE

Dated: 13 July 2018

Chair holder:

Dr.ir. R. C. Alderliesten

Committee members:

Dr. D. Zarouchas

Dr.ir. J. M. J. F. van Campen

Abstract

In general, damage models for Fibre-Reinforced Polymers (FRPs) can be divided into two categories: Continuum Damage Models (CDMs) and Fracture Mechanics Damage Model (FMDM). Damage models within each of these categories are advantageous for different types of failure mechanisms. Therefore, it is of interest to exploit different CDMs and FMDMs in a unified framework. The aim of blending multiple models is to enhance the predictive capabilities for simulations involving FRPs. Previous work has focussed on the development of such a framework for quasi-static loading. The goal of this study is to formulate a unified framework which extends the blending methodology to the fatigue domain, identifying the challenges that have to be tackled before the framework can be used for practical applications and to start the development of the numerical implementation of the framework.

The framework has to be formulated for Progressive Blended Damage Models (PBDMs). These are models that progressively simulate the damage of FRPs under quasi-static or fatigue loading, while combining several CDMs and FMDMs. In order for the framework to be applicable to high cycle fatigue, it is deemed necessary to implement the ability to skip cycles. From a variety of different approaches a disjoint type of framework has been formulated which uses a cycle jumping algorithm to skip cycles. The disjoint methodology entails that the calculations involving fatigue are performed outside of an Finite Element Analysis (FEA) environment. A limited amount of assumptions have been introduced for the formulation of the framework in order to achieve a general high-fidelity approach.

In order to model an arbitrary FRP structure in an FEA environment, a Layer-Wise (LW) approach has been used. With this approach every layer in the laminate is modelled by one element through-the-thickness. For the constitutive model of a lamina, a linear constitutive model has been extended with models accounting for non-linearities, such as non-linear shear behaviour and material damage. Furthermore, the observed discrepancy between the strength of a UniDirectional (UD) lamina and a lamina in an arbitrary laminate has been accounted for, by using an in-situ strength model.

Three damage models were considered for fibre, matrix and delamination failure. For fibre failure a CDM is used, for matrix failure an eXtended Finite Element Method (XFEM)-based approach and for delaminations a Cohesive Zone Model (CZM). For each model, a proposed formulation for quasi-static as well as for fatigue loading has been presented. For each of the models, a cycle jump algorithm is proposed that has to be used in conjunction with each other in order to determine the number of cycles to jump.

Due to time constraints, the scope of the numerical implementation has been limited. It has been decided to implement the general outline of the framework, CDM for quasi-static and fatigue loading and the CZM for quasi-static loading only.

Overall, the concept of the blending methodology shows potential. However, in the short term, the feasibility of the framework in a practical implementation is deemed to be unrealistic, as several challenges have to be tackled first. First of all, the development of the implementation of the PBDM should be continued and validated. A major part of the validation is the evaluation of the cycle jump methodology and the application of fatigue damage after skipping cycles. Secondly, by combining different models within a single framework, a large input data set is required. For quasi-static loading, the inputs are available in literature; however, the inputs required to address fatigue are limiting the PBDM in this aspect. This issue should be addressed with either an elaborate experimental campaign or with the development of novel models that require fewer inputs. Lastly, attempts have to be made to reduce the computational effort. For the quasi-static loading case, this is less stringent as a quasi-static analysis only has to be performed once. For fatigue loading, however, this analysis is repeated several times in conjunction with other processes not used for the quasi-static case. Therefore, it is of importance to reduce the required computational effort to evaluate the model. Possible solutions for reducing the computational effort is to make a more efficient translation from the theoretical framework/model(s) to a software representation and further use of parallel processing.

Table of Contents

List of Figures

List of Tables

List of Symbols

Symbols

A	Area, coefficient
A_0	Nominal area
a	Crack length, variable, lower interval boundary
a_0	Initial crack length
B	Body, coefficient
b	Variable, upper interval boundary
C	Fitting parameter, coefficient
c	Fitting parameter, coefficient
$\underline{\underline{\mathbf{D}}}$	Material stiffness matrix
d	damage parameter, fitting parameter
da	Increase in crack length
dN	Number of cycles to increase
E	Young's modulus, stiffness, energy
E'	Equivalent elastic modulus
E_s	Initial stiffness
e	Difference between values
$\underline{\mathbf{F}}$	Load vector
F	Load, force
FI	Failure index
f	Frequency, function
G	Strain Energy Release Rate (SERR), shear modulus
g	Function
h	Function
i	Index, integer
$\underline{\underline{\mathbf{J}}}$	Material Jacobian
$\mathbf{J}$	Set
j	Index, integer
$\mathbf{K}$	Set
K	Ramberg-Osgood fitting parameter, stiffness
k	Index, integer, stiffness, Stress-Cycle (SN) fitting parameter
k	Index, integer, element

$\mathbf{L}$	Set
L	Characteristic element length
l	Length
$\mathbf{M}$	Set
m	Coefficient,increment index
$\mathbf{N}$	Set
N	Cycle
$N_{current}$	Current cycle
N_f	Number of cycles until failure
N_{fixed}	Fixed number of cycles
N_{jump}	Number of cycles to jump
N_{max}	Maximum number of cycles
n	Ramberg-Osgood fitting parameter, increment index
n_{elem}	Elements per layer
n_{layers}	Number of layers
P	Coefficient
p	Point, variable
Q	Coefficient
R	Stress ratio
r	Fitting parameter
S	Strength
$\underline{\mathbf{t}}$	Prescribed lamina thicknesses
T	Chebyshev coefficients
t	Thickness, time, traction
$\underline{\mathbf{X}}$	Mesh seeds
x	Variable
y	Variable, function
α	Fitting parameter, specified factor, fracture angle
α_0	LaRC-05 parameter
β	Hahn-Tsai fitting parameter, displacement mode mixity
γ	Shear strain
ΔG	SERR range
ΔN	Range of cycles
$\Delta\sigma$	Stress range
δ	Displacement, relative error, tolerance
δ^0	Displacement corresponding to softening initiation
δ^f	Failure displacement
ϵ	Normal strain
η	Fitting parameter, arbitrary material property
η_L	LaRC-05 parameter
η_T	LaRC-05 parameter
θ	Misalignment angle
θ_0	Initial misalignment angle
ν	Poisson's ratio
$\underline{\sigma}$	Stress tensor
σ	Stress, normal stress, cyclic stress

σ_0	SN fitting parameter
σ_a	Stress amplitude
σ_m	Mean stress
χ	User-specified fraction
Ψ	Kink band angle
ψ	Mode mixity
ω	Angle

Subscripts

c	Critical, compression
cz	Cohesive zone
e	Element
eq	Equivalent (mixed-mode)
FFC	Compressive fibre failure
FFT	Tensile fibre failure
f	Fibre
I	Mode I
II	Mode II
III	Mode III
i	Initial
L	Longitudinal
MF	Matrix failure
MFC	Compressive matrix failure
MFT	Tensile matrix failure
m	Matrix, misalignment frame
max	Maximum
min	Minimum
N	Normal
r	Residual
s	Shear mode, shear
T	Transverse
t	Tensile
th	Threshold

Superscripts

f	Fatigue
$intra$	Intralaminar
$inter$	Interlaminar
is	In-situ
m	Misalignment frame
max	Maximum
new	New state
old	Old state
s	Static
tot	Total
u	Ultimate
Ψ	Kink band frame
$*$	Damaged
$(+)$	Tension

$(-)$	Compression

List of Abbreviations

4-ENF	Four-point bending End Notched Flexure
ACZ	Augmented Cohesive Zone
C-C	Compression-Compression
C-T	Compression-Tension
CA	Constant Amplitude
CAE	Complete Abaqus Environment
CC	Compact Compression
CDM	Continuum Damage Model
CE	Cohesive Element
CFRP	Carbon Fibre Reinforced Polymer
CLD	Constant Life Diagram
CLT	Classical Laminate Theory
CT	Compact Tension
CZM	Cohesive Zone Model
DCB	Double Cantilever Beam
ELS	End Load Split test
ESL	Equivalent Single Layer
FE	Finite Element
FEA	Finite Element Analysis
FEM	Finite Element Method
FF	Fibre Failure
FFC	Compressive Fibre Failure
FFT	Tensile Fibre Failure
FMDM	Fracture Mechanics Damage Model
FNM	Floating Node Method
FPBDM	Fatigue Progressive Blended Damage Model
FPCDM	Fatigue Progressive Continuum Damage Model
FPDA	Fatigue Progressive Damage Analysis
FPFMDM	Fatigue Progressive Fracture Mechanics Damage Model
FRP	Fibre-Reinforced Polymer
FSDT	First-order Shear Deformation Theory
GFRP	Glass Fibre Reinforced Polymer

GMDM	Gradual Material Degradation Model
HSDT	Higher-order Shear Deformation Theory
IFF	Inter Fibre Failure
INRSE	Integral Normalised Mean Square Error
ISO	International Organization of Standardization
LEFM	Linear Elastic Fracture Mechanics
LW	Layer-Wise
MDM	Material Degradation Model
MF	Matrix Failure
MFC	Compressive Matrix Failure
MFT	Tensile Matrix Failure
MMB	Mixed-Mode Bending
MMELS	Mixed-Mode End Load Split test
NMAE	Normalised Mean Absolute Error
NMSE	Normalised Mean Squared Error
OHT	Open-Hole Tensile
PBDA	Progressive Blended Damage Analysis
PBDM	Progressive Blended Damage Model
PCDM	Progressive Continuum Damage Model
PDA	Progressive Damage Analysis
PDM	Progressive Damage Model
PFMDM	Progressive Fracture Mechanics Damage Model
PNM	Phantom Node Method
QSPBDM	Quasi-Static Progressive Blended Damage Model
QSPCDM	Quasi-Static Progressive Continuum Damage Model
QSPDA	Quasi-Static Progressive Damage Analysis
QSPFMDM	Quasi-Static Progressive Fracture Mechanics Damage Model
RCCM	Rainflow Cycle Counting Method
RE	Residual stiffness
RS	Residual Strength
SN	Stress-Cycle
SERR	Strain Energy Release Rate
SMDM	Sudden Material Degradation Model
T-C	Tension-Compression
T-T	Tension-Tension
UD	UniDirectional
UQSTC	Unidirectional Quasi-Static Test Case
VA	Variable Amplitude
VCCT	Virtual Crack Closure Technique
VCE	Virtual Crack Extension
WWFE-I	First World Wide Failure Exercise
WWFE-II	Second World Wide Failure Exercise
XFEM	eXtended Finite Element Method

Preface

Dear reader,

FRPs provide advantages in terms of, for example, structural efficiency and performance, for a wide range of applications. However, the full potential of FRPs has not been reached due to the limited predicting capabilities of developed models, which in turn, can be attributed to a lack of understanding of the underlying damage mechanisms. This study attempts to formulate a framework in which the predictive capabilities for FRPs for fatigue can be improved, by exploiting the advantages of different models.

During my thesis, my supervisor Dr.ir. D. Zarouchas has provided me with guidance and lengthy discussions for which I am grateful. Moreover, I would like to thank Ruben and Daan for accommodating welcome distractions and discussions involving a wide range of topics. Furthermore, I would like to express my gratitude to Agnes, as she took it upon herself to proofread my entire thesis. Lastly, I would like to thank my parents, who provided emotional and financial support throughout my studies for which I am eternally grateful.

Delft, University of Technology — M.P. Bobeldijk
July 13, 2018

Chapter 1

Introduction

Fibre-Reinforced Polymers (FRPs) are widely used throughout a range of industries and it is foreseen that their use will only increase in the future. [1–4] The increasing use can be attributed to the advantages of FRPs with respect to other materials such as metals. Among the advantages are the superior strength-to-weight ratio and improved part consolidation when compared to metals. However, despite the increasing use of FRPs throughout the last few decades, the mechanical behaviour is still not fully understood due to a lack of understanding regarding the underlying damage mechanisms. [5] In order to fully exploit the potential benefits that FRPs can provide, it is required to understand the underlying damage mechanisms.

In literature, the methods used to predict damage in FRPs can be divided into two categories: Continuum Damage Models (CDMs) and Fracture Mechanics Damage Models (FMDMs). Academia is struggling to develop new failure theories upon a physical basis that leads to a unified model for multiple failure mechanisms. [6] CDMs and FMDMs are advantageous for different failure mechanisms; therefore, it is of interest to integrate (blend) both methods in order to obtain the best representation of failure mechanisms. In a parallel research, van Dongen [6] and van Oostrum [7] developed a blending framework for quasi-static loading. The aim of such a framework is to not only determine the failure strength but also simulate the damage evolution in FRPs and better represent the failure patterns. Improved prediction of damage progression and failure patterns may lead to advantageous developments for, for example, maintenance scheduling and the assessment of the severity of in-service damage.

Researchers have not yet attempted to develop a general unified blending framework for fatigue. For fatigue, most models aim to predict the fatigue life and/or residual strength of FRPs, but not to accurately capture the damage evolution (amongst others, Mitrousias [8] and Eliopoulos [9]). Research found in literature that attempts to simulate the damage evolution of FRPs (at least to a certain extent) either use a purely CDM-based approach (for example, Nikishkov et al. [10]) or a FMDM-based approach (for example, Nixon-Pearson et al. [11]). In light of the apparent success of blending models for the quasi-static domain, it is of interest to develop a similar framework for the fatigue domain. Therefore, the following research question is addressed in this report:

> How can a practical implementation of the blending methodology be achieved for quasi-static and fatigue loading?

The research question can be decomposed into three subquestions:

1. What is a suitable framework for a blending methodology for quasi-static and fatigue loading?
2. How do existing CDMs and FMDMs fit in such a framework?
3. What challenges have to be tackled to achieve a practical implementation of the framework?

The following hypothesis is proposed:

> A practical implementation of the blending framework can be achieved by simulating a limited amount of cycles with a quasi-static Finite Element Analysis (FEA).

In order to fully confirm the hypothesis, it is required to:

- Formulate a unified framework
- Develop a fully functional numerical implementation of the framework
- Validate the methodology with results obtained from experiments.

The development of the numerical implementation of the proposed framework is a time-consuming task. It is not possible to create the full implementation, and perform the validation thereof, in the time allocated for this thesis. It is decided to make a start with the numerical implementation, but with the acknowledgement that future work is required to finish the development and prove the merit of the framework. Therefore, this thesis will only partially address the hypothesis, but serves as a stepping stone for future research.

In order to use the blending methodology for a wide range of loading types and geometries, it is desirable to aim for a general high-fidelity framework. The main goal of the research presented in this report is formulated as:

> Formulate a unified framework for a Progressive Blended Damage Model (PBDM) in which CDMs and FMDMs under both fatigue and quasi-static loading can be integrated and lay the groundwork for a numerical implementation thereof.

The first research subquestion is addressed in Chapter 2, along with important concepts and terminology related to the framework. The second research subquestion is addressed in Chapters 3 and 4. The selection of suitable CDMs and FMDMs for fibre, matrix and delamination failure is presented in Chapter 3. Furthermore, Chapter 3 discusses the Quasi-Static Progressive Blended Damage Model (QSPBDM) which is part of the PBDM. The extension to fatigue loading is discussed in Chapter 4. The overview of the numerical implementation and the associated numerical considerations for the used models are presented in Chapter 5. In Chapter 6, the third research subquestion is addressed by identifying the challenges of the framework and the implementation of the said framework. Lastly, the recommendations for future work can be found in Chapter 7.

Chapter 2

Framework for Progressive Blended Damage Analysis (PBDA)

The proposed framework relies on several concepts such as Progressive Damage Analysis (PDA), Continuum Damage Models (CDMs) and Fracture Mechanics Damage Models (FMDMs). Section 2.1 discusses several concepts that are used by the framework and throughout this report. In Section 2.2, the framework is outlined in terms of expected inputs, set requirements and some initial notions regarding the implementation of the framework. Lastly, the framework itself is discussed in Section 2.3, where also the various components of the framework are outlined.

2.1 Fundamentals

In Section 2.1.1, the fatigue loading of a structure is briefly discussed. The difference between CDMs and FMDMs is discussed in Section 2.1.2. Furthermore, the concept of PDA and the classification of Progressive Damage Models (PDMs) are discussed in Section 2.1.3. Lastly, on several occasions in this report, the need for a root-finding algorithm arises which is discussed in Section 2.1.4.

2.1.1 Fatigue

Consider a repeating and time-varying load $F(t)$ that is applied to an arbitrary body B (structure) with a cut-out. This situation is sketched in Figure 2.1. In the figure, a cut-out has been included to illustrate that even if body B would be symmetric, a non-uniform stress-state will be present throughout the material due to the stress concentration. In practice most structures will not have a uniform stress-state due to:

- The global geometry of the structure, for example, the presence of a flange
- A local stress concentration due to a local disturbance such as a hole
- A local stress concentration due to a local discontinuity such as a surface scratch.

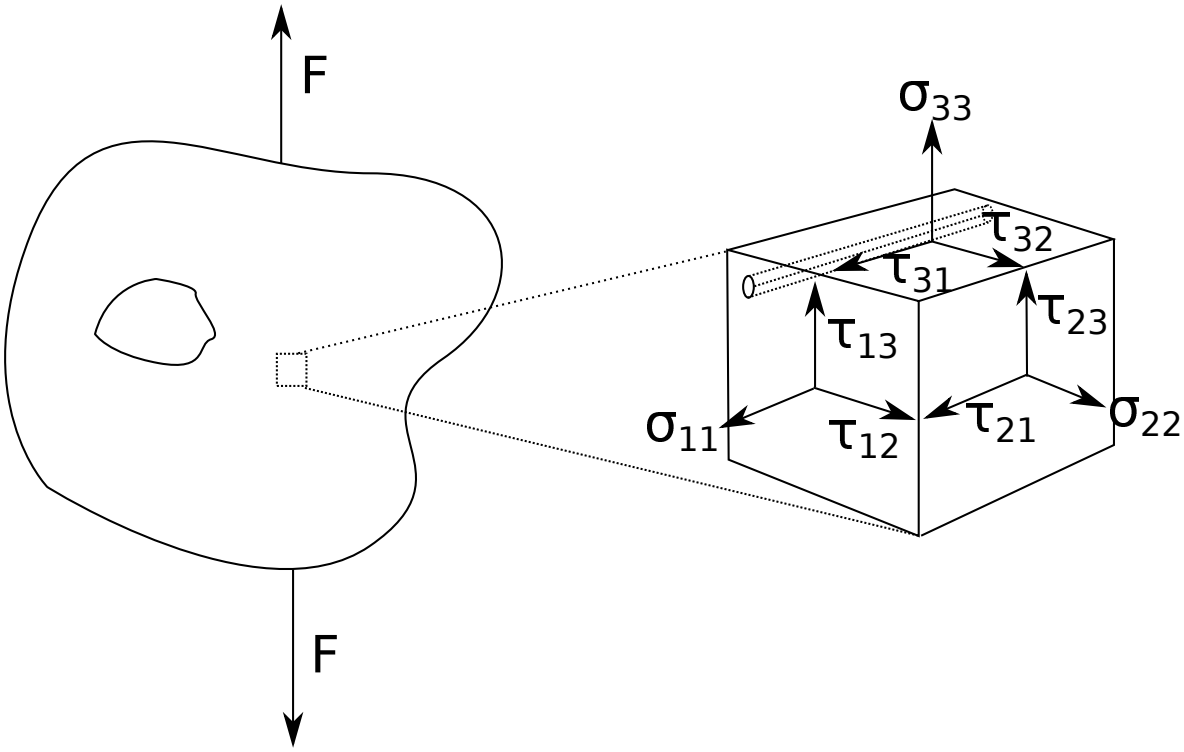

Figure 2.1: Sketch of the stress-state of a material element of an arbitrary body B. The material element is contained in one of the laminae of the FRP.

The fatigue loading can be described in terms of:

1. Components of cyclic load $\underline{\mathbf{F}}(t)$
2. Components of cyclic stress $\underline{\underline{\sigma}}(t)$.

The former is convenient for describing the fatigue loading on the global (structure) level and the latter for describing the fatigue loading on the global (structure) and local (material element, see Figure 2.1) level. In order to use the cyclic stress description on the global level, there has to be a notion of nominal stress as the stress will vary throughout the structure and material. The description of the fatigue loading in terms of cyclic load and stress are similar. The discussion of fatigue loading in the remainder of this section will be presented in terms of cyclic stress, however the same concepts will apply for the cyclic load description. Furthermore, for simplicity, only a single stress component σ is considered. Considering the load situation shown in Figure 2.1, σ can be defined in terms of the nominal area A_0 as $\frac{F}{A_0}$.

The cyclic stress σ can exhibit a Constant Amplitude (CA) or a Variable Amplitude (VA) behaviour. Both types of fatigue loading are shown in Figure 2.2. In practice, fatigue loads are mostly of the VA type. As shown in the figure, several parameters are required in order to fully define the CA and VA stress behaviour.

CA cyclic stress can be described in terms of three parameters: the stress amplitude σ_a defined in Equation 2.1, the mean stress σ_m defined in Equation 2.2 and the stress ratio R defined in Equation 2.3. In the equations, σ_{max} is the maximum applied stress and σ_{min} is

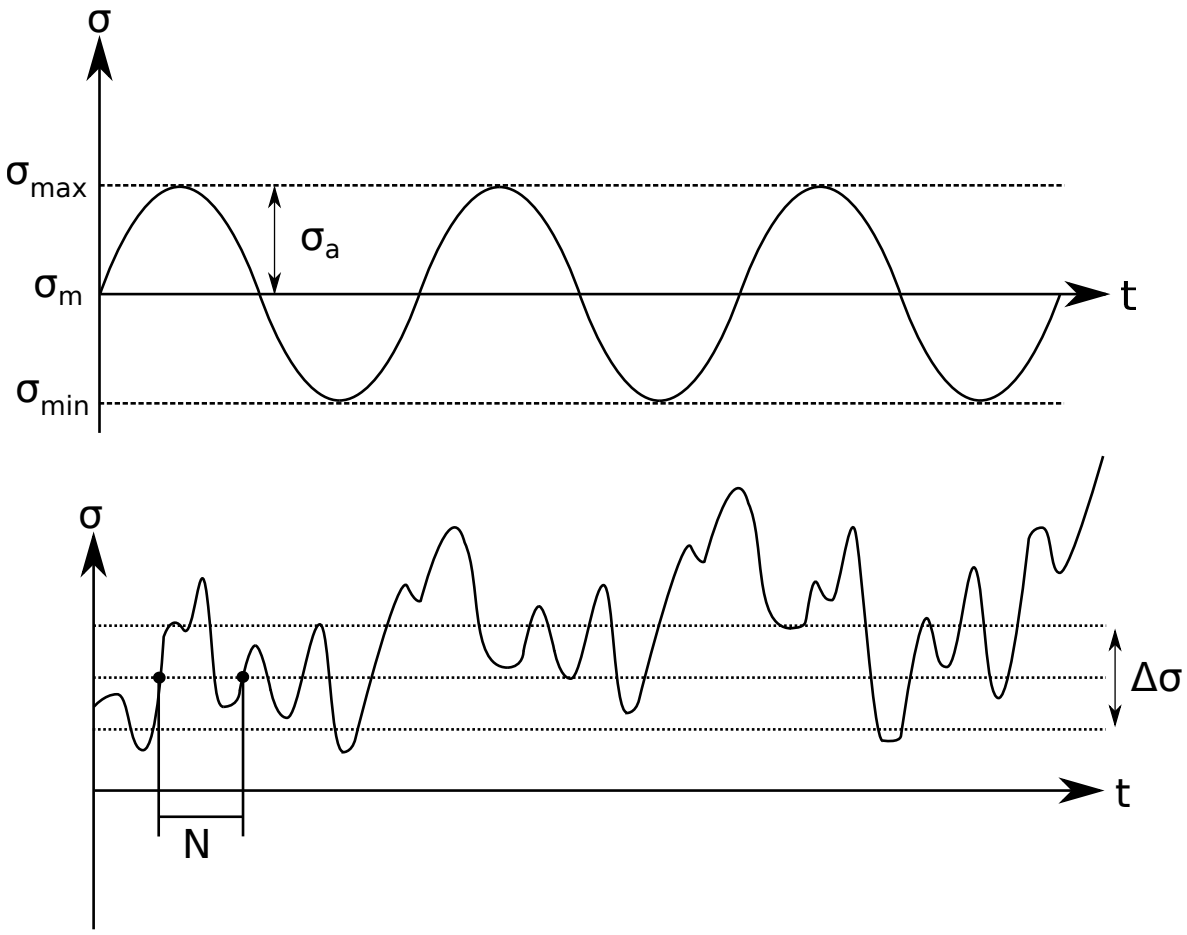

Figure 2.2: Examples of CA (top) and VA (bottom) cyclic stress.

the minimum applied stress, where $\sigma_{max} > \sigma_{min}$. Furthermore, for $R \neq -1$, σ_a and σ_m are related through Equation 2.4.

$$\sigma_a = \frac{\sigma_{max} - \sigma_{min}}{2} \tag{2.1}$$

$$\sigma_m = \frac{\sigma_{max} + \sigma_{min}}{2} \tag{2.2}$$

$$R = \frac{\sigma_{min}}{\sigma_{max}} \tag{2.3}$$

$$\sigma_a = \frac{1 - R}{1 + R}\sigma_m \tag{2.4}$$

In order to describe VA cyclic stress, the stress history is divided into individual cycles and corresponding equivalent stress ranges $\Delta\sigma$, as is shown for a single cycle in Figure 2.2. Note that by doing so, it is assumed a set of CA load spectra exists that is equivalent to the VA loading. Such an approach will only produce an approximation of the VA load.

However, simulating the entire VA spectrum is not feasible in practice. Therefore, such an approximation is justified.

There are several methods to translate VA cyclic stress into a set of cycles and corresponding equivalent stress ranges, for example the well-known Rainflow Cycle Counting Method (RCCM). [12] This leads to a distribution of stress ranges. A useful visual representation of the stress range distribution is a stress histogram. The stress histogram consists of multiple blocks that are characterised by a stress range and the number of cycles of that stress range. In case linear fatigue damage accumulation is assumed, the order of the blocks within the stress histogram does not matter. In case a non-linear fatigue damage accumulation is assumed, the specific order of the stress ranges has to be taken into account. An example of a stress histogram is shown in Figure 2.3, where the VA cyclic stress is converted into a set of CA cyclic stress levels. Note that the stress histogram is a convenient visual representation, but that for each stress range one more variable is required to fully define the fatigue loading (e.g. σ_{max}).

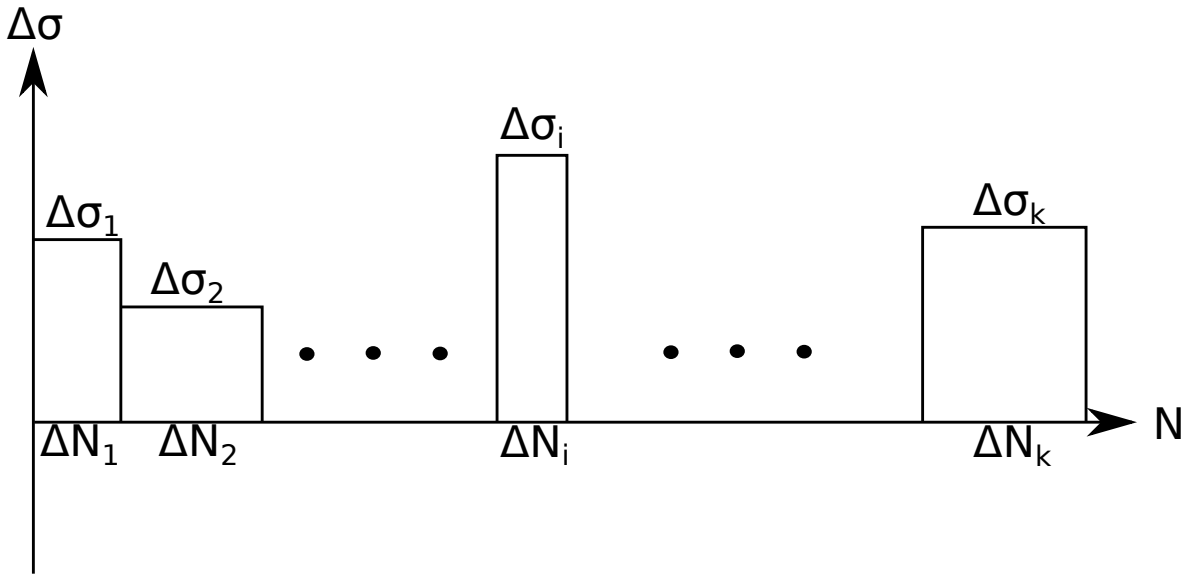

Figure 2.3: Example of a stress histogram.

2.1.2 Continuum Damage Models (CDMs) and Fracture Mechanics Models (FMDMs)

The main difference between CDMs and FMDMs is the used methodology to take into account damage initiation and/or progression. CDMs use a damage state-variable which reduces the mechanical properties selectively in order to model the effect of damage. This approach effectively smears the damage over the volume of the considered material (in case of a Finite Element Analysis (FEA), an element). CDMs have shown to provide satisfactory predictions of the ultimate failure load for quasi-static and fatigue loading, for the cases addressed by the researchers. [9, 13] However, the smearing of damage undermines the physical meaning of damage. Physically, the damage will be due to the formation of micro- and macrocracks which do not necessarily have a uniform distribution throughout the material. The effect

of the damage smearing by CDMs is that the damage patterns are not always accurately predicted. [7]

FMDMs are concerned with modelling the fracture themselves (e.g. taking into account crack geometry) instead of statistically smearing them out over the material. Such models take into account, for example, the geometry of cracks and the creation of fracture surfaces.

In general, CDMs are of interest to model the degradation of the material until the formation of a macrocrack. For macrocracks, FMDMs are of interest. The definitions of a micro- and macrocrack depends on the considered scale. Note that both the CDMs and FMDMs use a stress-strain or similar approach to determine damage initiation. The approach on how to account for damage progression is fundamentally different.

2.1.3 Progressive Damage Analysis (PDA)

The aim of PDA is to not only predict the point of failure but also the evolution (degradation) of the properties in the structure throughout the loading history. Models capable of PDA are called PDMs. PDMs can be developed on analytical grounds, however the state-of-the-art PDMs use numerical methods (mostly Finite Element Method (FEM) implementations). The PDMs are classified in subclasses based on the type of damage models and load type validity. In Figure 2.4, the classification of different PDMs is shown.

The classification depends on the applied load (quasi-static and/or fatigue) and the type of model (CDM or FMDM). For CDMs, the models are classified into Quasi-Static Progressive Continuum Damage Models (QSPCDMs) for quasi-static loading and Fatigue Progressive Continuum Damage Models (FPCDMs) for fatigue loading. In case the model accounts for both quasi-static and fatigue loading, the model is classified as a Progressive Continuum Damage Model (PCDM).

For FMDMs, the models are classified into Quasi-Static Progressive Fracture Mechanics Damage Models (QSPFMDMs) for quasi-static loading and Fatigue Progressive Fracture Mechanics Damage Models (FPFMDMs) for fatigue loading. In case a model accounts for both quasi-static and fatigue loading, the model is classified as a Progressive Fracture Mechanics Damage Model (PFMDM).

It is also possible that a model integrates both a CDM and FMDM, this is referred to as blending. A blended model that accounts for quasi-static loading is classified as a Quasi-Static Progressive Blended Damage Model (QSPBDM) and for fatigue loading as a Fatigue Progressive Blended Damage Model (FPBDM). In case the model accounts for both type of loads, the model is classified as a Progressive Blended Damage Model (PBDM).

Analog to the classification of PDMs, PDA can be divided into Fatigue Progressive Damage Analysis (FPDA), Quasi-Static Progressive Damage Analysis (QSPDA) and Progressive Blended Damage Analysis (PBDA). The only difference with the classification of PDMs is that no distinction is made between the type of method (CDM or FMDM) that is used for PDA.

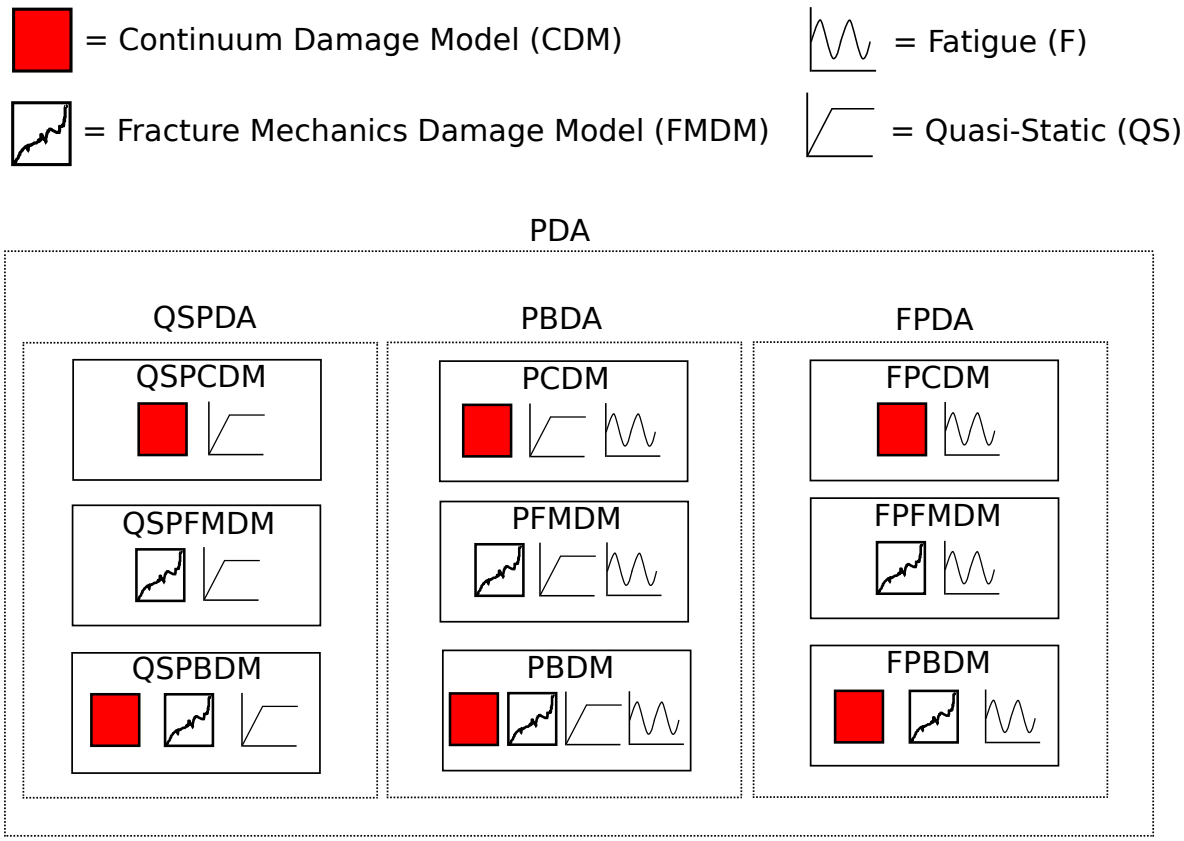

Figure 2.4: Overview of the classification of PDMs. The classification is based on the type of loading for which the model is valid (quasi-static, fatigue or both); and the type of damage model (CDM, FMDM or both).

2.1.4 Root-finding algorithm

On several occasions i the present work, equations that do not have an analytical solution for some variable x are encountered. In Equation 2.5, a general format of such a problem is shown for the variable x. The methodology to solve such problems is to find the root of a function $h(x)$ that is the difference of the functions $f(x)$ and $g(x)$, as shown in Equation 2.6. Therefore, a problem of the form shown in Equation 2.5 can be solved by employing root-finding methods.

$$f(x) = g(x) \tag{2.5}$$

$$h(x) = f(x) - g(x) = 0 \tag{2.6}$$

The root-finding algorithm is developed for continuous single variable functions. The outline of the algorithm is shown in Figure 2.5. The root-finding algorithm consists of three root-finding methods: the modified Newton-Raphson, Brent's method and the Chebyshev approximation. The modified Newton-Raphson is a well-performing root-finding algorithm that can achieve local quadratic convergence and has the robustness of the bisection method.

However, the modified Newton-Raphson requires the first-order derivative $h'(x)$. In case this is not available, Brent's method is used. Brent's method does not require the derivative, exhibits superlinear convergence characteristics and has the robustness of the bisection method. However, in case interval $[a, b]$ contains multiple roots and when a specific root or all roots have to be obtained, the modified Newton-Raphson and Brent's method are ill-suited. In order to overcome this problem, a Chebyshev approximation is used to obtain approximate roots of the function $h(x)$. Then, based on i roots, i intervals $[a_i, b_i]$ are created. Each of the intervals now contains one root $[a_i, b_i]$ and either the modified Newton-Raphson and/or Brent method can be used to obtain the roots. More information and references regarding the modified Newton-Raphson, Brent's and Chebyshev methods is provided in Appendix A.

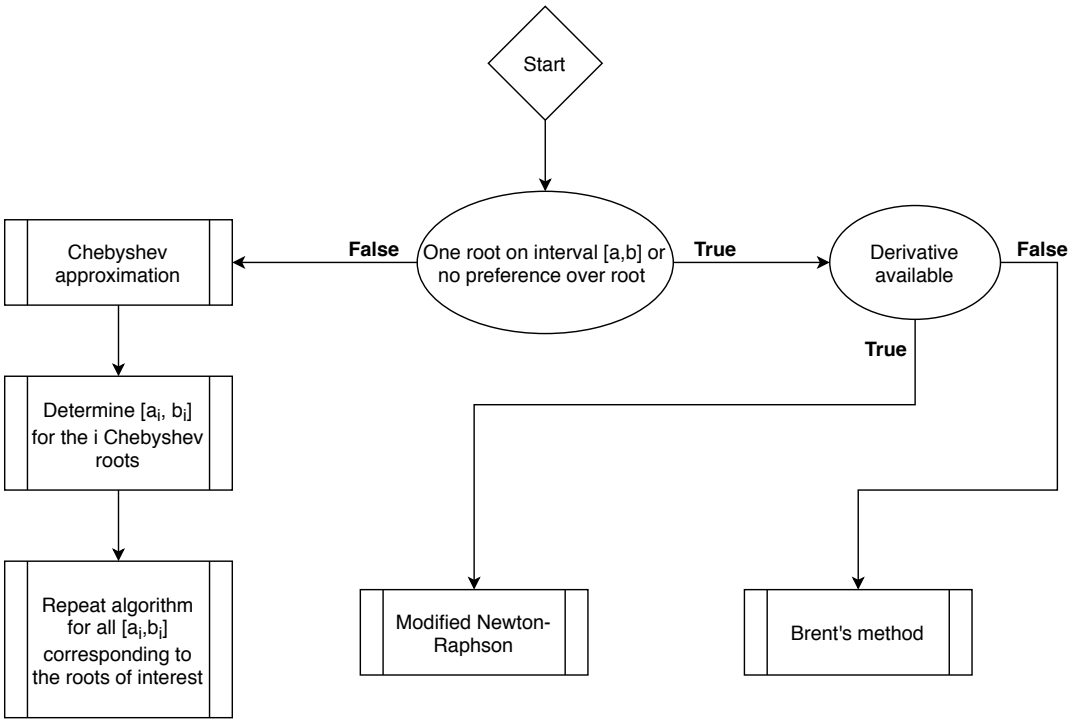

Figure 2.5: Overview of the proposed root-finding algorithm for continuous single-variable functions. The algorithm consists of the modified Newton-Raphson, Brent's method and the Chebyshev approximation.

2.2 Framework concept

Before proposing a general framework, some preliminary notions and assumptions are discussed first. Assumptions regarding the inputs of the framework and the corresponding challenges are briefly discussed in Section 2.2.1. In order to formulate the framework some fundamental requirements are imposed which are discussed in Section 2.2.2. Lastly, the motivation of the concept of the framework proposed in Section 2.3 is discussed in Section 2.2.3.

2.2.1 Inputs

For the general framework, it is assumed that all required material and model inputs for the considered CDMs and FMDMs are available. The number of material and model inputs required by the general framework depends on the specific CDMs and FMDMs chosen by the user. However, in general, considering the models proposed in this report, the required number of inputs for common CDMs and FMDMs can pose a problem. Especially, when combining such models. A large number of required inputs is unfortunately an inherent challenge for a framework that aims to use different models in conjunction. This challenge is discussed in more detail in Chapter 6.

2.2.2 Requirements

Requirements are formulated in order to define the domain of the framework. The framework should be applicable for arbitrary:

- Loading
- Geometry
- FRP materials
- Material (damage) models.

These requirements are chosen as to achieve a high level of universality. Furthermore, no assumptions are made regarding the used models which is essential for developing a framework in which CDMs and FMDMs can be blended. However, this universality will come at a price. Due to the specified requirements, the framework covers a broad domain. This results in a reduction of the number of assumptions that can be made and will in practice result in more computationally exhaustive implementations than when the previously stated requirements would be relaxed. The required computational effort is another challenge of the proposed framework which will be discussed in more detail in Chapter 6. For the present work, the required computational effort is not deemed an issue, as the main goal is to formulate a generally applicable framework. Future work can reduce the computational effort by introducing additional assumptions and relaxing the stated requirements on a case-by-case basis.

2.2.3 Concept

The purpose of this section is to discuss several concepts for a general framework for a PBDA. It is decided to use FEM for the framework. This choice is motivated in Section 2.2.3.1. By using FEM, the available framework concepts can be subdivided into two categories: joint and disjoint implementations. This is subject of discussion in Section 2.2.3.2. The joint implementation is discussed in more detail in Section 2.2.3.3 and the disjoint implementation in Section 2.2.3.4. In Section 2.2.3.5 a concept is chosen, which will be used for the framework.

On an important note, a large part of the motivation arises from a practical point-of-view regarding commercial FEM implementations. However, this is purely based on the author's

experience with Abaqus [1] and initial research regarding Ansys [2] and Comsol [3]. Therefore, the motivation for the choice of the concept may be subject to discussion when new information is available. This is not deemed to be a severe limitation of the present work, as parts of the concept can be reused for other types of frameworks.

2.2.3.1 Finite Element Method

In the last decades, FEA has shown to be a powerful tool in order to simulate the mechanical behaviour of structures. In terms of damage evolution in FRPs, research in literature is limited. Nixon-Pearson et al. [11] investigated the damage evolution in Carbon Fibre Reinforced Polymer (CFRP) Open-Hole Tensile (OHT) specimens and provided a numerical model using a Cohesive Zone Model (CZM) for both quasi-static and fatigue loading. Nikishkov et al. [10] investigated delamination initiation and progression sites in CFRP specimens with a CDM approach. Van Oostrum [7] has shown promising results for the damage evolution in CFRP OHT specimens under quasi-static loading by combining one CDM with two FMDMs. Therefore, the following assumption has been made for the concept of the framework:

- A FEM implementation provides the means to accurately simulate the damage evolution in FRPs.

This assumption is purely based on the results and developments in literature which makes the author believe that this assumption is justified. However, it should be noted that the accuracy of the FEM implementation depends on:

- The underlying models used for simulating the material behaviour
- The underlying assumption that when one takes the limit of the number of elements to infinity, the result converges to the exact solution dictated by the used model.

However, there can be cases that the latter is not true such as, when:

- The size of the elements is lower than the floating point accuracy of the system used to run the FEA
- Numerical issues arise due to non-linearities that may lead to unbalanced derived forces
- Numerical issues arise due to model approximations and coupling between different models.

In practice, for the mentioned numerical issues, it may be difficult to identify the causes. Furthermore, depending on the model formulations and combinations of used models, the solution might not converge for very a large number of elements. However, such models may still be used under the premise that the region of applicability is determined by validation with experiments.

[1] https://www.3ds.com/products-services/simulia/products/abaqus/
[2] https://www.ansys.com/
[3] https://www.comsol.com/

2.2.3.2 Modelling approaches

As established in Section 2.2.3.1 a FEM implementation is used. Two types of frameworks can be distinguished with respect to the method of implementation:

- Joint implementations
- Disjoint implementations.

The joint implementation performs the entire simulation procedure within the FEA environment. The inherent limitations of joint implementations are of a practical kind, namely:

- By implementing the entire simulation in the FEA environment, the model is only valid for the specifically used FEA environment. In order to port the implementation to another FEA environment, the model has to be revalidated
- Depending on the used FEA environment, specific implementations may be difficult to achieve. Widely used FEA commercial environments do provide some flexibility in implementing user-defined functionality. However, this flexibility is limited by the implementation of the FEA environment itself and due to the lack of access to the source code of the FEA environment.

For disjoint implementations, parts of the framework are located outside of the FEA environment. In context of the present work, this refers to the modelling of the fatigue behaviour outside of the FEA environment. The disjoint implementation aims to use the high-fidelity capabilities of FEM but also use the flexibility of user-developed source code. Such an implementation aims to alleviate the inherent limitations of joint implementations. However, the alleviation is only partial as the FEA environment is still used for part of the analysis. Furthermore, disjoint implementations may experience issues related to computational efficiency because of mixing different implementation environments. This may result in a slower overall implementation. To which degree depends on the specific implementation and used environments.

Joint and disjoint implementations are discussed in more detail in Section 2.2.3.3 and Section 2.2.3.4, respectively.

2.2.3.3 Joint implementations

For joint implementations, the entire simulation procedure is performed within an FEA environment. Simulating each cycle within such an environment is infeasible (especially for high-cycle fatigue) due to the required computational resources. In order to tackle such a problem different approaches can be used.

A possible workaround for this issue, used by several authors (amongst others Robinson et al. [14], Turon et al. [15] and Kawashita et al. [16]), is to keep the applied load within the FEA environment fixed and superimpose a fatigue damage model. Such an approach is referred to as the load envelope approach. As it is not possible for FEM implementations to instantly apply a load, the load will start at a value of 0. Next, the load is ramped from 0 towards

the maximum applied load. Furthermore, in case of Tension-Tension (T-T) or Compression-Compression (C-C) loading, the stress-state at the minimum (or maximum) applied fatigue load is obtained during the ramping. This information is required for the fatigue damage model. In Figure 2.6, the load envelope approach is shown for T-T CA fatigue loading. In case of Compression-Tension (C-T) or Tension-Compression (T-C) fatigue loading, one could first ramp the applied load to the negative minimum fatigue load and afterwards ramp up to the maximum applied load. The load envelope approach has the following limitations:

- By keeping the load fixed at a specific level and superimposing a fatigue damagem model, it is implicitly assumed that the material will fail at this load. However, for T-C or C-T fatigue loading this is debatable as the failure processes in tension and compression are fundamentally different. This may become important when combining arbitrary CDMs and FMDMs
- By only considering the stress-state at the minimum applied fatigue load at the beginning, certain fatigue parameters may not be represented accurately throughout the simulation. For example, the stress ratio R is only updated for the changing stress-state at the maximum applied load or remains constant throughout the simulation. It is debatable whether this is valid as the behaviour of R may be non-linear and/or non-monotonic, especially for complex geometries.

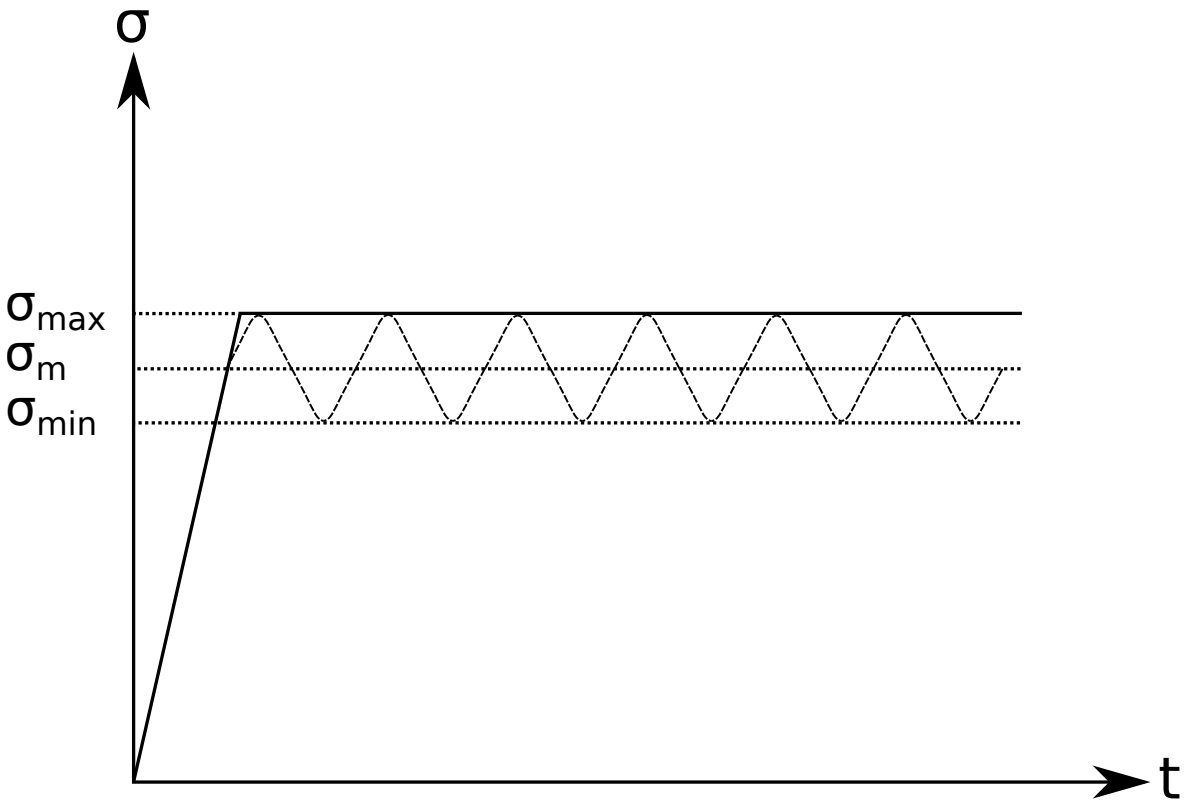

Figure 2.6: An overview of the load envelope approach in case of T-T CA fatigue loading.

Both limitations of the load envelope approach can be addressed by simulating one entire cycle after a certain number of cycles ΔN. ΔN is determined based on a specified cycle

jumping criterion. This alteration to the original formulation is shown in Figure 2.7. As shown in the figure, the load is ramped up to σ_{max} and kept there for ΔN_1 cycles, where the fatigue degradation model(s) is/are superimposed through time in order to model the fatigue degradation. Then after ΔN_1 cycles, the entire cycle N_i is evaluated and this process is repeated until failure. Using such an approach will be more computational exhaustive than the load envelope method. Furthermore, changing the applied load in the FEA environment during the simulation based on results obtained during the simulation is not trivial and may not be possible within a commercial FEA environment.

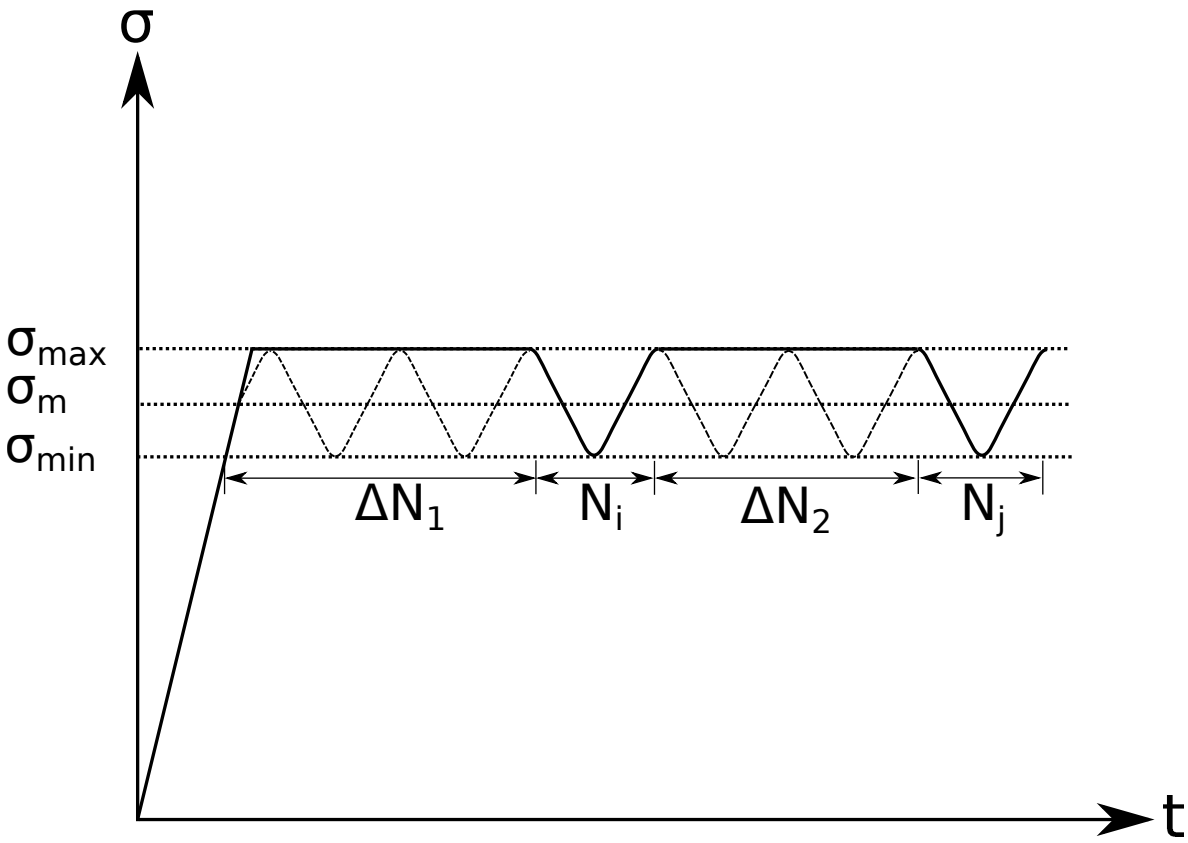

Figure 2.7: An overview of the load envelope approach with discrete cycle evaluation. The situation is sketched in case of T-T CA fatigue loading.

A joint implementation that may address the issue of changing the applied load during the simulation, is the joint constant cycle jump approach. This approach assumes a constant number of cycles to jump (ΔN) throughout the simulation. If the maximum number of cycles are known beforehand, the number of cycles to simulate is known a priori and given by Equation 2.7. In the equation, N_{jump} is the number of cycles to simulate, N_{max} the maximum number of cycles and ΔN the constant number of cycles to jump. Note that N_{max} follows from the scale of interest or an a priori known fatigue life.

$$N_{jump} = \lfloor \frac{N_{max}}{\Delta N} \rceil \tag{2.7}$$

With the joint constant cycle jump approach the number of cycles to evaluate is known

beforehand. Therefore, this number of cycles can be modelled without the need for changing the boundary conditions during the simulation. Furthermore, VA loading can be simulated with such an approach by transforming the load spectrum to a set of CA loads. Then for each CA spectrum i, the number of cycles to jump, $N_{jump,i}$, has to be specified. For this case, the number of cycles is given by Equation 2.8. In the equation, i indicates the CA spectrum number, ΔN_i is the number of cycles that the CA spectrum i contains and $\Delta N_{jump,i}$ is the specified number of constant cycle to jump for CA spectrum i. Moreover, it is deemed necessary to simulate at least one full cycle at the beginning of each CA spectrum i to characterise the CA cycles for spectrum i.

$$N_{jump} = \sum_{i=1}^{I} \min\left[1, \lfloor \Delta N_i \rfloor N_{jump,i}\right] \tag{2.8}$$

Another approach is the single-analysis joint adaptive cycle jump approach. This approach determines the number of cycles to jump, N_{jump}, based on the simulation results. Therefore, the cycles to jump will vary throughout the simulation. In order to avoid changing the boundary conditions during the simulation, the cyclic loading has to be specified beforehand. For CA loading this is possible with the joint methodology. At the beginning of the simulation, the cyclic load is defined by a number of cycles which will never be reached. The amount of cycles has to be determined based on experience or a very large number is used for which it is likely that it is not exceeded. Then, after each load cycle that is simulated in the FEA environment, the analysis is paused and a number of cycles to jump is determined based on the results of the previous cycle. The latter is achieved with a cycle jump algorithm that relies on simplifying assumptions. Next, the fatigue damage is imposed based on some arbitrary model(s) after which the next cycle is simulated. This approach is not possible for VA loading.

The last discussed approach is the multi-analysis joint adaptive cycle jump approach. This approach is similar to the single-analysis joint adaptive cycle jump approach, however the approach aims to alleviate some of the shortcomings. A load envelope approach is used at first. Parallel to this analysis, a cycle jump algorithm is evaluated. The algorithm determines after how many cycles a full cycle should be modelled. Upon reaching the determined number of cycles, the analysis is stopped and a quasi-static analysis of an entire cycle is performed. After the quasi-static analysis, the model is updated and a load envelope approach is initiated again. This is repeated until the end of the analysis. Such an approach alleviates the issues related to modelling the cycles. The boundary conditions do not have to be changed, the analysis does not have to be paused and no large number of cycles has to be specified as input load to model the problem at hand. Furthermore, in principle, this method allows for VA loading. However, after each new CA spectrum, a quasi-static analysis has to be performed which is computationally exhaustive. To avoid the simulation of a full cycle each time the loading changes, relieving assumptions have to be imposed. For example, the assumption that the local R-ratio of a material element scales one-on-one with the global R-ratio. The validity of such assumptions will differ on a case-by-case basis and has to be ratified.

2.2.3.4 Disjoint implementations

For disjoint implementations, parts of the framework are located outside of the FEA environment. In this thesis, the separation of the fatigue damage and FEA is considered. With such

an approach, a cycle is simulated with a quasi-static analysis within the FEA environment, while the fatigue behaviour is processed outside of the FEA environment. Such an implementation addresses the limitations of the joint implementations to a great extent. However, user-defined models used for the quasi-static simulation can still experience those limitations. Furthermore, the input and output of the FEM implementation has to be matched with the fatigue behaviour implementation.

A disjoint implementation addresses all of the issues of the joint load envelope approach and does not experience the issue of changing the boundary conditions during the simulation. However, as mentioned in Section 2.2.3.2, the computational effort for a disjoint implementation may be higher than for a joint implementation. For a practical implementation this is due to:

1. The required pre-processing for FEA environments every time a simulation is started
2. The disjoint implementation has to alternate between loads more often than some disjoint implementations (load envelope approach). The load behaviour of the entire considered cycle is taken into account (instead of keeping the load at a constant level).

The second reason only applies to the original discussed load envelope implementation. In case the first and second limitations of the load approach are addressed by simulating one entire cycle after a certain number of cycles, ΔN, the improvement in terms of computational effort is cancelled. On a last note, for the cycle jumping procedure of a disjoint implementation it is not possible to use FEM (based on computational effort considerations). Therefore, simplifying models and assumptions are required for the cycle jumping of the disjoint approach.

2.2.3.5 Selected concept

Considering the discussion presented in Sections 2.2.3.3 and 2.2.3.4, the multi-analysis joint adaptive cycle jump approach and the disjoint approach are identified as the best concepts for a high-fidelity tool for several reasons, as stated next.

- Both models are capable of simulating the entire cycle. This is deemed necessary for correct characterisation of the cyclic load. It is expected that this simulates the underlying physical mechanisms more accurately. This is especially important for blending arbitrary CDMs and FMDMs. First of all, the behaviour of an arbitrary CDM or FMDM may be influenced. Secondly, the interaction between arbitrary CDMs and FMDMs may be influenced due to the nature of the load cycle. Hence, in order to formulate a general framework for PBDA, it is required to simulate the entire load spectrum of the considered cycles
- Both models can simulate an entire cycle without having to change the applied load within the FEA environment during the simulation based on previous results. Doing so in an FEA environment is not trivial and may not be possible within a commercial FEA environment
- General applicability of the framework is considered as one of the primary objectives, therefore it should be possible to implement CA and VA fatigue loading in the framework

- Even though the required computational effort is important, it is considered a secondary issue for the proposed framework. Attempts will be made to address the issue of computational effort but this will be attempted from a top-down approach. In order to predict the damage evolution within arbitrary FRP structures, it is deemed necessary to simulate the entire load behaviour of a cycle. With the annotation that a cycle jump algorithm would be required to achieve acceptable run times. The use of a cycle jump algorithm will influence the accuracy of the method.

The disjoint methodology is preferred for the present work due to practical motivations, namely:

- The implementation of the multi-analysis joint adaptive cycle jump approach is deemed to be more complicated. One of the limitations is that the ease of implementation is limited within a commercial FEA environment in comparison to a programming language outside of this environment
- The disjoint implementation can achieve compatibility for different available FEA environments to a greater extent than the joint implementation. By separating the fatigue behaviour from the FEA environment, this part can potentially be compatible with different FEM implementations.

However, a disadvantage of the disjoint implementation is that the cycle jumping has to be based on simplifying models and assumptions. The multi-analysis joint adaptive cycle jump approach can update the state of the structure on a more regular basis with less simplifying assumptions from an FEA. Keeping this side note in mind, several methodologies and concepts discussed in this work will also be applicable to the multi-analysis joint adaptive cycle jump approach. The present work will only consider the disjoint implementation, however it is recommended to re-evaluate the possibility of the multi-analysis joint adaptive cycle jump approach in future research.

2.3 Framework

This section discusses the proposed general framework for PDA in FRPs. The framework is based on the discussion in Section 2.2, where it is decided to use a disjoint FEA implementation type of framework. An overview of the proposed framework is presented in Section 2.3.1 The framework consists of several primary components. These components are discussed in more detail in Sections 2.3.2, 2.3.3, 2.3.4, 2.3.5 and 2.3.6.

2.3.1 Framework overview

Consider the situation illustrated in Figure 2.1, where an arbitrary body B is subjected to an arbitrary cyclic load F. The cyclic load can be of the CA or VA type (see Section 2.1.1). Now consider a small material element of body B which is located in one of the laminae (i.e. an element cannot contain layers with different orientations), as shown in Figure 2.1. In general, stresses will act on such an element along every axis and plane, where σ_{ii} denotes the normal

stress components and τ_{ij} the shear stress components. Due to the varying nature of the load F, the stress tensor $\underline{\underline{\sigma}}$ varies over time or cycles as well. Note that even though the body B is loaded uniaxially, the material element can experience a triaxial stress-state.

As stated before, determining the stress-state of a material element for an arbitrary geometry and loading can be achieved with FEA. In light of the discussion in Section 2.2, it is proposed that an FEA tool is used for the quasi-static analysis of a structure and that the fatigue behaviour is processed outside of an FEA environment. This leads to the framework shown in Figure 2.8 which is based on the progressive fatigue damage methodology by Shokrieh and Lessard [17].

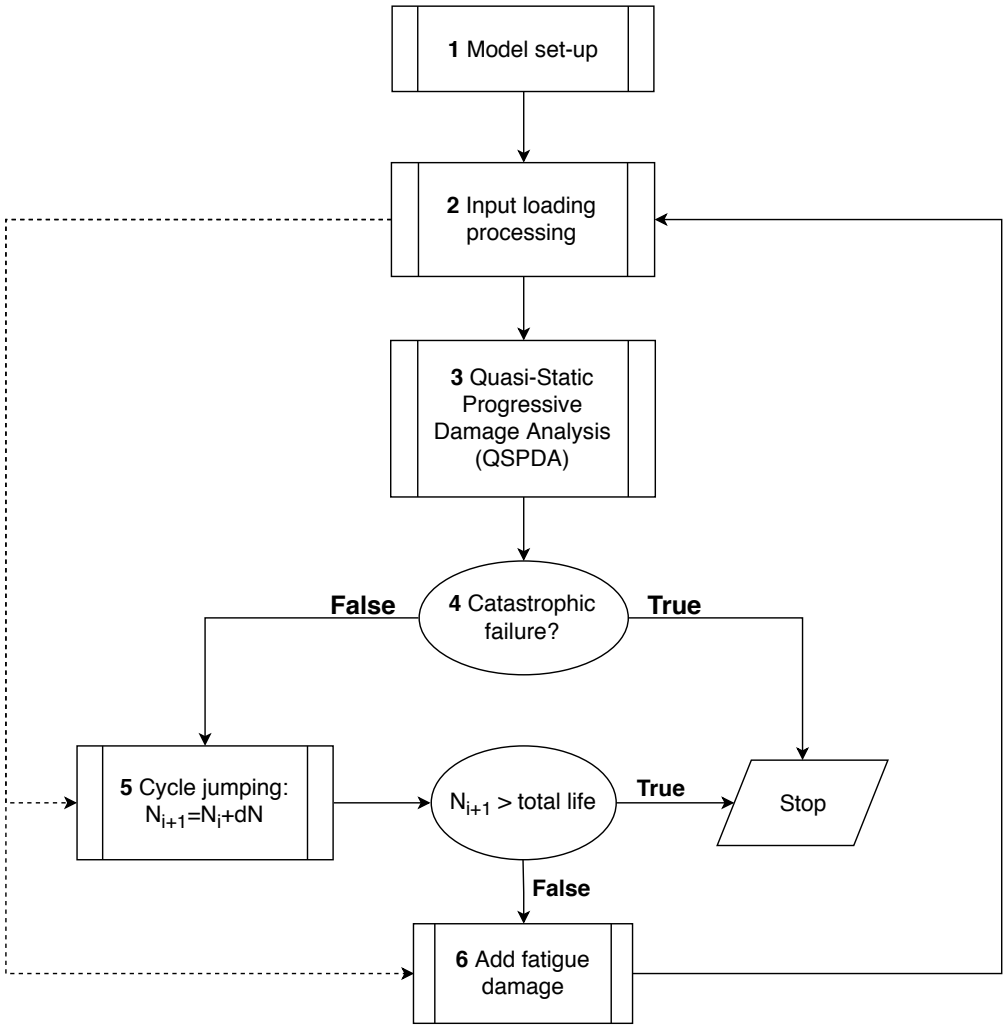

Figure 2.8: A general framework for PDMs.

The first component of the framework is the model set-up. This entails, for example, setting-up the FEA model, material properties and model specific properties. Part of the model set-up can be made model independent such as the geometry of the structure in the FEA

model. Other aspects may, unavoidably, be model specific. Examples are: altering elements in the FEA model to enable the use of eXtended Finite Element Method (XFEM) and/or CZMs. See Section 3.4 for more information regarding XFEM and CZMs.

The second component is denoted as 'input load processing'. In order to, incorporate the possibility of VA loading (for each cycle) the appropriate load has to be analysed for the quasi-static loading. Furthermore, in case of VA loading, the load also influences the cycle jumping and the fatigue damage which is indicated with the dashed arrows. In Section 2.3.2, the input load processing is discussed.

The third component is the PDA for quasi-static loading, the QSPDA, in a FEM implementation. This is discussed in more detail in Section 2.3.3.

The fourth component determines whether catastrophic failure has occurred. This determination is discussed in more detail in Section 2.3.4.

Next, a number of cycles have to be skipped as it is infeasible to evaluate each cycle N. This is referred to as cycle jumping. The cycle jumping component is discussed in more detail in Section 2.3.5.

After the number of cycles to jump is determined, it is checked whether the number of cycles exceeds the total life. The total life is only known when fatigue failure data is available for the structure under consideration. However, this is not always the case; therefore, the total life has a secondary meaning in this context: the user-specified maximum number of cycles under consideration. This may be based on the application for which the fatigue analysis is performed. For example, when analysing a component that has to withstand 10^6 cycles. Hence, the fatigue behaviour after 10^6 cycles is not of interest.

The last component in the proposed framework is concerned with applying the effect of fatigue for a given number of cycles which is based on the number of cycles that are jumped. The fatigue damage component is discussed in more detail in Section 2.3.6.

2.3.2 Input loading processing

The purpose of the 'input loading processing' component in the framework is to handle CA and VA fatigue loading. The case for VA fatigue loading in combination with non-linear damage accumulation will yield the most complicated situation. For this case, the fatigue damage behaviour of the material will be history dependent to a large extent. Consider the stress histogram shown in Figure 2.3. For a VA load and non-linear damage accumulation, the fatigue damage behaviour of the material will depend on the previous load peaks and even the order of these load peaks. In order to account for these effects, the cycle jumping and fatigue damage models have to take into account in the load history. This relation is shown in Figure 2.8 with dashed arrows.

At the other side of the spectrum is CA loading with linear damage accumulation. In this case, the load history dependence is removed and only the history damage state of the material has to be taken into account. Therefore, the 'input loading processing' component does not influence the cycle jumping and fatigue damage components directly.

For the intermediate case that VA loading is considered with linear damage accumulation, the cycle jumping and fatigue damage components have to take into account the load spectrum.

This is illustrated by considering cycle jumping. For ΔN_1 cycles, the stress range is $\Delta\sigma_1$. Then after ΔN_1 cycles, there will be a stress range of $\Delta\sigma_2$ for ΔN_2 cycles. Now, if the cycle jump component is going to estimate how many cycles to jump, the change of the stress range from $\Delta\sigma_1$ to $\Delta\sigma_2$ after ΔN_1 cycles has to be taken into account. Jumping N_{jump} cycles for a constant stress range $\Delta\sigma_1$, even though N_{jump} also contains (or part of) the range ΔN_2 is not a correct representation of the problem at hand. Due to the assumption of linear damage accumulation, the cycle jumping component is not load history dependent but does require information regarding the future load. The same type of argumentation applies for the fatigue damage component of the framework.

Lastly, it is noted that the proposed framework does not make any assumption regarding the type of fatigue loading and damage accumulation. However, for a practical implementation of the framework, this should be considered. Modelling VA loading with non-linear damage accumulation results in a complicated procedure and in case this is not required it is recommended to make some simplification.

2.3.3 Quasi-Static Progressive Damage Analysis (QSPDA)

The QSPDA component of the framework consists of an FEA for quasi-static loading. The QSPDA is performed at the start of the framework (after the model definition) and after each time N_{jump} cycles are jumped. The load that is applied during the QSPDA depends on the current cycle. Consider the load behaviour shown in Figure 2.3 (in terms of nominal stress). Note that the cycles indicated in the figure are a range of cycles and not a single cycle. At the start of the analysis, the first cycle is considered (cycle contained in range ΔN_1 shown in Figure 2.3). This means that the applied quasi-static load will follow the load behaviour corresponding to a CA cycle as defined in interval ΔN_1. At some point, the range ΔN_k will be reached and the quasi-static load will follow the behaviour defined in interval ΔN_k.

For an FEA it is not possible to instantly apply a load. Therefore, the FEA will always start at a load of zero even if the specified load behaviour does not start at zero (for example at interval N_k). Instead, the FEA will ramp from zero to the starting value of the specified load behaviour. Let σ_{min} be the stress at which the specified behaviour starts. Furthermore, the stress level at which the previous cycle ends is connected continuously to σ_{min}. If the latter would not be the case, the problem is no longer quasi-static, but dynamic (impact) which is not in the scope of the current research. If the material would fail in between a load of zero and σ_{min}, this implies that the material would already have failed in the previous cycle or in the transition between the two cycles. Therefore, this ramping behaviour is not deemed to be an issue in the implementation of the QSPDA.

In Figure 2.9, a general overview is provided of the progressive damage procedure used for the QSPDA for an arbitrary element at an arbitrary (pseudo-)time point during the simulation. As an input, the procedure requires the stress-state of the current element (which is provided by the FEA code/package) and element and material properties that are specified during the model set-up (component 1 of the framework).

In general, the progressive damage models can be divided into a damage initiation and progression component. The damage initiation component is some specified criterion which determines whether macroscopic damage occurs within the element. After damage has initiated, the damage progression component determines the response of the element due to the

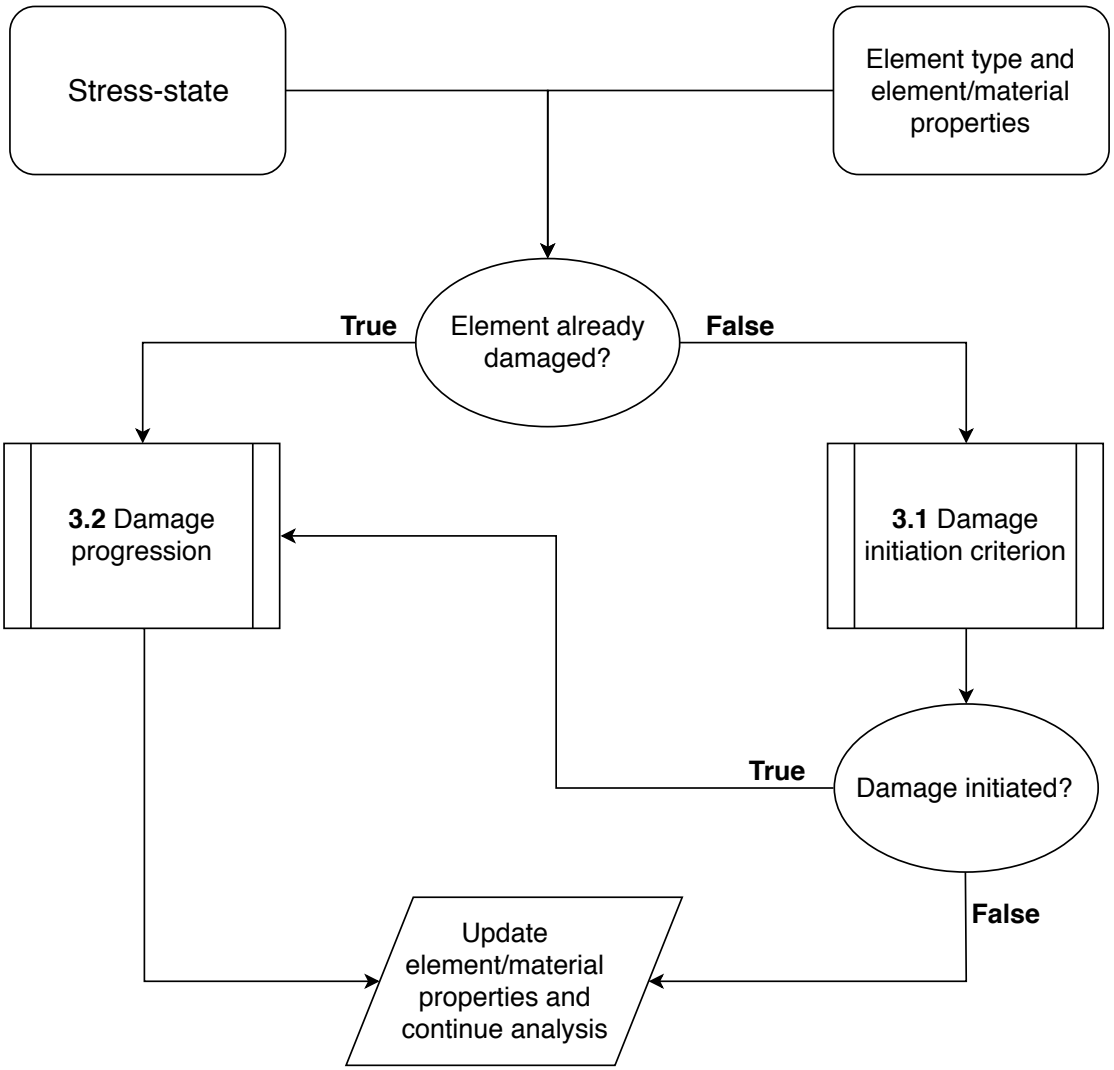

Figure 2.9: Procedure for progressive damage behaviour used by the QSPDA. This procedure is valid for every element at an arbitrary (pseudo-)time point during the simulation.

damage. Note that the element type can influence the models used for the damage initiation and progression. For example, when a model consists of elements using a CDM for matrix and fibre failure and Cohesive Elements (CEs) for delaminations. These elements use different damage initiation and progression models to update the state of the elements (i.e. mechanical properties).

2.3.4 Catastrophic failure

Catastrophic failure is defined as the state of the structure for which the user of the PDA considers the structure as failed. In general, it is difficult to define 'catastrophic failure'

and depends on a case-by-case basis. Therefore, the criterion which determines whether catastrophic failure has occurred should be determined on a case-by-case basis.

2.3.5 Cycle jumping

Cycle jumping is an essential component of the framework. It is only possible to evaluate a select amount of cycles due to the involved computational effort. Different methodologies can be used to skip cycles. First, the simplest implementation is to define a fixed step size ΔN. The disadvantage of this method is that this can lead to inaccuracies in the solution and a 'good' guess for such a step size depends from case to case and has to be determined by trial-and-error by the user. The disadvantage of the fixed step size can be addressed by using an adaptive step size method. In an adaptive step size method, a certain model approximates the step size ΔN. The advantage is that the user does not have to specify a pre-defined step size, however a disadvantage is that such a method is more complicated to implement. Furthermore, one has to be aware of the underlying assumptions of the method as these dictate the accuracy.

An adaptive cycle jump algorithm aims to find the number of cycles for which a significant failure event occurs (specified by the user), whereas for a fixed step size ΔN such events are more likely to be skipped. Furthermore, an adaptive cycle jump algorithm has the potential of general applicability, whereas for a fixed step size this is not possible. Therefore, an adaptive cycle jump algorithm is implemented, following Mitrousias [8].

The first step in an adaptive step size algorithm is to calculate the step size based on an approximate model. This could, for example, be a root-finding method that finds the intersection of the fatigue strength degradation of the material and the damage initiation criterion. A similar method can be used for damage propagation. This method is straightforward to implement but does not consider, for example, interactions between various fatigue and damage initiation mechanisms. The next step is to either use the approximate step size as the final step size or use the approximate step size as a starting point for a more sophisticated model. The former is easier to implement and computationally more efficient than the latter; however, the latter has the potential to be more accurate.

The adaptive cycle jump procedure in the framework attempts to predict a certain number of cycles, N_{jump}, after which a QSPDA leads to a failure event. The definition of a failure event is, once again, user-specified. A general format for the cycle jump procedure is outlined in Figure 2.10. The cycle jump algorithm has the following inputs:

- The stress/load/damage-state at the minimum and maximum of the cyclic loading
- Model specific inputs
- Damage and/or failure indices at the minimum and maximum of the cyclic loading.

Note that with the term 'model' an arbitrary CDM or FMDM is indicated. Furthermore, the damage parameters depend on the implemented model(s) and can relate to damage initiation as well as progression components (see Section 2.3.3).

For the cycle jumping procedure, several assumptions have to be made regarding the state of the material elements in the structure, namely:

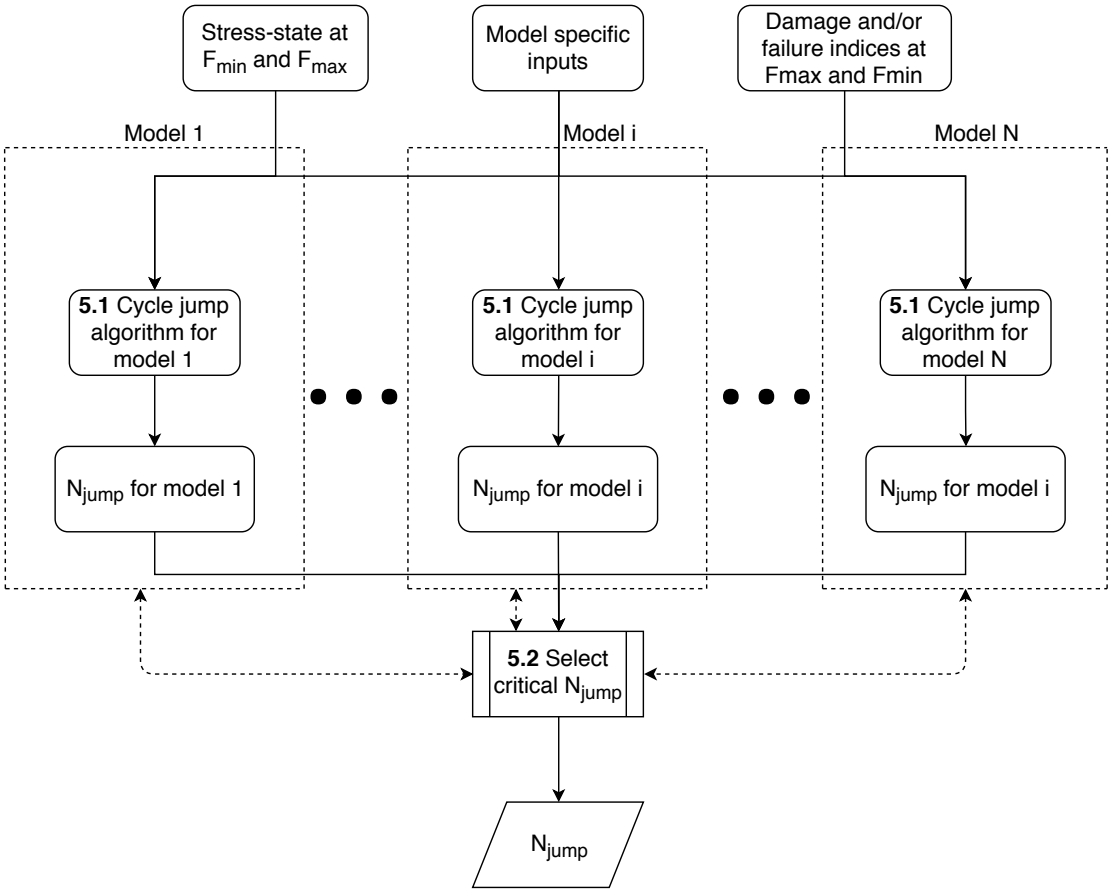

Figure 2.10: General format of the cycle jump procedure for an arbitrary number of models i, where $i = 1..N$.

1. For an arbitrary structure and loading each element will experience their most severe states ($\underline{\underline{\sigma}}_{\mathbf{min}}$ and $\underline{\underline{\sigma}}_{\mathbf{max}}$) at the extreme values of $\underline{\mathbf{F}}$ ($\underline{\mathbf{F}}_{\mathbf{min}}$ and $\underline{\mathbf{F}}_{\mathbf{max}}$)
2. The stress-state of the material remains constant throughout the cycle jump procedure, i.e. the stress-state is not a function of N.

The goal of the first assumption is to reduce the amount of load levels that have to be considered for the output processing of the FEA results. The two states corresponding to the loads $\underline{\mathbf{F}}_{\mathbf{min}}$ and $\underline{\mathbf{F}}_{\mathbf{max}}$ will provide the necessary inputs (maximum and minimum stresses and damage parameters) to model the fatigue behaviour.

The second assumption is made to avoid the iterative calculation of a new stress-state and corresponding damage parameters of the structure. As the stress-state and damage parameters are obtained from the FEA, for each guess of cycle N, an FEA will be required. Doing this would significantly increase the computational time; and potentially render the implementation of the framework unusable. For this reason assumption 2 is made. However, this assumption should be taken with a critical note. By assuming a constant state for a certain

number of cycles ΔN, effectively a linear integration scheme is used. This will affect the accuracy as the behaviour is non-linear. The extent to which this simplification is acceptable should be investigated with future research. Especially, since this may differ between models. A possible work-around is to use a low-fidelity tool to give an approximative update that is more accurate than the constant state assumption. However, it is questionable whether a general low-fidelity tool can be developed that returns acceptable accurate results for an arbitrary structure and loading. Therefore, it is more likely that such a low-fidelity tool has to be developed on a case-by-case basis or that it is not possible to obtain such a tool. The possibility of a low-fidelity tool used in conjecture with the cycle jumping of the framework is not further considered in this report. For the remainder of this report it is assumed that the constant state assumption is valid for a certain range of cycles ΔN. However, future investigation is warranted into determining the maximum range of cycles ΔN that can be used in order to still obtain acceptable accuracy.

Returning to Figure 2.10, each of the models follow a model-specific algorithm to determine the number of cycles to jump. From these number of cycles, the critical number of cycles is selected. However, the critical N_{jump} may also be influenced by a combination of the different models. For example, consider a CZM for delaminations and a CDM for the plies themselves. Let the predicted cycles N_{CZM} and N_{CDM} be the cycles to be jumped for these methods and $N_{CZM} > N_{CDM}$. Based on this information, the algorithm would use N_{CDM} as the cycles to be jumped. However, for this number of cycles, the created delamination damage zone in combination with the CDM damage zone may represent a severe damage event exceeding the tolerance of the user. Therefore, it would be possible to jump over the cycle at which the desired magnitude of the damage event occurs. This illustrates that it may be required to allow for possible interaction between the models. This is indicated with the dotted bidirectional connectors.

An attempt is made to provide a general format for the cycle jump algorithms, irrespective of the model. The general format of the cycle jump algorithm is shown in Figure 2.11. A set of elements $\mathbf{K}$ is selected upon which the number of cycles to jump, N_{jump}, is based. Which elements to select depends on a specified selection criterion. In the extreme case, $\mathbf{K}$ contains all elements. However, this is not recommended as it is computationally expensive to do the cycle jump procedure for all elements. In order to make a selection, the elements are ranked based on the likelihood that the element will fail before others. This can be based on, for example, damage parameters. After obtaining the set of elements $\mathbf{K}$, the number of cycles until failure, N_f, for each element is evaluated. The method to do so depends on the type of PDM. From all of the failure cycles N_f of all elements in $\mathbf{K}$, a cycle has to be selected which will be used as the number of cycles to jump N_{jump}. Which N_f to use, depends on the user-specified criterion.

As stated in Section 2.3.1 and shown in Figure 2.8, the type of fatigue loading can have an influence on the cycle jumping procedure. In case VA loading is considered, the stress-state and damage parameters have to be updated in case the load changes. There are two methods to deal with this. Let N_1 be the number of cycles where load $\underline{\mathbf{F}}_{\mathbf{1}}(t)$ starts to be applied, N_2 be the number of cycles where load $\underline{\mathbf{F}}_{\mathbf{2}}(t)$ starts to be applied and the current cycle is $N_1 + \Delta N$, where $\Delta N \leq N_2 - N_1$. Hence, load $\underline{\mathbf{F}}_{\mathbf{1}}(t)$ is applied for cycles $N_1 \leq N < N_2$ and load $\underline{\mathbf{F}}_{\mathbf{2}}(t)$ is applied for cycles $N \geq N_2$. The first method is to use the cycle jumping algorithm to determine N_{jump}. If $N_{jump} > N_2$ then $N_2 - 1$ cycles are jumped instead of N_{jump} cycles. Hence, each change in load is succeeded by a QSPDA. The second method is to assume that

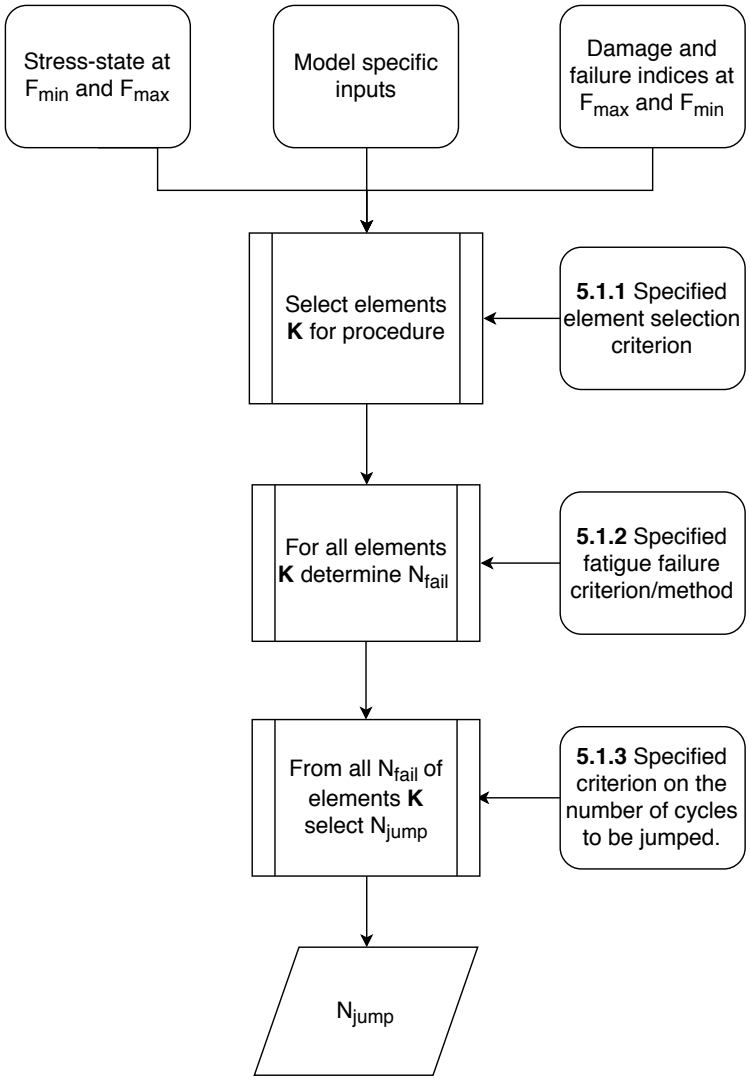

Figure 2.11: General format of the cycle jump algorithm for an arbitrary model.

the stress-state and damage parameters scale proportionally with the applied load. Hence, the cycle jumping algorithm is used to determine N_{jump}. In case the number of cycles for which the fatigue loading changes is exceeded, the following procedure is used:

1. Account for the fatigue damage until cycle $N_2 - 1$
2. Change the stress-states $\underline{\underline{\sigma}}_{\mathbf{min}}$ and $\underline{\underline{\sigma}}_{\mathbf{max}}$, damage parameters and other load dependent parameters proportionally to the load ($\underline{\mathbf{F}}_{\mathbf{min}}$ and $\underline{\mathbf{F}}_{\mathbf{max}}$)
3. Repeat this procedure until an N_{jump} is determined.

In case the relation between the fatigue load and a parameter is known beforehand this relation is used instead of the proportional assumption.

Another loading influence is in the case of non-linear damage accumulation, where the strength degradation of the material depends on the cyclic history. In literature, there is no proposed method to account for this effect without using experimental data. For an arbitrary loading and geometry, this is inconvenient as it is not feasible to do experiments for each combination of stress level and load spectrum. Therefore, for the models in subsequent chapters, linear damage accumulation is assumed. Hence, the strength degradation law is independent of the loading history.

2.3.6 Fatigue damage

The last component of the framework is to determine the residual properties of the material after experiencing N_{jump} number of fatigue cycles. A general format of the fatigue damage procedure is outlined in Figure 2.12.

The influence of fatigue on the mechanical properties of the material can be divided into two domains: pre-failure and post-failure fatigue. The former refers to the degradation of material properties before damage is initiated. The latter refers to the degradation of material properties after damage is initiated. Both the pre-failure and post-failure damage models depend on the type of damage model used for the elements. Note that for post-fatigue damage, one could instantly reduce the material properties and assume total element failure after damage onset. However, this would physically be equivalent to a phenomenon that immediately after the formation of a macroscopic crack, the crack will branch out in all directions throughout the element discounting the properties. Therefore, it is more sound to use a progressive type of post-failure fatigue damage model.

The pre-failure and post-failure fatigue damage models are used to evaluate the fatigue damage due to N_{jump} cycles of the applied fatigue loading. The material properties are then updated for each element and are provided as input to the QSPDA procedure.

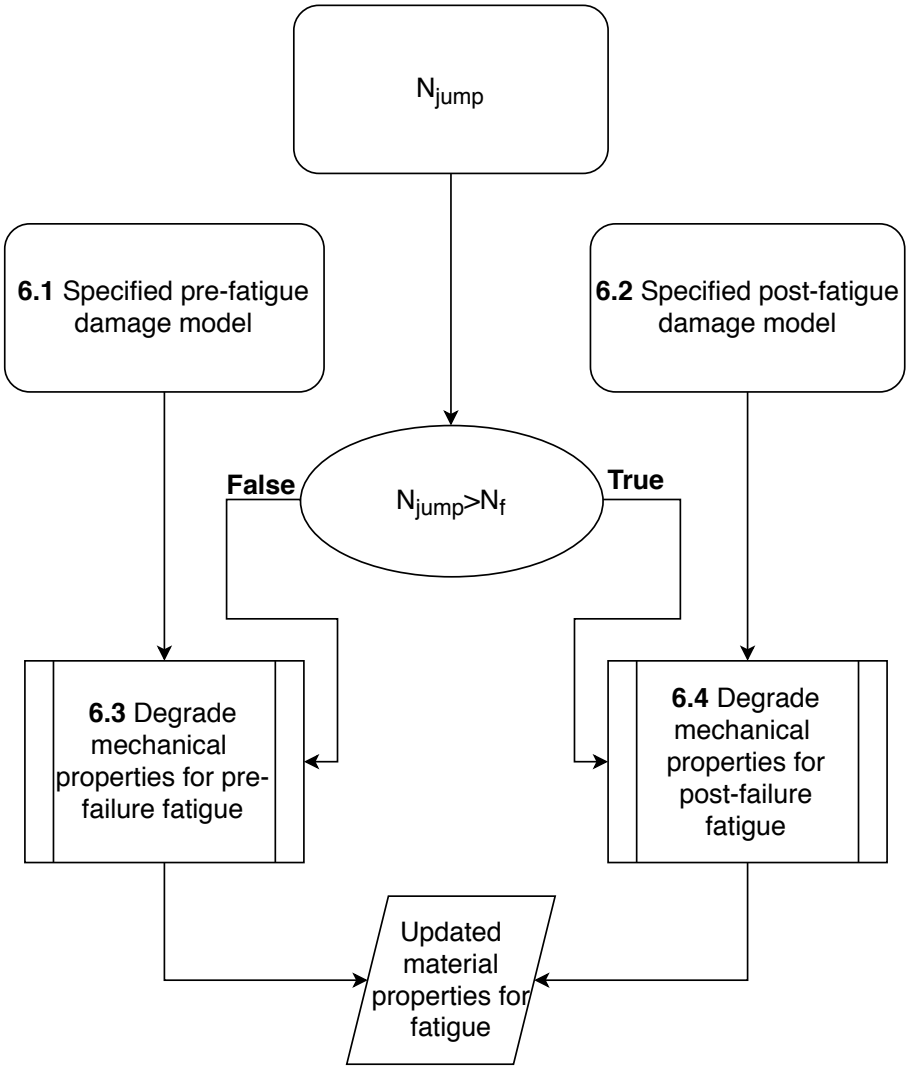

Figure 2.12: General format of the fatigue damage procedure.

Chapter 3

Quasi-Static Progressive Blended Damage Model (QSPBDM)

This chapter focuses on the development of a Quasi-Static Progressive Blended Damage Model (QSPBDM) by combining different types of damage models. Three different types of failure phenomena are considered: fibre failure, matrix failure and delaminations.

The material definition of the Fibre-Reinforced Polymer (FRP) with the Finite Element Method (FEM) is discussed in Section 3.1. On several occasions in this chapter, data is required to verify and compare models. This data is obtained from several test cases. These test cases are briefly discussed in Section 3.2. The constitutive model describes the material behaviour of FRPs and is discussed in Section 3.3. Section 3.3 also includes a brief discussion regarding the notion of in-situ strength and the influence of two different non-linear shear models on the in-situ strength are investigated. In Section 3.4 models are selected for fibre failure, matrix failure and delaminations. Furthermore, as stated in Chapter 2, a Quasi-Static Progressive Damage Analysis (QSPDA) can generally be separated into damage initiation and progression. The selected models are casted into such a format. The damage initiation is discussed in Section 3.5; and the damage progression is discussed in Section 3.6.

3.1 Material definition of Fibre-Reinforced Polymers (FRPs) in the Finite Element Method (FEM)

In Section 2.2.3.1, it has been established to use an Finite Element Analysis (FEA) in the framework. In order to define the FRP material in FEM, two approaches can be distinguished: the Equivalent Single Layer (ESL) and Layer-Wise (LW) approach.

The ESL approach homogenises the composite material; the heterogeneous laminate is treated as a statically equivalent single layer. [18] The ESL approach does not take into account the effect of bimaterial interfaces and assumes that the through-thickness displacement field is first order continuous. Commonly used ESL theories are Classical Laminate Theory (CLT) (Altenbach et al. [19]), First-order Shear Deformation Theory (FSDT) (Altenbach et al. [19]) and Higher-order Shear Deformation Theory (HSDT) (Murty and Vellaichamy [20]). Various researchers have obtained acceptable results with the ESL approach. [13, 21, 22]

With the LW, approach each lamina in the laminate is modelled separately. By doing so, the material heterogeneity is addressed explicitly; and the behaviour of the laminate is defined geometrically instead of materially, as was the case for the ESL approach. [23] By modelling the laminate per lamina, the transverse and interlaminar stresses are more accurately represented than for the ESL approach. [6] However, the LW approach is generally more expensive due to an increase in degrees of freedom per element. [24] In literature, the LW approach is used by several authors for Progressive Damage Analysis (PDA) under quasi-static as well as fatigue loading. [6–8, 10, 23, 25, 26]

In addition to the LW and ESL approaches, a hybrid model could be used. For a hybrid model, an LW approach is used locally for the critical locations; and for the rest of the model, an ESL approach is used. However, in order to apply such an approach, the critical locations have to be known beforehand which results in a loss of generality. Therefore, such an approach will not be considered any further.

The choice between an ESL and an LW approach is a trade-off between accuracy and computational effort. The ESL approach is generally less accurate than the LW approach. [6, 27] Therefore, for a general high-fidelity Progressive Damage Model (PDM) framework, as discussed in this report, the LW approach is deemed more suitable than the ESL approach. In case the generality requirement is relaxed, the ESL approach can be reconsidered for cases where:

- The influence of transverse and interlaminar effects is not stringent
- Computational effort is more important than the loss of accuracy.

3.2 Test cases

In order to compare models and verify the implementation of models, experimental data is required. The concerning models are either material constitutive behaviour models or Continuum Damage Models (CDMs). Therefore, no fracture data is required with the exception of some parameters for the bilinear softening. As individual elements will only span a single lamina (see Section 3.1, it is sufficient to consider UniDirectional (UD) specimens only. Eight test cases have been selected from literature and will be referred to as the Unidirectional Quasi-Static Test Cases (UQSTCs). The UQSTCs are defined in Table 3.1. All of the UQSTCs consider UD FRP materials.

The material properties corresponding to the test cases are provided in Appendix B. UQSTC-1 provides biaxial data for a high-strength Carbon Fibre Reinforced Polymer (CFRP). UQSTC-2, UQSTC-3 and UQSTC-4 are data sets generated by the First World Wide Failure Exercise (WWFE-I) (Kaddour et al. [28]). Unfortunately, the original source was unavailable to the author and the experimental data was obtained from the secondary sources: van Dongen [6] and Puck and Schurmann [29].

UQSTC-5 to UQSTC-8 are obtained from the Second World Wide Failure Exercise (WWFE-II) (Hinton and Kaddour [30]) and correspond to triaxial loading cases with and without shear.

Table 3.1: The eight considered UQSTCs obtained from literature. The mechanical properties of the materials corresponding to the UQSTCs are provided in Appendix B.1.

ID	Material	Stress state	Reference
UQSTC-1	IM7/977-2	$\sigma_{11} - \sigma_{22}$; $\sigma_{33} = \tau_{12} = 0$	[31]
UQSTC-2	E-glass/LY556	$\sigma_{22} - \tau_{12}$; $\sigma_{33} = \sigma_{11} = 0$	[6] and [29]
UQSTC-3	T300/BSL914C	$\sigma_{11} - \tau_{12}$; $\sigma_{22} = \sigma_{33} = 0$	[6] and [29]
UQSTC-4	E-glass/MY750	$\sigma_{11} - \sigma_{22}$; $\sigma_{33} = \tau_{12} = 0$	[6] and [29]
UQSTC-5	E-glass/MY750	$\sigma_{22} - \sigma_{33}$; $\sigma_{11} = \sigma_{33}$, $\tau_{12} = 0$	[30]
UQSTC-6	T300/PR319	$\sigma_{11} - \tau_{12}$; $\sigma_{11} = \sigma_{22} = \sigma_{33}$	[30]
UQSTC-7	S2-glass/Epoxy 2	$\sigma_{11} - \sigma_{33}$; $\sigma_{22} = \sigma_{33}$, $\tau_{12} = 0$	[30]
UQSTC-8	AS/Epoxy 1	$\sigma_{11} - \sigma_{33}$; $\sigma_{22} = \sigma_{33}$, $\tau_{12} = 0$	[30]

3.3 Constitutive model of a lamina

This section is concerned with the constitutive model of a lamina. The constitutive model describes the stress-strain relationship of the material. The simplest possible constitutive model is linear and such a model is widely used in literature to model the behaviour of FRP laminae. This can be attributed to computational considerations. [6, 32] The linear model can approximate the material behaviour well for a certain region of application. However, in reality, the FRP laminae will exhibit non-linear behaviour. The non-linear material behaviour is primarily caused by:

- Inherent material non-linearity
- Damage to the material.

The used constitutive model is based on the linear constitutive model which is extended with methods to account for non-linear behaviour. In Section 3.3.1, the linear constitutive model is discussed. The extensions of this model to account for non-linearity are discussed in Section 3.3.2. In order to account for the, so-called, in-situ strength of a lamina, the original shear and transverse tensile ultimate strengths of the material have to be altered. This is discussed in Section 3.3.3.

3.3.1 Linear constitutive model

In Equation 3.1, the general format of a linear elastic orthotropic material is defined.

$$\begin{bmatrix} \sigma_{11} \\ \sigma_{22} \\ \sigma_{33} \\ \tau_{12} \\ \tau_{13} \\ \tau_{23} \end{bmatrix} = \begin{bmatrix} D_{11} & D_{12} & D_{13} & 0 & 0 & 0 \\ & D_{22} & D_{23} & 0 & 0 & 0 \\ & & D_{33} & 0 & 0 & 0 \\ & & & D_{44} & 0 & 0 \\ & & & & D_{55} & 0 \\ & \text{sym.} & & & & D_{66} \end{bmatrix} \begin{bmatrix} \epsilon_{11} \\ \epsilon_{22} \\ \epsilon_{33} \\ \gamma_{12} \\ \gamma_{13} \\ \gamma_{23} \end{bmatrix} \tag{3.1}$$

The elements of the material stiffness matrix, $\underline{\underline{\mathbf{D}}}$, shown in Equation 3.1 are defined by engineering constants which are given in Equation 3.2. [32]

$$D_{ij} = \begin{cases} D_{11} = E_{11}\frac{1-\nu_{23}\nu_{32}}{\nu} \\ D_{22} = E_{22}\frac{1-\nu_{13}\nu_{31}}{\nu} \\ D_{33} = E_{22}\frac{1-\nu_{12}\nu_{21}}{\nu} \\ D_{12} = E_{22}\frac{\nu_{12}+\nu_{32}\nu_{13}}{\nu} \\ D_{13} = E_{22}\frac{\nu_{13}+\nu_{12}\nu_{23}}{\nu} \\ D_{23} = E_{22}\frac{\nu_{23}+\nu_{21}\nu_{13}}{\nu} \\ D_{44} = G_{12} \\ D_{55} = G_{13} \\ D_{66} = G_{23} \\ \nu = 1 - \nu_{12}\nu_{21} - \nu_{23}\nu_{32} - \nu_{13}\nu_{31} - 2\nu_{32}\nu_{21}\nu_{13} \end{cases} \tag{3.2}$$

According to Maxwell's theorem, the Poisson ratios are related as shown in Equation 3.3.

$$\begin{aligned} \nu_{21} &= \nu_{12}\frac{E_{22}}{E_{11}} \\ \nu_{31} &= \nu_{13}\frac{E_{33}}{E_{11}} \\ \nu_{32} &= \nu_{23}\frac{E_{33}}{E_{22}} \end{aligned} \tag{3.3}$$

Considering the relations given by Equations 3.2 and 3.3, the constitutive behaviour of an FRP lamina can be described by nine engineering constants (E_{11}, E_{22}, E_{33}, G_{12}, G_{13}, G_{23}, ν_{12}, ν_{13} and ν_{23}). The engineering constants can be reduced to five by assuming transverse isotropy. This assumption, however, is not valid for damaged composites. [23] Therefore, nine engineering constants will be required to fully describe the constitutive behaviour of an FRP lamina. Furthermore, when the out-of-plane loads are negligible or not present at all, the constitutive behaviour can be reduced to a two-dimensional model by disregarding all stress and strain components except σ_{11}, ϵ_{11}, σ_{22}, ϵ_{22}, τ_{12} and γ_{12}. For general applicability, the three-dimensional model, defined by Equation 3.1, is used.

3.3.2 Non-linearities

The linear elastic constitutive model forms the basis of the constitutive model used. However, in order to obtain a more accurate description of the material behaviour of FRP laminae, non-linear behaviour should be accommodated. The non-linear behaviour arising from damage is accounted for by using a damage progression model. This will be discussed in Section 3.6. The inherent material non-linearity of an FRP lamina is primarily exhibited in the transverse and shear moduli. [6, 8, 9, 26] The need for modelling the transverse non-linearity is generally case dependent. For example, based on the Glass Fibre Reinforced Polymer (GFRP) data of Eliopoulos [9], it is observed that the shear non-linearity is larger than the transverse non-linearity. Also, Mitrousias [8] suggests that the transverse non-linearity mainly occurs in the compressive region which is outside of the critical area of CFRP Open-Hole Tensile (OHT) specimens. In this work, transverse non-linearity is not taken into account. However, in case a material does exhibit transverse non-linearity and this is apparent in the region of application of the structure under consideration, it is recommended to revisit this assumption.

The material non-linearity is implemented in the constitutive behaviour by fitting experimental stress-strain curves. In order to achieve this, one can use interpolation or extrapolation. However, as explained by van Dongen [6], semi-empirical extrapolation methods are not fit for FEM implementation due to the incompatibility with FEM formulations. Therefore, the non-linearity has to be taken into account by one of the interpolation methods. Which interpolation method to use depends on the available data and restrictions on the computational effort. Three methods commonly found in literature will be discussed next: the Hahn-Tsai, Ramberg-Osgood and spline fits.

The most common method to address the shear non-linearity is the Hahn-Tsai fit (see Hahn and Tsai [33]) due to its simplicity (compared to other methods) and strong theoretical background. [34] The non-linearity is approximated by Equation 3.4, where β is a fitting parameter that has to be determined from experimental data.

$$\gamma_{12} = \frac{\tau_{12}}{G_{12}} + \beta\tau_{12}^3 \tag{3.4}$$

The Ramberg-Osgood fit (see, amongst others, Bogetti et al. [35], Rose et al. [36] and Johnson et al. [37]) is a two-parameter fit, as shown in Equation 3.5, where K and n are fitting parameters determined from experimental data.

$$\gamma_{12} = \frac{\tau_{12}}{G_{12}} + K(\frac{\tau_{12}}{G_{12}})^n \tag{3.5}$$

The spline fit methods are based on a piecewise interpolation between the available datapoints. In literature various order of spline fits can be found. [38–41] For a larger number of experimental data points the spline fit methods provide more accurate results, as for an increasing number of data points the error at the intervals between two data points decreases. A disadvantage of spline methods is that the implementation is less straightforward and the computational effort can be higher than for other interpolation methods. This is due to the piecewise nature of the spline fits. When evaluating the spline fit, before the calculation, the correct spline has to be found depending on the current interval where the value of interest resides in.

Mainly due to additional effort of implementing a spline fit for an arbitrary data set, it is decided to use interpolation fits such as the Hahn-Tsai and the Ramberg-Osgood fits. The Hahn-Tsai and Ramberg-Osgood fits have been evaluated for the materials of the UQSTCs. The Hahn-Tsai and Ramberg-Osgood coefficients are found by using the Levenberg-Marquardt algorithm. [42] Selecting an error measure in order to compare the fits is not trivial and error measures can lead to erroneous conclusions in certain cases. Furthermore, the meaning of error measures is not always straightforward. However, by using multiple error measures a qualitative comparison of the fits is attempted. The following forecasting error measures are used: Normalised Mean Absolute Error (NMAE), Normalised Mean Squared Error (NMSE) and Integral Normalised Mean Square Error (INRSE). [43, 44] The measures are defined in Equations 3.6, 3.7 and 3.8, where e_i is the difference between the experimental value y_i at x_i and the predicted value $f_i(x_i)$. Note that the measures have been normalised by the maximum experimental value y_{max}. In order to account for the different stress magnitudes of the various materials. Furthermore, for the NMAE, NMSE and INRSE measures, it holds that the model

with the lowest value performs best. It is assumed that when all three criteria are in favour of the same model, then that model performs the best (in comparison to the other model(s)).

$$NMAE = \frac{1}{N \cdot y_{max}} \Sigma_{i=1}^{N} \left[|e_i|\right] \tag{3.6}$$

$$NMSE = \frac{1}{N \cdot y_{max}} \Sigma_{i=1}^{N} \left[e_i^2\right] \tag{3.7}$$

$$INRSE = \frac{1}{\Sigma_{i=1}^{N} \left[y_i\right] \cdot y_{max}} \sqrt{\Sigma_{i=1}^{N} \left[e_i^2\right]} \tag{3.8}$$

In Table 3.2, the values of the error measures for the materials of the UQSTCs are given for the Hahn-Tsai and Ramberg-Osgood fits. Plots of the Hahn-Tsai and Ramberg-Osgood fits for the materials are provided in Appendix B.2. The corresponding mechanical properties can be found in Appendix B.1. From the values in the table, it is clear that the Ramberg-Osgood fit out-performs the Hahn-Tsai fit for all cases. By visual inspection, the Ramberg-Osgood fit seems to closely predict the experimental observations for the CFRPs, however for GFRPs the Ramberg-Osgood fit slightly deviates from the experimental observations in the transition area from linear to non-linear behaviour. The Hahn-Tsai fit shows poor performance for materials that exhibit a sharp transition from linear to non-linear behaviour. This can be seen from the relative difference between the Hahn-Tsai and Ramberg-Osgood fits which is higher for such materials (E-glass/LY556, E-glass/MY750, S2-glass/Epoxy-2 and T300-BSL914C). Due to the difference in accuracy, it is decided to use the Ramberg-Osgood fit to account for non-linear shear behaviour. However, it should be noted that the evaluation of the Ramberg-Osgood shear model to obtain the shear stress is computationally more intensive, as no closed form solution for arbitrary constant K and n can be obtained. The latter is possible for the Hahn-Tsai fit.

3.3.3 Lamina in-situ strength

From experimental observations it is known that the strength of a lamina depends on the material, thickness and the location of the lamina in the laminate. [45] Hence, the strength of a lamina in a laminate is not necessarily equal to the measured UD strength of the material. The transverse and shear strength of a lamina increases for a lower thickness and by embedding laminae. [45] The latter is because cracks are more likely to develop at unconstrained surfaces.

Van Dongen [6] compared failure envelopes for various models with and without the incorporation of in-situ strengths. It was found that excluding the effect of the in-situ strength results in overly conservative failure initiation predictions. For final failure, the use of in-situ strengths does not significantly increase predictive accuracy. Van Oostrum [7] considered CFRP OHT specimens and found that excluding in-situ effects leads to unphysical failure patterns. Hence, from a progressive damage point-of-view, taking into account in-situ strengths is important. Furthermore, van Oostrum [7] confirmed the statements of van Dongen [6] that incorporating in-situ strengths does increase the predictive accuracy of final failure but not significantly ($2-3\%$ for an IM7-8552 OHT specimen).

Table 3.2: The NMAE, NMSE and INRSE measures for the Hahn-Tsai and Ramberg-Osgood fits for the materials of the UQSTC. The relative difference is calculated with respect to the Ramberg-Osgood error measure. The corresponding material properties can be found in Appendix B.1 and the experimental data is provided in Appendix B.2.

	E-glass LY556			**E-glass MY750**		
	NMAE	**NMSE**	**INRSE**	**NMAE**	**NMSE**	**INRSE**
Hahn-Tsai	$3.80 \cdot 10^{-1}$	$1.59 \cdot 10^{1}$	$1.10 \cdot 10^{-1}$	$3.62 \cdot 10^{-1}$	$1.51 \cdot 10^{1}$	$9.97 \cdot 10^{-2}$
Ramberg-Osgood	$2.78 \cdot 10^{-1}$	$1.11 \cdot 10^{1}$	$9.15 \cdot 10^{-2}$	$2.64 \cdot 10^{-1}$	$1.06 \cdot 10^{1}$	$8.35 \cdot 10^{-2}$
Relative difference [%]	36.6	43.2	19.7	37.4	42.6	19.4
	S2-glass Epoxy 2			**IM7 977-2**		
	NMAE	**NMSE**	**INRSE**	**NMAE**	**NMSE**	**INRSE**
Hahn-Tsai	$5.36 \cdot 10^{1}$	$2.74 \cdot 10^{1}$	$2.56 \cdot 10^{-1}$	$4.28 \cdot 10^{-1}$	$2.90 \cdot 10^{1}$	$1.90 \cdot 10^{-1}$
Ramberg-Osgood	$4.42 \cdot 10^{-1}$	$2.07 \cdot 10^{1}$	$2.23 \cdot 10^{-1}$	$4.02 \cdot 10^{-1}$	$2.68 \cdot 10^{1}$	$1.83 \cdot 10^{-1}$
Relative difference [%]	21.2	32.3	15.0	6.45	8.36	4.09
	T300 BSL914C			**T300 PR319**		
	NMAE	**NMSE**	**INRSE**	**NMAE**	**NMSE**	**INRSE**
Hahn-Tsai	$5.05 \cdot 10^{-1}$	$2.78 \cdot 10^{1}$	$2.30 \cdot 10^{-1}$	$5.58 \cdot 10^{-1}$	$3.89 \cdot 10^{1}$	$2.89 \cdot 10^{-1}$
Ramberg-Osgood	$4.12 \cdot 10^{-1}$	$2.10 \cdot 10^{1}$	$2.00 \cdot 10^{-1}$	$5.09 \cdot 10^{-1}$	$3.38 \cdot 10^{1}$	$2.69 \cdot 10^{-1}$
Relative difference [%]	22.4	32.2	15.0	9.60	15.0	7.22
	AS Epoxy 1					
	NMAE	**NMSE**	**INRSE**			
Hahn-Tsai	$5.01 \cdot 10^{-1}$	$2.49 \cdot 10^{1}$	$2.61 \cdot 10^{-1}$			
Ramberg-Osgood	$4.47 \cdot 10^{-1}$	$2.14 \cdot 10^{1}$	$2.42 \cdot 10^{-1}$			
Relative difference [%]	12.0	16.6	8.00			

Considering the influence of in-situ effects on the progressive damage behaviour, it is decided that in-situ strengths have to be considered for the QSPBDM. In addition, the predictive accuracy for final failure is expected to slightly increase. A model for calculating the in-situ strengths, based on a fracture mechanics approach, has been introduced by Pinho et al. [26] and Camanho et al. [45]; and will be discussed in Section 3.3.3.1. The model is based on the Hahn-Tsai non-linear shear fit; and is henceforth referred to as the Hahn-Tsai in-situ model. As stated in Section 3.3.2, the Hahn-Tsai fit does not always produce satisfactory results. Therefore, the in-situ model by Pinho et al. [26] and Camanho et al. [45] is modified to incorporate the Ramberg-Osgood fit instead; and is henceforth referred to as the Ramberg-Osgood in-situ model. This model is discussed in Section 3.3.3.2. Finally, in Section 3.3.3.3, the two models are compared.

3.3.3.1 Hahn-Tsai in-situ model

The in-plane shear in-situ strength, $\tau_{12}^{u,is}$, is given in Equation 3.9. [45] In the equation, ϕ is given by Equation 3.10, β is the Hahn-Tsai fitting parameter (see Section 3.3.2) and t is the lamina thickness. [45]

$$\tau_{12}^{u,is} = \sqrt{\frac{\sqrt{1+\beta\phi G_{12}^2}-1}{3\beta G_{12}}} \tag{3.9}$$

$$\phi = \begin{cases} 12\frac{{\tau_{12}^u}^2}{G_{12}} + 18\beta {\tau_{12}^u}^4 \\ 48\frac{G_{II,c}}{\pi t} \\ 24\frac{G_{II,c}}{\pi t} \end{cases} \tag{3.10}$$

The in-situ transverse tensile strength is given by Equation 3.11, where Δ_{22}^0 is given by Equation 3.12. [26]

$$\sigma_{22,t}^{u,is} = \begin{cases} 1.12\sqrt{2}\sigma_{22,T}^u \\ \sqrt{\frac{8G_{I,c}}{\pi t \Delta_{22}^0}} \\ 1.79\sqrt{\frac{G_{I,c}}{\pi t \Delta_{22}^0}} \end{cases} \tag{3.11}$$

$$\Delta_{22}^0 = 2\left(\frac{1}{E_2} - \frac{\nu_{21}^2}{E_{11}}\right) \tag{3.12}$$

Note that $\tau_{12}^{u,is}$ for embedded plies is equal to the highest estimate between thin embedded and thick embedded plies. Hence, the lower bound of $\tau_{12}^{u,is}$ for embedded plies is equal to $\tau_{12}^{u,is}$ for a thick embedded ply. The fracture toughnesses $G_{I,c}$ and $G_{II,c}$ are determined with Double Cantilever Beam (DCB) and Four-point bending End Notched Flexure (4-ENF) tests, respectively.

3.3.3.2 Ramberg-Osgood in-situ model

The in-plane in-situ shear strength in Equation 3.9 is based on a Hahn-Tsai fit to describe the non-linear shear behaviour. However, in Section 3.3.2 it has already been determined that the Hahn-Tsai fit does not necessarily provide a good fit for all types of FRPs. The Ramberg-Osgood fit was shown to provide a better fit for the materials from the test cases introduced in Section 3.2. Therefore, it is warranted to investigate the influence of using the Ramberg-Osgood fit instead of the Hahn-Tsai fit.

Following the derivation by Camanho et al. [45]: for a thick embedded ply the mode II fracture toughness in transverse direction is given by Equation 3.13.

$$G_{II,c} = \pi a_0 \int_0^{\gamma_{12}^u} \sigma_{12} d\gamma_{12} \tag{3.13}$$

The integral is solved by integration by substitution. In Equation 3.14, the relation between an infinitesimal stress $d\tau_{12}$ and an infinitesimal strain $d\gamma_{12}$ is derived by using the Ramberg-Osgood relation given by Equation 3.5. Substituting this relation into Equation 3.13 and changing the integral boundaries from $[0, \gamma_{12}^{u}]$ to $[0, \tau_{12}^{u,is}]$ (which is a result of the change in variable), yields the expression given by Equation 3.15.

$$\begin{aligned} \frac{d\tau_{12}}{d\gamma_{12}} &= \frac{1}{\frac{d\gamma_{12}}{d\tau_{12}}} = \frac{1}{\frac{1}{G_{12}} + \frac{Kn}{G_{12}}(\frac{\tau_{12}}{G_{12}})^{n-1}} \\ \rightarrow d\gamma_{12} &= \left[\frac{1}{G_{12}} + \frac{Kn}{G_{12}}(\frac{\tau_{12}}{G_{12}})^{n-1}\right] d\tau_{12} \end{aligned} \tag{3.14}$$

$$G_{II,c} = \pi a_0 \left[\frac{\left(\tau_{12}^{u,is}\right)^2}{2G_{12}} + \frac{Kn}{n+1} G_{12} \left(\frac{\tau_{12}^{u,is}}{G_{12}}\right)^{n+1}\right] \tag{3.15}$$

The fracture toughness for a UD laminate is given by Equation 3.16. According to Camanho et al. [45], a UD laminate can be seen as a thick laminate with unconstrained outer surfaces. Therefore, Equation 3.15 is equal to Equation 3.16. The evaluation of the integral in Equation 3.16 yields the equality shown in Equation 3.17. Solving Equation 3.17 for $\tau_{12}^{u,is}$ results in the in-situ shear strength.

$$G_{II,c} = 2\pi a_0 \int_0^{\gamma_{12}^{u}} \tau_{12} d\gamma_{12} = 2\pi a_0 \left[\frac{(\tau_{12}^{u})^2}{2G_{12}} + \frac{Kn}{n+1} G_{12} \left(\frac{\tau_{12}^{u}}{G_{12}}\right)^{n+1}\right] \tag{3.16}$$

$$\frac{\left(\tau_{12}^{u,is}\right)^2}{2G_{12}} + \frac{Kn}{n+1} G_{12} \left(\frac{\tau_{12}^{u,is}}{G_{12}}\right)^{n+1} = \frac{(\tau_{12}^{u})^2}{G_{12}} + \frac{2Kn}{n+1} G_{12} \left(\frac{\tau_{12}^{u}}{G_{12}}\right)^{n+1} \tag{3.17}$$

For a thin embedded ply, the fracture toughness is given by Equation 3.18. [45] By again using integration by substitution, the in-situ shear strength is obtained by solving Equation 3.19.

$$G_{II,c} = \frac{\pi t}{4} \int_0^{\gamma_{12}^{u}} \tau_{12} d\gamma_{12} \tag{3.18}$$

$$\frac{G_{II,c}}{\pi t} = \frac{\left(\tau_{12}^{u,is}\right)^2}{8G_{12}} + \frac{Kn}{4(n+1)} G_{12} \left(\frac{\tau_{12}^{u,is}}{G_{12}}\right)^{n+1} \tag{3.19}$$

For thin outer plies, the fracture toughness is given by Equation 3.20. [45] Hence, the in-situ shear strength is obtained by solving Equation 3.21.

$$G_{II,c} = \frac{\pi t}{2} \int_0^{\gamma_{12}^{u}} \tau_{12} d\gamma_{12} \tag{3.20}$$

$$\frac{G_{II,c}}{\pi t} = \frac{\left(\tau_{12}^{u,is}\right)^2}{4G_{12}} + \frac{Kn}{2(n+1)} G_{12} \left(\frac{\tau_{12}^{u,is}}{G_{12}}\right)^{n+1} \tag{3.21}$$

Due to the format of Equations 3.17, 3.19 and 3.21 it is difficult (if not impossible) to find an analytical expression for $\tau_{12}^{u,is}$ for arbitrary values of K and n. Therefore, the modified Newton-Raphson algorithm discussed in Section 2.1.4 is employed to solve for $\tau_{12}^{u,is}$. The transverse in-situ tensile strength remains equal to the expression shown in Equation 3.11.

3.3.3.3 Model comparison

In order to investigate the influence of the shear model on the estimation of the in-situ shear strength, the in-situ strengths for embedded and outer plies have been calculated for each of the UQSTC materials. For each of the materials, the in-situ strength is calculated by using a linear, Hahn-Tsai and Ramberg-Osgood shear model. From the evaluation it becomes apparent that a linear shear model provides extremely conservative shear strengths (especially for thin plies). Therefore, the linear shear model illustrates the requirement of a non-linear shear model and is not further considered for the calculation of in-situ strengths. The maximum errors between the Hahn-Tsai and Ramberg-Osgood in-situ models are shown in Table 3.3. The errors are calculated with respect to the in-situ strength predicted by the Hahn-Tsai in-situ model. Furthermore, the minimum and maximum error are calculated on the interval $t = [0.1, 1.0]$ to accommodate for practical lamina thicknesses and to avoid the asymptotic behaviour close to $t = 0$. In Appendix B.4, the predicted in-situ shear strengths for the UQSTC materials are plotted. Note that in the figures in Appendix B.4 the term 'ply' is used instead of 'lamina'.

Table 3.3: Relative errors of the in-situ strength of embedded and outer laminae between the Hahn-Tsai and Ramberg-Osgood in-situ models. The provided errors are relative to the Hahn-Tsai in-situ model.

	E-glass LY556		**E-glass MY750**		**S2-glass Epoxy 2**	
	δ_{min} [%]	δ_{max} [%]	δ_{min} [%]	δ_{max} [%]	δ_{min} [%]	δ_{max} [%]
Embedded	11.50	25.92	11.60	24.03	9.65	20.92
Outer	−14.69	13.46	−16.11	11.61	−14.29	10.61
	IM7 977-2		**T300 BSL914C**		**T300 PR319**	
	δ_{min} [%]	δ_{max} [%]	δ_{min} [%]	δ_{max} [%]	δ_{min} [%]	δ_{max} [%]
Embedded	5.06	23.77	10.78	41.11	13.84	28.13
Outer	0.32	17.70	−6.29	28.23	−2.77	11.81
	AS Epoxy 1					
	δ_{min} [%]	δ_{max} [%]				
Embedded	−38.95	0.00				
Outer	−39.22	0.00				

The errors in Table 3.3 clearly show that the Hahn-Tsai in-situ model predicts higher in-situ strengths when compared to the Ramberg-Osgood in-situ model for embedded laminae. Furthermore, for thin outer laminae, the Hahn-Tsai in-situ model predicts higher in-situ strengths; while for thick outer laminae, the Ramberg-Osgood in-situ model predicts higher in-situ strengths. Considering that large maximum relative errors (up to 41.11%) arise when

using a different shear model, it is recommended to investigate the modelling of the in-situ strength in more detail in future research.

3.4 Model selection

The failure of composites can be characterised by three types of failure: fibre, matrix and delamination failure. [46] Delamination failure can be considered as a special type of matrix failure. Important considerations for selecting a model for these failure types are accuracy, computational efficiency and generality. Rarely, a chosen model is in favour of all considerations; therefore, a trade-off has to be made.

In this section, the application of several methodologies, to the discussed type of failures, will be discussed. The detailed discussion of the methodologies is out of the scope of the current work and only a brief discussion, where deemed necessary, will be provided. Furthermore, the CDM (discussed by, amongst others, van Dongen [6]), Cohesive Zone Model (CZM) (discussed by, amongst others, Camanho et al. [47] and Turon et al. [15]), Virtual Crack Closure Technique (VCCT) (discussed by, amongst others, Krueger [48]) and eXtended Finite Element Method (XFEM)-based models (discussed by, amongst others, Mohammadi [49]) have been identified as the main methodologies for PDA for quasi-static loading as well as fatigue loading. A variation on the VCCT, Virtual Crack Extension (VCE), has not been considered based on the review by Van Oostrum [7]. Van Oostrum [7] observed that no practical applications of the VCE for mixed-mode are available in literature; therefore, this method is not further considered. Note that some additional information and references for the CZM have been provided in Appendix D.

In Section 3.4.1, fibre failure is discussed. Matrix failure is discussed in Section 3.4.2 and delamination is discussed in Section 3.4.3.

3.4.1 Fibre failure

Fibre failure can be distinguished by Tensile Fibre Failure (FFT) and Compressive Fibre Failure (FFC). For the prediction and modelling of FFT onset, the stress-based criterion of the form shown in Equation 3.22 is often encountered in literature. The main reason for the common use of the criterion, shown in Equation 3.22, is that it correlates well to experimental data. [50]

$$\frac{\langle \sigma_{11} \rangle_+}{\sigma^u_{11,t}} \geq 1 \tag{3.22}$$

For the prediction and modelling of FFC onset, either numerical micromechanical models (Pimenta et al. [51] and Gutkin et al. [52]) or analytical stress-based criteria (Puck and Schurmann [29], Gutkin et al. [53] and Pinho et al. [50]) are used. The numerical micromechanical models are not suitable in this work as the integration of such a model will lead to a multi-scale analysis which significantly increases the computational effort. Therefore, it has been decided to use a stress-based criterion for FFC.

In literature for both FFT and FFC, the property degradation after damage onset is based on degradation methods corresponding to CDMs. [54, 55] Considering the methods used in literature to predict damage initiation and account for damage progression, the only available option to model FFT and FFC is by using a CDM. The damage initiation of the CDM is discussed in Section 3.5.1 and damage progression in Section 3.6.1.

3.4.2 Matrix failure

The term matrix failure does not only refer to the failure initiation of the matrix but also to the progression of such failure to other parts of the structure. In recent literature the PDA methods for modelling matrix failure are: CDMs discussed in Section 3.4.2.1, interface (CZM) or spring elements discussed in Section 3.4.2.2 and XFEM-based models discussed in Section 3.4.2.3. Finally, in Section 3.4.2.4 a model for matrix failure is selected.

3.4.2.1 Continuum Damage Models (CDMs)

The advantage of CDMs is that they are readily evaluated and do not require significant computational effort. However, CDMs have the tendency to smear out damage. Macroscopic cracks will in reality not consist of a smeared out damage are but instead of a fracture surface formed by cracking. Therefore, CDMs have a reduced physical basis when compared to Fracture Mechanics Damage Models (FMDMs). Especially, considering that fracture is not driven by the stress-state of the material but rather to the energy release due to the forming of fracture surfaces. Van Oostrum [7] has shown, for CFRP OHT specimens under quasi-static loading, that a fracture mechanics method for matrix cracking shows better correspondence to experimental data in terms of both damage patterns and predicted failure loads. A disadvantage of an FMDM approach is the increase in computational effort in comparison to a CDM. However, the expected increase in accuracy in terms of both damage patterns and failure load is deemed to be of more importance. Therefore, it is decided to use an FMDM instead of a CDM for matrix failure.

3.4.2.2 Interface or spring models

Interface or spring elements for the modelling of matrix cracking have been used by, amongst others, Jiang et al. [56] and Wisnom and Chang [57]. The use of spring elements, requires prior knowledge of the crack such as the orientation and path of the crack during loading. Therefore, such elements are not considered.

For CZMs, a distinction can be made between intrinsic and extrinsic models. Extrinsic CZMs start at a non-zero traction at zero separation. For such models, the cohesive element is added in the model after an ultimate strength/criterion has been surpassed. This requires that the mesh topology is updated during the analysis which leads to implementation complexity and increase in computational effort. [58] This increase due to updating the mesh topology will lead to unrealistic computational time. Especially, considering that multiple FEAs have to be performed in the case of fatigue loading. Therefore, extrinsic CZMs are deemed to be unsuitable for the problem at hand. Note that this concerns a pure extrinsic CZMs approach

and does not discount the extrinsic CZMs to be used in conjunction with another type of method.

Intrinsic CZMs start with zero traction at zero separation and intrinsic cohesive elements are added to the model during the model generation. In order to do so, a priori knowledge of the fracture plane is required. A possible solution for the latter is to add intrinsic CZMs elements in between all other elements. However, this is unfortunately not possible because:

- The CZM artificially changes the stiffness of the structure
- The stiffness matrix becomes ill-conditioned [7]
- By adding intrinsic cohesive elements the possible fracture planes along which the crack can propagate is dictated by the mesh. Even when cohesive elements are in between all other elements, the possible fracture path is still constrained. This does not allow for general problem dependent crack growth.

Considering the previous discussion regarding interface and spring elements, it is concluded that these methods are not suitable for the modelling of matrix failure and progression.

3.4.2.3 eXtended Finite Element Method (XFEM)-based models

In literature, several implementations and variations of XFEM for the modelling of matrix cracks can be found. [7, 58–60] All such models will be referred to as XFEM-based models. The models under consideration are pure XFEM as formulated by Belytschko and Black [61], Phantom Node Methods (PNMs) [7, 59, 62, 63] and Floating Node Methods (FNMs) [64, 65]. All three methods are applicable for modelling matrix cracks and have as main feature that the crack can be represented within an element. This avoids the need for remeshing. Furthermore, the fracture surface does not have to be known a priori and follows progressively from the simulation. These two advantages already give a preference of an XFEM-based method over the previously discussed methods and VCCT.

A pure XFEM approach is rarely used nowadays because:

- The modelling of the crack-tip singularity is computationally expensive. In order to model this accurately, the crack has to be tracked constantly. Furthermore, for a non-isotropic material, the crack singularity depends on the location of the crack [66]
- XFEM does not provide the means to predict progression. In order to do this, a different type of model/criterion has to be used.

Both disadvantages make the use of pure XFEM for anything other than stationary cracks inconvenient. Therefore, a pure XFEM implementation is not considered any further.

The PNM was introduced to allow for simplifications of the implementation of XFEM in existing FEA codes. The advantages of the PNM is lower computational cost (compared to XFEM) and little mesh dependence. [63] Note that the latter is only applicable in case the mesh is refined enough to capture the underlying physics. Furthermore, it has been observed by Song et al. [63] that the crack tip speed is affected to some extent by the mesh size. This

is attributed to the incapability of the PNM to model partially cracked elements. The main disadvantages of the PNM are the inability to partially model cracked elements and model the near-tip singularity. Note that the PNM is not able to determine the progression of the crack and has to be used in conjunction with another method, such as the extrinsic CZM.

The FNM is a variation of the PNM. De Carvalho et al. [65] state the following advantages of the FNM over the PNM and XFEM.

- Mapping to the natural coordinates with the FNM does not introduce an error on the crack geometry
- No partial domain numerical integration is required
- FNM is capable of modelling multiple networks of different type of discontinuities
- The FNM obtains the same solution as for the case where the discontinuity is explicitly represented
- The FNM has a simpler concept than PNM and XFEM.

Similar to the PNM, the FNM is not able to model the progression of the crack and another FMDM is required. De Carvalho et al. [64,65] used the VCCT in order to model matrix cracks. In order to improve the crack tip representation, the elements within a specified enrichment radius of the crack tip are refined. This refinement occurs locally in an element; therefore, no global remeshing is required which is one of the main disadvantages of the VCCT. However, using the VCCT in conjuction with FNM still seems to require pre-cracks. The FNM has also been used together with extrinsic CZM. [60,67] The main disadvantages of the FNM are that:

- The near-tip singularity cannot always be modelled. In combination with VCCT it is possible to model this; however, local mesh refinement and a pre-crack are required
- The modelling of a wide variety of possible discontinuities requires a large amount of floating nodes per element. This may influence the computational effort and lead to practical restrictions in terms of model size.

A general shortcoming of the XFEM-based methods is that there is no detailed comparison of, amongst others, computational effort, mesh-dependency and accuracy. Therefore, it is recommended for future work to compare such models in order to identify the relative shortcomings and challenges of these methods.

3.4.2.4 Matrix failure model

Based on the brief evaluation of several models in Sections 3.4.2.1 to 3.4.2.3, it is decided to use an XFEM-based model. Due to a lack of a thorough qualitative and quantitative comparison of such models, it is not straightforward to select the 'best' method. Therefore, it has been decided to select the standard XFEM-based method in Abaqus as this avoids the creation of user-defined element behaviour. If future work dictates that this model is

insufficient, an improved user-defined XFEM model can be created as previously shown by Giner et al. [68] and de Carvalho et al. [65].

The model used by Abaqus is an XFEM-based cohesive segment method which uses the PNM. [66] More information regarding this model is provided in Chapters 3.5.3 and 3.6.3; and the Abaqus Analysis User's Guide [66].

3.4.3 Delamination failure

Based on available literature, three types of methodologies are considered for delaminations: CDMs discussed in Section 3.4.3.1, VCCT discussed in Section 3.4.3.2 and CZM discussed in Section 3.4.3.3. Finally, in Section 3.4.3.4 a delamination model is selected.

3.4.3.1 Continuum Damage Models (CDMs)

In literature, several stress-based delamination initiation criteria can be found such as criteria by Lee [69], Ochoa and Engblom [70], Long [71], Shokrieh et al. [72] and Tong [73]. Such criteria are of a similar format and are based on a limited physical basis. Furthermore, most of literature using a CDM type of approach use an instant total property discount in case of delamination failure (amongst others, Tserpes et al. [22]). It is questionable whether this is true; even though the element cannot transfer load to the next lamina (due to the separation), it may still be able to carry loads transferred within the lamina. Furthermore, the instant discount of properties may pose numerical issues.

Both stress-based initiation and progression approaches seem to be unable to reliably capture the effects of delaminations. It is therefore not surprising that from the turn of this century, stress-based models are scarce in literature and FMDMs are favoured. Therefore, stress-based criteria (CDM) will not be considered for delaminations.

3.4.3.2 Virtual Crack Closure Technique (VCCT)

VCCT has been used by several authors such as Elisa [74] and Shen et al. [75]. However, the application of VCCT to PDA is rarely encountered in literature. The advantages of VCCT are that:

- There is a physical basis founded on Linear Elastic Fracture Mechanics (LEFM), where the crack growth is fully determined from fracture mechanics without the need of stress measures
- VCCT is a mature model based on extensive literature and research. See, for example, Krueger [48] for an elaborate overview.

The main disadvantages of the VCCT are that:

- An existing crack with given shape and size is required
- The crack path is mesh dependent

- A very fine mesh, in comparison to the rest of the structure, is required to sufficiently capture the effect of the crack tip
- In order to advance the crack front, moving mesh techniques are required that increase implementation complexity and computational effort
- Due to the dependence on topological information and nodal variables of the nodes behind and ahead of the crack front, the computational effort is further increased [15]
- Multiple cracks are not allowed to coalesce. [7]

The FNM discussed in Section 3.4.2.3 may alleviate some of the issues regarding implementation complexity, computational effort and the mesh dependent crack path. The FNM allows for locally refining the mesh which mitigates the need for a global mesh update. Furthermore, due to the portioning of elements, the crack path is not necessarily defined along the faces of the elements. However, even with the FNM, an initial existing crack is required and cracks cannot coalesce. Furthermore, it is not clear to what extent the use of the FNM in conjunction with VCCT reduces the computational effort. Therefore, it is recommended to investigate the limitations and the advantages of the FNM in conjunction with VCCT in future research.

3.4.3.3 Cohesive Zone Models (CZMs)

Extrinsic CZMs will require a significant amount of mesh updating, as the element is added after a certain ultimate strength/criterion has been surpassed. Therefore, extrinsic CZMs will not be considered for the modelling of delaminations.

Intrinsic CZMs lend themselves well to the modelling of delaminations as the fracture plane is typically constraint (in-plane). The advantages of intrinsic CZM for the modelling of delaminations are:

1. The capability of predicting the onset as well as the propagation of delaminations [15]
2. The suitability for general structures and loading. No assumptions have to be made regarding the fracture surface
3. Cohesive zones are inserted as separate elements. This poses no requirements on the surrounding mesh (and element type) which is beneficial for a blending philosophy [7]
4. The failure is defined within the formulation of CZMs. This mitigates the need of remeshing.

For the second advantage, it has to be pointed out that it depends on the other used methods. For example, consider using CDM elements for the laminae and intrinsic cohesive elements in between the elements. Vigueras et al. [58] point-out that, due to using two fundamentally kinematic representations, not all interactions can be captured. Therefore, depending on the situation, the imposed behaviour of the surrounding elements does matter.

The intrinsic CZMs does have several shortcomings.

1. Generally, a small mesh size is required for accurate delamination predictions

2. A decrease in physical basis when compared to VCCT
3. Depending on the formulation of the CZM, the cohesive elements cannot correctly account for the transfer of load from cracked solid elements to the interface of the lamina [76]
4. Depending on the formulation, decohesion elements may cause numerical difficulties. These difficulties may arise due to the stiffness of the cohesive relation and convergence issues related to softening constitutive models. [15]

The third shortcoming can be solved by using different formulated CZMs such as the Augmented Cohesive Zone (ACZ) method proposed by Fang et al. [76]. Such a model aims to accurately model the cracks that merge into or branch away from the lamina interface. Formulations that do not take this into account can still be used. However, one should take into account that the previously mentioned type of cracks are less accurately modelled. Furthermore, the last shortcoming depends on the formulation of the used decohesion elements. However, in general, the addition of intrinsic CZM to model delaminations lead to slower convergence than compared to a model without such elements.

3.4.3.4 Delamination model

Based on the brief discussion in Sections 3.4.3.1, to 3.4.3.3, it is found that the VCCT and intrinsic CZMs are the only contenders for delamination modelling. It has been decided to use an intrinsic CZM for the following reasons.

- The VCCT requires a priori knowledge regarding the crack, whereas for CZMs this is not required. The latter is therefore of more interest for a general high-fidelity tool
- CZMs allow for delamination fronts to join, whereas for the VCCT this is not possible. [7]
- The CZM is preferred in terms of computational efficiency, because the VCCT generally takes more computational effort to evaluate. This is especially apparent in the case of fatigue, where VCCT are only used for the evaluation of low-cycle fatigue and/or relatively small models (see, amongst others, Pradhan and Tay [77] and Davila and Bisagni [78])
- Results obtained in literature for CZMs for quasi-static (see amongst others, Lampani [79] and Ankersen and Davies [80]), as well as fatigue loading (see amongst others, Kawashita and Hallett [16] and Bak et al. [81]), have shown to produce reasonably accurate results. However, it should be kept in mind that in order to produce such results a relatively fine mesh is required.

The increase in computational efficiency for CZMs with respect to the VCCT has not been clearly quantified in literature. Pirondi et al. [82] compared an intrinsic CZM with a VCCT for fatigue loading. Simulations of DCB, End Load Split test (ELS), Mixed-Mode End Load Split test (MMELS) and a single-lap joint experiments were evaluated. A reduction of up to one order of magnitude in the computational effort was reported in case CZMs were used instead of the VCCT. However, for this comparison, a user-defined CZM and the built-in

VCCT in Abaqus were used. The built-in VCCT uses a direct cyclic procedure within Abaqus which can require a large number of iterations to converge. Therefore, this comparison is influenced by the implementation in conjunction with the model formulations. In literature, the general consensus is that CZMs are more efficient than the VCCT; however, a thorough quantification of the improvement in efficiency has not been encountered. Based on the consensus in literature regarding this subject, the argument that CZMs are less computationally expensive than the VCCT is maintained in this work.

3.5 Damage initiation criterion

This section discusses the damage initiation part of the QSPDA, indicated as module 3.1 in Figure 2.9. The damage initiation criterion for the CDM is discussed in Section 3.5.1. The damage initiation criteria of the CZM for delaminations is discussed in Section 3.5.2 and the XFEM-based model for matrix failure is discussed in Section 3.5.3.

3.5.1 Continuum Damage Model (CDM)

The damage initiation part of the CDM consists of a stress-based model. This model is primarily used for the initiation of fibre damage. Furthermore, as will be further explained in Section 3.5.3, a stress-based criterion will be used for matrix damage onset as well. The advantage of such models is that they can be efficiently evaluated and provide the means to define a starting point for computationally more exhaustive methods that capture the damage progression more accurately. Macroscopic stress-strain-based failure criteria can be classified in two main categories: mode independent and mode dependent failure criteria. For both categories various reviews can be found in literature such as Van Dongen [6], Garnich and Akula [32], Wicaksono and Chai [46], Echaabi et al. [83], Orifici et al. [84] and Talreja [85].

Mode independent criteria can be defined as a mathematical curve or surface in stress-strain space which predict failure of the material but do not (directly) identify the failure mode or damage mechanisms. [32] The most common form of independent criteria are the so-called polynomial criteria. A commonly used polynomial criterion is the quadratic Tsai-Hill or Azzi-Tsai criterion. [86] Most of the polynomial criteria used in literature are quadratic criteria. It is reported that there exist some higher-order polynomial (mostly cubic) failure criteria. [46, 83, 87] However, the increase in accuracy by using a higher-order polynomial is accompanied with a significant increase in complexity which requires the determination of additional parameters. [46, 83, 87] Other mode independent approaches are the parametric criteria, where the failure surface in stress space is described in a parametric form. [87–91]. However, as reported by Echaabi et al. [83] the parametric method is not more precise or systematic than other mode independent failure criteria. The literature on parametric criteria is therefore limited compared to the polynomial criteria which were developed earlier.

Mode dependent criteria do not only predict damage and failure of a composite, but also consider different types of failure methods. The lack of the latter is a significant shortcoming of the mode independent methods. Hashin and Rotem [92, 93] were one of the first to make a real distinction between failure modes. However, the Hashin-Rotem criterion was still based on polynomial fitting and reasoning instead of insight in the failure mechanisms. A significant

improvement on the Hashin-Rotem methods was introduced by Puck and Schurmann [29]. This so-called Puck criterion distinguishes between Fibre Failure (FF) and Inter Fibre Failure (IFF), based on physical mechanisms. The main drawback of the Puck criterion is that seven constants have to be determined from test data. [85] Furthermore, in order to determine the fracture plane, one has to iterate over the fracture angle which results in more computational effort. Fortunately, as reported by van Dongen [6], there are guidelines available for the selection of the inclination parameters of CFRPs and GFRPs which mitigates the former drawback. After Puck and Schurmann [29], Cuntze and Freund [94] developed a failure mode concept for multidirectional laminates. However, the criterion is based on probabilistic curve fitting rather than physical mechanisms which reduces the general applicability of this method. [6] Based on the criterion by Puck and Schurmann [29], state-of-the-art criteria in the form of the LaRC-03, LaRC-04 and LaRC-05 have been developed. The LaRC-03 criterion, developed by Davila et al. [95], showed a number of similarities to the Puck model but also had some drawbacks such as only being applicable to two-dimensional applications. The LaRC-04 criterion, introduced by Pinho et al. [26], addressed several of the shortcomings of the LaRC-03 and extended the criterion to three-dimensions. However, the LaRC-04 criterion requires more computational effort. The last installment in the LaRC criterion series is the LaRC-05 criterion. [50] The criterion is similar to the LaRC-04 criterion, however with some changes with respect to the LaRC-04 criterion, the LaRC-05 criterion achieves improved computational efficiency while keeping good predictive capability. [6]

The mode dependent criteria are preferred above mode independent criteria, as the former is capable of predicting the failure mode and, as shown in literature, provide more accurate results. Van Dongen [6] compared the Hashin, Hashin-Rotem, Cuntze, Puck, LaRC-03, LaRC-04 and LaRC-05 criteria based on experimental data of five tests cases generated by the first Worldwide Failure Exercise [28]. Based on this comparison it was found that the Puck, LaRC-04 and LaRC-05 criteria showed the best performance. These criteria have comparable performance, and without a more thorough comparison with more experimental data, the choice between these three criteria is arbitrary. For the implementation of the Quasi-Static Progressive Continuum Damage Model (QSPCDM) model in this report, the LaRC-05 criterion has been chosen. First of all, the LaRC-05 provides similar accuracy as the LaRC-04 criterion while having a lower computational cost, which favors the LaRC-05 over the LaRC-04 criterion. Secondly, the Puck criterion has already been used in several fatigue models by, amongst others, Eliopoulos [9] and Mitrousias [8], whereas a LaRC-05 implementation in such a model has not been encountered in literature. Therefore, it is of interest to implement the LaRC-05 criterion to illustrate the merit of this criterion for PDA.

The LaRC-05 model distinguishes between Tensile Matrix Failure (MFT), Compressive Matrix Failure (MFC), FFT and FFC. For damage initiation all of these damage modes will be used. In Appendix C.1.1 more information and references are provided concerning the LaRC-05 model.

3.5.2 Cohesive Zone Model (CZM)

The bilinear mixed-mode traction-separation relation formulated by Camanho and Davila [96] is selected for modelling delaminations. The motivations for choosing such a model are:

- The simple formulation of the bilinear traction-separation relation

- The wide use in literature
- This formulation is included in the standard implementation of Abaqus

The discussion regarding the validity of the bilinear traction-separation relation with respect to the underlying physical mechanisms is not in the scope of this research. The motivation is primarily based on the reasonable results obtained in literature with such a formulation. [7, 96, 97] However, the subject of such validity is briefly discussed in Appendix D.2.

A crack has three possible opening modes which are shown in Figure 3.1. With each crack mode different mechanisms are involved. Furthermore, it is possible that the crack experiences combinations of these modes; a situation called mixed-mode. Therefore, for a general purpose application of CZMs, the bilinear traction-separation relation is formulated for mixed-mode.

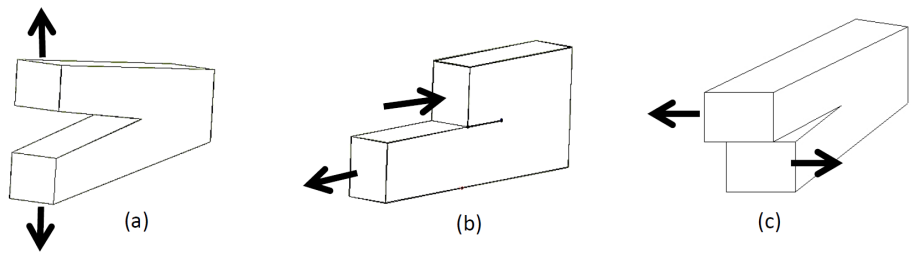

Figure 3.1: Illustration of the mode I, II and III crack opening modes. Copied from Khan [98].

For pure mode decohesion, it is assumed that the traction t_i increases linearly with the relative displacement δ_i until some value δ_i^0 is reached. The constitutive relation in this region is $t_i = k_i\delta_i$, where k_i is the initial stiffness of the cohesive element. Beyond δ_i^0 the material is softened according to a linear relation that is determined from limits on the tractions in the tangential and normal directions and the critical Strain Energy Release Rate (SERR) for the considered mode. The area under the curve is equal to the energy dissipated in the process and is equal to the critical SERR $G_{i,c}$, where i specifies the mode.

In order to account for mixed-mode loading, an equivalent (or total effective) displacement δ_{eq} is used which is a function of the relative displacements for which softening occurs under mixed mode. [96] The mixed-mode behaviour can be decomposed in the mode I, II and III components. However, as stated by Camanho and Davila [96], it is difficult to test for mode III loading. Furthermore, as reported by Pascoe et al. [5] and Blanco Villaverde [99], research in literature is mainly focussed on modes I and II as for the examined loading conditions the mode III component is usually negligible. The mode III contribution in delamination growth is generally small due to the constraint of the adjacent laminae, this has been supported by investigations of Jensen and Sheinman [100] and Glaessgen et al. [101]. Therefore, in case of negligible contribution, the mode III component for delamination growth can be neglected. Another approach, instead of neglecting the contribution, is based on the work of Li [102,103], where the shear mode SERR, $G_s = G_{II} + G_{III}$, is used instead. Li et al. [104] have shown for graphite epoxy laminates that the mode II critical SERR is lower than for mode III. Therefore, the applicability of G_s is questionable and seems to be only valid for the case where $\frac{G_{II}}{G_{III}} << 1$. For the remainder of this report either mode III is neglected or the shear fracture toughness G_s is used; depending on the context. In case mode III cannot be neglected, it is recommended to revisit these assumptions.

In literature, two criteria are often used to describe the interaction between the SERRs of the three modes. The first criterion is the power law criterion introduced by Wu and Reuter Jr. [105]. The power law criterion adapted for the shear mode SERR is shown in Equation 3.23. The other criterion is the Benzeggagh-Kenane (B-K) criterion introduced by Benzeggagh and Kenane [106]. This criterion gives an expression for the equivalent critical SERR; and when the equivalent SERR is larger than the equivalent critical SERR failure occurs. The expression for the equivalent critical SERR by Benzeggagh and Kenane [106] is shown in Equation 3.24.

$$\left(\frac{G_I}{G_{I,c}}\right)^{\alpha} + \left(\frac{G_s}{G_{s,c}}\right)^{\alpha} = 1 \tag{3.23}$$

$$G_{eq,c} = G_{I,c} + (G_{s,c} - G_{I,c}) \left(\frac{G_s}{G_I + G_s}\right)^{\eta} \tag{3.24}$$

Camanho and Davila [96] compared the power law criterion and the B-K criterion with experimental data from Reeder [107]. Based on this comparison, the B-K criterion shows better results for epoxy and thermoplastic composites. As the scope of this report is limited to FRPs, it is decided to select the B-K criterion.

The equivalent displacement, δ_{eq}, is defined by Equations 3.25 and 3.26. Analogous, an equivalent traction t_{eq} is defined as shown in Equations 3.27 and 3.28.

$$\delta_{eq} = \sqrt{\langle \delta_1 \rangle^2 + (\delta_s)^2} \tag{3.25}$$

$$\delta_s = \sqrt{(\delta_2)^2 + (\delta_3)^2} \tag{3.26}$$

$$t_{eq} = \sqrt{(t_1)^2 + (t_s)^2} \tag{3.27}$$

$$t_s = \sqrt{(t_2)^2 + (t_3)^2} \tag{3.28}$$

The subscripts of the tractions and displacements, used in this report, refer to the corresponding mode. For example, t_1 corresponds to mode I crack opening. This is a different notation than previously used for defining stresses and care should be taken to not mix-up the notations. Moreover, the used displacement for mode III, only captures the sliding of mode III. The torsion (rotation) due to the scissoring movement is not captured with the used formulation. However, in light of the assumption that mode III is negligible, this discrepancy is deemed acceptable. A graphical representation of the bilinear mixed-mode softening law is provided in Figure 3.2.

In order to determine damage initiation, a damage onset criterion is required. The damage onset criterion provides a damage initiation locus which dictates the maximum stress before softening occurs. A variety of damage initiation criteria can be used. In literature several authors such as Camanho and Davila [96], Turon et al. [97], Pinho et al. [108] and Amiri-Rad

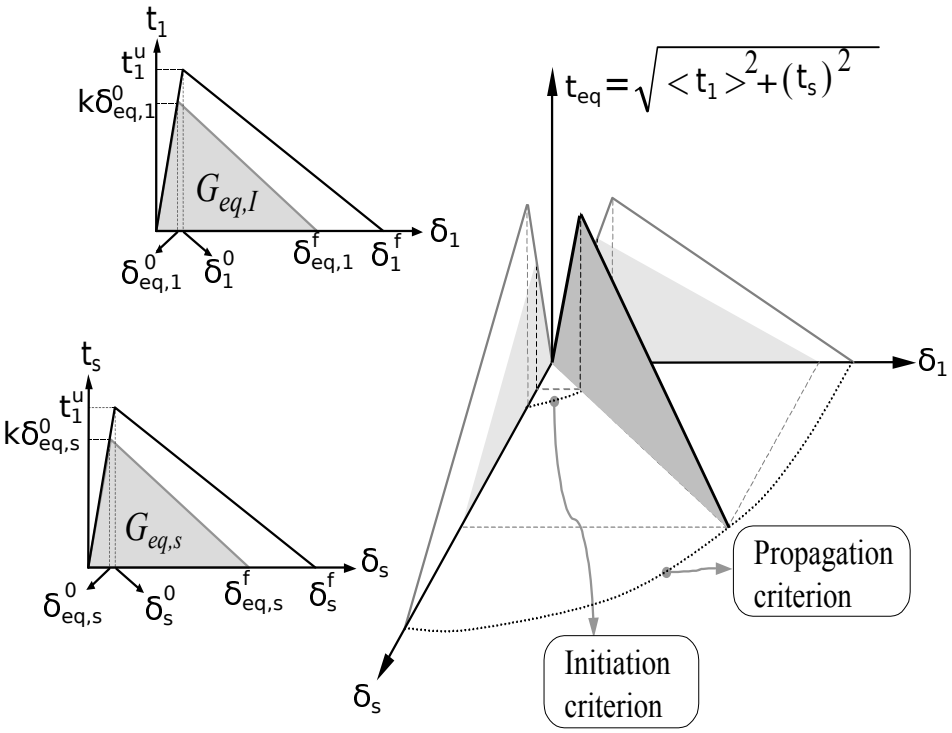

Figure 3.2: Graphical representation of the bilinear mixed-mode softening law. The figure is adapted from Pinho et al. [108].

and Mashayekhi [109] use the quadratic failure criterion. For the present work it is decided to also use the quadratic failure criterion as multiple researchers obtained acceptable results with this criterion. Furthermore, this criterion is already implemented in Abaqus which allows for a straightforward implementation. The quadratic failure criterion is shown in Equation 3.29, where $t_1^u = \sigma_{33}^u$ is the interlaminar normal tensile strength and $t_2^u = \tau_{12}^u$ and $t_3^u = \tau_{13}^u$ the interlaminar shear strengths. Often it is assumed that $t_2^u = t_3^u$.

$$\left(\frac{\langle t_1 \rangle}{t_1^u}\right)^2 + \left(\frac{\langle t_2 \rangle}{t_2^u}\right)^2 + \left(\frac{\langle t_3 \rangle}{t_3^u}\right)^2 = 1 \tag{3.29}$$

The effective relative displacement δ_{eq}^0 at which damage initiation occurs for mixed-mode is given by Equation 3.30, where β is defined by Equation 3.31. [96] For the derivation of this expression, it is assumed that $t_2^u = t_3^u$ and the quadratic failure criterion has been used.

$$\delta_{eq}^0 = \begin{cases} \delta_1^0 \delta_s^0 \sqrt{\frac{1+\beta^2}{(\delta_s^0)^2 + (\beta \delta_1^0)^2}} & \text{if } \delta_1 > 0 \\ \delta_s^0 & \text{if } \delta_1 \leq 0 \end{cases} \tag{3.30}$$

$$\beta = \max\left\{0, \frac{\delta_s}{\delta_1}\right\} \tag{3.31}$$

3.5.3 eXtended Finite Element Method (XFEM)

In order to initiate an XFEM crack, a stress-based criterion is used. Following the same motivation as for the selection of the CDM initiation criterion, the LaRC-05 initiation criterion is selected. For XFEM, only the matrix failure criteria of the LaRC-05 are considered. The governing equations of the LaRC-05 can be found in Appendix C.1.1.

3.6 Damage progression

This section concerns the damage progression part of the QSPDA, indicated as module 3.2 in Figure 2.9. After damage onset has been determined, a damage progression method is used to determine the evolution of the damage. In Section 3.6.1, the damage progression model for the CDM is discussed. Furthermore, in Section 3.6.2 the damage progression for the CZM is discussed. Lastly, the damage progression method for the XFEM-based model is discussed.

3.6.1 Continuum Damage Model (CDM)

In general two damage progression methods for CDM can be distinguished: Sudden Material Degradation Models (SMDMs) and Gradual Material Degradation Models (GMDMs). SMDMs degrade the various properties of the composite materials instantly when damage initiation (failure) occurs. SMDMs have been used by, amongst others, Tserpes et al. [22], Lee [69], Pachajoa et al. [110] and McCarthy et al. [111]. A detailed review of SMDMs is provided by Garnich and Akula [32]. In literature, either a total discount of the element/ply or a degradation with a specified degradation factor is used. The former means that the material properties are reduced to zeros or a value close to zero in order to avoid numerical issues. The latter is applied with only limited justifications. In general, SMDMs are posed without justification other than comparison with limited experimental results. [6]

GMDMs degrade the properties gradually after damage initiation. Most GMDMs employ some sort of softening models to degrade the properties. Note that softening laws do not only apply to GMDMs but also to, for example, CZMs. There are a variety of softening methodologies and an extensive review has been provided by Park and Paulino [112]. Only the bilinear softening model will be discussed further due to its common use in literature, amongst others, by Pinho et al. [50,113], van Dongen [6], Lapczyk and Hurtado [25], van der Meer and Sluys [114] and Zhang et al. [115]. For the bilinear softening model, an equivalent strain or stress is used which takes into account the principal stresses or strains and their interactions. [50,113] One should note that such a definition of an equivalent parameter does not have any physical basis. The bilinear softening model defines the slope between damage initiation and total discount of the material property.

Van Dongen [6] compared three SMDMs (Camanho and Matthews [54], Lee [69] and McCarthy et al. [111]) and two GMDMs (Puck [55] and bilinear softening). Van Dongen [6] determined that the bilinear softening model was the best choice for implementation in FEM. The main advantages of the bilinear softening are that mesh dependency can be alleviated, the results are in decent comparison to the test cases of the WWFE-I (see Kaddour et al. [28]) and the gradual degradation reduces the risk of numerical instabilities. Based on this reasoning, it is

decided to also use the bilinear softening model as Material Degradation Model (MDM) in the QSPCDM. Additional information regarding the bilinear softening damage model can be found in Appendix C.2.

3.6.2 Cohesive Zone Model (CZM)

The damage progression is dictated by the relative failure displacement. A criterion that determines the displacement at which complete decohesion occurs is also referred to as the complete decohesion criterion. Effectively, the complete decohesion criterion predicts the critical SERR for the considered mixed-mode loading. In Figure 3.2, the locus of the propagation criterion is indicated.

The equivalent failure displacement δ_{eq}^{f} for the B-K criterion (see Section 3.5.2) is given by Equation 3.32. [96]

$$\delta_{eq}^{f} = \begin{cases} \frac{2}{k\delta_{eq}^{0}} \left[G_{I,c} + (G_{s,c} - G_{I,c}) \left(\frac{\beta^2}{1+\beta^2} \right)^{\eta} \right] & \text{if } \delta_1 > 0 \\ \sqrt{\left(\delta_2^f\right)^2 + \left(\delta_3^f\right)^2} & \text{if } \delta_1 \leq 0 \end{cases} \tag{3.32}$$

The softening of the cohesive zone is incorporated in the bilinear format as $\tau_i = D_{ij}\delta_j$, where D_{ij} is given by Equation 3.33 and d by Equation 3.34. [96] The Kronecker delta is denoted as $\hat{\delta}_{ij}$. Furthermore, the maximum equivalent displacement δ_{eq}^{max} is given by Equation 3.35.

$$D_{ij} = \begin{cases} \hat{\delta}_{ij} k & \text{if } \delta_{eq}^{max} \leq \delta_{eq}^{0} \\ \hat{\delta}_{ij} \left[(1-d)\, k + k d \hat{\delta}_{i1} \frac{\langle -\delta_1 \rangle}{-\delta_1} \right] & \text{if } \delta_{eq}^{0} < \delta_{eq}^{max} < \delta_{eq}^{f} \\ \hat{\delta_{i1}} \hat{\delta_{1j}} \frac{\langle -\delta_1 \rangle}{-\delta_1} k & \text{if } \delta_{eq}^{max} \geq \delta_{eq}^{f} \end{cases} \tag{3.33}$$

$$d = \frac{\delta_{eq}^{f} \left(\delta_{eq}^{max} - \delta_{eq}^{0} \right)}{\delta_{eq}^{max} \left(\delta_{eq}^{f} - \delta_{eq}^{0} \right)} \tag{3.34}$$

$$\delta_{eq}^{max} = \max \left\{ \delta_{eq}^{max}, \delta_{eq} \right\} \tag{3.35}$$

3.6.3 eXtended Finite Element Method (XFEM)

As discussed in Section 3.5.3, the LaRC-05 criterion is used to evaluate matrix crack initiation. A convenient property of the LaRC-05 criterion is that for matrix failure, the angle of the plane where the failure occurs is also known. However, according to van der Meer et al. [59, 114], matrix cracks are necessarily oriented in the direction of the fibres. This implies that the orientation of the matrix crack may be assumed to be equal to the lamina orientation. On the other, van Oostrum [7] has shown that by using the matrix failure angle from a CDM can results in cracks that closely resemble experiments. Furthermore, the matrix failure angle may still be required for transverse matrix cracks. For the present work, the matrix failure angle obtained by the LaRC-05 is used to dictate the orientation of the initiated crack. However, it

is recommended to further investigate the influence of using the matrix failure angle obtained from a CDM in terms of accuracy.

After crack initiation, an extrinsic CZM is used to model the debonding of the two surfaces being separated by the crack. The XFEM-based implementation in Abaqus allows for a linear and non-linear softening behaviour. It is not clear which behaviour should be preferred for matrix cracking. For the current work the linear softening is selected with the same motivation as for the CZM for delaminations (see Section 3.5.2). See Appendix D.2 for a brief discussion regarding the influence of the shape of CZMs.

Similar to the intrinsic CZM, the surface beneath the traction-separation relation is equal to the critical SERR. In order to determine the equivalent critical SERR under mixed-mode, the same criterion as for the delamination CZM is used: the B-K criterion. However, the critical SERR in this context is for intralaminar fracture instead of interlaminar fracture. There are tests available to determine intralaminar fracture. For mode I, Compact Tension (CT) tests are used. [116, 117] For mode II, modified Iosipescu tests have been used. [118] Furthermore, for mixed-mode, intralaminar fracture tensile tests have been used on specimens with pre-cracked specimens. [119]

Finally, when complete decohesion is reached, the phantom nodes can move independently from the parent nodes. This results in the separation of the cracked element into a real domain and a phantom domain. The displacements in the real domain are then obtained by interpolation based on the nodal degrees of freedom in the phantom domain. In order to achieve the displacement jump due to the crack, the integration is only performed over the area of one side of the real domain. The Abaqus Analysis User's Guide [66] and Song et al. [63] provide a more detailed outline of the procedure.

Chapter 4

Fatigue Progressive Blended Damage Model (FPBDM)

In this chapter, the Quasi-Static Progressive Blended Damage Model (QSPBDM) is extended into the fatigue domain: the influence of fatigue on Fibre-Reinforced Polymers (FRPs) is taken into account. Following the fatigue damage component of the framework shown in Figure 2.12, a distinction is made between pre-failure and post-failure fatigue. For pre-failure fatigue, the material properties are degrading due to the subjection of the material to a repeating alternating load. This alternating loading degrades the material for each cycle that is applied. Post-failure fatigue is concerned with the material degradation due to fatigue after macroscopic damage has been initiated. After macroscopic damage is initiated it may not be accurate to fully discount the material as it may still have residual strength and properties left.

In Section 4.1, the pre-failure fatigue is discussed. The post-failure fatigue is discussed in Section 4.2. Lastly, in Section 4.3 the cycle jumping algorithms for the selected damage models are discussed.

4.1 Pre-failure fatigue

With the term pre-failure fatigue, the fatigue behaviour of undamaged materials is meant (i.e. damage initiation has not yet occurred). This section discusses the pre-failure fatigue models used for the selected Continuum Damage Model (CDM) in Section 4.1.1, Cohesive Zone Model (CZM) in Section 4.1.2 and eXtended Finite Element Method (XFEM) model in Section 4.1.3.

4.1.1 Continuum Damage Model (CDM)

In literature, the topic of CDM-based fatigue models has extensively been reviewed by, amongst others, Wicaksono and Chai [46] and Degrieck and van Paepegem [120]. Three main groups of composite fatigue models can be distinguished: fatigue life, phenomenological and progressive damage models. [46] The progressive fatigue models (Fatigue Progressive

Continuum Damage Models (FPCDMs)) are the state-of-the-art models for predicting the fatigue behaviour of composites and are primarily used in recent literature. [10, 25, 121, 122] Therefore, also the present work will use such an approach. It should be noted that FPCDMs are synergies of different type of models (e.g. different models for residual strengths, failure criteria, assumptions and implementations of the models in Finite Element Analysis (FEA)); therefore, a large range of different FPCDMs can be made with varying properties (e.g. in terms of accuracy for certain materials and required computational resources). However, overall, FPCDMs have the following shortcomings:

- FPCDMs use empirical fitting parameters. The progressive fatigue models rely on the use of Stress-Cycle (SN) curves obtained from experiments. By data fitting for a specified relation, parameters of that relation are determined. The same applies for the residual strength and stiffness models. The models are developed from trends observed from experiments. It should be noted that such an approach has limited physical foundation but still has to be used due to the lack of understanding of fatigue mechanisms in composites
- The progressive fatigue models still suffer from the damage smearing properties of the CDMs when predicting the damage patterns.

The last shortcoming is not deemed an issue for the Fatigue Progressive Blended Damage Model (FPBDM), as Fracture Mechanics Damage Models (FMDMs) are used for the modelling of matrix cracks and delaminations. The first step in determining the influence of fatigue is to find the number of cycles until failure of the material under arbitrary loading. This will be discussed in Section 4.1.1.1. The reduction in strength for an arbitrary load after a certain number of cycles is discussed in Section 4.1.1.2. Lastly, the reduction in stiffness for an arbitrary load after a certain number of cycles is discussed in Section 4.1.1.3.

4.1.1.1 Failure cycle determination

It is of interest to determine when a structure (or in this case a material element) fails due to the subjection of the material to Constant Amplitude (CA) loading. Therefore, a model should be developed to achieve this. For Variable Amplitude (VA) loading, the same approach applies, as the VA spectrum can be converted to a set of CA loads (see Section 2.1.1).

The representation of the number of cycles until failure for a known maximum stress or stress amplitude is done with so-called SN curves. As the maximum stress or stress amplitude does not fully characterise the CA loading, the representation is only valid for certain fixed conditions. For example, a fixed stress-ratio R. In order to obtain an SN curve, experiments are performed for different maximum stresses or stress amplitudes. By fitting a curve to these data points an SN curve is obtained. The SN curve is sensitive to a variety of variables such as the frequency f, material, geometry, load spectrum (e.g. CA or VA), temperature T and the ratio between the minimum and maximum applied stress R. For the present work, the loading type, R-ratio, material and geometry are taken into account. The effect due to the frequency is not in the scope of the current research and is therefore not considered. Furthermore, any effect on the fatigue behaviour due to temperature is disregarded and room temperature is assumed. However, when input data is used, it should be checked whether the temperature

maintains acceptable levels during testing. Imposing a threshold on the temperature, also limits the possible frequencies that can be used during testing, as high frequencies will lead to an increase in temperature. Furthermore, the effect of changing the material is already taken into account in the experimental data (i.e. for the simulation of material A, SN data for material A is used). For the geometry it is assumed that the effect is already taken into account by using a FEA (effect of geometry is captured in the state of the elements). The effect of variable loading is taken into account with the approach discussed in Section 2.1.1 and in the residual strength model discussed in Section 4.1.1.2. Furthermore, the effect of the R-ratio will be discussed in the current section. Moreover, it is assumed, in the present work, that coupon data is representable for material elements in FEA. The validity of this scaling is not in the scope of the present work and it is recommended to look into scaling effects in future research.

Different fitting relations for the S-N curves are developed ranging in complexity. Several of such formulations have been reviewed by Broer [123] and will not be discussed any further. For the present work, the fitting relation shown in Equation 4.1 is used. In the equation, σ_a is the amplitude stress, σ_0 and k are fitting parameters based on experimental data and N is the number of cycles. The choice of such an SN curve formulation does not influence the validity of the discussion in this section. The chosen model only represents the linear part of the SN behaviour (on a log-scale) which is deemed a reasonable representation for high-cycle fatigue loading ($N > 10^4$ [5]) of FRPs. In case a more complex model is required (for example, to capture the threshold effect), only the definition of the SN fitting relation changes and all of the other methods discussed in this section remain unaltered.

$$\sigma_a = \sigma_0 N^{-\frac{1}{k}} \tag{4.1}$$

In general, the stress-state in a structure is non-constant; therefore, the R-ratio varies throughout the structure. When only using SN curves to characterise the fatigue behaviour, a large amount of SN experiments have to be performed for each R-ratio encountered in the structure (or at least a subset of enough R-ratios that lead to accurate results). Also, in the case of VA loading, the R-ratio can change throughout the applied cycles. However, having to do a large amount of SN experiments is expensive and infeasible. Therefore, it is required to interpolate between SN data for a limited amount of R-ratios. The two primary interpolation/extrapolation methods are the master SN curve and the Constant Life Diagram (CLD) approach. Both methods have been reviewed by Broer [123] and from this review it is apparent that only the CLD approach is suitable for the present work.

The CLD procedure allows interpolation between SN curves in the material direction i. From this interpolation, the remaining fatigue life for an arbitrary stress ratio R_i and stress amplitude $\sigma_{a,i}$ can be determined. Graphically, the CLD represents the (σ_a-σ_m) plane which is defined by Equation 4.1. In Figure 4.1, the general format of a CLD is shown. Four regions can be identified in the figure, corresponding to the four cyclic regions: Compression-Compression (C-C), Compression-Tension (C-T), Tension-Compression (T-C) and Tension-Tension (T-T). Note that the value of σ_m is bounded for $\sigma_a = 0$, where $\sigma^u_{i,t}$ corresponds to the upper bound and the $\sigma^u_{i,c}$ to the lower bound.

Consider an arbitrary SN curve z for the strength in material direction i obtained for a prescribed stress ratio $R_i^{(z)}$. This SN curve lies on the line $R_i^{(z)}$ in the $(\sigma_a - \sigma_m)$ plane.

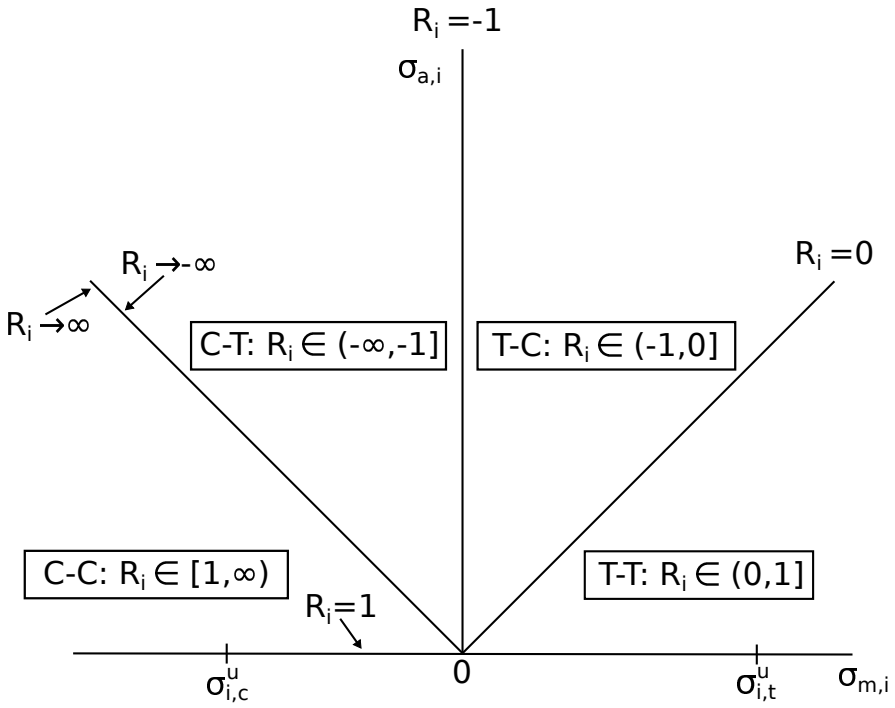

Figure 4.1: General format of a CLD. The four cyclic regions are indicated and bounded by limiting R-ratios.

Hence, each value of $\sigma_{a,i}$ on the line $R_i^{(z)}$ corresponds to a failure cycle N (the variable of the SN curve). When there are more SN curves available, it is possible to interpolate between the points $(\sigma_{a,i} = 0; \sigma_{m,i} = \sigma^u_{i,c})$, $(\sigma_{a,i} = 0; \sigma_{m,i} = \sigma^u_{i,t})$ and the points $P_{i,z}(N) = (\sigma_{a,i} = \sigma_{a,i,z}(N); \sigma_m = \frac{1+R^{(z)}}{1-R^{(z)}}\sigma_{a,i,z}(N))$.

A number of different interpolation schemes are proposed in literature. A possible interpolation scheme is the piecewise linear interpolation used by Philippidis and Vassilopoulos [124]. Consider that three SN curves (a, b and c) are available for three different stress ratios ($R_i^{(a)}$, $R_i^{(b)}$, $R_i^{(c)}$). For a fixed number of cycles one can linearly interpolate between $\sigma^u_{i,c}$, $\sigma^u_{i,t}$, $\sigma_{a,i}(N_{fixed}, R_i^{(a)})$, $\sigma_{a,i}(N_{fixed}, R_i^{(b)})$ and $\sigma_{a,i}(N_{fixed}, R_i^{(c)})$. A CLD with a piecewise linear interpolation for three SN curves is shown schematically in Figure 4.2 for a fixed number of cycles. Such a curve can be created for any number of cycles N_{fixed}, where $N_{fixed} = N_f$ for the loading conditions along that line. The number of cycles until failure N_f for an arbitrary choice of R and σ_a can now be determined. First, the stress amplitude values for a number of cycles are calculated with Equation 4.2, where j indicates the cycle number. The values $\sigma_{a,i}^{(j)}$ are then used for a linear regression in order to derive an SN curve for the prescribed value of R. The fatigue life is then obtained by the intersection of the derived SN curve and the prescribed stress $\sigma_{a,i}$. The advantage of the piecewise linear interpolation method is that it only requires a limited number of SN curves. According to Vassilopoulos et al. [125], the piecewise linear interpolation scheme produces acceptable results when 3 or more SN curves are used.

$$\sigma_{a,i}^{(j)} = \sigma_{a,i}(R, N_j);\ j = 1..J \tag{4.2}$$

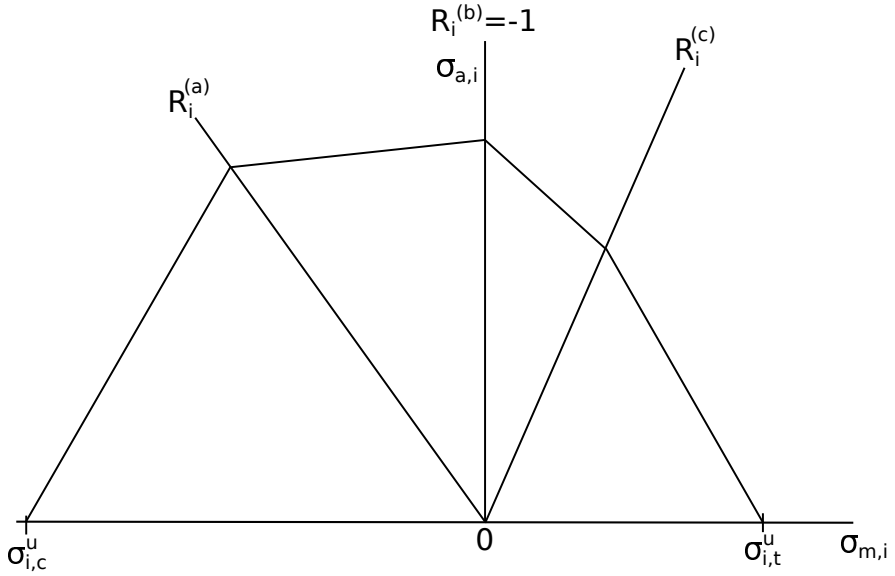

Figure 4.2: A CLD with piecewise linear interpolation. In the figure it is assumed that $R_i^{(b)} = -1$. For $R_i^{(a)}$ and $R_i^{(c)}$ no assumptions are made, except for the region of occurrence.

Next to the linear piecewise interpolation method, there are more interpolation methods available in literature. The simplest model is the linear CLD, where it is assumed that the behaviour in tension and compression is equivalent for the same load amplitude and only a single SN curve is required to derive other SN curves. [125] The non-linear bell-shaped CLD was introduced by Harris [126] and is a semi-empirical model that requires the determination of six fitting parameters. The original CLD of Harris [126] allows constant life lines to intersect. In order to avoid this, Eliopoulos [9] modified the bell-shaped CLD by Harris [126]. Additionally, the modified bell-shaped CLD allows for a semi-empirical expression for the number of cycles instead of having to numerically solve the non-linear equation. [9] Boerstra [127] proposed a multislope model that can construct the CLD with random fatigue data; and hence, does not require the stress ratio R. Boerstra's method requires five parameters that are obtained from the fatigue data by using a multi-objective optimisation procedure. Moreover, Vassilopoulos et al. [125] used the formulation of a piecewise non-linear CLD in conjuction with the model by Kassapoglou [128]. Due to the assumptions of Kassapoglou's [128] model, no fatigue testing is required. However, the validity of this approach has been questioned by various authors. [129, 130] Lastly, parallel to this thesis, Broer [123] worked on a CLD approach that only required a single S-N curve for each material direction. This method shows great potential of reducing the required input. However, for the method by Broer [123] and the other CLD methods discussed previously, the validation in literature is limited.

All of the previous models with the exception of Broer's model, have been compared by Vassilopoulos et al. [125] for three Glass Fibre Reinforced Polymer (GFRP) laminates with varying lay-up. The coefficient of multiple determination was used as a measure for the performance of the models. From the results obtained by Vassilopoulos et al. [125], it was concluded that the piecewise linear CLD provided the most accurate results in case a sufficient amount of S-N curves was used. As an improvement upon the piecewise linear model, Vassilopoulos et al. [131] developed a piecewise non-linear CLD model. The piecewise non-linear CLD model

seems to produce more accurate results than the other discussed models while requiring only a limited amount of SN curves (3 for each material direction). However, in order to draw definitive conclusions, the CLD models have to be validated more thoroughly on larger data sets and preferably for different materials (e.g. GFRPs and Carbon Fibre Reinforced Polymers (CFRPs)). Only then, a reliable conclusion can be drawn regarding which method provides the best interpolation scheme. Doing so is not in the scope of the current work. Due to the lack of such data sets and a more thorough review in literature, a CLD model is chosen based on the work of Vassilopoulos et al. [125, 131]. It has been decided to implement the piecewise non-linear CLD in the FPCDM.

The piecewise non-linear CLD model requires SN curves for $R = -1$, $R = \pm\infty$ and $R = 0$. However, in practice, most of the data is for $R = 0.1$ instead of $R = 0$ and $R = 10$ instead of $R = \pm\infty$. According to Vassilopoulos et al. [131] this is allowed as the model still produces a sufficiently accurate model, however, the definition of the coefficients in the method have to be altered. The piecewise non-linear CLD model for known SN curves for $R = -1$, $R = 0.1$ and $R = 10$ are given by Equations 4.3 to 4.12. [9]

$$\sigma_{a,i}^{(R_i)} = (1 - R_i)\left(\frac{A_1}{R_i} + \frac{B_1}{R_i^2}\right) \qquad R_i \in (-\infty, -1] \tag{4.3}$$

$$\sigma_{a,i}^{(R_i)} = \frac{1 - R_i}{A_2 R_i + B_2} \qquad R_i \in (-1, 0] \tag{4.4}$$

$$\sigma_{a,i}^{(R_i)} = \frac{1 - R_i}{A_2 R_i + B_2} \qquad R_i \in (0, 1] \tag{4.5}$$

$$\sigma_{a,i}^{(R_i)} = (1 - R_i)\left(\frac{A_4}{R_i} + \frac{B_4}{R_i^2}\right) \qquad R_i \in (1, +\infty) \tag{4.6}$$

$$A_1 = A_4 = \frac{0.045 \cdot UCS - \sigma_{a,i}^{(R_i^{(c)})}}{0.81} \tag{4.7}$$

$$B_2 = B_3 = \frac{0.9 - \frac{2\sigma_{a,i}^{(R_i^{(c)})} \cdot 10^{-3}}{\sigma_{i,t}^{u}}}{0.999 \cdot \sigma_{a,i}^{(R_i^{(a)})}} \tag{4.8}$$

$$B_1 = \frac{\sigma_{a,i}^{(R_i^{(b)})}}{2} + A_1 \tag{4.9}$$

$$B_4 = -\frac{\sigma_{i,c}^{u}}{2} - A_1 \tag{4.10}$$

$$A_2 = B_2 - \frac{2}{\sigma_{a,i}^{(R_i^{(b)})}} \tag{4.11}$$

$$A_3 = \frac{2}{\sigma_{i,t}^{u}} - B_2 \tag{4.12}$$

An example of the piecewise non-linear CLD is given in Figure 4.3. The CLD corresponds to a 0° UniDirectional (UD) PPG2002/Prime-20 GFRP laminate under longitudinal fatigue loading.

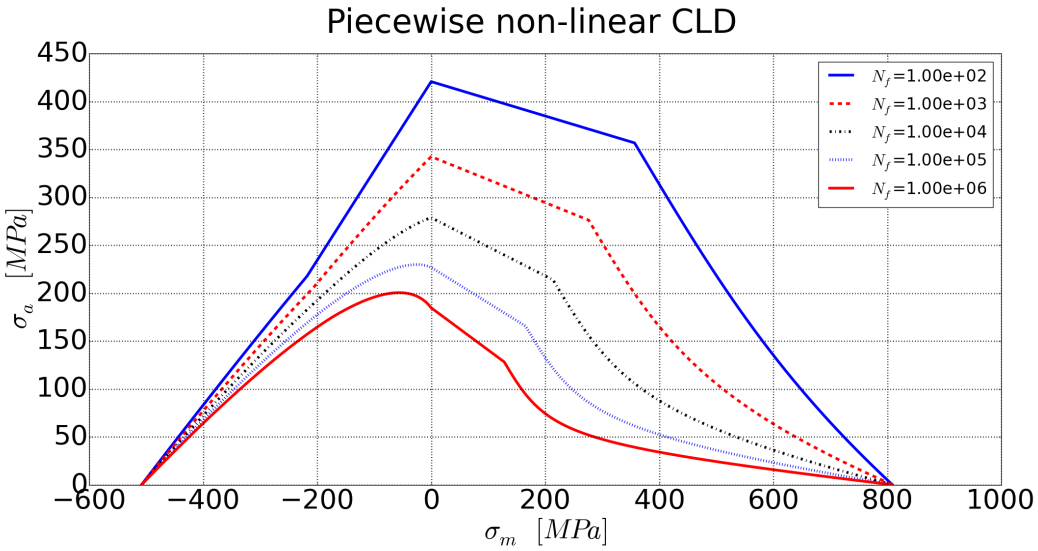

Figure 4.3: The piecewise non-linear CLD for the PPG2002/Prime-20 FRP material in the 0° direction, for a number of failure cycles. The required SN data is obtained from the Optidat database [132].

4.1.1.2 Residual strength

In literature, various residual strength models can be found. Extensive reviews regarding this subject are provided, amongst others, by Post et al. [133, 134] and Passipoularidis and Philippidis [135,136]. A wide range of residual strength models can be described by the general relation given in Equation 4.13. [137] This results in the expression for the residual strength S_r given by Equation 4.14. In case $A = 0$ and $C >> 1$, a sudden death type of behaviour is obtained; and in case of $A = 0$ and $C < -1$, there is a rapid initial loss of strength. [138] Moreover, in case of variable amplitude loading, the relation given in Equation 4.14 is of the form shown in Equation 4.15, where $N_{eq,i-1}$ is given by Equation 4.16. [133] Note that for VA loading it is assumed that the residual strength remains constant during the transition from a load step to the next load step.

$$\frac{dS_r(N)}{dN} = -B\frac{CN^{C-1}}{AS_r(N)^{A-1}} \tag{4.13}$$

$$S_r(N,S)^A = S_u^A - \left(S_u^A - S^A\right)\left(\frac{N}{N_f}\right)^C \tag{4.14}$$

$$S_{r,i} = \left[S_u^{A_i} - \left(S_u^{A_i} - S_i^{A_i}\right)\left(\frac{N_i + N_{eq,i-1}}{N_{f,i}}\right)^{C_i}\right]^{\frac{1}{A_i}} \tag{4.15}$$

$$N_{eq,i-1} = N_{f,i}\left[\frac{S_u^{A_i} - S_{r,i-1}^{A_i}}{S_u^{A_i} - S_i^{A_i}}\right]^{\frac{1}{C_i}} \tag{4.16}$$

Following the results of the review by Passipoularidis and Philippidis [136], there is no model that produces consistently better results than other models for varying fatigue cases (e.g. different materials). Therefore, it is decided to choose the relatively simple Broutman-Sahu residual strength relation. The main advantage of the Broutman-Sahu relation is that no additional fitting parameters are required which limits the amount of required input data. The Broutman-Sahu relation is a special case of the general relation by Sarkani et al. [137] given in Equation 4.13. The Broutman-Sahu relation is obtained from Equation 4.14 when $A = C = 1$. In general, it is expected that C_i is not constant for all spectrum cycles i as for each cycle the stress-state can be different. [139] If the FPCDM is used for general applications, it is not realistic to determine the term C_i for each possible cycle loading i. Since there is no analytical expression for C_i available in literature, it is decided to set $C_i = 1$ for all i.

4.1.1.3 Residual stiffness

From experiments it has been observed that the stiffness of a composite material reduces when subjected to cyclic loading. [140–142] Literature reviews regarding phenomenological residual stiffness fatigue models are provided by Wicaksono and Chai [46], Degrieck and van Paepegem [120] and van Paepegem [143]. All of the residual stiffness models, found in literature, depend on a stiffness related parameter and the use of fitting parameters to describe the stiffness reduction as a function of the number of cycles. The fitting parameters are influenced by a number of lay-up dependent factors such as geometry and lay-up (Shirazi and Varvani-Farahani [144]), thickness of the individual layers (Soutis and Kashtaylan [145]) and load conditions (Wicaksono and Chai [46]). Therefore, in order to properly determine the fitting parameters, experiments have to be performed which simulate the same stress-state as the real structure.

In literature, no thorough comparison between the various residual stiffness models has been found. Therefore, it is not possible to select a model based on known performance. For the present work, the model by Eliopoulos [9] is used to account for the stiffness degradation. However, it is recommended for future research to attempt a more thorough comparison between the different residual stiffness models on more diverse data sets. The residual stiffness fit is given in Equation 4.17, where E_r is the residual stiffness, E_s the initial stiffness, c_i and d_i are constants determined from experimental data and i indicates the plane/direction of the property.

$$E_{r,i}(N) = E_{s,i}\left[1 - (1 - c_i)\left(\frac{N}{N_{f,i}}\right)^{d_i}\right] \tag{4.17}$$

4.1.2 Cohesive Zone Model (CZM)

This section is concerned with the implementation of fatigue damage for the CZM. A fatigue threshold behaviour is observed in experiments; therefore, fatigue damage does not always initiate in the cohesive zone. The fatigue initiation for the CZM is discussed in Section 4.1.2.1. After fatigue damage has initiated, the fatigue damage has to be applied to the CZM. This is discussed in Section 4.1.2.2.

4.1.2.1 Fatigue initiation

The crack growth rate for delaminations in FRPs shows correlation with the Strain Energy Release Rate (SERR). Furthermore, in general, the crack growth rate behaviour can be subdivided into three regions.

1. A threshold region for which effectively there is no crack growth (the crack growth rate is close to zero)
2. A region where the crack growth rate increases gradually. The behaviour of this region is dictated by a so-called Paris relation which will be discussed in Section 4.1.2.2
3. A region for which the rate of crack growth rapidly increases for a small increase in SERR (or another fracture mechanics parameter).

In the third region, the crack grows so fast that in a few cycles the crack effectively leads to failure. This region is often not considered and failure is assumed at the onset of this region. The onset is determined with the equivalent critical SERR. Note that the term equivalent is used to also account for mode mixity. This section will discuss the threshold region. Most of literature considers CFRPs when discussing the fatigue crack growth rate threshold behaviour; therefore, the discussion in the remainder of this section is limited to CFRPs.

The threshold region is determined with a certain equivalent threshold SERR which is obtained experimentally. This equivalent threshold SERR corresponds to the SERR for which no crack growth is observed for an arbitrary number of fatigue cycles. In order to determine this value, an infinite number of fatigue cycles have to be tested for which no crack growth is allowed to occur. Obviously, in practice this is not possible; therefore, the threshold is determined by considering no crack growth rate for a large number of cycles or if the crack growth rate remains below a certain value. In literature, no consistent definitions are used. For example, Asp et al. [146] determines the threshold value by observing no crack growth rate for $1.8 \cdot 10^6$ cycles. However, Zhang et al. [147] uses the threshold criteria that the crack growth rate should stay below $1 \cdot 10^{-7}$ N/mm for $5 \cdot 10^5 - 1 \cdot 10^6$ cycles. Therefore, the validity of a threshold criterion, based on experimental data, depends on a case-by-case basis as there is no consistent definition of the threshold. The dimensions, maximum number of fatigue cycles and the effect of a crack in the structure have to be considered to determine whether the experimental data can be used.

The threshold SERR is different for different modes; therefore, mode mixity has to be taken into account. [146–148] In order to do so, often a B-K type of relation is used as is shown in Equation 4.18.

$$\Delta G_{eq,th} = \Delta G_{I,th} + (\Delta G_{s,th} - \Delta G_{I,th}) \left(\frac{G_s}{G_I + G_s} \right)^{\eta} \tag{4.18}$$

The fitting parameter η is different from the one in Equation 3.24 as the relation between the threshold SERRs is generally different from the relation between the critical SERRs. [146]

For the CZM, fatigue damage will be initiated if the condition in Equation 4.19 is satisfied, where $\Delta G_{eq,th}$ is calculated with Equation 4.18.

$$\Delta G_{eq} > \Delta G_{eq,th} \tag{4.19}$$

There are several shortcomings related to this approach.

1. Additional experimental data is required
2. The lay-up of the laminae of the considered interface may influence the results
3. The initiation criterion relies on the used definitions of 'no crack growth' and 'large number of cycles' which is not consistently defined in literature
4. The method is a purely empirical relation without consideration of the underlying physical mechanisms.

The second shortcoming is because most of the experimental data in literature is obtained for small off-axis interfaces. However, when other interfaces are considered, the threshold SERR and the behaviour due to mode mixity may change. Therefore, it either has to be assumed that this effect is negligible or experimental data has to be generated for different interface orientations.

Despite the shortcomings, the initiation criterion discussed in this section is deemed the only feasible approach to account for threshold crack growth. Furthermore, such an approach has as advantage that new delamination fronts can be initiated without the need for pre-existing delaminations.

4.1.2.2 Cohesive zone fatigue progression

In literature various fatigue models for CZMs have been proposed. However, such models are not fit for the current framework. Providing a review of the available models in literature is not deemed a primary objective of the thesis, however a brief overview with references and discussion is provided in Appendix D.3. The fatigue models for CZMs in literature are not applicable for the proposed framework due to one or more of the following reasons.

- Parameters are used that are not directly linked to the damage rate. These parameters have to be determined iteratively by comparing simulations to experiments, effectively tuning the model manually on a case-by-case basis. This undermines the purpose of a general high-fidelity tool
- The model is formulated within the load envelope framework as discussed in Section 2.2.3.3. As the current framework uses a disjoint implementation such formulations cannot be used directly.

Clearly, models that use parameters that are not directly linked to the damage rate are not fit for implementation in the framework, as they undermine the purpose of a general high-fidelity tool. Furthermore, the load envelope approach models are not suitable for implementation in the framework because:

- The models directly influence the damage parameter of the CZM. For a disjoint implementation, such an approach can only be implemented with a user-defined element that loads the fatigue damage parameter portion at the start of each FEA. This increases the implementation difficulty and computational effort and decreases the universality of the used model
- The load envelope approach aims to keep the failure displacement equal to the displacement under maximum static load and to incorporate the fatigue to only decrease the maximum strength t_{eq}^0. [149] For a disjoint implementation, this is not applicable as the load is not fixed at its maximum.

In light of the previous, a CZM is proposed that enforces energy conservation and allows for subsequent quasi-static FEAs. Ideally, after ΔN cycles are skipped, the CZM retains the bilinear formulation but the shape is altered to capture the fatigue effect on the delamination. In order to achieve this, the growth of the delamination due to static and fatigue loading is treated as the creation of a fracture surface. In case the element is not damaged, the energy that is required to fully separate the element with area A is given by Equation 4.20. Note that this energy is mode dependent, as the critical SERR depends on the mode mixity.

$$E_{eq,c} = G_{eq,c}A \tag{4.20}$$

It is assumed that when an area is damaged, the SERR remains constant. Hence, the remaining energy is given by Equation 4.21, where A^* is the damaged area.

$$E_{eq,c}^* = G_{eq,c}(A - A^*) \tag{4.21}$$

Combining Equations 4.20 and 4.21 leads to the relation shown in Equation 4.22, where d_A is the damage parameter defined in terms of area.

$$\frac{E_{eq,c}^*}{E_{eq,c}} = 1 - \frac{A^*}{A} = 1 - d_A \tag{4.22}$$

Unfortunately, energy cannot be used directly in the CZM formulation and instead an energy density (the SERR) is required. The CZM formulation does not physically model the creation of a fracture surface, but uses the traction-separation relation instead. Therefore, in order to capture the release of energy due to the creation of fracture surfaces, an equivalence approach is used. The remaining energy that can be released, E^*, is spread over the initial area A. Physically, this does not have any meaning, however this allows to account for energy dissipation in the CZM formulation. The relation between the damaged equivalent critical SERR, $G_{eq,c}^*$, and the corresponding remaining energy $E_{eq,c}^*$ is given in Equation 4.23.

$$E_{eq,c}^* = G_{eq,c}^*A \tag{4.23}$$

Effectively, it is assumed that the creation of fracture surface can be captured in the CZM formulation by reducing the effective SERR with the expression given in Equation 4.24. The advantage of this method is that it is guaranteed that no more energy can dissipate due to

static and fatigue loading. Nonetheless, the physical connection between the energy and the fracture area is lost. However, this is unavoidable due to the formulation of the CZM.

$$G^*_{eq,c} = G_{eq,c}\,(1 - d_A) \tag{4.24}$$

After every ΔN cycles, an FEA is performed. To account for the fatigue damage during the cycles, the pristine parameters t^0_{eq}, k and δ^f_{eq} have to be altered. In order to obtain the parameters corresponding to the damage state, at least two requirements have to be specified. The first requirement follows from the definition of the CZM that the area under the traction-separation relation has to be equal to the critical SERR. For the damage state, this is the $G^*_{eq,c}$ defined by Equation 4.24. The second requirement is based on the assumption that the failure traction δ^f_{eq} is independent of fatigue damage. The traction at failure is then only dependent on the mode mixity. By using geometry and the bilinear CZM formulation the traction-separation parameters for the damaged state are provided by Equations 4.25, 4.26 and 4.27.

$$t^{0^*}_{eq} = \frac{2G^*_{eq,c}}{\delta^{f^*}_{eq}} \tag{4.25}$$

$$\delta^{0^*}_{eq} = \delta^0_{eq} + \frac{t^0_{eq} - t^{0^*}_{eq}}{t^0_{eq}} \left(\delta^f_{eq} - \delta^0_{eq}\right) + \delta^0_{eq} \tag{4.26}$$

$$k^* = \frac{t^{0^*}_{eq}}{\delta^{0^*}_{eq}} \tag{4.27}$$

In general, the damaged area A^* can be caused by static as well as fatigue loading. For static loading the increase in damaged area is determined by the decrease in SERR. Considering the standard Abaqus CZM implementation, the static damage parameter can be obtained from the FEA outputs. Based on the traction-separation parameters of the previous analysis, the dissipated energy due to the quasi-static loading can be found. By using the relation given in Equation 4.28, the damaged area can be calculated. The subscript 'old' refers to the value prior to the FEA and the subscript 'new' refers to the value after the FEA.

$$A^{new^*} = A\left(1 - \frac{G^{new^*}_{eq,c}}{G^{old^*}_{eq,c}}\left(1 - \frac{A^{old^*}}{A}\right)\right) \tag{4.28}$$

To determine the increase in damaged area A^* due to fatigue, a Paris-like relation is used. The Paris-like relation predicts the crack growth rate $\frac{da}{dN}$ as a function of some fracture parameter. When using such a Paris-like relation to obtain the crack growth rate, the required fracture parameter(s) are obtained from the FEA. Often the SERR range ΔG is used. A common definition of ΔG, found in literature, is given by Equation 4.29.

$$\Delta G = G_{max} - G_{min} \tag{4.29}$$

However, as argued by Rans et al. [150], the use of the definition in Equation 4.29 is incorrect. Instead, the definition of ΔG provided in Equation 4.30 should be used, as this definition is

derived from the same basis for similitude as used in metals. [150] In practice, only a small difference is observed between the definitions as the ratio of $\frac{G_{min}}{G_{max}}$ is proportional to R^2. [5] Hence, for the common R-ratio of 0.1, G_{max} is almost equal to ΔG for both definitions. However, for larger R-ratios this does not hold. Therefore, the definition in Equation 4.30 is used.

$$\Delta G = (\sqrt{G_{max}} - \sqrt{G_{min}})^2 \tag{4.30}$$

Another shortcoming of most Paris-like relations is the use of only one fracture parameter. By using one parameter, it is not possible to sufficiently describe a load cycle. As argued by Pascoe et al. [151] this is the reason why an R-ratio effect is observed: "..the so-called R-ratio effect is really only a reflection of the inadequacy of using only G_{max} or ΔG to describe the load cycle". Therefore, the Paris-like relation should be a function of two fracture parameters that can describe the load cycle uniquely. For example, ΔG and G_{mean}.

The Paris-like relation developed by Blanco et al. [152] is commonly used for recently developed CZMs such as by Harper and Hallett [153], Kawashita and Hallett [16], Bak et al. [81] and Amiri-Rad and Mashayekhi [109]. The model by Blanco et al. [152] is a mixed-mode crack growth rate relation for delaminations based on the Paris relation format. Blanco et al. [152] argued that, based on experimental data, the mode mix dependence is non-monotonic and that therefore parabolic equations should be used to model the propagation parameters of the Paris-like relation. The model of Blanco et al. [152] is provided in Equations 4.31 to 4.33. Note that for the equations, the original format proposed by Blanco et al. [152] is used; and therefore, the shear mode (as discussed in Section 3.5.2) has not been used.

$$\frac{da}{dN} = C(\frac{\Delta G}{G_c})^r \tag{4.31}$$

$$\log(C) = \log(C_I) + \log(C_m)\left[\frac{G_{II}}{G}\right] + \log\left(\frac{C_{II}}{C_I C_m}\right)\left[\frac{G_{II}}{G}\right]^2 \tag{4.32}$$

$$r = r_I + r_m\left[\frac{G_{II}}{G}\right] + (r_{II} - r_I - r_m)\left[\frac{G_{II}}{G}\right]^2 \tag{4.33}$$

The coefficients C_I, C_{II} and C_m are determined by Equation 4.34 for pure mode I, mode II and mixed-mode respectively, indicated with index i. The coefficients c_1, c_2 and c_3 are fitting parameters.

$$\log(C_i) = c_1 + c_2\left(\frac{G_{II}}{G}\right) + c_3\left(\frac{G_{II}}{G}\right)^2 \tag{4.34}$$

The coefficients r_I, r_{II} and r_m are obtained in an analogous manner from Equation 4.35, where r_1, r_2 and r_3 are fitting parameters.

$$r_i = r_1 + r_2\left(\frac{G_{II}}{G}\right) + r_3\left(\frac{G_{II}}{G}\right)^2 \tag{4.35}$$

Lastly, the critical SERR is also a function of the mode mixity and is obtained by curve fitting Equation 4.36, where g_1, g_2 and g_3 are fitting parameters.

$$G_c = g_1 + g_2 \left(\frac{G_{II}}{G}\right) + g_3 \left(\frac{G_{II}}{G}\right)^2 \tag{4.36}$$

There are a few remarks regarding the model by Blanco et al. [152]. First of all, the model contains the earlier discussed fallacy of $\frac{da}{dN} = f(\Delta G, \psi)$, where ψ is the mode mixity. This form cannot describe the full load cycle; and should therefore, contain an additional parameter. For example, $\frac{da}{dN} = f(\Delta G, G_m, \psi)$. Furthermore, the data used by Blanco et al. [152] contains significant scatter. As shown by Burger [154], the scatter may partly be responsible for the observed non-monotonic behaviour. The determination of the fitting parameters for such scatter introduce non-monotonic behaviour. Zhang et al. [147] compare the model by Blanco et al. [152] with other experimental data, however only four datapoints are used to illustrate the fit and no scatter bands are provided. Therefore, the same considerations as discussed before apply. Lastly, in order to apply such a model, at least 21 tests have to be performed. The number of tests will even be larger, in order to increase the confidence of the obtained fitting parameters. This is a costly undertaking; therefore, the use of the model by Blanco et al. [152] may not be appropriate. This emphasises the need for a different approach than the empirical methodology of Paris-like relations. However, as Bak et al. [81] put it: "..currently there are no alternatives to challenge Paris-like models on the capability of representing fatigue crack growth observations". Therefore, due to the lack of better models, a Paris-like relation has to be used in order to account for delamination growth due to fatigue.

The Paris-like relation describes the crack length rate. In order to use this relation for the CZM discussed earlier in this section, the crack length has to be converted to an area. In order to relate the crack growth rate to an area, analytical expressions can be derived that relate the crack length and crack orientation to the damaged element area. However, easier approaches may be employed. The first method uses a characteristic element length and multiplies this length with the crack growth rate in order to obtain a measure of area growth rate. Another method is to determine the maximum crack length that the element will experience for a constant crack orientation; and normalise the area of the element with this length. Hence, when the crack has fully progressed through the element, all of the area has been damaged. Both methods require a relative fine mesh and do not direct represent the physical mechanisms at a local level. Another method would be to use user-defined element formulations where the delamination orientations and damaged area are tracked. This would allow for changing delamination orientations within an element but will result in an increase in implementation difficulty. Whether such an approach will result in an increase or decrease in computational effort is not known as the model could support a coarser mesh but would require more computational exhaustive elements. Moreover, the use of the area instead of crack length is expected to only have an influence locally and not globally. Therefore, it is not known whether the additional effort required to use the fracture area pays-off. If not, the crack length could be used and multiplied with the element width/length in order to obtain a measure of area. In any case, this thesis does not consider the assessment and validation of the fatigue model; therefore, the choice of the model to relate the crack length to the area is left for future research. Therefore, from this point on it is assumed that A^* is known.

The proposed fatigue CZM for the disjoint framework is as follows:

1. Initiate the FEA model with pristine traction-separation parameters
2. Evaluate the FEA for quasi-static loading. In case of damage during the quasi-static loading, calculate the increase in damaged area with Equation 4.28
3. For an arbitrary ΔN (determined with the cycle jump algorithm discussed in Sections 2.3.5 and 4.3), predict the increase in damaged area by using a Paris-like relation. Furthermore, the remaining SERR, $G^*_{eq,c}$, is calculated with Equation 4.24
4. Update the traction-separation parameters with Equations 4.25, 4.26 and 4.27.

The approach discussed in this section aims to incorporate the effect of static and fatigue damage for the CZM. However, this approach introduces some strong assumptions. In order to evaluate the validity of these assumptions and of the model as a whole, simulations have to be compared to experiments. This has not be done in the present work; therefore, this approach should be taken with a critical note. It is recommended for future research to assess the validity of this approach.

4.1.3 eXtended Finite Element Method (XFEM)

Before matrix damage has initiated, XFEM is not used. However, the material will degrade due to fatigue loading even before damage has initiated. Therefore, in order to account for the degradation of the material before damage initiation, the FPCDM approach, as discussed in Section 4.1.1, is used. Whereas the CDM primarily considers fibre failure, the CDM will also consider matrix failure for pre-failure fatigue. This means that SN data for all three material directions (0°, 45° and 90°) is required as input.

4.2 Post-failure fatigue

After damage has been initiated, post-failure fatigue has to be taken into account. The model to do so for the CDM is discussed in Section 4.2.1, for the CZM in Section 4.2.2 and for XFEM in Section 4.2.3.

4.2.1 Continuum Damage Model (CDM)

Often a sudden degradation model is used after damage has initiated such as by Eliopoulos [9], Nikishkov et al [10] and Lian and Yao [121]. Several researchers have reported degradation factors to degrade the material properties based on the failure mode. In Table 4.1, several discounting factors for Sudden Material Degradation Models (SMDMs) are provided.

Based on the values of Table 4.1, it seems that there is not a consensus in literature regarding the properties to decrease for a certain failure mode and to what extent these properties should be degraded. Gradual Material Degradation Models (GMDMs) for fatigue loading has not been encountered in literature. However, the bilinear softening approach used for the Quasi-Static Progressive Continuum Damage Model (QSPCDM) described in Chapter 3 has shown to provide better results than SMDMs for quasi-static loading. Therefore, it is worth

Table 4.1: Sudden degradation models by several researchers. 1) FFT = tensile fibre failure; 2) FFC = compressive fibre failure; 3) MFT = tensile matrix failure; and 4) MFC = compressive matrix failure.

Model	Failure mode	Properties to zero	Other
Eliopoulos [9]	FF	E_{11}, E_{22} and G_{12}	
	MFT and MFC	E_{22} and G_{12}	
Lian and Yao [121]	FF	E_{11}, E_{22}, E_{33}, G_{12}, G_{13} G_{23}, ν_{12}, ν_{13} and ν_{23}	
	MF	E_{22}, G_{12} and G_{23}	
Chang and Chang [21]	FFT	E_{22}, G_{12} and G_{23}	
	FFC	E_{11}, E_{22}, E_{33}, G_{12}, G_{13} G_{23}, ν_{12}, ν_{13} and ν_{23}	
	MFT	E_{22} and ν_{12}	
	MFC	E_{22} and ν_{12}	
Camanho and Matthews [54]	FFT		$0.07 \cdot E_{11}$
	FFC		$0.14 \cdot E_{11}$
	MFT		$0.2 \cdot E_{22}$, $0.2 \cdot G_{12}$ and $0.2 \cdot G_{23}$
	MFC		$0.2 \cdot E_{22}$, $0.2 \cdot G_{12}$ and $0.4 \cdot G_{23}$

considering whether an analogy can be drawn from the quasi-static to the fatigue methodology. The main motivations to use such a model were the numerical considerations for gradually decreasing the properties of the material and the documented indication of obtaining better results with such methods than SMDMs. The property of the bilinear softening approach that can be used in the fatigue domain is the gradual degradation of material properties that are not related to the initial failure mode of the material. Both the SMDM and GMDM approach show a lack of physical basis and there is no definitive proof which method provides a better result when applied to fatigue. Therefore, the choice of a method seems arbitrary and the GMDM approach is chosen, based on the performance for quasi-static loading. However, it is left for future work to evaluate whether such an approach has more merit in terms of accuracy than SMDMs for fatigue loading.

It is proposed to use a bilinear softening approach to account for static as well as fatigue damage. The bilinear softening model uses a damage parameter consisting of a static (d^s) and fatigue (d^f) component, as is shown in Equation 4.37.

$$d^{tot} = d^s + d^f \tag{4.37}$$

Assuming linear damage accumulation, the total damage parameter can be described as shown in Equation 4.38, where N is the number of cycles, N_f the number of cycles until failure and j indicates the type of damage (fibre, matrix or shear). Note that the static damage parameter for shear, d^s_s, is equal to $1-(1-d^s_f)(1-d^s_m)$. The value of d^{tot}_j is used to degrade the mechanical properties for the next quasi-static analysis, as is shown in Equation 4.39. The out-of-plane

properties are only degraded by the static damage parameter as out-of-plane fatigue is not considered. It is expected that (except for out-of-plane loading) the degradation of the out-of-plane properties is limited. Moreover, when delaminations occur, the properties will degrade as stipulated in Section 4.1.2.

$$d_j^{tot} = d_j^s + \frac{N_j}{N_{f,j}} \tag{4.38}$$

$$E_{11} = E_{11}\left(1 - d_f^{tot}\right) \tag{4.39}$$
$$E_{22} = E_{22}\left(1 - d_m^{tot}\right) \tag{4.40}$$
$$E_{33} = E_{33} \tag{4.41}$$
$$G_{12} = G_{12}\left(1 - d_s^{tot}\right) \tag{4.42}$$
$$\nu_{12} = \nu_{12}\left(1 - d_f^{tot}\right) \tag{4.43}$$
$$\nu_{13} = \nu_{13}\left(1 - d_f^{tot}\right) \tag{4.44}$$
$$\nu_{21} = \nu_{21}\left(1 - d_m^{tot}\right) \tag{4.45}$$
$$\nu_{23} = \nu_{23}\left(1 - d_m^{tot}\right) \tag{4.46}$$
$$\nu_{31} = \nu_{31} \tag{4.47}$$
$$\nu_{32} = \nu_{32} \tag{4.48}$$

In order to avoid numerical issues due to severe discontinuities between the mechanical properties throughout the material, a limitation is imposed on the minimum value that the properties can have. This limitation is given by Equation 4.49, where α is a specified factor, η is an arbitrary material property specified in Equation 4.39 and η_i is the initial value of the said property.

$$\eta = \begin{cases} \eta & \text{if } \eta \geq \alpha\eta_i \\ \alpha\eta_i & \text{if } \eta < \alpha\eta_i \end{cases} \tag{4.49}$$

The bilinear softening approach discussed in this section is only activated after failure has been initiated. Furthermore, the CDM only concerns fibre failure; and therefore, once matrix failure has initiated, this approach is not used. It may also occur that fibre failure is initiated first. This leads to the bilinear softening approach. However, after a new quasi-static FEA, it may occur that the criterion for matrix failure is satisfied. This will enable the XFEM procedure and the bilinear softening approach for fatigue will be disabled. It is expected that such an approach will provide compatibility between XFEM and the CDM approach. However, the performance of this method has to be evaluated in future work.

4.2.2 Cohesive Zone Model (CZM)

For the CZM, no distinction is made between pre-failure and post-failure fatigue. The procedure discussed in Section 4.1.2 applies for both cases.

4.2.3 eXtended Finite Element Method (XFEM)

For XFEM, the same methodology as discussed for the CZM in Section 4.1.2 is considered. The only difference is that an extrinsic formulation is used instead of an intrinsic. However, the methodology to relate the change in traction-separation parameters due to the creation of a fracture surface remains the same.

An issue with XFEM that has to be solved is the crack progression to other elements during the skipped cycles ΔN. There are several possibilities to solve this issue. First of all, a restriction can be posed on the skipped cycles ΔN that limits the magnitude of ΔN to the number of cycles for which an XFEM element will fail. However, this may lead to a significant increase in computational effort as for each small crack increase an FEA must be performed.

Another approach is to assume that if an XFEM element fails, the crack will continue in the same direction and orientation. Hence, it is known which element will fail next to continue the crack path. To account for continued crack growth after a new element has failed, the extrinsic CZM has to be considered outside of the FEA and continue the fatigue damage by using the approach discussed in Section 4.1.2. Then, when a new FEA is performed, the elements have to be updated. This means manually enabling the XFEM and updating the extrinsic CZMs of these elements. The main assumption and issue for such approach has already been discussed in Section 2.3.5. Namely, the state of the elements (e.g. in terms of stress) is assumed to remain constant and equal to the state obtained from the previous FEA. Obviously, when the damage progresses, the load will be redistributed and the state changes. Furthermore, in order to account for the fatigue damage, the mixed-mode SERR parameter has to be known. In case an element has not failed in the FEA and XFEM has not yet been enabled, this value is unknown. Therefore, it has to be assumed that the value is equal to the mixed-mode SERR parameter of the closest element, within the same crack, where XFEM was enabled during the FEA. Effectively, this approach boils down to the linearisation of the crack growth based on the previous state.

For the numerical implementation of this framework, XFEM has not yet been considered. Therefore, this issue has not been investigated in-depth and is not considered any further during this thesis. However, it is recommend that this issue is investigated in the future. This includes investigating the maximum value of ΔN for which the approach produces acceptable results.

4.3 Cycle jump algorithm

As discussed in Section 2.3.5, it is not possible to simulate each cycle. Therefore, it is required to skip cycles and solve for a discrete number of cycles. In the perfect case, only the number of cycles are skipped where no change in the macroscopic damage state occurs. This means that only cycles should be considered where either new damage is initiated or the damage has progressed sufficiently. The latter should be defined by the user. In order to achieve this, a cycle jump algorithm has to be used. The current section is only concerned with the proposal of cycle jump algorithms for the three selected models. The integration of these models to generate a single number of cycles to jump and the fundamental assumptions related to cycle jump algorithms, have already been discussed in Section 2.3.5.

The proposed cycle jump algorithm for the CDM is discussed in Section 4.3.1, for the CZM in Section 4.3.2 and for XFEM in Section 4.3.3.

4.3.1 Continuum Damage Model (CDM)

For the FPCDM, an adaptive cycle jump algorithm is used. The implementation is constraint by the amount of time it takes to evaluate the cycle jump algorithm, as this procedure has to be performed several times when considering fatigue loading. To comply with these constraints, additional assumptions are introduced. For the LaRC-05 criterion, the function $FI_{i,max} - 1$ (where i indicates the failure mode) the following assumptions are made. The function:

1. Is at least first-order continuous
2. Contains one root at the interval $(N_{current}, N_f]$.

Both assumptions are imposed to allow the use of Brent's root-finding algorithm (see Appendix A.2). Based on the observed behaviour of the maximum failure index obtained from the LaRC-05 criterion, this is deemed to be an acceptable assumption.

Following the framework, the concept of the cycle jump algorithm is to calculate the number of cycles N_k for which the criterion $F_{max}(\sigma_{\mathbf{k}}, N_k) = 1$ is satisfied. Then, the number of cycles has to be selected from the calculated values of N_k. Here, $k \in K$ denotes the element, $\mathbf{K}$ the set of considered elements and $\sigma_{\mathbf{k}}$ the stress-state of element k. The selection is based on a user-defined criterion. There are several possibilities for the set $\mathbf{K}$. First of all, $\mathbf{K}$ can be taken as the set of all elements. However, due to the first assumption of the cycle jump algorithm in Section 2.3.5, it is reasonable to assume that the elements that have the highest FI_{max} will be the first to fail. As the failure indices of the different failure modes will generally show different responses to the number of cycles N, it is required to consider the elements per failure mode. In this case, the set $\mathbf{K}$ will consist of n_{elem} elements per layer per failure type that exhibit the highest $FI_{j,max}$, where j denotes the failure mode. For the FPCDM, this approach is used.

The procedure starts with selecting $\chi \frac{n_{elem}}{n_{layer}}$ number of elements per layer i that have the highest failure index FI for failure mode j. The factor χ is a user-specified fraction, n_{elem} the total number of elements used in the analysis and n_{layers} the total number of layers. The set of elements per layer per failure mode is defined as $\mathbf{L_{ij}}$, for which $|\mathbf{L_{ij}}| = \chi \frac{n_{elem}}{n_{layer}}$. All of the elements considered for this procedure are contained the set $\mathbf{K}$, for which $|\mathbf{K}| = \chi \cdot n_{elem}$ (considering that each layer contains equal amounts of elements) and $\mathbf{L_{ij}} \subset \mathbf{K}$ $\forall i, j$. The failure indices are directly obtained from the FEA.

Next, for each element l_{ijm} in $\mathbf{L_{ij}}$ (where $m = 1..|\mathbf{L_{ij}}|$), the number of cycles until failure, N_{fail}, is calculated. The cycles until failure are elements of set $\mathbf{N}$ for which each element N_{ik} corresponds to element K_{ik}; therefore, $|\mathbf{N}| = |\mathbf{K}|$. Each element should be considered only once, as an element will fail irrespective of which failure index is evaluated. Hence, in case the element l_{ijm} is considered for multiple failure modes, the most critical failure mode is used, i.e. $N_{ik} = \min(N_{f,j,m})$.

Lastly, when all of the element sets $\mathbf{L_{ij}}$ have been evaluated, the failure cycle N_f is selected from $\mathbf{N}$ so that $\chi \cdot n_{elem}$ elements in $\mathbf{K}$ will fail. This is equal to the number of cycles to be jumped, N_{jump}.

In Figure 4.4, an overview of the proposed cycle jumping algorithm is provided. The overview follows the general cycle jumping algorithm framework of Figure 2.11. For the modules 5.1 and 5.2, this leads to a superfluous depiction as parts of both procedures are the same. However, in the current format, the connection to the general framework is more clear.

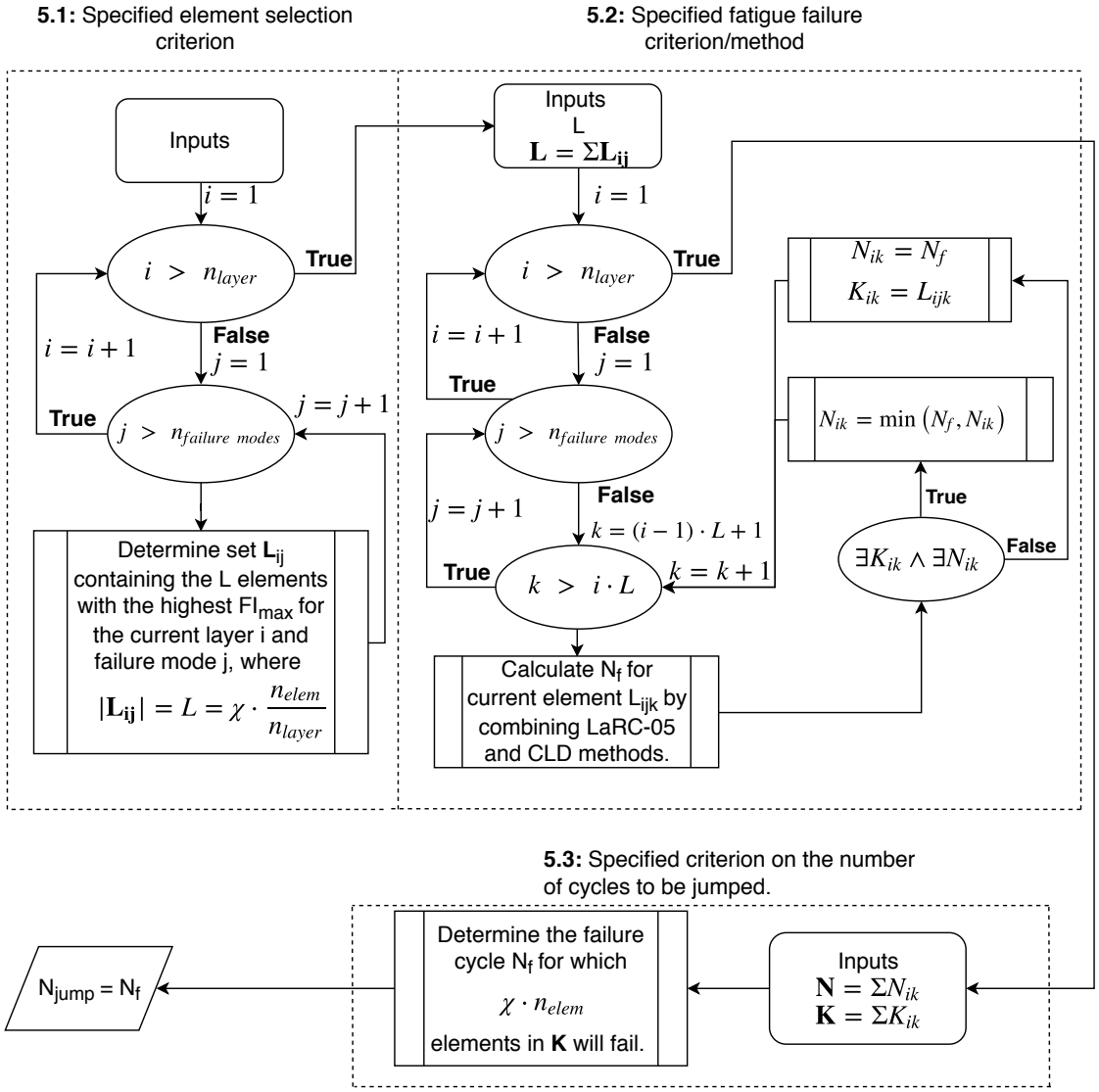

Figure 4.4: Overview of the algorithm for the CDM used to determine the number of cycles to be jumped.

Next to the assumptions and possible pitfalls discussed in Section 2.3.5, the cycle jump algorithm for the FPCDM, proposed in this section, has one additional difficulty. By introducing the parameter χ, the issue of a 'good' guess for the step size is not fully addressed. The cycle jump algorithm requires the specification of a parameter χ whose definition is the fraction of pristine elements that are allowed to fail in fatigue before a next FEA simulation is performed.

The parameter χ aims to be less arbitrary than a fixed step-size and automatically scales the step over time (at a later stage more elements will fail sequentially than at the beginning). However, it is not clear at this stage what value of χ allows for acceptable results. In order to overcome this issue, one could take $\chi = \frac{1}{n_{elem}}$ and $L = 1$. This results in jumping N cycles until one pristine element fails. However, this would result in a significant amount of FEAs and undermines the motivation for using a cycle jumping algorithm. Therefore, it is recommend to investigate the performance and sensitivity of the parameter χ in future work. Furthermore, attempts to relate χ to the structure (such as material, geometry, etc.) is recommended. Such a relation will not make the choice of χ universal but makes the choice of χ less arbitrary with a connection to the physical nature of the problem.

4.3.2 Cohesive Zone Model (CZM)

The cycle jump algorithm for the CZM is shown in Figure 4.5. Just as for the CDM, the format of the general cycle jumping algorithm framework of Figure 2.11 is explicitly used.

For the selection of the elements that are considered, the delamination fronts in every layer have to be identified and tracked. In order to find delamination fronts, a pattern recognition type of algorithm is required. Such an algorithm should provide the means to identify delamination fronts without evaluating the state of every element. A possible delamination front tracking algorithm has been proposed by Kawashita and Hallett [16]. In order to handle delamination initiation and progression, a delamination tracking algorithm will have to fulfil two functions:

1. Identifying new delamination fronts
2. Tracking existing delamination fronts.

The development and numerical implementation of such an algorithm is not in the scope of the present research; and is therefore, left to future research.

For every delamination front, the elements at the delamination tip are identified. Furthermore, the global direction of the delamination front should be determined. It is assumed that the entire delamination front will move into the same direction. If this is not the case, a procedure has to be developed that determines the delamination direction per element or per subgroup of elements.

The fatigue failure criterion entails the specification of a maximum allowed delamination progression length, da_{max}. In this context, the length is a suitable parameter and delamination area does not have to be considered. The length is defined as the distance between the point of delamination in the current element to the delamination front after ΔN cycles. As the maximum allowed length and direction of the delamination progression are known, ΔN can be determined. In order to determine the location of the delamination within an element, the damaged area (see Section 4.1.2.2) and delamination progression direction can be used.

The fatigue failure criterion is evaluated for each element at the delamination front and the minimum number of cycles is used as the number of cycles to jump.

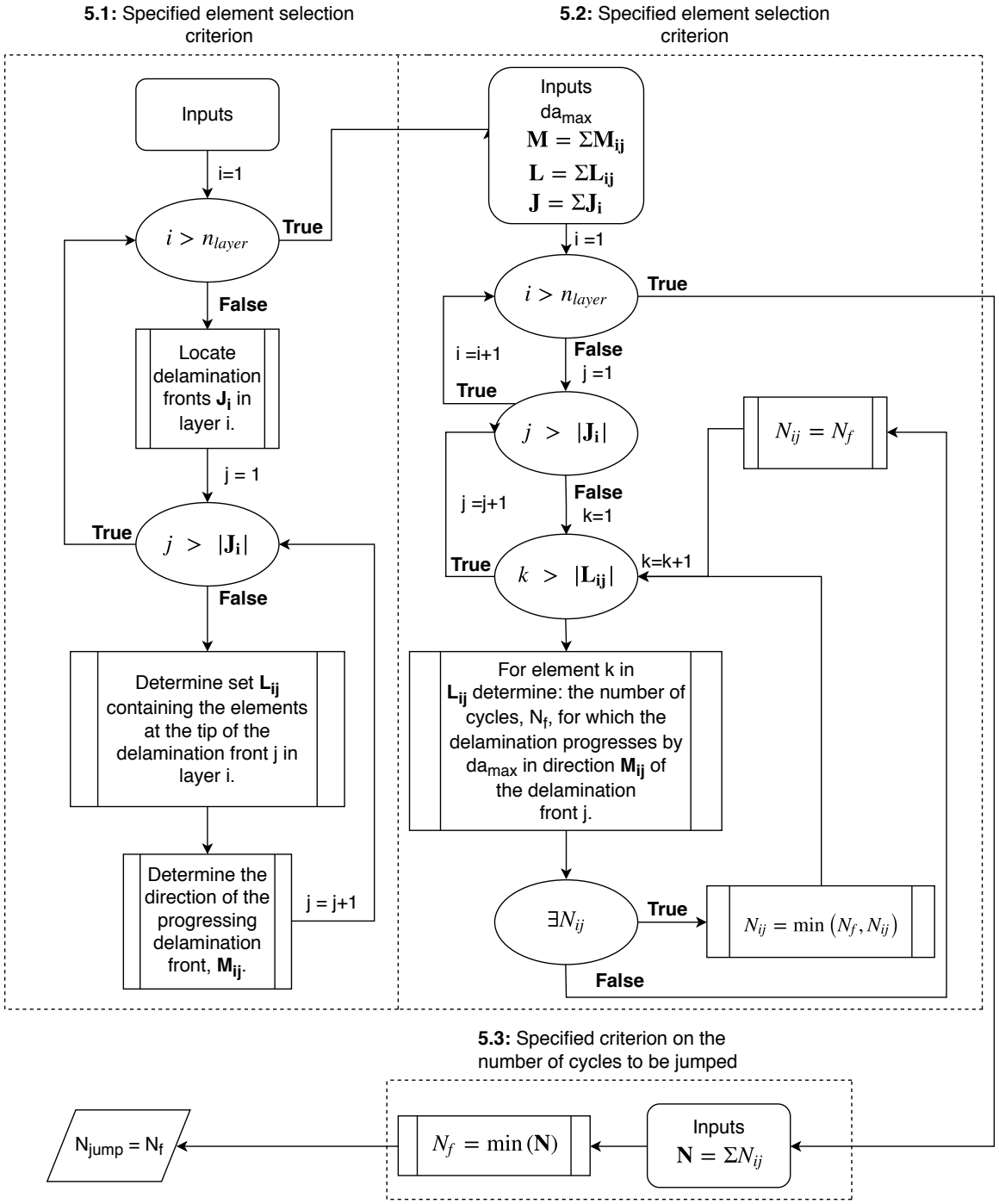

Figure 4.5: Overview of the algorithm for the CZM to determine the number of cycles to be jumped.

4.3.3 eXtended Finite Element Method (XFEM)

The cycle jump algorithm for XFEM is shown in Figure 4.6. The formulation is similar to that of the CZM. The main difference is that instead of a delamination front, the tips of matrix cracks are considered.

First, all of the matrix cracks in the layers have to be identified. A similar type of algorithm as for identifying the delamination fronts can be used. When a matrix crack has been identified once (after initiation), the crack can be tracked by following the elements for which XFEM is enabled. An element corresponds to the crack tip of a matrix crack if the element:

- Is only linked with one other XFEM initiated element
- Has not yet failed (extrinsic CZM does not evaluate to complete decohesion).

As stated previously in Section 4.3.2, the development of such an algorithm is not in the scope of the present investigation and is therefore left to future research.

Next, just as for the CZM, a specified da_{max} is used to determine the number of cycles to jump. Generally, the value of da_{max} is different than for the CZM. Furthermore, instead of an entire front, only one element has to be considered per crack. Note that cracks that grow into two directions simultaneously, are considered as two cracks. The minimum number of cycles for a crack to reach the specified da_{max} is used as the number of cycles to jump.

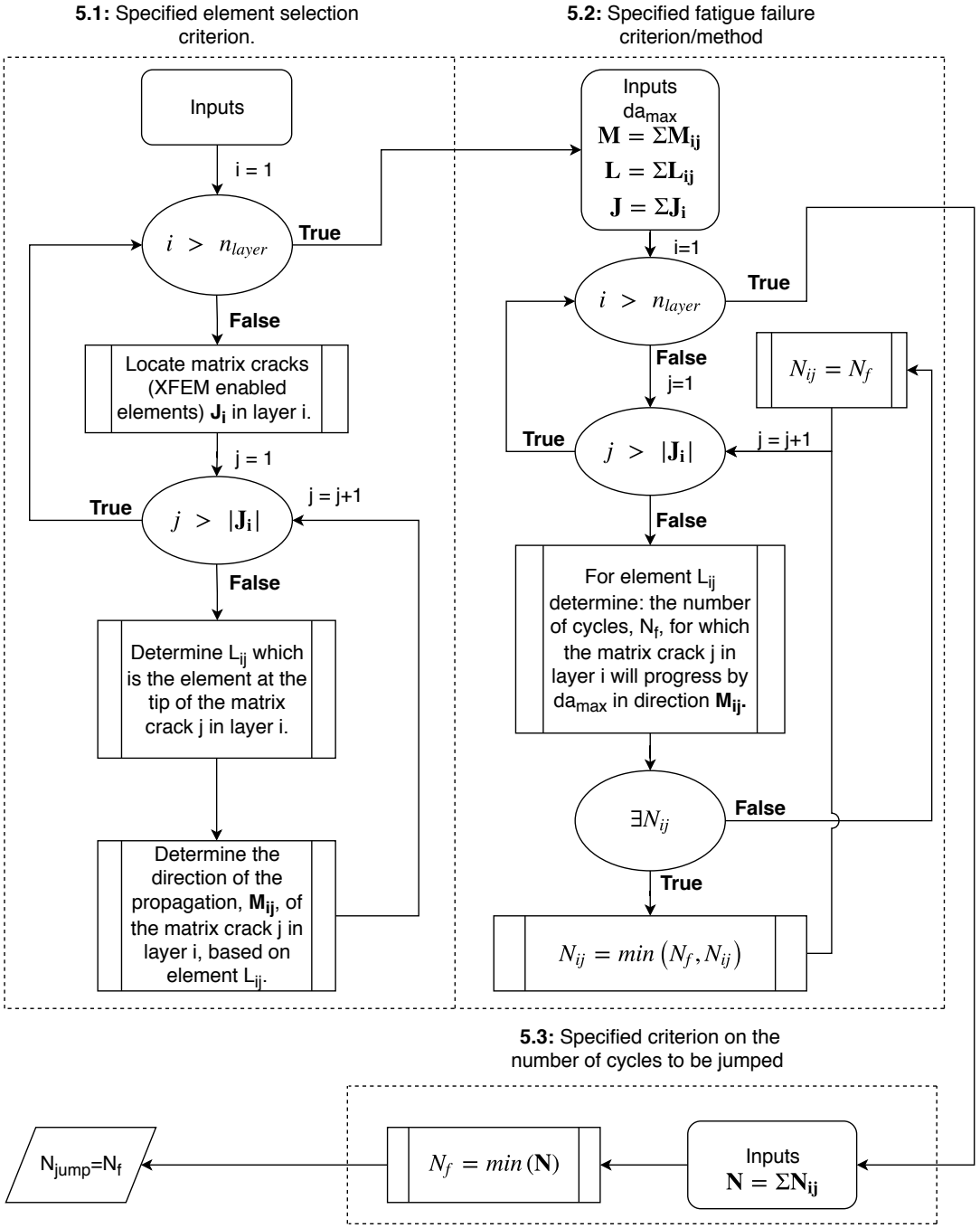

Figure 4.6: Overview of the algorithm for the XFEM to determine the number of cycles to be jumped.

Chapter 5

Numerical implementation

Part of the project described in this report, is the start of the development of a practical numerical implementation of the proposed framework. The numerical implementation of the framework consists of several modules and environments as shown in Figure 5.1. 'Abaqus Python' indicates that Python is used within the Complete Abaqus Environment (CAE), 'external Python' indicates that pure Python is used and 'Abaqus Fortran' indicates that Fortran is used within the Abaqus solver environment.

Due to time constraints, it is not realistic to implement and verify the implementation of all of the models and methods discussed in Chapters 3 and 4. Therefore, the following goals have been set concerning the numerical implementation.

1. Create a numerical framework in which arbitrary Continuum Damage Models (CDMs) and Fracture Mechanics Damage Models (FMDMs) can be incorporated.
2. Implement the CDM discussed in Chapters 3 and 4
3. Implement the Cohesive Zone Model (CZM) for delaminations discussed in Chapter 3 for quasi-static loading; and allow for the extension to fatigue loading as discussed in Chapter 4. Hence, the implementation of fatigue for the CZM is not considered.

The numerical implementation is verified with the simulation of Open-Hole Tensile (OHT) specimens as investigated by Nixon-Pearson et al, [11] and Green et al, [155]. The same data has been used by van Oostrum [7] to verify the implemented Quasi-Static Progressive Blended Damage Model (QSPBDM) part of the framework. As no new insights or sensitivities are considered, the verification of the quasi-static part has not been included in this report. In order to verify the Fatigue Progressive Blended Damage Model (FPBDM) part of the implementation, a consistent data set of quasi-static and fatigue parameters is required. The creation of such a data set is not in the scope of the present research. Furthermore, when using input data from literature, several issues can arise. These issues are discussed in more detail in Chapter 6. Therefore, also the fatigue verification will not be considered. Instead, the chapter only focusses on the numerical implementation itself.

The first goal of the numerical implementation entails the creation of a software framework of which the functionality can be readily expanded by additional user-written code. The

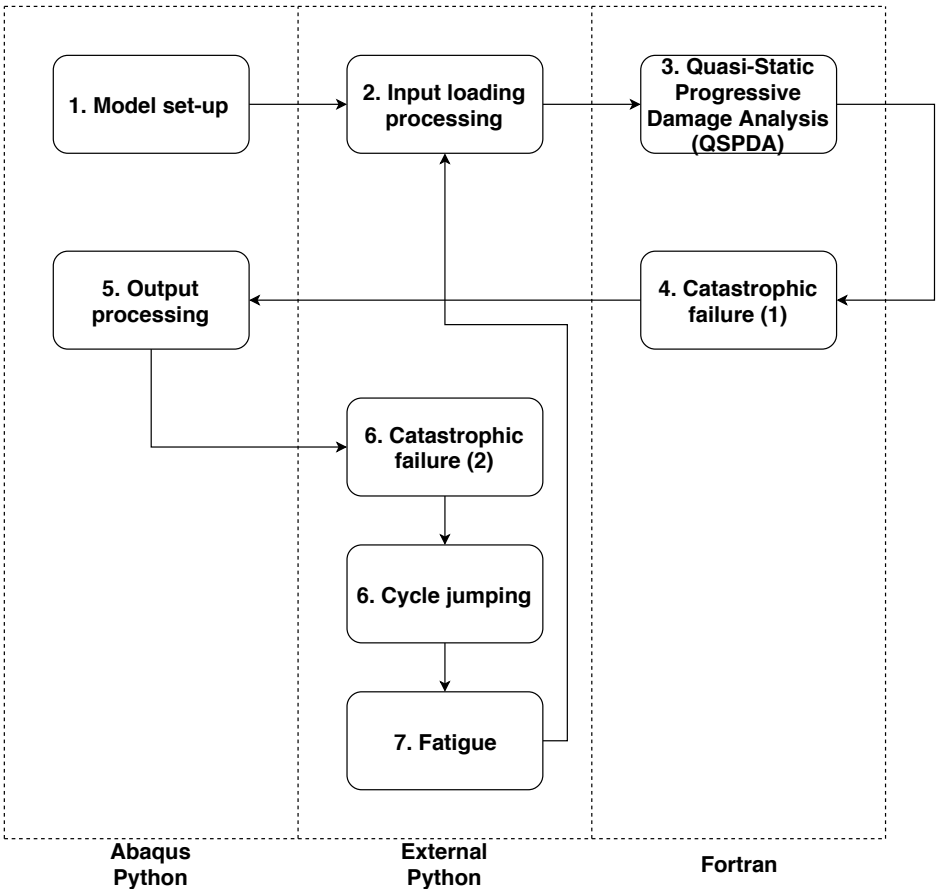

Figure 5.1: Flow chart of the numerical implementation of the framework. For each part of the implementation it is indicated which software (or combinations thereof) are used.

second goal and third goal are to start the development of an implementation of the blended framework, and illustrate how the CDM and CZM models fit in the software framework.

The numerical implementation, presented in this work, has the following features:

- A modular implementation of the framework discussed in Chapter 2 and as shown in Figure 5.1
- Automatic model generation for an arbitrary lay-up and an OHT or Tension-Tension (T-T) rectangular specimen
- The Quasi-Static Progressive Continuum Damage Model (QSPCDM) as discussed in Chapter 3, including the Hahn-Tsai and Ramberg-Osgood shear and in-situ strength fits
- The Fatigue Progressive Continuum Damage Model (FPCDM) as discussed in Chapter 4
- The implementation of the CZM for delaminations, referred to as the Quasi-Static Progressive Fracture Mechanics Damage Model (QSPFMDM), as discussed in Chapter 3.

The model set-up is discussed in Section 5.1. In Section 5.2, the input loading processing is briefly discussed. Furthermore, the Quasi-Static Progressive Damage Analysis (QSPDA) is discussed in Section 5.3 which concerns the Finite Element Analysis (FEA) implementation. Internally in Abaqus catastrophic failure criteria have been implemented that terminate the QSPDA. This is discussed in Section 5.4. The output processing is straight-forward and only consists of reading the data from the Abaqus generated output file; and therefore, no section will be dedicated to the output processing. In case catastrophic failure cannot be determined within the QSPDA or the criteria are insufficient, the catastrophic failure is evaluated outside of the Abaqus environment. This is also discussed in Section 5.4. Remarks for the numerical implementation of the cycle jump algorithm are discussed in Section 5.5. Lastly, remarks regarding the fatigue damage evaluation are provided in Section 5.6.

5.1 Model set-up

The first component of the numerical implementation is the model set-up. During the model set-up, the geometry, material and analysis settings are created within Abaqus CAE by using Python.

Two types of geometries are incorporated: OHT and T-T specimens. The dimensions and other characteristics of the geometries (such as symmetry) are left as input for the user.

In order to employ user-defined material behaviour, it is required to load material properties from an external text file. In order to incorporate the fatigue model, it is required to define each material property per element separately. Furthermore, this allows for a readily extension to stochastic models as the material properties can be assigned throughout the structure based on a statistical distribution. For the current implementation, the element material properties are based on a master material file that contains the material mechanical properties. Some of the properties depend on the location of the element, such as the in-situ strengths. Each of the material files are distributed throughout directories based on the layer that the element resides in. A limit is imposed on the maximum number of text files per directory due to performance issues. At the start of the FEA analysis by the QSPBDM, the material files are opened, read and loaded into the Abaqus solver. Opening and reading a large number of files will decrease the computational efficiency and for a large number of files it is recommended to merge the properties of multiple elements in one file. An optimum can be found between opening m files with n lines and opening m/p files with $n \cdot p$ lines, where m, n and p are integers. For the present work the number of elements remain in an acceptable range to use the representation of one element per file. In Figure 5.2, the structure of the material files is sketched schematically.

The analysis settings of the FEA are assigned, based on the user-specified inputs which allows for flexibility. Among the analysis settings inputs are: mesh seeds, boundary conditions and solver settings. Furthermore, several CDM initiation, progression and delamination initiation models have been ported from the implementation by Van Dongen [6]. The following CDM initiation criteria have been ported:

- Hashin
- Cuntze

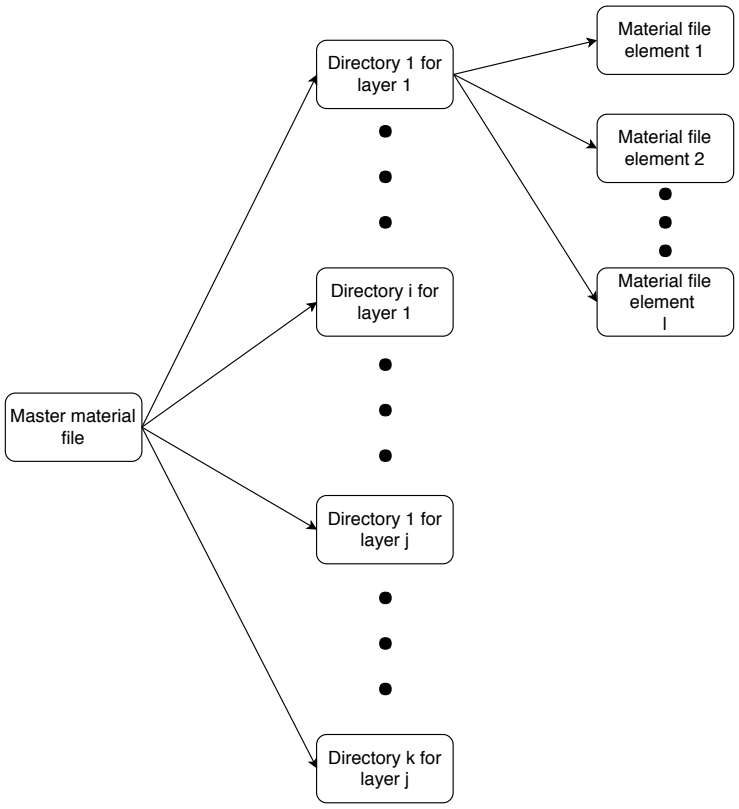

Figure 5.2: The material file structure used by the numerical implementation of the framework. This structure allows for each element to be treated separately and provides an easy means to alter material properties due to statistical variations of the material and influence of fatigue.

- Puck.

The following CDM propagation criteria have been ported:

- Bilinear softening
- McCarthy
- Camanho.

Furthermore, CDM delamination initiation criteria, that can be used instead of the CZM, have been ported:

- Lee
- Ochoa-Engblom
- Long

- Shokrieh
- Tong.

5.2 Input loading processing

The input loading processing is not considered in the current implementation. The model has been implemented for Constant Amplitude (CA) loading with linear damage accumulation which mitigates the need of this module. However, the option for implementing this module has been left open, in order to extend the implementation to the simulation of Variable Amplitude (VA) loading.

5.3 Quasi-Static Progressive Blended Damage Model (QSPBDM)

This section discusses the numerical implementation of the QSPBDM that is used to evaluate the model as created in Section 5.1. In Section 5.3.1 it is decided whether to use an explicit or implicit analysis for the QSPBDM. Furthermore, whether to use load or displacement control for the QSPBDM is discussed in Section 5.3.2. In order to accelerate the solving procedure, the numerical implementation has been made compatible for parallel processing; and is discussed in Section 5.3.3. Numerical consideration regarding the QSPCDM are discussed in Section 5.3.4. Finally, numerical consideration regarding the QSPFMDM are discussed in Section 5.3.5.

5.3.1 Explicit vs implicit analysis

Comparisons between explicit and implicit finite element methods can be found in several publications in literature such as Prior [156], Sun et al. [157], Yang et al. [158] and Kim et al. [159]. Most of the comparisons are made with respect to metal sheet forming, however the involved principles are valid in general. This section will briefly touch upon the difference between explicit and implicit finite element methods and motivate the choice for the method for the QSPBDM.

The primary difference between the explicit and implicit method is that the explicit method solves for $t+\delta t$ using the state at t, whereas the implicit method solves for $t+\delta t$ using states at t and $t+\delta t$. As the state at $t+\delta t$ is not known beforehand, an iterative procedure has to be used (such as the Newton-Raphson method). The implicit method is unconditionally stable, whereas the explicit method is conditionally stable. Note that for (quasi-)static problems, one speaks of pseudo-time instead of time. For convenience, only the term time will be used and the distinction should be clear from the context.

For a three-dimensional model, the unconditionally stable implicit method can run into convergence issues. The main reasons are: i) when the time increment continues to reduce, the computation of the tangent stiffness matrix increases and can eventually lead to diverging behaviour; ii) local instabilities may cause difficulty to achieve force equilibrium. [157, 159] Examples of the latter are contact problems or wrinkling.

For the explicit method, a large amount of increments is required. The maximum step size δt for the explicit method, depends on the smallest element length and the material properties (sonic speed). The application of the explicit method is limited to short transient problems (due to the small required time steps); and in case of quasi-static problems, the inertia effects must be negligible. [157]

Even though the explicit method requires more increments than the implicit method, the explicit method can be more efficient than the implicit method. For problems where the implicit method has difficulties to converge (e.g. due to contact or material complexities) the implicit method may require a significant amount of iterations which are expensive to evaluate. In this case, the explicit method becomes more efficient than the implicit method. Furthermore, the explicit method in Abaqus performs more calculations in memory, whereas the implicit method reads and writes more data to the hard disk. This also increases the efficiency of the explicit method in comparison to the implicit method.

For the QSPBDM, the implicit method (Abaqus/Standard) has been chosen. It is expected that the convergence behaviour of the implicit method will be acceptable (i.e. does not requires excessive iterations per time increment). Furthermore, it is expected that the implementation of the bilinear softening and viscous regularisation (see Section 5.3.4.1) lead to better convergence behaviour. These expectations have been based on the results of van Dongen [6] and van Oostrum [7].

5.3.2 Load or displacement control

Load control methods solve the system of non-linear equations by incrementally increasing the load. Displacement control methods solve the system of equations by incrementally changing the displacement. Load control methods generally have issues with limit points (i.e $\frac{dF}{du} = 0$) and are not capable of capturing snap-through and snap-back phenomena. [160] Displacement control methods are capable of handling limit points and snap-through phenomena but are not able to capture snap-back phenomena.

For quasi-static failure, displacement control is favoured as snap-through phenomena can be captured and issues with limit points are avoided. However, in case of fatigue, the behaviour is often defined in terms of load spectra. Therefore, the use of load control may be required in case the applied load is provided. For fatigue the disadvantages of load control may not necessarily be limiting. The biggest issue with load control is the occurrence of limit points. However, for most cases this will only occur at final failure and hence load control could be sufficient for a progressive fatigue model.

Based on the author's experience, it is deemed possible to write user subroutines in Abaqus to allow for a displacement-based control that will terminate or change boundary conditions after a specified load has been reached. However, the implementation of such a procedure is tedious, especially when allowing for parallel processing. Furthermore, for a multidirectional load case, the implementation is less straightforward; and it may not be possible to evaluate for arbitrary loads and structures. Therefore, it has been decided that for modelling quasi-static ultimate failure, the model will use displacement control; and for fatigue, load control is used.

5.3.3 Multi-core implementation

Nowadays, most computers use processors that have more than one core and/or have more than one processor. Therefore, it is a waste of resources if the evaluation of the QSPDA is only compatible for one core. Hence, the subroutines used for the Abaqus analysis are developed for parallel processing compatibility. In order to enforce this compatibility with both MPI and thread parallel processing, the following measures have been taken.

- The use of mutex protectors in the subroutines. Mutex protectors allow for protecting processes that change global variables (common blocks in Fortran). When a mutex is locked, all other threads will sleep until the thread using the mutex, unlocks the mutex again
- If common block are used, care is taken such that the common blocks are read-only. In the cases that this is not possible, mutex protectors have to be used
- In case files have to be accessed, a mutex protector is used. For the internal termination criteria (see Section 5.4), a temporary storage file of Abaqus has to be accessed. In order to avoid erroneous results and/or runtime errors, mutex protectors have been used to protect the access to the file.

In light of universality and flexibility, care is taken that the multi-core implementation allows for different operating systems. For a Windows system, the thread parallel computing option has to be used. For Linux based systems (such as most computing clusters), the MPI option should be used instead. By accounting for both thread and MPI parallel computing, the model can be run on a wide-variety of systems. The correctness of implementation is readily evaluated by running the same simulation twice: once with parallel computing enabled and once disabled.

5.3.4 Quasi-Static Progressive Continuum Damage Model (QSPCDM)

This section discusses important aspects regarding the numerical implementation of the QSPCDM and analysis in Abaqus. In order to avoid convergence issues with the chosen finite element method, viscous regularisation is employed, which is briefly discussed in Section 5.3.4.1. The approach on how to implement the non-linear shear behaviour and calculate the material Jacobian is discussed in Section 5.3.4.2. Furthermore, critical notes regarding the implementation of in-situ strengths is discussed in Section 5.3.4.3. Lastly, the element type for the CDM elements is discussed Section 5.3.4.4.

5.3.4.1 Viscous regularisation

In order to reduce possible convergence issues of the implicit method, an artificial viscosity is included in the bilinear softening behaviour. By adding such a viscosity, the energy dissipated by the damage evolution is increased. The purpose of adding this viscosity is to make the mechanical property degradation more gradual. As the energy dissipation due to the viscosity is artifical, the viscosity should be kept small. The implementation of viscous regularisation has been ported from the implementation by Van Dongen [6]. For details regarding the method and implementation of viscous regularisation, the reader is referred to van Dongen [6].

5.3.4.2 Material Jacobian and non-linear shear

Abaqus/Standard uses the material Jacobian $\underline{\underline{\mathbf{J}}}$, defined by Equation 5.1, to determine the strain for the next increment (or iteration), where m indicates the current increment. Hence, the material Jacobian is imperative for the convergence behaviour of the model but does not influence the solution. Following, amongst others, McCarthy et al. [39], the material Jacobian is simply the material stiffness matrix $\underline{\underline{\mathbf{D}}}$ given by Equation 3.1 but with each of the material properties multiplied by $1 - d_k$. Here, d_k is the damage parameter corresponding to the material property k. The D_{ij} coefficients are given in Equation 3.2.

$$\underline{\underline{\mathbf{J}}} = \frac{\partial \Delta \sigma_{ij}^{m+1}}{\partial \Delta \epsilon_{ij}^{m+1}} \tag{5.1}$$

The material Jacobian in the discussed form is only valid if the damage parameters are not varying during the load history. Otherwise, a complicated relation will arise, as is shown by van der Meer and Sluys [114] (which also include partial derivatives of the viscous regularisation). As a rule-of-thumb: a more accurate material Jacobian results in a higher convergence rate. [161] However, in some cases it may be less computational expensive to approximate the material Jacobian with a simpler representation and accept a slower convergence rate. Based on the work of Van Dongen [6] and van Oostrum [7]; and the experience of the author, the approximation of the material Jacobian by the material stiffness matrix is sufficient to obtain satisfactory convergence behaviour.

The material stiffness matrix and material Jacobian in the current form, are derived for linear material behaviour. In order to account for non-linear shear behaviour, the material stiffness matrix coefficient D_{44} has to be altered. However, D_{44} will be a function of the stress τ_{12}; and therefore, τ_{12}^{m+1} has to be determined before D_{44}^{m+1}. Furthermore, τ_{12}^{m+1} has to be accurately calculated in order to obtain acceptable results in terms of accuracy and stable numerical behaviour. Also, D_{44} will be a function of the damage parameter d_s. It is assumed that non-linear shear fitting parameters are not affected by damage, i.e. β, K and n. The damage parameter will therefore only have an influence on the pristine shear modulus G_{12}^0.

In order to determine the stress τ_{12}^{m+1} it has been decided to use an absolute approach instead of an incremental approach. This means that instead of evaluating Equation 5.2, the non-linear shear relation given by Equation 5.3 is evaluated directly at each increment m.

$$\sum_{i=1}^{N} \left(\frac{d\tau_{12}}{d\gamma_{12}} \right)_i \Delta \gamma_{12}^{i+1} \tag{5.2}$$

$$\gamma_{12} = f\left(\tau_{12}\right) \tag{5.3}$$

For a general function $f(\tau_{12})$ it is not always possible to obtain an expression for τ_{12}. Therefore, the general approach is to find the root of $g(\tau_{12}, \gamma_{12}, d_s) = f(\tau_{12}, d_s) - \gamma_{12}$, where γ_{12} and the shear damage parameter d_s are known. For an iterative scheme, the strain at step $m+1$ is equal to $\gamma_{12}^{m+1} = \gamma_{12}^{m} + \Delta\gamma_{12}^{m+1}$, where $\Delta\gamma_{12}^{m+1}$ is determined by Abaqus with the material Jacobian from the previous step. The stress for iteration $m+1$ is then obtained by solving Equation 5.4.

$$g\left(\tau_{12}^{m+1}, \gamma_{12}^{m+1}, d_s\right) = f\left(\tau_{12}^{m+1}, d_s\right) - \gamma_{12}^{m+1} = 0 \tag{5.4}$$

Equation 5.4 is solved by using the modified Newton-Raphson method discussed in Appendix A.1, where the first derivative is given by Equation 5.5.

$$\frac{dg}{d\tau_{12}^{m+1}} = \frac{df}{d\tau_{12}^{m+1}} \tag{5.5}$$

For the Ramberg-Osgood relation, the root function and the derivative of the root function are given by Equations 5.6 and 5.7.

$$g = \left[\frac{\tau_{12}^{m+1}}{G_{12}^0} + \frac{K}{(1-d_s)^{n-1}}\left(\frac{\tau_{12}^{m+1}}{G_{12}^0}\right)^n\right]\frac{1}{(1-d_s)} - \gamma_{12}^{m+1} \tag{5.6}$$

$$\frac{dg}{d\tau_{12}^{m+1}} = \left[\frac{1}{G_{12}^0} + \frac{Kn}{G_{12}^0\,(1-d_s)^{n-1}}\left(\frac{\tau_{12}^{m+1}}{G_{12}^0}\right)^{n-1}\right]\frac{1}{(1-d_s)} \tag{5.7}$$

For the Ramberg-Osgood relation, the damaged tangential stiffness at step $m+1$ is given by Equation 5.8 which leads to the material Jacobian entry J_{44} $(= D_{44})$.

$$J_{44}^{m+1} = G_{12}^{m+1} = \frac{d\tau_{12}^{m+1}}{d\gamma_{12}^{m+1}} = \frac{1}{\frac{d\gamma_{12}^{m+1}}{d\tau_{12}^{m+1}}} = \frac{1}{\left(\frac{1}{G_{12}^0} + \frac{Kn}{G_{12}^0(1-d_s)^{n-1}}\left(\frac{\tau_{12}^{m+1}}{G_{12}^0}\right)^{n-1}\right)\frac{1}{(1-d_s)}} \tag{5.8}$$

For the Hahn-Tsai relation, the roots can be obtained analytically, where the solution corresponds to the real root. The analytical solution for the stress τ_{12}^{m+1} is given in Equation 5.9, where the coefficients A and B are given in Equation 5.10.

$$\tau_{12}^{m+1} = \frac{A}{(2)^{\frac{1}{3}}3^{\frac{2}{3}}G_{12}\beta B} - \frac{(\frac{2}{3})^{\frac{1}{3}}}{A} \tag{5.9}$$

$$\begin{aligned} A &= \left[9G_{12}^3\beta^2B^3\gamma_{12}^{m+1} + \sqrt{81G_{12}^6\beta^4B^6\left(\gamma_{12}^{m+1}\right)^2 + 12G_{12}^3\beta^3B^3}\right]^{\frac{1}{3}} \\ B &= (1-d_s) \end{aligned} \tag{5.10}$$

The material Jacobian entry J_{44} for the Hahn-Tsai relation is given by Equation 5.11.

$$J_{44}^{m+1} = \frac{1}{\left[\frac{1}{G_{12}^0(1-d_s)} + 3\beta\left(\tau_{12}^{m+1}\right)^2\right]} \tag{5.11}$$

5.3.4.3 In-situ strengths

The in-situ strengths have been incorporated as discussed in Section 3.3.3. However, it should be noted that it is questionable whether the in-situ strength remains constant in a progressive damage analysis. When neighbouring elements start to fail (matrix failure or delamination), the surfaces of elements start to become less constrained; and therefore, the constrained surface assumptions of the in-situ strength model become invalid. In order to circumvent this issue, it is recommended to develop an in-situ strength updater which changes the in-situ strength of elements according to the damage state of neighbouring elements. An important consideration for the in-situ strength updater is the required additional computational effort. However, this is not considered any further in the present work and is recommended for future research.

5.3.4.4 Element type

Following the discussion by van Oostrum [7], it is decided to use C3D8 elements with reduced integration for the following reasons:

- C3D8 elements are compatible with eXtended Finite Element Method (XFEM)
- A simple interface with adjacent elements
- A limited number of degrees of freedom in comparison to other available elements which results in less required computational effort
- Is shown to obtain acceptable results for thin laminate type of structures.

Even though XFEM is not considered in the present model, the option for future implementation is kept open. This limits the choice to the C3D8, C3D4 and C3D10 elements. The C3D4 and C3D10 elements are not preferred due to the significant increase in degrees of freedom. Therefore, the C3D8 element is selected. A disadvantage of the C3D8 element is its poor through-thickness approximation of stresses. However, for thin layers subjected to in-plane loading the through-thickness stresses are not significant in comparison to the in-plane stresses. Therefore, the choice of the C3D8R element is justified for a wide range of Fibre-Reinforced Polymer (FRP) laminates. However, other element types should be considered in the case of significant out-of-plane stresses. Here, significant indicates the out-of-plane stresses for which the C3D8R element cannot correctly represent the state of the real structure under consideration.

In order to reduce the degrees of freedom, and therefore, decrease the required computational time, it is decided to use reduced integration (C3D8R element). This results in one integration point per element. By using reduced integration, hourglassing of the elements can occur. In order to mitigate this issue, hourglass stiffness control is enabled in Abaqus. The used stiffness for the hourglass control is given by Equation 5.12. [7]

$$G = \frac{G_{12} + G_{23} + G_{13}}{3} \tag{5.12}$$

5.3.5 Progressive Quasi-Static Fracture Mechanics Damage Model (QSPFMDM)

For the numerical implementation of the QSPFMDM, a CZM for delaminations has been implemented. This section discusses the element type in Section 5.3.5.1 and additional considerations for cohesive elements in Section 5.3.5.2.

5.3.5.1 Cohesive element type for delaminations

Abaqus provides two default cohesive zone elements: the COH3D8 and COH3D6 elements. Both of these elements are continuous. It is also possible to use SPRINGA elements that are discontinuous, however the use of such elements requires user defined material behaviour. The COH3D8 elements can interface with the C3D8 elements and are therefore chosen for the present model. The COH3D8 elements fortunately follow the damage initiation and progression discussed in Chapter 3; and therefore, no user-defined element or material behaviour is required. The main advantage of not having to implement any user-defined subroutine is the avoidance of tedious verification and validation. This is also the reason to not use the discontinuous cohesive elements. However, as will be discussed in Section 5.3.5.2, the chosen CZM has some issues. Therefore, if in future work these (or other) issues are addressed, a user-defined subroutine is most likely required.

5.3.5.2 Cohesive element considerations for delaminations

The use of intrinsic CZMs lead to several numerical issues. These difficulties have to be addressed for successfully implementing cohesive elements for delaminations. The identified problems are, the:

- Mesh dependence of the cohesive process zone
- Slower convergence of the QSPFMDM compared to the QSPCDM.

Both of the mentioned issues are addressed in the remainder of this section.

Mesh dependence of the cohesive process zone: As stated by Turon et al. [162], in order to obtain accurate results with a CZM, the tractions in the cohesive process zone must be properly represented by finite element spatial discretisation. Failing to do so results in poor accuracy. This is one of the inherent issues of CZM as discussed in Section 3.4. In order to address the mesh sensitivity of the CZM, the 'engineering' approach by Turon et al. [162] is used.

The in-plane dimensions of the cohesive zone are constrained by evaluating the mode I and mode II cohesive zone length l_{cz}. Mode III is assumed to be similar to the mode II delamination growth. However, based on the discussion in Section 3.5.2, this assumption should be revisited in case of significant mode III contribution (relative to the mode I and II). The model proposed by Turon et al. [162] only considers mode I. Harper and Hallett [163] extended the methodology to mode II by using different expressions for the stiffness of the cohesive zone. The cohesive zone lengths for mode I and mode II can be calculated with Equations 5.13 and 5.14. In the equations, m is a parameter between 0.21 and 1 (according to the models

considered by Turon et al. [162]), $E_I^{'}$ and $E_{II}^{'}$ are equivalent elastic moduli for mode I and mode II, respectively; and, t_1^u and t_2^u are the interlaminar shear strengths of the interface ($t_1^u = \sigma_{33}^u$ and $t_2^u = \tau_{12}^u$).

$$l_{cz,I} = mE_I^{'}\frac{G_{I,c}}{(\tau_1^u)^2} \tag{5.13}$$

$$l_{cz,II} = mE_{II}^{'}\frac{G_{II,c}}{(\tau_2^u)^2} \tag{5.14}$$

The cohesive elements model a thin layer of resin in between the laminae. It is assumed that the resin behaves isotropically. Turon et al. [162] use the transverse stiffness for $E_I^{'}$. Harper and Hallett [163] calculate the cohesive zone length based on analytical expressions for $E_I^{'}$ and $E_{II}^{'}$ which assumes a crack in an infinite body of an orthotropic material under plane stress conditions. However, Harper and Hallett [163] use equations that are derived by considering multiple laminae as one layer, whereas the current implementation models the layers individually. Considering that the cohesive elements in the present model represent an isotropic material, the equations used by Harper and Hallett [163] are modified for an isotropic material. The resulting equations are shown in Equation 5.15.

$$E_I^{'} = E_{II}^{'} = \frac{1}{\sqrt{\frac{1}{2E^2}\left(1-\nu+\frac{E}{2G}\right)}} \tag{5.15}$$

Equation 5.15 assumes that an thin isotropic layer of pure resin is added in between the layers; and therefore, the values of E, ν and G are matrix properties. However, as the cohesive layer is constrained between two layers and co-cured with these layers; and due to the presence of fibres in the cohesive layer (e.g. due to fibre bridging), it is likely that the properties will differ from the pure matrix properties. Therefore, in case the pure matrix properties are not available, it is deemed acceptable to use the properties of the anistropic material instead: $E \approx E_{22}$, $\nu \approx \nu_{32}$ and $G \approx G_{23}$. The advantages of making this approximation are:

- The material inputs of the model are already in terms of the orthotropic material and therefore directly available
- Not all required pure matrix properties can be readily found in literature or datasheets from the manufacturer.

The number of elements in the cohesive zone is given by Equation 5.16, where $l_{e,i}$ is the mesh size (element length) in the direction of the crack propagation for mode i.

$$N_{cz,i} = \frac{l_{cz,i}}{l_{e,i}} \tag{5.16}$$

The cohesive zone lengths given by Equations 5.13 and 5.14 may become small, which would require a very fine mesh. This is not always possible and in order to still be able to use cohesive elements for coarse meshes, a correction is required. The correction method presented by

Turon et al. [162] is used for the present model. The method entails a so-called effective interfacial strength to account for the lack of a sufficient number of elements in the cohesive zone. The method has been applied by van Oostrum [7] and yielded better results compared to not using the strength correction.

By combining Equation 5.16 with Equations 5.13 and 5.14, an expression can be derived for the effective interfacial strength $\bar{t}_i^u$, where i indicates the mode. The resulting expression is given in Equation 5.17, where $N^0_{cz,i}$ is the desired number of elements in the cohesive zone.

$$\bar{t}_i^u = \sqrt{\frac{mE_i' G_{i,c}}{N^0_{cz,i} l_{e,i}}} \tag{5.17}$$

The effective strength t_i^{eff} is then determined with Equation 5.18, where i indicates the mode and t_i^u is the original strength.

$$t_i^{eff} = \min\left(\bar{t}_i^u\right) \ \forall\ i \tag{5.18}$$

Two more problems remain: 1) what is a suitable choice for $N^0_{cz,i}$?; and 2) what value should be used for $l_{e,i}$ for an arbitrary varying mesh?

In literature there is no consensus regarding the minimum number of elements required in the cohesive zone. Moes and Belytschko [164] state that the number of elements should be higher than 10, Carpinteri et al. [165] suggest more than 10 elements, Davila et al. [166] used 3 elements and Turon et al. [162] used 5 elements. As it is not clear which number has preference and there is no physical basis on selecting such number, it is decided to choose the arbitrary number of 5 elements. A sensitivity analysis for parameter $N^0_{cz,i}$ is warranted. Note that $N^0_{cz,I} = N^0_{cz,II}$ is used for the present model.

Determining the mesh size in the direction of crack propagation $l_{e,i}$ is difficult for a general model. First of all, a varying mesh would lead to different values of $l_{e,i}$ depending on the location in the mesh. Furthermore, for a general geometry and/or loading it is not known how the crack will propagate. For the modelling of delaminations it is reasonable to assume that the crack will grow in-plane of the cohesive layer, however there are still a lot of possibilities in which direction the delamination will grow (longitudinally, transversely or under an arbitrary angle). To overcome these issues it is decided to use the largest element size encountered in the model. This guarantees that everywhere in the model at least $N^0_{cz,i}$ elements will be in the cohesive zone. For regions where the elements are of smaller lengths there will be more than $N^0_{cz,i}$ elements in the cohesive zone.

Even though the proposed approach uses a physical phenomenon to decrease the mesh sensitivity, the approach is only based on a limited physical basis and simulations which seem to imply that the approach provides better results. However, if the CZM truly aims to capture the material behaviour of the cohesive material, it is expected that the model would not be mesh dependent to such an extent. The approach by Turon et al. [162] is purely used for its simplicity and no other approaches are considered. However, a future investigation into the topic of CZM mesh sensitivity is warranted in order to find a more physically-based approach to reduce the mesh sensitivity.

Convergence performance: The addition of cohesive zone elements in between the layers results in poorer convergence characteristics than obtained for only using the QSPCDM. In order to improve the convergence characteristics of the QSPCDM, the mesh is slightly randomised. Molinari et al. [167] showed that for a slightly randomised mesh, the convergence behaviour for cohesive elements is better while retaining accuracy. The randomness is achieved by shifting the nodal x, y and z coordinates from their prescribed values with random uniformly distributed increments dx, dy and dz. The increments dx and dy are distributed on the interval $\left[-c\frac{\min(\underline{\mathbf{X}})}{2}, c\frac{\min(\underline{\mathbf{X}})}{2}\right]$, where $\underline{\mathbf{X}}$ are the mesh seeds that define the nodal locations on geometry boundaries; and c is a factor between 0 and 1. The coefficient c is introduced to control the randomness and avoid ill-defined geometries. The increments dz are distributed on the interval $\left[-c\frac{\max(\underline{\mathbf{t}})}{2}, c\frac{\max(\underline{\mathbf{t}})}{2}\right]$, where $\underline{\mathbf{t}}$ are the prescribed lamina thicknesses.

5.4 Catastrophic failure evaluation

A catastrophic failure criterion and evaluation of such a criterion for fatigue has not been developed in the present work. By considering catastrophic failure as the point where the structure is not able to carry the imposed loads, the evaluation of catastrophic failure can follow from the termination of the Abaqus analysis. As the fatigue load is applied with load control, the Abaqus analysis is expected to crash when the load cannot be sustained. However, it is recommended to implement an explicit criterion to evaluate this as it will avoid unnecessary iterations within the implicit analysis scheme and provide a more reliable method to assess catastrophic failure. Another approach is to impose a maximum allowed displacement of the structure, as this is often constraint by practical considerations. In any case, the failure evaluation for fatigue is left to future investigation and not considered any further in this report.

For the assessment of catastrophic failure under quasi-static loading, a displacement-based criterion has been used. The advantages of using a catastrophic failure criterion for quasi-static loading are that no unnecessary iterations/steps are evaluated. The criterion is as follows.

1. The reaction force, F, at specified node set $\mathbf{K}$ is calculated at (pseudo-)time step i
2. If i is the first step or the reaction force is larger than in any previous time steps j ($F_i > F_j$), then $F_{max} = F_i$. Else, see step 3
3. If $F_i < \chi F_{max}$, then terminate analysis. Else, continue the analysis.

The parameter χ is a user-defined fraction and depends on the user's definition of catastrophic failure. For example, Nixon-Pearson et al. [11] and Green et al. [155] use a load drop of 5% as a criterion. The validity of the criterion depends on the following assumptions.

- The applied quasi-static loading is increased until failure of the structure
- A node set $\mathbf{K}$ can be defined from which a representable reaction force behaviour for the entire structure can be obtained.

5.5 Cycle jumping algorithm

The cycle jump algorithm has been implemented for the CDM as dictated in Section 4.3.1 with all corresponding critical notes and assumptions. Parallel processing is not considered in the current implementation, however it is recommended to allow for this in future implementations as it will decrease the required computational time.

5.6 Fatigue damage

The fatigue damage has been implemented for the CDM as dictated in Sections 4.1.1 and 4.2.1. Just as for the implementation of the cycle jump algorithm, the option for parallel processing has not been considered. However, such an implementation is feasible and recommended for future implementations, in order to decrease the required computational time.

Chapter 6

Framework challenges

The proposed framework aims to provide the means of developing a high-fidelity tool which can be used to model the damage evolution in arbitrary Fibre-Reinforced Polymer (FRP) components. However, several challenges have to be tackled before the framework can successfully be applied for its intended purpose. This chapter will focus on challenges that are mostly inherent to the framework and not to specific Continuum Damage Models (CDMs) or Fracture Mechanics Damage Models (FMDMs). Challenges and critical notes regarding the CDM, Cohesive Zone Model (CZM) and eXtended Finite Element Method (XFEM) implementations for quasi-static and fatigue loading have been discussed in Chapters 3 and 4, respectively.

Three main challenges of the framework have been identified. First of all, the cycle jumping methodology poses a difficulty and is discussed in Section 6.1. Secondly, the required number of inputs pose another difficult task and is discussed in Section 6.2. The third challenge is the required computational effort. This is discussed in Section 6.3.

6.1 Cycle jumping

To use the high-fidelity capabilities of Finite Element Analysis (FEA), it is, unavoidably, required to impose assumptions that simplify the modelling of large number of cycles. In order to use such an approach, a trade-off has to be made between a loss in accuracy and decrease in computational effort.

The disjoint framework, discussed in the majority of the present work, uses a linear interpolation type of simplification in order to impose the effect of fatigue over a number of cycles ΔN. Clearly, such an assumption can only yield an acceptable approximation for a certain maximum number of cycles ΔN. The determination of a range of acceptable ΔN, identifying the influencing factors and formulate an approach to determine this for an arbitrary structure under arbitrary loading, is not in the scope of this research. However, before implementing, further research into these aspects should be conducted.

The multi-analysis joint adaptive cycle jump approach discussed in Section 2.2.3 provides a promising alternative for the disjoint framework when considering cycle jumping. For such

an approach the imposed assumptions are less constraining. The imposed assumptions are that:

- The stress ratio R does not change during the analysis
- The fatigue behaviour is captured with the use of (semi-)empirical models.

The advantage of the multi-analysis joint adaptive cycle jump approach over the disjoint approach is that the stress-, damage- and crack-state can be modelled for each cycle. Hence, part of the non-linear behaviour can be captured; and a linearisation approach is not required. The primary motivation to choose the disjoint approach over the multi-analysis joint adaptive cycle jump approach is related to the feasibility of implementing such a model in a commercial FEA environment. However, there is no definitive proof that it is impossible. Therefore, it may be of interest for future research to investigate the feasibility of the multi-analysis joint adaptive cycle jump approach as it clearly does present advantages in terms of cycle jumping. Of course also other factors have to be taken into account such as the computational effort.

6.2 Inputs

By blending CDMs and FMDMs for fatigue, the required number of inputs is larger than for the case where only one type of model would be considered. Especially when combining these two type of models for the fatigue domain, the required data is exhaustive. Furthermore, in order to relate errors in the prediction to the used models and underlying assumptions, it is imperative that the appropriateness and the quality of the used data is guaranteed. The appropriateness of the data refers to measuring the correct quantity under the correct conditions for the purpose that the data is intended to be used. The term quality refers to the accuracy and confidence of the measurements. Both of these aspects are essential for obtaining representative results of the used models and framework, from which conclusions regarding the accuracy of the models can be drawn. In case the inputs are erroneous, the results may be influenced which will introduce an inaccurate depiction of the performance of the model. When the data is both of sufficient quality and appropriate, the input data set is consistent. Combining separate data sets in literature may result in issues related to the consistency.

The exhaustive amount of required data (for the models discussed in this report) will be addressed in Section 6.2.1. The quality of input data is discussed in Section 6.2.2. Lastly, the appropriateness of input data is discussed in Section 6.2.3.

6.2.1 Input data set size

This section will discuss the data required for using the framework discussed in this thesis. As for different CDMs and FMDMs the required inputs may differ, the CDM, CZM and XFEM as discussed in this report are used. Furthermore, it should be mentioned that there is not a clear consensus regarding the required number of experiments to determine the various material properties. Therefore, for the remainder of the discussion the number of experiments will not be elaborated upon. Furthermore, mode III crack opening parameters are not discussed.

In Table 6.1, the inputs for the Quasi-Static Progressive Continuum Damage Model (QSPCDM) are provided. Furthermore, the inputs for the CZM for quasi-static loading are provided in Table 6.2 and for XFEM for quasi-static loading in Table 6.3.

Table 6.1: Inputs required for the QSPCDM discussed in Chapter 3.

Mechanical properties	Ultimate strengths	Fracture properties	Miscellaneous
E_{11}	$\sigma^u_{11,t}$	$G^{(+)}_{m,c}$	K
E_{22}	$\sigma^u_{11,c}$	$G^{(-)}_{m,c}$	n
E_{33}	$\sigma^u_{22,t}$	$G^{(+)}_{f,c}$	α_0
G_{12}	$\sigma^u_{22,c}$	$G^{(-)}_{f,c}$	η_L
G_{13}	τ^u_{12}		
G_{23}	τ^u_{23}		
ν_{12}			
ν_{13}			
ν_{23}			

Table 6.2: Inputs required for the CZM for quasi-static loading as discussed in Chapter 3.

Mechanical properties	Ultimate strengths	Fracture properties
k	σ^u_{33}	$G^{inter}_{I,c}$
	τ^u_{12}	$G^{inter}_{II,c}$
	τ^u_{13}	η^{inter}

Table 6.3: Inputs required for XFEM for quasi-static loading as discussed in Chapter 3.

Mechanical properties	Ultimate strengths	Fracture properties
k	σ^u_{33}	$G^{intra}_{I,c}$
	τ^u_{12}	$G^{intra}_{II,c}$
	$\tau 13^u$	η^{intra}

The mechanical and ultimate strength properties can be determined by either:

1. Micromechanics-based models
2. Experiments.

The first option relies on a formulated model that uses the material properties of the resin and fibres to predict the resulting properties of the composite. In literature, this is a topic of recent research such as by Younes et al. [168], Chamis et al. [169] and You et al. [170]. The advantage of such models is that the fibre and matrix properties are often readily available

from the manufacturer. Therefore, no additional tests have to be performed. However, such models do not yet have the capability of reliably predicting all of the mechanical properties for arbitrary composites. Therefore, such models have to be thoroughly validated when applied to new materials. In case of the absence of experimentally determined material properties, micromechanics-based models can provide the means to generate this data. However, one should be aware of the limitations of such models.

The second option is to do experiments and measure the properties. In practice, this is currently the most reliable option. It is required to do multiple tests due to the stochastic nature of composites in order to evaluate the confidence bounds of the properties. The tests required for the mechanical and ultimate strength properties can be reduced as several properties can be measured with one type of test. Furthermore, such tests are relatively fast (when compared to fatigue tests). Lastly, in literature, mechanical and ultimate strength properties are in abundance for a range of different FRPs. Note that the stiffness K for the intrinsic and extrinsic CZM is shown as a mechanical property. However, in practice, K is chosen for numerical considerations and is therefore not really a mechanical property.

The fracture properties in Tables 6.1, 6.2 and 6.3 are more difficult to determine. For the CZM only interlaminar properties are required. The critical mode I interlaminar Strain Energy Release Rate (SERR), $G_{I,c}^{inter}$, is determined by Double Cantilever Beam (DCB) tests. [13] The mode II interlaminar SERR, $G_{II,c}^{inter}$, is determined with Four-point bending End Notched Flexure (4-ENF) tests. [13] To account for the influence of mode mixity, Mixed-Mode Bending (MMB) tests have to be performed in order to obtain the required parameters for the B-K relation.

For the bilinear softening model, intralaminar longitudinal tension and compression and transverse tension and compression fracture energies are required. The intralaminar transverse fracture properties, $G_{m,c}^{+}$ and $G_{m,c}^{-}$, are assumed to be equal to the interlaminar SERR. The underlying assumptions is that the transverse matrix cracking is equivalent to the cracking of the resin material. However, the influence of fibres in transverse cracking is not taken into account. From a practical point-of-view it is not feasible to take this influence into account. Therefore, $G_{m,c}^{+}$ is determined with DCB tests and $G_{m,c}^{-}$ with 4-ENF tests. The intralaminar longitudinal fracture energies, $G_{f,c}^{+}$ and $G_{f,c}^{-}$, are determined with Compact Tension (CT) and Compact Compression (CC) tests. [113] For the bilinear softening model, mode mixity is not of importance.

According to van der Meer et al. [59, 114], matrix cracks are necessarily oriented in the direction of the fibres. Therefore, for XFEM, the longitudinal intralaminar fracture energies are required. The mode I fracture energy is determined with CT tests. [113] The mode II fracture energy can be determined with modified Iosipescu tests. [118] In order to determine the longitudinal mixed-mode behaviour, the method by Andersons et al. [119] can be used. However, on a critical note, not all of the methods are standardised. An in-depth investigation in the stated methods is not in the scope of this work; and therefore, not discussed any further.

Czabaj and Ratcliffe [117] reviewed literature that compared intralaminar (longitudinal) and interlaminar mode I fracture toughness. From the review it is clear that the interlaminar and intralaminar mode I fracture toughnesses are different. Therefore, it is not correct to use the same fracture toughnesses for interlaminar failure, as modelled by CZM, and intralaminar failure as modelled by XFEM. In conclusion, a total of seven different tests have to be

performed (in multitude to characterise the variation in measurements) for a material in order to determine all of the required fracture energies under quasi-static loading.

On a last note, the miscellaneous properties K and n in Table 6.1 are obtained from shear-strain measurements which are readily available in literature. The properties α_0 and η_L are often approximated due to prior observations.

The required inputs for the Fatigue Progressive Continuum Damage Model (FPCDM) for fatigue are shown in Table 6.4. The inputs required for the FPCDM are relatively more difficult to obtain than the QSPCDM parameters. First of all, fatigue tests often take longer to perform especially for high cycle fatigue. Furthermore, the currently selected Constant Life Diagrams (CLDs) requires three Stress-Cycle (SN) curves at different R-ratios. Also, for the FPCDM, three material directions are required to fully characterise the fatigue behaviour of a unidirectional FRP. The amount of data can be reduced by assuming that the behaviour in the 45° direction can be described by a linear symmetric CLD. Considering that each SN curve requires several tests, the total number of required fatigue tests is high. SN data generally shows high scatter and therefore it is necessary to do several tests for the same stress level in order to obtain confidence in the SN curve. As mentioned previously, in Section 4.1.1.1, Broer [123] made an attempt to develop a CLD that requires less SN curves as input while maintaining similar accuracy. The model has been validated for various Carbon Fibre Reinforced Polymer (CFRP) lay-ups and the results are promising. However, more validation effort is required to fully evaluate the merit of this model. Therefore, it is recommended to look into further improving and/or validating the model by Broer [123], as this will alleviate the required amount of data for the FPCDM.

Table 6.4: Inputs required for the FPCDM discussed in Chapter 4.

S-N data	Miscellaneous
0°; $R = -1$	χ
0°; $R = 0.1$	Residual Strength (RS) parameters
0°; $R = 10$	Residual stiffness (RE) parameters
90°; $R = -1$	
90°; $R = 0.1$	
90°; $R = 10$	
45°; R =any	

The RS and RE parameters refer to the fitting parameters for such models. For the FPCDM discussed in Chapter 4, no RS parameters are required. In case a model does require parameters, additional residual strength tests have to be performed. Just as for fatigue, the residual strength of composite materials can exhibit high scatter. Therefore, multiple tests have to be performed for the same fatigue life. The same applies for the RE parameters, however the evaluation of the residual stiffness is non-destructive. Therefore, it may be possible to combine the determination of the residual stiffness with other tests reducing the total number of required tests. The parameter χ is a user-specified input required for the cycle jump algorithm discussed in Section 4.3.1.

Overall, it is difficult to obtain all required fatigue data as a large amount of tests is needed. Furthermore, test data from different sources in literature for the same material are often

generated under different conditions (such as different frequencies). Therefore, it is difficult to combine SN data from different sources. Additionally, the quality of the SN data can vary between sources which further increases the difficulty to combine such data.

The inputs required for fatigue for the CZM are provided in Table 6.5 and for XFEM in Table 6.6. For both models da_{max} has to be specified which is used for the cycle jump algorithm discussed in Sections 4.3.2 and 4.3.3. In general, it is expected that this parameter is different for interlaminar and intralaminar crack growth.

Table 6.5: Inputs required for the CZM for fatigue loading as discussed in Chapter 4.

Fracture properties	Miscellaneous
$\frac{da}{dN}^{inter}$	da_{max}^{inter}
G_{th}^{inter}	

Table 6.6: Inputs required for XFEM under fatigue loading as discussed in Chapter 4.

Fracture properties	Miscellaneous
$\frac{da}{dN}^{intra}$	da_{max}^{intra}
G_{th}^{intra}	

The largest challenge for both FMDMs is the generation of the fracture properties $\frac{da}{dN}^{inter}$, $\frac{da}{dN}^{intra}$, G_{th}^{inter} and G_{th}^{intra}. For the threshold values, mode I, mode II and at least one mixed-mode fatigue threshold experiment have to be performed. Of course each experiment has to be repeated several times in order to account for variability. The same applies for the determination of the crack growth rate $\frac{da}{dN}$. Moreover, the type of tests are different for inter- and intralaminar fracture. In total, six different type of tests have to be performed with several repetitions in order to determine the required properties. Based on the results of Blanco et al. [152], it is clear that such data contains high scatter. Therefore, a large amount (not further specified here) of repititions are required to measure the variability of the measurements sufficiently. The determination of the fracture data for fatigue is deemed to be the most expensive and exhaustive of all inputs discussed in this section.

Overall, a large data set is required to blend the CDM and Fatigue Progressive Fracture Mechanics Damage Models (FPFMDMs) discussed in this report. For the quasi-static models, the required input data can be found in literature for a selection of materials. The fatigue models are the limiting factor in this aspect. A sufficient amount of data is generally not available in literature for the same material. Furthermore, combining several data sets from different sources is not always possible due to, for example, different test conditions. Therefore, the input data set size is a limiting challenge for the Progressive Blended Damage Model (PBDM) and experimental campaigns and/or the development of less input exhaustive models are required.

6.2.2 Input quality

Another possible issue with input data is the quality of the data. This is also part of the reason that data sets from different sources cannot always be combined, even though the data is obtained for the same (or at least very similar) conditions. The quality of the data does not only entail the results but also the corresponding documentation. Both of these aspects are briefly discussed; and examples are provided based on observations of data sets in literature.

First of all, the quality of the results of tests is discussed. One of the issues encountered for data sets in literature, is the use of too few test results for the intended application. An example would be to generate an SN curve based on only a few data points (for example, 5 or less). By using such a small data set, it is possible to obtain an SN curve that fits the limited data points well but fails to model the real behaviour. This real behaviour would be more clearly observed when more tests would have been performed. Furthermore, if the data points are concentrated in a certain region of the SN domain, it is not known whether the obtained fit correctly models the entire S-N domain. Another possible issue encountered in literature is the incompatibility between static and fatigue parameters. For example, SN data is generated for higher stresses than the static ultimate strength. A possible explanation for this observation is the use of an anti-buckling device during the fatigue tests but not for the static compression strength tests. It is then questionable whether the static strength can be used in combination with the obtained fatigue data.

The second major issue is lack of documentation accompanying the presented data. The lack of documentation can relate to several aspects, such as an incomplete description of the test setup/conditions, lack of descriptions of the events that lead to deviating data points and not providing error measures. The first aspect refers to, for example, not mentioning that an anti-buckling device has been used; or not mentioning the test frequencies (in case of fatigue tests). The lack of descriptions of the events that lead to deviating data points refers to, for example, not indicating that a strain measure is wrong due to a malfunction strain gauge, fatigue tests have been interrupted after a certain number of cycles, or, that the test specimen is reused from a different test. All of these examples can influence the results obtained from experiments that are not related to the material/specimen itself but to the testing conditions. The last aspect is not providing error measures (such as the coefficient of variation). When no error measures are provided, there is no notion of parameter variability. This can lead to incorrect results and/or conclusions based on this input data. Furthermore, knowing the variability assists with sensitivity analyses.

6.2.3 Input appropriateness

The last issue regarding input data is the input appropriateness. This concerns whether the measured quantity is the appropriate quantity used by the model. It should be noted that it is still possible to use less appropriate data as input for models. Often it is not possible (with the current approaches) to accurately measure a desired quantity without any undesirable influences. The point made in this section is that ideally one should aspire for measuring the desired quantity as correctly as possible; and in case this is not possible, investigate the influence of the quantity on the model. Being more aware of the input appropriateness will aid in avoiding contamination of conclusions regarding developed models and methods due to

incorrect inputs. For the remainder of this section, several examples will be briefly discussed to demonstrate considerations regarding input appropriateness.

Consider the determination of fracture parameters for a UniDirectional (UD) composite layer. Based on the review by Laffan et al. [171], CT tests seem to be the most widely used tests to measure the translaminar fracture toughness of composites. When the translaminar fracture toughness for a single lamina, is required it is not clear how to measure this quantity. Prewo [172] showed that in boron reinforced composites, the fracture toughness depends on the relative number of 0° and 90° plies and the lay-up sequence. It was observed that by increasing the size of 0° layer blocks, the fracture toughness was higher. Observing the fracture surfaces it was found that blocking 0° resulted in more fibre pull-out. This observation is explained by the reduced restriction on matrix deformations and fracture in the regions parallel to the 0° fibre direction. Laffan et al. [173] observed similar behaviour for CFRPs. This questions the reliability of the translaminar fracture toughness for a UD lamina. Especially since tests with multiple plies already introduce an in-situ influence depending on the used lay-up. Therefore, this is case dependent. In order to address this issue, a sensitivity analysis should be performed in order to determine the variability of models with regards to this parameter.

A similar argument can be made for, for example, DCB tests. The lay-up does not only influence the stress-state at the crack tip but also introduces effects such as fibre bridging. For example, Franklin and Christopher [174] found that the fracture toughness of a UD Glass Fibre Reinforced Polymer (GFRP) exhibits more fibre bridging during propagation than an angle-ply and a cross-ply laminate. Therefore, if for example a cross-ply laminate is used to measure the mode I fracture SERR, the results of a model using only UD laminae underestimates the fracture toughness.

Another example is the use of International Organization of Standardization (ISO) coupons for obtaining the shear strength. As reported by Eliopoulos [9], for GFRP ISO coupons, significant normal stresses are developed in the transverse direction. This implies that the measured failure strength is not the pure shear strength of the material. However, the CDM requires the pure shear strength as input. Hence, using the results of the ISO specimen for the model is inappropriate. Note that this is only valid for GFRP ISO coupons and not CFRP ISO coupons. [9]

In this section, several examples have been introduced to demonstrate that quantities that are measured are not always the same quantities used by the models. Several options to overcome this issue is by performing sensitivity analyses. Sensitivity analyses reveal the change in the accuracy of the method when input parameters are varied. From the results an indication can be obtained, regarding the appropriateness of using the measured value. For example, consider a measured quantity that is not appropriate for the input and can only be considered a crude approximation. If the sensitivity of the model for this parameter is high, then it is most likely that this measured value is inappropriate to use. Conversely, in case the sensitivity is low, the use of the measured parameter can still be justified on grounds of practicality. Another option is to shift the focus of research to developing models to correct measured data to decrease the influence of conditions that should not be present in the measured quantity. The goal is to obtain a measure of the quantity that does not depend on, for example, lamina thickness and orientations. This is especially important for a framework such as the one discussed in this report. Such a framework models laminates on the lamina level and therefore the used

quantities should be valid on the lamina level.

6.3 Computational effort

Reducing the computational effort of the proposed framework is a significant challenge that has to be tackled in order to make full use of the Fatigue Progressive Blended Damage Model (FPBDM). The computational effort arises from the inherent behaviour of the framework due to:

- The modelling of the full cycle
- Exiting and re-entering the FEA environment during analysis
- Combining different models and formulations which can result in convergence problems.

This section will discuss the bottlenecks of the numerical implementation of the proposed framework and possible improvements of the numerical implementation of the framework. Focussing on the framework and the numerical implementation thereof, the model can be separated in modules. These modules are defined based on the computational effort and are as follows:

- Model creation
- FEA
- Output processing
- Cycle jumping
- Fatigue damage.

The computational efficiency for the model creation is discussed in Section 6.3.1. The FEA is discussed in Section 6.3.2 and the output processing of the FEA results is discussed in Section 6.3.3. Furthermore, the computational efficiency of the cycle jumping algorithm is discussed in Section 6.3.4 and the fatigue damage is discussed in Section 6.3.5.

6.3.1 Model creation

The creation of the model only has to be performed once for each Fatigue Progressive Damage Analysis (FPDA); and therefore, in light of the entire analysis, the model creation is only a fraction of the total required computational time. However, the model itself will be used throughout the entire analysis. Therefore, simplifications of the model can reduce the required computational effort. Adding simplifications, that are automatically incorporated after being specified by the user, does not reduce the generality of the high-fidelity framework. Possible simplifications are to:

- Allow for symmetry boundary conditions

- Use substructures (i.e. superelements) based on prior knowledge of the locations of critical and non-critical areas
- Use less sophisticated models that can be more readily evaluated in case a reduced accuracy is acceptable.

6.3.2 Finite Element Analysis (FEA)

One of the most computational exhaustive components of the framework is the FEA. The FEA can be separated in an initiation phase and an analysis phase. For both these phases, the computational efficiency can be increased by:

1. Choosing a convenient set of models
2. Optimising the code
3. Reformulating the implementation
4. Using parallel processing.

The first option is trivial and not pursuit further as the framework should be valid for an arbitrary blend of models.

During the initiation phase, the inputs are loaded into the solver of the FEA package. Furthermore, for the implementation discussed in this report, the input files are read and stored internally. This phase takes relatively less time than the analysis phase. Due to the implementation in Fortran and the use of common blocks it is not possible to use a multi-thread implementation. Therefore, improvement of this part of the FEA is limited unless an approach that does not require global storage variables can be formulated.

The analysis phase of the FEA concerns solving the Finite Element (FE) problem. The computational efficiency can be improved by re-evaluating the implemented user subroutines and optimising the code. Furthermore, the inputs that influence the behaviour of the solver can be optimised to decrease the computational effort. However, tweaking such values is case dependent and therefore may not be a realistic improvement if a large number of varying models (e.g. different structures) have to be evaluated. Other than the previous mentioned improvements, room for increased efficiency is limited as the solver is inaccessible to the user.

6.3.3 Output processing

The output processing entails the extraction of outputs of the FEA in a workable format. This workable format is then used for the fatigue evaluation.

Based on the current numerical implementation, significant improvement is possible. In the current implementation, no parallel processing is used for extracting the outputs. By dividing the elements into groups, multiple threads can be used to extract the relevant data of each element in the group. The data is then stored in a local structure that, at the end of the output processing, can be merged in a global structure. This global structure contains all of the required data. Note that the term structure refers to a data structure such as an array, dictionary or list. By using such an implementation, the output processing can be increased significantly.

6.3.4 Cycle jumping

The cycle jump algorithm is one of the most crucial components of the framework. Not only dictating accuracy but also the computational effort. A correct implemented cycle jump algorithm keeps the accuracy within specified bounds and jumps as many cycles as possible while satisfying these bounds. Hence, the formulation of the cycle jump algorithm has a big impact on the computational efficiency and further research of this topic is recommended.

Furthermore, for the current implementation, no parallel processing is used for the cycle jump algorithm. Due to the nature of the cycle jump algorithm, where multiple elements are evaluated to identify the number of cycles to jump, this can readily be casted in a parallel processing format. It should be taken into account that in case the damage state of an element has non-local dependency, no conflicts should arise when using multiple threads. Of course further optimisation of the code will also result in improvements of the computational efficiency.

6.3.5 Fatigue damage

The computational efficiency of the fatigue damage is purely based on the implementation. For the current implementation, no parallel processing has been used. Just as for the cycle jumping and output processing, the fatigue damage processing can readily be casted in a parallel processing format. This is because the damage is evaluated per element which can be separated. The same remark for non-local dependency as for cycle jumping applies. Of course further optimisation of the code will also result in improvements of the computational efficiency.

6.3.6 Concluding remarks

Due to the general and high-fidelity nature of the formulation, the decrease of computational effort can only be achieved by efficient numerical implementation, parallel processing or re-formulating models so that a more efficient numerical implementation becomes feasible. A numerical efficient implementation refers to the translation from the theoretical framework/-model(s) to a software representation. Furthermore, the use of parallel processing will for most case significantly reduce the required computational time. However, care should be taken that the solution is unaffected by the use of parallel processing. On a last note, it is recommended to not impose additional assumptions on the used models, as this would harm the general and high-fidelity nature of the framework.

Chapter 7

Conclusions and recommendations

This last chapter presents the conclusions regarding the work in this report and highlights the most important recommendations for improvements and future work. The conclusions can be found in Section 7.1 and the recommendations in Section 7.2.

7.1 Conclusions

In this thesis, a framework is proposed which aims to not only accurately predict fatigue life, but also to accurately describe the damage evolution during the life of a structure. This report focused on the:

- Formulation of a unified framework
- Demonstration of the application of the framework for a Continuum Damage Model (CDM) and two Fracture Mechanics Damage Models (FMDMs)
- Start of a numerical implementation of the proposed framework.

The formulation of the framework has been kept as general as possible in order to aspire for a general high-fidelity framework. Furthermore, the chosen CDM was shown to readily fit within the proposed framework. For the Cohesive Zone Model (CZM) the modelling of the fatigue behaviour posed to be the main challenge. Furthermore, the eXtended Finite Element Method (XFEM) was shown to fit in the proposed framework as well.

The CZM formulations in literature are based on a joint Finite Element Analysis (FEA) model, whereas the proposed framework is of the disjoint type. By smearing the remaining energy of a damaged element, it was aimed to provide a fatigue formulation within the disjoint framework. The merit and accuracy of such a method has to be investigated further.

Based on the concept of the framework and the discussed CDM and FMDMs, the development of the numerical implementation of the framework is initiated. This numerical implementation was verified for the combination of the CZM and CDM for quasi-static loading. Parallel processing was incorporated in the numerical implementation in order to decrease the computational effort.

The hypothesis, as stated in Chapter 1, is as follows:

A practical implementation of the blending framework can be achieved by simulating a limited amount of cycles with a quasi-static FEA.

The hypothesis has partially been addressed in this thesis. A framework is formulated that allows for the integration (blending) of arbitrary CDMs and FMDMs and uses a quasi-static FEA in conjunction with a cycle jump algorithm. An important part of the 'practical implementation' is that the framework implementation can obtain acceptable results in terms of predictive capability of damage progression in Fibre-Reinforced Polymers (FRPs) due to quasi-static and fatigue loading; and that the analysis is performed within an acceptable time frame. Both of these aspects have to be specified on a case-by-case basis and is user dependent. However, in order to assess whether the proposed blending framework is capable of doing so, future research is required. Therefore, on a short term it is not deemed feasible to develop a fully functioning practical implementation of the framework. However, in case the work on the numerical implementation is continued and the identified challenges are tackled, it is deemed feasible to achieve a general high-fidelity implementation of the blending methodology.

7.2 Recommendations

During the development of the framework several challenges and issues have been identified. To solve these, future research and steps have to be undertaken. The recommendations are separated in different sections and each section covers a different aspect. Section 7.2.1 presents future improvements regarding the proposed framework. In Section 7.2.2, future improvements regarding the models used in the present work are provided. Furthermore, Section 7.2.3 provides recommendations regarding the required input data for the models of the framework. Finally, the recommendations for the framework implementation and validation are discussed in Section 7.2.4 and Section 7.2.5, respectively.

7.2.1 Framework

An investigation into the feasibility of the multi-analysis joint adaptive cycle jump approach (as discussed in Section 2.2.3.3) is warranted. If such an approach is feasible, it may relieve future issues related to imposing the fatigue damage after ΔN cycles are jumped. In case the disjoint approach, as discussed in the present work, is used, it is imperative that the cycle jumping procedure is validated. Cycle jumping has the potential of alleviating the computational effort of Fatigue Progressive Blended Damage Model (FPBDM), however it is not known to what extent certain assumptions can be made to formulate such a cycle jumping algorithm. This requires further work and validation.

7.2.2 Models

The recommendations related to the models used in this report are separated into several categories: general, CDM, Fatigue Progressive Continuum Damage Model (FPCDM), Quasi-Static Progressive Fracture Mechanics Damage Model (QSPFMDM) and Fatigue Progressive

Fracture Mechanics Damage Model (FPFMDM). The general category is used for recommendations that covers multiple models or are high level recommendations.

In general, it is recommended to:

- Reduce the amount of required fitting in methods to describe the material behaviour and work towards more physical-based models in order to capture the physical mechanisms at work and to be able to identify discrepancy sources of models more clearly
- Investigate the formulation of da/dN fitting models. For example, by using two fracture parameters to fully define the fatigue cycle
- Investigate possibilities to reduce the amount of required inputs.

For the CDM, it is recommended to:

- Investigate the influence of transverse non-linearity and whether it is a correct assumption to neglect the non-linear behaviour
- Further investigate the influence of shear models on the in-situ strength. If a better shear model (better correspondence to experimental data) shows worse results it is an indication that the in-situ model is not sufficient: i.e. errors imposed by the assumptions within the model seem to be compensated with a worse approximation of the shear behaviour. Therefore, it is recommended to calculate the in-situ strength with a spline fit, as generally this provides a better fit than the Ramberg-Osgood relation. Furthermore, the influence of in-situ strengths should also be investigated in the blended model that includes XFEM
- Further improve CDMs. Even though the state-of-the-art LaRC-05 shows promising results, the LaRC-05 is not able to capture all types of observed failures for all types of materials. Amongst these failures types are the cases of triaxial compression (likely due to crushing)
- Investigate the influence of using a non-linear shear model in the LaRC-05 criterion. A non-linear shear behaviour would introduce an additional failure mode that competes with the matrix cracking failure mode and may, therefore, influence the results.

For the FPCDM, it is recommended to:

- Investigate whether analytical/numerical models can be developed that rely less on experimental data by having a stronger connection to the underlying physical mechanisms. The FPCDM uses Stress-Cycle (SN) curves and Constant Life Diagrams (CLDs) to account for the fatigue damage in the CDM elements. Such models rely on experimental data that are obtained under specific circumstances, for example, specimen geometry and fatigue frequency. Hence, the validity of using this data for an arbitrary loading and geometry for the same material is debatable. Repeating these tests for a large number of combinations of variables is not feasible in terms of costs and resources. It is acknowledged that progressive models using SN curves and CLDs are the available state-of-the art CDMs but in the future it is recommended to step away from such methods. Models which are less input data exhaustive are preferred.

- Attempt to develop models for the residual strength and stiffness, that have a physical basis and rely less on experimental data. It is known that the influence of fatigue on the residual strength and stiffness is history dependent. However, to account for this influence using currently available models, experimentally determined parameters are required. For Variable Amplitude (VA) fatigue loads, this leads to an excessive amount of required experiments in order to define the influence for a variety of VA fatigue loads. This is not feasible for a high-fidelity model where the experimentally determined parameters have to account for arbitrary geometry and loading. A possible approach may be to look into models with an energy basis.
- Validate the cycle jump methodology of the FPCDM and perform a sensitivity analysis for the involved variables.

For the QSPFMDM, it is recommended to:

- Look into methods that can improve the numerical behaviour of the CZM for modelling delaminations, in terms of convergence rate. However, even with the disadvantage in terms of convergence rate, the CZM has shown to provide acceptable results and at least provides a better representation of delaminations than a CDM delamination method. An improvement in terms of the computational effort increases the feasibility of a practical implementation of the framework
- Look into CZM formulations that are less mesh dependent and thus allow for coarser meshes
- Investigate the application of the Floating Node Method (FNM) for the blending methodology for XFEM and CZMs.

For the FPFMDM, it is recommended to:

- Investigate the method for damage progression when ΔN cycles are skipped. The proposed methodology in the present work assumes that the state of the elements are constant during the cycle jumping. This poses issues when having to model the damage progression of matrix cracks and delaminations
- Investigate the merit of the proposed cycle jumping algorithms for CZM and XFEM.

7.2.3 Input data

First of all, it is imperative to obtain a consistent and complete data set that is suitable for the validation and evaluation of Progressive Blended Damage Models (PBDMs). Currently, it is not possible to obtain such a data set for a single material under the same test conditions from literature. Furthermore, having such a data set is not only beneficial for validating the framework discussed in this report, but also for the validation of a wide range of other models.

Secondly, tests that measure a certain quantity should be reviewed critically whether the measured quantity is the desired quantity. If this is not the case, it is recommended to look

into the influencing factors and try to characterise what the effects of these factors are. For example, UniDirectional (UD) data obtained from multidirectional laminates suffer from this.

Finally, it is recommended to set-up a platform that facilitates a joint database for academia to share experimental data. To set up such a database, a collaboration is required in order to determine guidelines. These guidelines should include what format the data should have and what type of documentation should accompany the input data. Both of these aspects are test dependent. Furthermore, such a platform can also allow for data requests. These data requests can reduce the amount of tests and allow for more efficient allocation of resources. Furthermore, by dictating guidelines (rules) for the documentation of the data, the quality can be guaranteed to a further extent than when these guidelines are absent.

7.2.4 Framework implementation

For the framework implementation, the primary recommendation is to continue and further investigate the work started in this report. When the implementation is finished, the validation of the methods and submethods is possible.

Recommendations related to the framework implementation as of this thesis, are to:

- Revisit the in-situ strength method. In the current implementation, the in-situ strength is evaluated during the model set-up. However, when surrounding elements start to fail, an element will experience different boundary conditions than used for the derivation of the in-situ strengths. It is expected that not taking into account this effect, introduces errors in the predictions
- Optimise the code for a decrease in computational effort.

7.2.5 Validation

The framework proposed in the present work lacks sound validation. Therefore, it is recommended to validate the merit of the framework based on experimental data. However, before validation is possible, the numerical implementation should be finished and the issues related to input data have to be solved.

References

[1] Global Aerospace Market Outlook and Forecast. Technical report AIAC Phase 3, Deloitte, October 2010. http://aiac.ca/wp-content/uploads/2015/11/AIAC-Phase-3-Report$_$FINAL.pdf (accessed April 13, 2018).

[2] A. P. Mouritz, E. Gellert, P. Burchill, and K. Challis. Review of Advanced Composite Structures for Naval Ships and Submarines. *Composite Structures*, 53(1):21–42, July 2001.

[3] V. M. Karbhari and L. Zhao. Use of Composites for 21st Century Civil Infrastructure. *Computer Methods in Applied Mechanics and Engineering*, 185(2-4):433–454, May 2000.

[4] K. Ishikawa, T.and Amaoka, Y. Masubuchi, T. Yamamoto, A. Yamanaka, M. Arai, and J. Takahashi. Overview of Automotive Structural Composites Technology Developments in Japan. *Composites Science and Technology*, 155(8):221–246, February 2018.

[5] J. A. Pascoe, R. C. Alderliesten, and R. Benedictus. Methods for the Prediction of Fatigue Delamination Growth in Composites and Adhesive Bonds - A Critical Review. *Engineering Fracture Mechanics*, 112-113:72–96, November 2013.

[6] B. R. van Dongen. *Progressive Damage Modelling of FRPs using a Blendend Stress-Strain and Fracture Mechanics Approach in FEM.* Master of science thesis, Delft University of Technology, Faculty of Aerospace Engineering, Delft, June 2017.

[7] A. P. van Oostrum. *Application of Fracture Mechanics in a Blended Numerical Framework for Progressive Damage Analysis of CFRPs in FEM.* Master of science thesis, Delft University of Technology, Faculty of Aerospace Engineering, Delft, October 2017.

[8] A. M. Mitrousias. *Predicting Residual Strength of Composites After Cyclic Loading: A Numerical, Progressive Damage Analysis Based Approach.* Master of science thesis, Delft University of Technology, Faculty of Aerospace Engineering, Delft, July 2017.

[9] E. N. Eliopoulos. *Numerical Simulation of Damage Progression in GFRP Composites under Cyclic Loading.* Phd thesis, University of Patras, Patras, July 2013.

[10] Y. Nikishkov, A. Makeev, and G. Seon. Progressive Fatigue Damage Simulation Method for Composites. *International Journal of Fatigue*, 48:266–279, March 2013.

[11] O. J. Nixon-Pearson, S. R. Hallett, P. J. Withers, and J. Rouse. Damage Development in Open-Hole Composite Specimens in Fatigue. Part 1: Experimental Investigation. *Composite Structures*, 106:882–889, December 2013.

[12] I. Rychlik. A New Definition of the Rainflow Cycle Counting Method. *International Journal of Fatigue*, 9(2):119–121, April 1987.

[13] P. Maimi, P. P. Camanho, J. A. Mayugo, and C. G. Davila. A Continuum Damage Model for Composite Laminates: Part I - Constitutive Model. *Mechanics of Materials*, 39(10):897–908, October 2007.

[14] P. Robinson, U. Galvanetto, D. Tumino, G. Bellucci, and D. Violeau. Numerical Simulation of Fatigue-Driven Delamination Using Interface Elements. *International Journal for Numerical Methods in Engineering*, 63(13):1824–1848, August 2005.

[15] A. Turon, J. Costa, P. P. Camanho, and C. G. Davila. Simulation of Delamination in Composites Under High-cycle Fatigue. *Composites: Part A*, 38(11):2270–2282, November 2007.

[16] L. F. Kawashita and S. R. Hallett. A Crack Tip Tracking Algorithm for Cohesive Interface Element Analysis of Fatigue Delamination Propagation in Composite Materials. *International Journal of Solids and Structures*, 49(21):2898–2913, October 2012.

[17] M. M. Shokrieh and L. B. Lessard. Progressive Fatigue Damage Modeling of Composite Materials, Part I: Modeling. *Journal of Composite Materials*, 34(13):1056–1080, July 2000.

[18] W. Van Paepegem and J. Degrieck. Modelling Strategies for Fatigue Damage Behaviour of Fibre-Reinforced Polymer Composites. *European Journal of Mechanical and Environmental Engineering*, 46(4):217–227, 2001.

[19] H. Altenbach, J. Altenbach, and W. Kissing. *Mechanics of Composite Structural Elements*. Springer, 152 Beach Road, Gateway East, Singapore 189721, Singapore, 2018.

[20] A. V. Murty and S. Vellaichamy. On Higher Order Shear Deformation Theory of Laminated Composite Panels. *Composite Structures*, 8(4):247–270, 1987.

[21] F.-K. Chang and K.Y. Chang. A Progressive Damage Model for Laminated Composites Containing Stress Concentrations. *Journal of Composite Materials*, 21(9):834–855, September 1987.

[22] K. I. Tserpes, G. Labeas, P. Papanikos, and Th. Kermanidis. Strength Prediction of Bolted Joints in Graphite/Epoxy Composite Laminates. *Composites: Part B*, 33(7):521–529, October 2002.

[23] H. M. Deuschle. *3D Failure Analysis of UD Fibre Reinforced Composites: Puck's Theory Within FEA*. Phd thesis, University of Stuttgart, Institute of Statics and Dynamics of Aerospace Structures, September 2010.

[24] D. H. Robbins and J. N. Reddy. Modelling of Thick Composites Using a Layerwise Laminate Theory. *International Journal for Numerical Methods in Engineering*, 36(4):655–677, February 1993.

[25] I. Lapczyk and J. A. Hurtado. Progressive Damage Modeling in Fiber-Reinforced Materials. *Composites: Part A*, 38(11):2333–2341, November 2007.

[26] S. T. Pinho, C. G. Davila, P. P. Camanho, L. Iannucci, and P. Robinson. Failure Models and Criteria for FRP Under In-Plane or Three-Dimensional Stress States Including Shear Non-Linearity. Technical Memorandum NASA/TM-2005-213530, National Aeronautics and Space Administration, Hampton, Virgina 23681-2199, United States of America, February 2005.

[27] E. Carrera. An Assessment of Mixed and Classical Theories on Global and Local Response of Multilayered Orthotropic Plates. *Composite Structures*, 50(2):183–198, October 2000.

[28] A. S. Kaddour, M. J. Hinton, and P. D. Soden. *Failure Criteria in Fibre Reinforced Polymer Composites: The World-Wide Failure Exercise*. Elsevier Ltd, Oxford, 1st edition, 2004.

[29] A. Puck and H. Schurmann. Failure Analysis of FRP Laminates by Means of Physically Based Phenomenological Models. *Composites Science and Technology*, 62(12-13):1633–1662, September-October 2002.

[30] M. J. Hinton and A. S. Kaddour. Triaxial Test Results for Fibre-Reinforced Composites: The Second World-Wide Failure Exercise Benchmark Data. *Journal of Composite Materials*, 47(6-7):653–678, March 2013.

[31] J. S. Welsh, A.C. Biskner, and E. E. Nelson. Experimental and Numerical Failure Predictions of Biaxially-Loaded Unidirectional Carbon Composite Laminates. In *17th International Conference on Composite Materials*, Edinburgh, United Kingdom, July 2009. IOM Communications Ltd. http://www.iccm-central.org/Proceedings/ICCM17proceedings/Themes/Behaviour/COMPOSITES%20TEST%20&%20MODEL%20ID/F5.1%20Welsh.pdf (accessed January 15, 2018).

[32] M. R. Garnich and V. M. K. Akula. Review of Degradation Models for Progressive Failure Analysis of Fiber Reinforced Polymer Composites. *Applied Mechanics Reviews*, 62(1):1–33, January 2009.

[33] H. T. Hahn and S. W. Tsai. Nonlinear Elastic Behavior of Unidirectional Composite Laminae. *Journal of Composite Materials*, 7(1):102–118, January 1973.

[34] A. Sabik. Direct Shear Stress vs Strain Relation of Fiber Reinforced Composites. *Composites Part B*, 139:24–30, April 2018.

[35] T. A. Bogetti, C. P. R. Hoppel, V. M. Harik, J. F. Newill, and B. P. Burns. Predicting the Nonlinear Response and Progressive Failure of Composite Laminates. *Composites Science and Technology*, 64(3-4):329–342, March 2004.

[36] C. A. Rose, C. G. Davila, and F. A. Leone. Analysis Methods for Progressive Damage of Composite Structures. Technical Memorandum NASA/TM-2013-218024, Langley Research Center, Hampton, Virginia, United States of America, July 2013.

[37] S. Johnson, L. Kang, and H. M. Akil. Mechanical Behaviour of Jute Hybrid Bio-Composites. *Composites Part B*, 91:83–93, April 2016.

[38] S.M Mohensi Shakib and S. Li. Modified Three Rail Shear Fixture (ASTM D 4255/D 4225M) and an Experimental Study of Nonlinear In-Plane Shear Behaviour of FRC. *Composites Science and Technology*, 69(11-12):1854–1866, September 2009.

[39] C. T. McCarthy. A Cubic Spline Implementation of Non-linear Shear Behaviour in Three-Dimensional Progressive Damage Models for Composite Laminates. *Composite Structures*, 92(1):173–181, January 2010.

[40] A. Hallonet, L. Michel, and E. Ferrier. Investigation of the Bond Behaviour of Flax FRP Strengthened RC Structures Through Double Lap Shear Testing. *Composites Part B*, 100:247–256, September 2016.

[41] J. E. Yetman, A. J. Sobey, J. I. R. Blake, and R. A. Shenoi. Mechanical and Fracture Properties of Glass Vinylester Interfaces. *Composites Part B*, 130:38–45, December 2017.

[42] J. J. More. The Levenberg-Marquardt Algorithm: Implementation and Theory. In G. A. Watson, editor, *Numerical Analysis. Lecture Notes in Mathematics. Volume 630.*, pages 105–116. Springer, Berlin, Heidelberg, 1978.

[43] M. V. Shcherbakov, A. Brebels, N. L. Shcherbakova, A. P. Tyukov, T. A. Janovsky, and V. A. Kamaev. A Survey of Forecast Error Measures. *World Applied Sciences Journal (Information Technologies in Modern Industry, Education and Society)*, 24(24):171–176, January 2013.

[44] J. S. Armstrong and F. Collopy. Error Measures for Generalizing About Forecasting Methods: Empirical Comparisons. *International Journal of Forecasting*, 8(1):69–80, June 1992.

[45] P. P. Camanho, C. G. Davila, S. T. Pinho, L. Iannucci, and P. Robinson. Prediction of In Situ Strengths and Matrix Cracking in Composites Under Transverse Tension and In-Plane Shear. *Composites: Part A*, 37(2):165–176, February 2006.

[46] S. Wicaksono and G. B. Chai. A Review of Advances in Fatigue and Life Prediction of Fibe-Reinforced Composites. *Journal of Materials: Design and Applications*, 227(3):179–195, July 2012.

[47] P. P. Camanho, C. G. Davila, and M. F. de Moura. Numerical Simulation of Mixed-Mode Progressive Delamination in Composite Materials. *Journal of Composite Materials*, 37(16):1415–1438, August 2003.

[48] R. Krueger. Virtual Crack Closure Technique: History, Approach and Applications. *Applied Mechanical Reviews*, 57(2):109–143, March 2004.

[49] S. Mohammadi. *XFEM Fracture Analysis of Composites*. John Wiley & Sons. Ltd, The Atrium, Southern Gate, Chichester, West Sussex, PO19 8SQ, United Kingdom, 2012.

[50] S.T. Pinho, R. Darvizeh, P. Robinson, C. Schuecker, and P. P. Camanho. Material and Structural Response of Polymer-Matrix Fibre-Reinforced Composites. *Journal of Composite Materials*, 46(19-20):2313–2341, September 2012.

[51] S. Pimenta, R. Gutkin, S. T. Pinho, and P. Robinson. A Micromechanical Model for Kink-band Formation: Part I - Experimental Study and Numerical Modelling. *Composites Science and Technology*, 69(7-8):948–955, June 2009.

[52] R. Gutkin, S. T. Pinho, P. Robinson, and P. T. Curtis. Micro-Mechanical Modelling of Shear-Driven Fibre Compressive Failure and of Fibre Kinking for Failure Envelope Generation in CFRP Laminates. *Composites Science and Technology*, 70(8):1214–1222, August 2010.

[53] R. Gutkin, S. T. Pinho, P. Robinson, and P. T. Curtis. A Finite Fracture Mechanics Formulation to Predict Fibre Kinking and Splitting in CFRP Under Combined Longitudinal Compression and In-plane Shear. *Mechanics of Materials*, 43(11):730–739, November 2011.

[54] P. P. Camanho and F. L. Matthews. A Progressive Damage Model for Mechanically Fastened Joints in Composite Laminates. *Journal of Composite Materials*, 33(24):2248–2280, December 1999.

[55] A. Puck and H. Schurmann. Failure Analysis of FRP Laminates by Means of Physically Based Phenomenological Models. *Composite Science and Technology*, 58(7):1045–1067, July 1998.

[56] W.-G. Jiang, S. R. Hallett, B. G. Green, and M. R. Wisnom. A Concise Interface Constitutive Law for Analysis of Delamination and Splitting in Composite Materials and its Application to Scaled Notched Tensile Specimens. *International Journal for Numerical Methods in Engineering*, 69(9):1982–1995, 2007.

[57] M. R. Wisnom and F.-K. Chang. Modelling of Splitting and Delamination in Notched Cross-Ply Laminates. *Composites Science and Technology*, 60(15):2849–2856, November 2000.

[58] G. Vigueras, F. Sket, C. Samaniego, L. Wu, L. Noels, D. Tjahjanto, E. Casoni, G. Houzeaux, A. Makradi, M. Molina-Aldareguia, J. M. an Vazquez, and A. Jerusalem. An XFEM/CZM Implementation for Massively Parallel Simulations of Composite Fracture. *Composite Structures*, 125:542–557, July 2015.

[59] F. P. van der Meer, C. Oliver, and L. J. Sluys. Computational Analysis of Progressive Failure in a Notched Laminate Including Shear Nonlinearity and Fiber Failure. *Composites Science and Technology*, 70(4):692–700, April 2010.

[60] B. Y. Chen, T. E. Tay, S. T. Pinho, and V. B. C. Tan. Modelling the Tensile Failure of Composites with the Floating Node Method. *Computer Methods in Applied Mechanics and Engineering*, 308(15):414–442, August 2016.

[61] T. Belytschko and T. Black. Elastic Crack Growth in Finite Elements with Minimal Remeshing. *International Journal for Numerical Methods in Engineering*, 45(5):601–620, April 1999.

[62] A. Hansbo and P. Hansbo. A Finite Element Method for the Simulation of Strong and Weak Discontinuities in Solid Mechanics. *Computer Methods in Applied Mechanics and Engineering*, 193(33-35):3523–3540, August 2004.

[63] J.-H. Song, P. M. A. Areias, and T. Belytschk. A Method for Dynamic Crack and Shear Band Propagation with Phantom Nodes. *International Journal For Numerical Methods in Engineering*, 67(6):868–893, February 2006.

[64] S. T. Pinho, B. Y. Chen, N. V. De Carvalho, P. M. Baiz, and T. E. Tay. A Floating Node Method for the Modelling of Discontinuities Within a Finite Element. In *The 19th International Conference on Composite Materials*, Montreal, Quebec, Canada, July 2013. https://ntrs.nasa.gov/search.jsp?R=20140000841 (accessed June 20, 2018).

[65] N. V. De Carvalho, B. Y. Chen, S. T. Pinho, P. M. Baiz, J. G. Ratcliffe, and T. E. Tay. Floating Node Method and Virtual Crack Closure Technique for Modeling Matrix Cracking-Delamination Migration. In *The 19th International Conference on Composite Materials*, Montreal, Quebec, Canada, July 2013.

[66] Simulia. Abaqus 6.14, Analysis User's Guide, Section 10.7: Modeling Discontinuities as an Enriched Feature Using the Extended Finite Element Method. Online. http://localhost:2080/v6.14/books/usb/default.htm?startat=pt04ch10s07at36.html#usb-anl-aenrichment-cohesive (accessed May 20, 2018).

[67] X. Lu, B. Y. Chen, V. B. C. Tan, and T. E. Tay. Adaptive Floating Node Method for Modelling Cohesive Fracture of Composite Materials. *Engineering Fracture Mechanics*, 194:240–261, May 2018.

[68] E. Giner, N. Sukumar, J. E. Tarancon, and F. J. Fuenmayor. An Abaqus Implementation of the Extended Finite Element Method. *Engineering Fracture Mechanics*, 76(3):347–368, February 2009.

[69] J. D. Lee. Three Dimensional Finite Element Analysis of Damage Accumulation in Composite Laminate. *Computers and Structures*, 15(3):335–350, 1982.

[70] O. O. Ochoa and J. J. Engblom. Analysis of Progressive Failure in Composites. *Composites Science and Technology*, 28(2):87–102, 1987.

[71] R. S. Long. Static Strength of Adhesively Bonded ARALL-1 Joints. *Journal of Composite Materials*, 25(4):391–415, April 1991.

[72] M. M. Shokrieh, L. B. Lessard, and C. Poon. Three-Dimensional Progressive Failure Analysis of Pin/Bolt Loaded Composite Laminates. In *83rd Meeting of the AGARD Structures and Materials Panel*, Florence, Italy, September 1996.

[73] L. Tong. An Assessment of Failure Criteria to Predict the Strength of Adhesively Bonded Composite Double Lap Joints. *Journal of Reinforced Plastics and Composites*, 16(8):698–713, May 1997.

[74] P. Elisa. Virtual Crack Closure Technique and Finite Element Method for Predicting the Delamination Growth Initiation in Composite Structures. *Advances in Composite*

Materials - Analysis of Natural and Man- Made Materials, pages 462–480, September 2011.

[75] F. Shen, K. H. Lee, and T. E. Tay. Modeling Delamination Growth in Laminated Composites. *Composites Science and Technology*, 61(9):1239–1251, July 2001.

[76] X. J. Fang, Q. D. Yang, B. N. Cox, and Z. Q. Zhou. An Augmented Cohesive Zone Element for Arbitrary Crack Coalescence and Bifurcation in Heterogeneous Materials. *International Journal For Numerical Method in Engineering*, 88(9):841–861, April 2011.

[77] S. C. Pradhan and T. E. Tay. Three-Dimensional Finite Element Modelling of Delamination Growth in Notched Composite Laminates Under Compression Loading. *Engineering Fracture Mechanics*, 60(2):157–171, May 1998.

[78] C. G. Davila and C. Bisagni. Fatigue Life and Damage Tolerance of Postbuckled Composite Stiffened Structures with Initial Delamination. *Composite Structures*, 161:73–84, February 2017.

[79] L. Lampani. Finite Element Analysis of Delamination of a Composite Component with the Cohesive Zone Model Technique. *Engineering Computations: International Journal for Computer-Aided Engineering and Software*, 28(1):30–46, 2011.

[80] J. Ankersen and G. A. O. Davies. Interface Elements - Advantages and Limitations in CFRP Delamination Modelling. In W. M. Banks and M. R Wisnom, editors, *17th International Conference on Composite Materials*, Edinburgh, UK, July 2009.

[81] B. L. V. Bak, A. Turon, E. Lindgaard, and E. Lund. A Simulation Method for High-Cycle Fatigue-Driven Delamination Using a Cohesive Zone Model. *International Journal for Numerical Methods in Engineering*, 106(3):163–191, April 2016.

[82] A. Pirondi, G. Giuliese, F. Moroni, A. Bernasconi, and A. Jamil. Comparative Study of Cohesive Zone and Virtual Crack Closure Techniques for Three-Dimensional Fatigue Debonding. *The Journal of Adhesion*, 90(5-6):457–481, 2014.

[83] J. Echaabi, F. Trochu, and R. Gauvin. Review of Failure Criteria of Fibrous Composite Materials. *Polymer Composites*, 17(6):786–798, December 1996.

[84] A. C. Orifici, I. Herszberg, and R. S. Thomson. Review of Methodologies for Composite Material Modelling Incorporating Failure. *Composite Structures*, 86(1-3):194–210, November 2008.

[85] R. Talreja. Assessment of the Fundamentals of Failure Theories for Composite Materials. *Composites Science and Technology*, 105(10):190–201, December 2014.

[86] V. D. Azzi and S. W. Tsai. Anisotropic Strength of Composites. *Experimental Mechanics*, 5(9):283–288, September 1965.

[87] A. Makinde, K. W. Neale, and Z. Sacharuk. A Strain-Based Parametric Biaxial Failure Criterion for Fiber-Reinforced Composites. *Polymer Composites*, 13(4):263–272, August 1992.

[88] P. Labossiere and K. W. Neale. A General Strength Theory for Orthotropic Fiber-Reinforced Composite Laminae. *Polymer Composites*, 9(5):306–317, October 1988.

[89] K. W. Neale and P. Labossiere. Failure of Composite Laminae Under Biaxial Loading. *Polymer Composites*, 10(5):285–292, October 1989.

[90] S. C. Tan and S. Cheng. Failure Criteria for Fibrous Anisotropic Materials. *Journal of Material in Civil Engineering*, 5(2):198–211, May 1993.

[91] W. K. Lim, W. K. Jeong, and E. K. Tschegg. Failure of Fibrous Anisotropic Materials Under Combined Loading. *Composites Part B: Engineering*, 41(1):94–97, January 2010.

[92] Z. Hashin and A. Rotem. A Fatigue Failure Criterion for Fiber Reinforced Materials. Technical Report AFOSR-TR-73-0686, Air Force Office of Scientific Research, 1400 Wilson Boulevard, Arlington, Virgina, United States of America, March 1973.

[93] Z. Hashin. Failure Criteria for Unidirectional Fiber Composites. *Journal of Applied Mechanics*, 47(2):329–334, June 1980.

[94] R. G. Cuntze and A. Freund. The Predictive Capability of Failure Mode Concept-Based Strength Criteria for Multidirectional Laminates. *Composites Science and Technology*, 64(3-4):343–377, March 2004.

[95] C. G. Davila, P. P. Camanho, and C. A. Rose. Failure Criteria for FRP Laminates. *Journal of Composite Materials*, 39(4):323–345, February 2005.

[96] P. P. Camanho and C. G. Davila. Mixed-Mode Decohesion Finite Elements for the Simulation of Delamination in Composite Materials. Technical report TM-2002-211737, National Aeronautics and Space Administration, Langley Research Center, Hampton, Virginia 23681-2199, United States of America, June 2002.

[97] A. Turon, P. P. Camanho, J. Costa, and C. G. Davila. A Damage Model for the Simulation of Delamination in Advanced Composites Under Variable-Mode Loading. *Mechanics of Materials*, 38(11):1072–1089, November 2006.

[98] R. Khan. *Delamination Growth in Composites Under Fatigue Loading*. Phd dissertation, Delft University of Technology, Faculty of Aerospace Engineering, Delft, October 2013.

[99] N. Blanco Villaverde. *Variable Mixed-Mode Delamination in Composite Laminates Under Fatigue Conditions: Testing & Analysis*. Phd dissertation, Universitat de Girona, Faculty of Mechanical Engineering and Industrial Construction,Girona, October 2004.

[100] H. M. Jensen and I. Sheinman. Straight-sided, Buckling-Driven Delamination of Thin Films at High Stress Levels. *International Journal of Fracture*, 110(4):371–385, August 2001.

[101] E. H. Glaessgen, I. S. Raju, and C. C. Poe Jr. Analytical and Experimental Studies of the Debonding of Stitched and Unstitched Composite Joints. *Journal of Composite Materials*, 36(23):2599–2622, December 2002.

[102] J. Li and J. K. Sen. Analysis of Frame-To-Skin Joint Pull-Off Tests and Prediction of the Delamination Failure. In *42nd AIAA/ASME/ASCE/AHS/ASC Structures, Structural Dynamics, and Materials Conference and Exhibit*, number AIAA-2001-1484, Seattle, Washington, United States of America, April 2001. AIAA.

[103] J. Li. Three-Dimensional Effect in the Prediction of Flange Delamination in Composite Skin-Stringer Pull-Off Specimens. *Journal of Composites Technology and Research*, 24(2):182–189, July 2002.

[104] J. Li, S. M. Lee, E. W. Lee, and T. K. O'Brien. Evaluation of the edge crack torsion (ect) test for mode iii interlaminar fracture toughness of laminated composites. Technical Memorandum NASA-TM-110264, National Aeronautics and Space Administration, Langley Research Center, Hampton, Virginia, United States of America, August 1996.

[105] E. M. Wu and R. C. Reuter Jr. Crack Extension in Fiberglass Reinforced Plastics. Technical report 275, University of Illinois, Urbana, Illinois, United States of America, February 1965.

[106] M. L. Benzeggagh and M. Kenane. Measurement of Mixed-Mode Delamination Fracture Toughness of Unidirectional Glass/Epoxy Composites with Mixed-Mode Bending Apparatus. *Composites Science and Technology*, 56(4):439–449, 1996.

[107] J. R. Reeder. An Evaluation of Mixed-Mode Delamination Failure Criteria. Technical Memorandum 104210, National Aeronautics and Space Administration, Langley Research Center, Hampton, Virginia 23665, United States of America, February 1992.

[108] S. T. Pinho, L. Iannucci, and P. Robinson. Formulation and Implementation of Decohesion Elements in an Explicit Finite Element Code. *Composites: Part A*, 37(5):778–789, May 2006.

[109] A. Amiri-Rad and M. Mashayekhi. A Cohesive Zone Approach for Fatigue-Driven Delamination Analysis in Composite Materials. *Applied Composite Materials*, 24(4):751–769, August 2017.

[110] M. E. Pachajoa, M. K. Frances, and J. D. Lee. Stress and Failure Analysis of Composite Structures. *Engineering Fracture Mechanics*, 50(5-6):883–902, March-April 1995.

[111] C. T. McCarthy, M. A. McCarthy, and V. P. Lawlor. Progressive Damage Analysis of Multi-Bolt Composite Joints with Variable Bolt-Hole Clearances. *Composites: Part B*, 36(4):290–305, June 2005.

[112] K. Park and G. H. Paulino. Cohesive Zone Models: A Critical Review of Traction-Separation Relationships Across Fracture Surfaces. *Applied Mechanics Reviews*, 64(6):1–20, November 2011.

[113] S. T. Pinho. *Modelling Failure of Laminated Composites Using Physically-Based Failure Models*. Phd thesis, Imperial College London, London SW7 2AZ, U.K., 2005.

[114] F. P. van der Meer and L. J. Sluys. Continuum Models for the Analysis of Progressive Failure in Composite Laminates. *Journal of Composite Materials*, 43(20):2131–2156, September 2009.

[115] C. Zhang, N. Li, W. Wang, W. K. Binienda, and H. Fang. Progressive Damage Simulation of Triaxially Braided Composite Using a 3D Meso-Scale Finite Element Model. *Composite Structures*, 125:104–116, July 2015.

[116] S. T. Pinho, P. Robinson, and L. Iannucci. Fracture Toughness of the Tensile and Compressive Fibre Failure Modes in Laminated Composites. *Composites Science and Technology*, 66(13):2069–2079, October 2006.

[117] M. W. Czabaj and J. Ratcliffe. Comparison of Intralaminar and Interlaminar Mode-I Fracture Toughness of Unidirectional IM7/8552 Graphite/Epoxy Composite. In *15th US-Japan Conference on Composite Materials*, Arlington, Texas, United States of America, October 2012.

[118] G. Catalanotti and J. Xavier. Measurement of the Mode II Intralaminar Fracture Toughness and R-curve of Polymer Composites Using a Modified Iosipescu Specimen and the Size Effect Law. *Engineering Fracture Mechanics*, 138:202–214, Apri 2015.

[119] J. Andersons, E. Sparnins, and R. Joffe. The Onset of Mixed-Mode Intralaminar Cracking in a Cross-Ply Composite Laminate. *Mechanics of Composite Materials*, 44(6):549–556, December 2008.

[120] J. Degrieck and W. Van Paepgem. Fatigue Damage Modeling of Fibre-Reinforced Composite Materials. *Applied Mechanics Reviews*, 54(4):279–300, July 2001.

[121] W. Lian and W. Yao. Fatigue Life Prediction of Composite Laminates by FEA Simulation Method. *International Journal of Fatigue*, 32(1):123–133, January 2010.

[122] E. N. Eliopoulos and T. P. Philippidis. A Progressive Damage Simulation Algorithm for GFRP Composites Under Cyclic Loading. Part I: Material Constitutive Model. *Composites Science and Technology*, 71(5):742–749, March 2011.

[123] A. A. R. Broer. *Fatigue Life Prediction of Carbon Fibre-Reinforced Epoxy Laminates Using a Single S-N Curve*. Master thesis, Delft University of Technology, Faculty of Aerospace Engineering, Delft, May 2018.

[124] T. Philippidis and A. Vassilopoulos. Life Prediction Methodology for GFRP Laminates Under Spectrum Loading. *Composites Part A: Applied Science and Manufacturing*, 35(6):657–666, June 2004.

[125] A Vassilopoulos, B. Manshadi, and T. Keller. Influence of the Constant Life Diagram Formulation on the Fatigue Life Prediction of Composite Materials. *International Journal of Fatigue*, 32(4):659–669, April 2010.

[126] B. Harris. A Parametric Constant-Life Model for Prediction of the Fatigue Lives of Fibre-Reinforced Plastics. In B. Harris, editor, *Fatigue in Composites: Science and Technology of the Fatigue Response FIbre-reinforced Plastics*, pages 546–568. Woodhead Publishing Limited, 2003.

[127] G. Boerstra. The Multislope Model: A New Description for the Fatigue Strength of Glass Fibre Reinforced Plastic. *International Journal of Fatigue*, 29(2):1571–1576, August 2007.

[128] C. Kassapoglou. Fatigue Life Prediction of Composite Structures Under Constant Amplitude Loading. *Journal of Composite Materials*, 41(22):2737–2753, November 2007.

[129] M. Ciavarella, V. Vinogradov, and G. Carbone. A Critical Assessment on Kassapoglou's Statistical Model For Composite Fatigue. October 2013. https://www.researchgate.net/publication/257409820_A_critical_assessment_on_%27s_statistical_model_for_composites_fatigue (accessed November 25, 2017).

[130] J. Tomblin and W. Seneviratne. Determining the Fatigue Life of Composite Aircraft Structures Using Life and Load-Enhancement Factors. Technical Report DOT/FAA/AR-10/6, Federal Aviation Administration (FAA), Springfield, Virginia 22161, United States of America, June 2011. http://www.tc.faa.gov/its/worldpac/techrpt/ar10-6.pdf (accessed November 25, 2017).

[131] A. Vassilopoulos, B. Manshadi, and T. Keller. Influence of the Constant Life Diagram Formulation on the Fatigue Life Prediction of Composite Materials. *International Journal of Fatigue*, 32(4):659–669, April 2010.

[132] R. Nijssen. OptiDat Database. Knowledge Centre WMC, Juli 2014. http://www.wmc.eu/optimatblades_optidat.php (accessed February 4, 2018).

[133] N. L. Post, S. W. Case, and J. J. Lesko. Modeling the Variable Amplitude Fatigue of Composite Materials: A Review and Evaluation of the State of the Art for Spectrum Loading. *International Journal of Fatigue*, 30(12):2064–2086, December 2008.

[134] N.L. Post, J. J. Lesko, and S. W. Case. Chapter 3: Residual Strength Fatigue Theories for Composite Materials. In A. P. Vassilopoulos, editor, *Fatigue Life Prediction of Composites and Composite Structures*, pages 79–101. Woodhead Publishing, 2010.

[135] V. A. Passipoularidis and T. P. Philippidis. Strength Degradation Due to Fatigue in Fiber Dominated Glass/Epoxy Composites: A Statistical Approach. *Journal of Composite Materials*, 43(9):997–1013, May 2009.

[136] Philippidis. T. P. and V. A. Passipoularidis. Residual Strength After Fatigue in Composites: Theory vs Experiment. *International Journal of Fatigue*, 29(12):2104–2116, December 2007.

[137] S. Sarkani, G. Michaelov, D. P. Kihl, and D. L. Bonanni. Comparative Study of Nonlinear Damage Accumulation Models in Stochastic Fatigue of FRP Laminates. *Journal of Structural Engineering*, 127(3):314–322, March 2001.

[138] J. R. Schaff and B. D. Davidson. Life Prediction Methodology for Composite Structures. Part I - Constant Amplitude and Two-Stress Level Fatigue. *Journal of Composite Materials*, 31(2):128–157, January 1997.

[139] J. R. Schaff and B. D. Davidson. Life Prediction Methodology for Composite Structures. Part II - Spectrum Fatigue. *Journal of Composite Materials*, 31(2):158–181, January 1997.

[140] S. Ogin, P. Smith, and W. Beaumont. Matrix Cracking and Stiffness Reduction During the Fatigue of a (0/90)s GFRP Laminate. *Composites Science and Technology*, 22(1):23–31, 1985.

[141] F. Taheri-Behrooz, M. Shokrieh, and L. Lessard. Residual Stiffness in Cross-Ply Laminates Subjected to Cyclic Loading. *Composite Structures*, 85(3):205–212, October 2008.

[142] A. Varvani-Farahani and A. Shirazi. A Fatigue Damage Model for (0/90) FRP Composites Based on Stiffness Degradation of 0 and 90 Composite Plies. *Reinforced Plastics and Composites*, 26(13):1319–1336, September 2007.

[143] W. van Paepegem. Chapter 4: Fatigue Damage Modelling of Composite Materials with the Phenomenological Residual Stiffness Approach. In A. P. Vassilopoulos, editor, *Fatigue Life Prediction of Composites and Composite Structures*, pages 102–138. Woodhead Publishing, 2010.

[144] A. Shirazi and A. Varvani-Farahani. A Stiffness Degradation Based Fatigue Damage Model for FRP Composites of $0/\theta$ Laminate Systems. *Applied Composite Materials*, 17(2):137–150, April 2010.

[145] C. Soutis and M. Kashtaylan. Residual Stiffness of Cracked Cross-ply Composite Laminates Under Multi-Axial In-Plane Loading. *Applied Composite Materials*, 18(1):31–43, February 2011.

[146] L. E. Asp, A. Sjogren, and E. S. Greenhalgh. Delamination Growth and Thresholds in a Carbon/Epoxy Composite Under Fatigue Loading. *Journal of Composites Technology and Research*, 23(2):55–68, April 2001.

[147] J. Zhang, L. Peng, L. Zhao, and B. Fei. Fatigue Delamination Growth Rates and Threshold of Composite Laminates Under Mixed Mode Loading. *International Journal of Fatigue*, 40:7–15, July 2012.

[148] M. Kenane, Z. Azari, S. Benmedakhene, and M. L. Benzeggagh. Experimental Development of Fatigue Delamination Threshold Criterion. *Composites: Part B*, 42(3):367–375, April 2011.

[149] C. Tao, J. Qiu, W. Yao, and H. Ji. A Novel Method for Fatigue Delamination Simulation in Composite Laminates. *Composites Science and Technology*, 128:104–115, May 2016.

[150] C. Rans, R. Alderliesten, and R. Benedictus. Misinterpreting the Results: How Similitude Can Improve Our Understanding of Fatigue Delamination Growth. *Composites Science and Technology*, 71(2):230–238, January 2011.

[151] J. A. Pascoe, R. C. Alderliesten, and R. Benedictus. On the Relationship Between Disbond Growth and the Release of Strain Energy. *Engineering Fracture Mechanics*, 133:1–13, January 2015.

[152] N. Blanco, E. K. Gamstedt, L. E. Asp, and J. Costa. Mixed-Mode Delamination Growth in Carbon-Fibre Composite Laminates Under Cyclic Loading. *International Journal of Solids and Structures*, 41(15):4219–4235, July 2004.

[153] P. W. Harper and S. R. Hallett. A Fatigue Degradation Law for Cohesive Interface Elements - Development and Application to Composite Materials. *International Journal of Fatigue*, 32(11):1774–1787, November 2010.

[154] D. B. Burger. *Mixed-Mode Fatigue Disbond on Metallic Bonded Joints*. Phd dissertation, Delft University of Technology, Faculty of Aerospace Engineering, Delft, February 2015.

[155] B. G. Green, M. R. Wisnom, and S. R. Hallett. An Experimental Investigation Into the Tensile Strength Scaling of Notched Composites. *Composites Part A: Applied Science and Manufacturing*, 38(3):867–878, March 2007.

[156] A. M. Prior. Applications of Implicit and Explicit Finite Element Techniques to Metal Forming. *Journal of Materials Processing Technology*, 45(1-4):649–656, September 1994.

[157] J. S. Sun, K. H. Lee, and H. P. Lee. Comparison of Implicit and Explicit Finite Element Methods for Dynamic Problems. *Journal of Materials Processing Technology*, 105(1-2):110–118, September 2000.

[158] D. Y. Yang, D. W. Jung, I. S. Song, D. J. Yoo, and J. H. Lee. Comparative Investigation into Implicit, Explicit and Iterative Implicit/Explicit Schemes for the Simulation of Sheet-Metal Forming Processes. *Journals of Materials Processing Technology*, 50(1-4):39–53, March 1995.

[159] J. Kim, Y. H. Kang, H. H. Choi, S. M. Hwang, and B. S. Kang. Comparison of Implicit and Explicit Finite-Element Methods for the Hydroforming Process of an Automobile Lower Arm. *Advanced Manufacturing Technology*, 20(6):407–413, September 2002.

[160] M. Yousaf, Z. A. Siddiqi, M. B. Sharif, and A. U. Qazi. Force- and Displacement-Controlled Non-Linear FE Analyses of RC Beam with Partial Steel Bonded Length. *International Journal of Civil Engineering*, 15(4):499–513, June 2017.

[161] Simulia. Abaqus 6.14, Abaqus User Subroutines Reference Guide, Section 1.1.41: UMAT. Online. http://localhost:2080/v6.14/books/sub/default.htm (accessed May 20, 2018).

[162] A. Turon, C. G. Davila, P. P. Camanho, and J. Costa. An Engineering Solution for Mesh Size Effects in the Simulation of Delamination Using Cohesive Zone Models. *Engineering Fracture Mechanics*, 74(10):1665–1682, July 2007.

[163] P. W. Harper and S. R. Hallett. Cohesive Zone Length in Numerical Simulations of Composite Delamination. *Engineering Fracture Mechanics*, 75(16):4774–4792, November 2008.

[164] N. Moes and T. Belytschko. Extended Finite Element Method for Cohesive Crack Growth. *Engineering Fracture Mechanics*, 69(7):813–833, May 2002.

[165] A. Carpinteri, P. Cornetti, F. Barpi, and S. Valente. Cohesive Crack Model Description of Ductile to Brittle Size-Scale Transition: Dimensional Analysis vs. Renormalization Group Theory. *Engineering Fracture Mechanics*, 70(14):1809–1839, September 2003.

[166] C. G. Davila, P. P. Camanho, and M. F. S. F. de Moura. Mixed-Mode Decohesion Elements for Analyses of Progressive Delamination. In *42nd AIAA/ASME/ASCE/AHS/ASC Structures, Structural Dynamics and Materials Conference*, number AIAA-01-1486, Seattle, Washington, April 2001.

[167] J. F. Molinari, G. Gazonas, R. Raghupathy, A. Rusinek, and F. Zhou. The Cohesive Element Approach to Dynamic Fragmentation: The Question of Energy Convergence. *International Journal for Numerical Methods in Engineering*, 69(3):484–503, January 2007.

[168] R. Younes, A. Hallal, F. Fardoun, and F. H. Chehade. Comparative Review Study on Elastic Properties Modeling for Unidirectional Composite Materials. In N. Hu, editor, *Composites and Their Properties*, pages 391–408. IntechOpen, 2012. Available from: https://www.intechopen.com/books/composites-and-their-properties/comparative-review-study-on-elastic-properties-modeling-for-unidirectional-composite-materials.

[169] C. C. Chamis, F. Abdi, M. Garg, L. Minnetyan, H. Baid, D. Huang, J. Housner, and F. Talagani. Micromechanics-Based Progressive Failure Analysis Prediction for WWFE-III Composite Coupon Test Cases. *Journal of Composite Materials*, 47(20-21):2695–2712, September 2013.

[170] Y.-J. You, J.-H. J. Kim, K.-T. Park, D.-W. Seo, and T.-H. Lee. Modification of Rule of Mixtures for Tensile Strength Estimation of Circular GFRP Rebars. *Polymers*, 9(12):682–695, 2017.

[171] M. J. Laffan, S. T. Pinho, P. Robinson, and A. J. McMillan. Translaminar Fracture Toughness Testing of Composites: A Review. *Polymer Testing*, 31(3):481–489, May 2012.

[172] K. M. Prewo. The effect of ply lay-up sequence on the fracture toughness of boron aluminum. *Journal of Composite Materials*, 12(1):40–52, April 1978.

[173] M. J. Laffan, S. T. Pinho, P. Robinson, and L. Iannucci. Measurement of the In Situ Ply Fracture Toughness Associated with Mode I Fibre Tensile Failure in FRP. Part I: Data Reduction. *Composites Science and Technology*, 70(4):606–613, April 2010.

[174] V. A. Franklin and T. Christopher. Fracture Energy Estimation of DCB Specimens Made of Glass/Epoxy: An Experimental Study. *Advances in Materials Science and Engineering*, 2013:1–7, 2013.

[175] W. H. Press, S. A. Teukolsky, W. T. Vetterling, and B. P. Flannery. *Numerical Recipes in C: The Art of Scientific Computing, Second Edition*. Press Syndicate of the University of Cambridge, The Pitt Building, Trumpington Street, Campbridge CB2 1RP, 2002.

[176] R. L. Burden and J. D. Faires. *Numerical Analysis: 9th edition*. Brook/Cole, Cengage Learning, 20 Channel Center Street, Boston, Maryland, United States of America, 2011.

[177] V Noferini and J. Perez Alvaro. Chebyshev Rootfinding Via Computing Eigenvalues of Colleague Matrices: When Is It Stable? *Mathematics of Computation*, 86(306):1, November 2016.

[178] P. D. Soden, M. J. Hinton, and A. S. Kaddour. Lamina Properties, Lay-up Configurations and Loading Conditions for a Range of Fibre-Reinforced Composite Laminates. *Composites Science and Technology*, 58(7):1011–1022, July 1998.

[179] A. S. Kaddour and M. J. Hinton. Input data for test cases used in benchmarking triaxial failure theories of composites. *Journal of Composite Materials*, 46(19-20):2295–2312, September 2012.

[180] A. M. Girao Coelho. Finite Element Guidelines for Simulation of Delamination Dominated Failures in Composite Materials Validated by Case Studies. *Archives of Computational Methods in Engineering*, 23(2):363–388, June 2016.

[181] P. Maimi, P. P. Camanho, J. A. Mayugo, and C. G. Davila. A Continuum Damage Model for Composite Laminates: Part II - Computational Implementation and Validation. *Mechanics of Materials*, 39(10):909–919, October 2007.

[182] P. P. Camanho, P. Maimi, and C. G. Davila. Prediction of Size Effects in Notched Laminates Using Continuum Damage Mechanics. *Composites Science and Technology*, 67(13):2715–2727, October 2007.

[183] R. K. Goldberg. Strain Rate Dependent Deformation and Strength Modeling of a Polymer Matrix Composite Utilizing a Micromechanics Approach. Technical Memorandum NASA/TM-1999-209768, National Aeronautics and Space Administration, Glenn Research Center, Cleveland, Ohio, United States of America, December 1999.

[184] S. T. Pinho, L. Iannucci, and P. Robinson. Phyiscally-Based Failure Models and Criteria for Laminated Fibre-Reinforced Composites with Emphasis on Fibre Kinking: Part I: Development. *Composites Part A: Applied Science and Manufacturing*, 37(1):63–73, January 2006.

[185] C. G. Davila and P. P. Camanho. Failure Criteria for FRP Laminates in Plane Stress. Technical Memorandum TM-2003-212663, National Aeronautics and Space Administration, Langley Research Center, Hampton, Virginia 23681-2199, United States of America, November 2003.

[186] C. S. Lopes, P. P. Camanho, Z. Gurdal, and B. F. Tatting. Progressive Failure Analysis of Tow-Placed Variable-stiffness Composite Panels. *International Journal of Solids and Structures*, 44(25-26):8493–8516, December 2007.

[187] M. J. Hinton, A.S. Kaddour, and P. D. Soden. A Comparison of the Predictive Capabilities of Current Failure Theories for Composite Laminates, Judged Against Experimental Evidence. *Composites Science and Technology*, 62(12-13):1725–1797, September-October 2002.

[188] Z. P. Bazant and B. H. Oh. Crack Band Theory for Fracture of Concrete. *Materiaux et Construction*, 16(3):155–177, May 1983.

[189] A. Matzenmiller, J. Lubliner, and R. L. Taylor. A Constitutive Model for Anisotropic Damage in Fiber-Composites. *Mechanics of Materials*, 20(2):125–152, April 1995.

[190] S. Abrate, J. F. Ferrero, and P. Navarro. Cohesive Zone Models and Impact Damage Predictions for Composite Structures. *Meccanica*, 50(10):2587–2620, October 2015.

[191] J. W. Hutchinson and A. G. Evans. Mechanics of Materials: Top-Down Approaches to Fracture. *Acta Materiala*, 48(1):125–135, January 2000.

[192] C. Shet and N. Chandra. Analysis of Energy Balance When Using Cohesive Zone Models to Simulate Fracture Processes. *Journal of Engineering Materials and Technology*, 37(16):1415–1438, August 2003.

[193] M. Kuna. *Finite Elements in Fracture Mechanics: Theory-Numerics-Applications*. Springer, Dordrecht, 2013.

[194] C. Shet and N. Chandra. Effect of the shape of traction-displacement cohesive zone curves on the fracture response. *Mechanics of Advanced Materials and Structures*, 11(3):249–275, 2004.

[195] Q. Yang and B. Cox. Cohesive Models for Damage Evolution in Laminated Composites. *International Journal of Fracture*, 133(2):107–137, May 2005.

[196] J. G. Williams and H. Hadavinia. Analytical Solutions for Cohesive Zone Models. *Journal of the Mechanics and Physics of Solids*, 50(4):809–825, April 2002.

[197] M. May and S. R. Hallett. An Advanced Model for Initiation and Propagation of Damage Under Fatigue Loading- Part I: Model Formulation. *Composite Structures*, 93(9):2340–2349, August 2011.

[198] S. Roth, G. Hutter, and M. Kuna. Simulation of Fatigue Crack Growth with a Cyclic Cohesive Zone Model. *International Journal of Fracture*, 188(1):23–45, July 2014.

[199] B. L. V. Bak, C. Sarrado, A. Turon, and J. Costa. Delamination Under Fatigue Loads in Composite Laminates: A Review on the Observed Phenomenology and Computational Methods. *Applied Mechanical Reviews*, 66(6):1–24, November 2014.

[200] K. L. Roe and T. Siegmund. An Irreversible Cohesive Zone Model for Interface Fatigue Crack Growth Simulation. *Engineering Fracture Mechanics*, 70(2):209–232, January 2003.

[201] A. Abdul-Baqi, P. J. G. Schreurs, and M. G. D. Geers. Fatigue Damage Modeling in Solder Interconnects Using a Cohesive Zone Approach. *International Journal of Solids and Structures*, 42(3-4):927–942, February 2005.

[202] B. L. V. Bak, A. Turon, E. Lindgaard, and E. Lund. A Benchmark Study of Simulation Methods for High-Cycle Fatigue-Driven Delamination Based on Cohesive Zone Models. *Composite Structures*, 164:198–206, March 2017.

Appendix A

Root-finding algorithm: Additional information

The root-finding algorithm introduced in Section 2.1.4 uses three root-finding methods. The modified Newton-Raphson method is discussed in Section A.1. Furthermore, Brent's method is discussed in Section A.2. The Chebyshev approximation is discussed in Section A.3.

A.1 Modified Newton-Raphson

The iterative Newton-Raphson scheme is given by Equation A.1. [175]

$$x_{n+1} = x_n + h = x_n - \frac{f(x_n)}{\frac{df(x_n)}{dx}} \tag{A.1}$$

Two cases where the Newton-Raphson method in its current form will fail are, in case:

1. Of the presence of local extrema
2. The method enters a non-convergent cycle.

The first case causes the Newton-Raphson method to jump to $-\infty$. This is because at a local extremum the derivative is zero; and therefore, h becomes ∞. The second case causes the Newton-Raphson method to continuously cycle between a limited amount of values. According to Press et al. [175], this is often encountered when f is obtained by table interpolation. In order to avoid these phenomena, the bisection method is included within the Newton-Raphson procedure.

The bisection method calculates the midpoint of the interval at each step, as shown in Equation A.2. In case $f(a_i)f(p_i) > 0$, $a_{i+1} = p_i$ and $b_{i+1} = b_i$. For any other case, $a_{i+1} = a_i$ and $b_{i+1} = p_i$. This procedure is continued after a maximum number of steps has been reached or if $|f(p)| < \delta$, where δ is a specified tolerance. More information regarding the bisection method is provided by Burden and Faires [176].

$$p_i = a_i + \frac{b_i - a_i}{2} \tag{A.2}$$

The modified Newton-Raphson method is implemented as proposed by Press et al [175]. The Newton-Raphson method is used as the primary method, however in case the Newton-Raphson method evaluates to solutions that are out of range or if the bounds of the interval are not decreasing fast enough, the bisection method is used. This method exploits the robustness of the bisection method, mitigates the poor global convergence of the Newton-Raphson methods and exploits the quadratic local convergence of the Newton-Raphson method.

A.2 Brent's method

Brent's method (also referred to as the van Wijngaarden-Dekker-Brent method) combines the bisection, secant and inverse quadratic interpolation methods. By combining these methods, Brent's method is able to obtain the reliability of the bisection method while also obtaining a higher convergence rate up to the convergence rate of less-reliable methods. Three points $[a, b, c]$ and their function values $[f(a), f(b), f(c)]$ can be defined. For these points, the next root estimate is given by Equation A.3, where P and Q are given by Equations A.4 and A.5. [175]

$$x = b + \frac{P}{Q} \tag{A.3}$$

$$P = \frac{f(b)}{f(a)}\left[\frac{f(b)}{f(c)}\left(\frac{f(b)}{f(c)} - \frac{f(a)}{f(c}\right)(c-b) - \left(1 - \frac{f(b)}{f(c)}\right)(b-a)\right] \tag{A.4}$$

$$Q = \left(\frac{f(a)}{f(c)} - 1\right)\left(\frac{f(b)}{f(c)} - 1\right)\left(\frac{f(b)}{f(a)} - 1\right) \tag{A.5}$$

In case the fraction $\frac{P}{Q}$ causes a correction that would exceed the bounds or when the bounds are not collapsing fast enough, Brent's method takes a bisection step instead.

A.3 Chebyshev approximation

The Chebyshev polynomial of degree n is given by Equation A.6 and follows the relation given in Equation A.7. [175]

$$T_n(x) = \cos(n \arccos(x)) \tag{A.6}$$

$$T_{n+1}(x) = 2xT_n(x) - T_{n-1}(x); \quad n \geq 1 \tag{A.7}$$

An arbitrary function $f(x)$ defined in the interval $[-1, 1]$ can be approximated by the Chebyshev approximation formula given in Equation A.8, where the coefficients c_k are given by Equation A.9 for $k = 0, .., N-1$. [175]

$$f(x) \approx \left[\sum_{k=0}^{N-1} c_k T_k(x)\right] - \frac{1}{2}c_0 \tag{A.8}$$

$$c_k = \frac{2}{N}\sum_{j=1}^{N} f(x_j)T_k(x_j) \tag{A.9}$$

The Chebyshev approximating polynomial is preferred over another approximating polynomial (such as the Taylor expansion) because the Chebyshev approximation smooths the error over the interval; and is nearly identical to the polynomial that has the smallest possible maximum deviation from the true function $f(x)$ for the approximation degree m. [175] The approximating polynomial of degree m that has the smallest maximum deviation from the true function $f(x)$ is called the minimax polynomial and is generally difficult to find, whereas the Chebyshev approximation is readily computed.

As the Chebyshev polynomial is only defined in the interval $[-1, 1]$, a change of variables is performed to change the range to an arbitrary interval $[a, b]$. The function $f(x)$ in the range $[a, b]$ is then approximated by a Chebyshev polynomial in y, where y is given by Equation A.10.

$$y = \frac{x - \frac{1}{2}(b + a)}{\frac{1}{2}(b - a)} \tag{A.10}$$

In order to calculate the roots of the Chebyshev polynomial, the eigenvalues of the companion matrix are calculated. [177]

Finding the roots of an arbitrary function by using the Chebyshev interpolation is a powerful method; if multiple roots are required, the interval for which the roots are required is unknown or (some of) the roots are complex. However, the computational effort for this method is higher than for the modified Newton-Raphson and Brent's method.

Appendix B

Mechanical properties: Unidirectional Quasi Static Test Cases

B.1 Mechanical properties

The mechanical properties for the materials of the Unidirectional Quasi-Static Test Cases (UQSTCs) are provided in Table B.1. The references from where the data is obtained are also included in the table.

Additionally, interlaminar and intralaminar toughnesses are required for the materials. Ideally, this data is determined for each of the UQSTC materials shown in Table B.1. Unfortunately, such data is not available for each of the materials. Therefore, some assumptions have to be made regarding these values. For the interlaminar fracture toughnesses for mode I and II ($G_{I,c}$ and $G_{II,c}$), only a distinction between Carbon Fibre Reinforced Polymers (CFRPs) and Glass Fibre Reinforced Polymer (GFRP) is made. Van Dongen [6] reported the interlaminar fracture toughness CFRP (from Pinho [113]) and GFRP (from Girao Coelho [180]) composites. For the intralaminar fracture toughnesses ($G_{f,c}^{(+)}$, $G_{f,c}^{(-)}$, $G_{m,c}^{(+)}$ and $G_{m,c}^{(-)}$), Van Dongen [6] reports data for: T300/1034C (from Maimi et al. [181]), a GFRP used in Glare (from Lapczyk and Hurtado [25]), IM7/8552 (from Camanho et al. [182]) and AS4/8552. In order to determine the values of the intralaminar fracture toughnesses for the materials used by the UQSTCs, the data from the most similar out of the four materials is used. The fracture toughnesses are given in Table B.2.

B.2 Non-linear shear behaviour

The experimental data, linear elastic approximation, Hahn-Tsai fit and Ramberg-Osgood relation for the shear stress-strain relation for the materials listed in Table B.1 are shown in Figures B.1, B.2, B.3, B.4, B.5, B.6 and B.7. The references from where the data is obtained is indicated in the captions of the figures.

The shear stress-strain data for IM7/977-2 obtained from Goldberg [183] is not in accordance with the IM7/977-2 properties in Table B.1. Therefore, the shear modulus used for the fits

Table B.1: Mechanical properties for the materials used by the UQSTCs. – indicates that the property has not been provided.

	E-glass LY556	E-glass MY750	S2-glass Epoxy 2	IM7 977-2	T300 BSL914C	T300 PR319	AS Epoxy 1
Reference	[178]	[179]	[179]	[31]	[178]	[179]	[179]
$\mathbf{E_1}$ **[GPa]**	53.5	45.6	52.0	153.1	138.0	129.0	140.0
$\mathbf{E_2}$ **[GPa]**	17.7	16.2	19.0	9.7	11.0	5.6	10.0
$\mathbf{E_3}$ **[GPa]**	–	16.2	19.0	9.7	–	5.6	10.0
ν_{12} [–]	0.278	0.278	0.30	0.27	0.28	0.318	0.318
ν_{13} [–]	–	0.278	0.30	0.27	–	0.318	0.318
ν_{23} [–]	0.40	0.40	0.42	0.41	0.40	0.50	0.50
$\mathbf{G_{12}}$ **[GPa]**	5.83	5.83	6.7	5.31	5.50	1.33	6.0
$\mathbf{G_{13}}$ **[GPa]**	–	5.83	6.70	5.31	–	1.33	6.0
$\mathbf{G_{23}}$ **[GPa]**	–	5.70	6.70	3.42	–	1.86	3.35
$\sigma^{\mathbf{u}}_{\mathbf{11,t}}$ **[MPa]**	1140	1280	1700	2861	1500	1378	1990
$\sigma^{\mathbf{u}}_{\mathbf{11,c}}$ **[MPa]**	570	800	1105	1551	900	950	1500
$\sigma^{\mathbf{u}}_{\mathbf{22,t}}$ **[MPa]**	35	40	63	76	27	40	38
$\sigma^{\mathbf{u}}_{\mathbf{22,c}}$ **[MPa]**	114	145	180	299	200	125	150
$\sigma^{\mathbf{u}}_{\mathbf{33,t}}$ **[MPa]**	–	40	50	76	–	40	38
$\sigma^{\mathbf{u}}_{\mathbf{33,c}}$ **[MPa]**	–	145	180	299	–	125	150
$\tau^{\mathbf{u}}_{\mathbf{12}}$ **[MPa]**	72	73	72	102	80	97	70
$\tau^{\mathbf{u}}_{\mathbf{13}}$ **[MPa]**	–	73	72	102	–	97	70
$\tau^{\mathbf{u}}_{\mathbf{23}}$ **[MPa]**	–	50	40	53	–	45	50

Table B.2: Fracture toughness data for the materials used by the UQSTCs.

	E-glass LY556	E-glass MY750	S2-glass Epoxy 2	IM7 977-2	T300 BSL914C	T300 PR319	AS Epoxy 1
$\mathbf{G_{I,c}}$ **[N/mm]**	0.18	0.18	0.18	0.258	0.258	0.258	0.258
$\mathbf{G_{II,c}}$ **[N/mm]**	0.36	0.36	0.36	1.080	1.080	1.080	1.080
$\mathbf{G^{(+)}_{f,c}}$ **[N/mm]**	12.5	12.5	12.5	81.5	52.5	52.5	92.0
$\mathbf{G^{(-)}_{f,c}}$ **[N/mm]**	12.5	12.5	12.5	106.3	45.8	45.8	80.0
$\mathbf{G^{(+)}_{m,c}}$ **[N/mm]**	1.0	1.0	1.0	0.28	0.13	0.13	0.20
$\mathbf{G^{(-)}_{m,c}}$ **[N/mm]**	1.0	1.0	1.0	0.80	0.45	0.45	0.80

is directly obtained from the experimental data based on the first two data points: $G_{12} = 9.56 \cdot 10^3\ MPa$.

B.3 LaRC-05 parameters

The parameters α_0 and η_L used as inputs for the UQSTCs are provided in B.3. The values for α_0 are reported to be $53° \pm 2°$ for CFRPs and GFRPs composites by various authors (such as Puck and Schurmann [29] and Pinho et al. [50]). The values for η_L for T300/PR319, E-

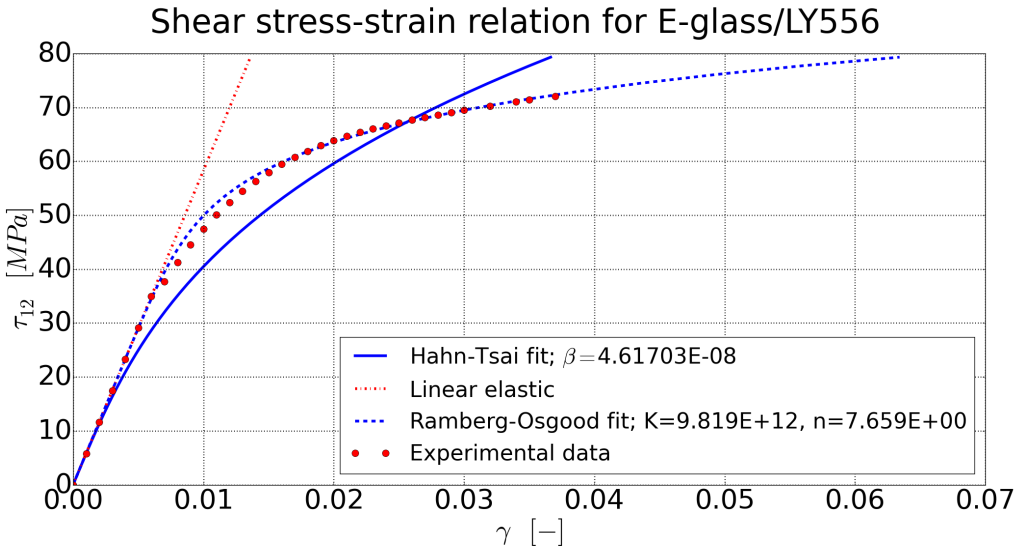

Figure B.1: A plot of the Hahn-Tsai shear model, linear elastic shear model and experimental data for a uni-directional E-glass/LY556 composite. The experimental data is obtained from Soden et al. [178].

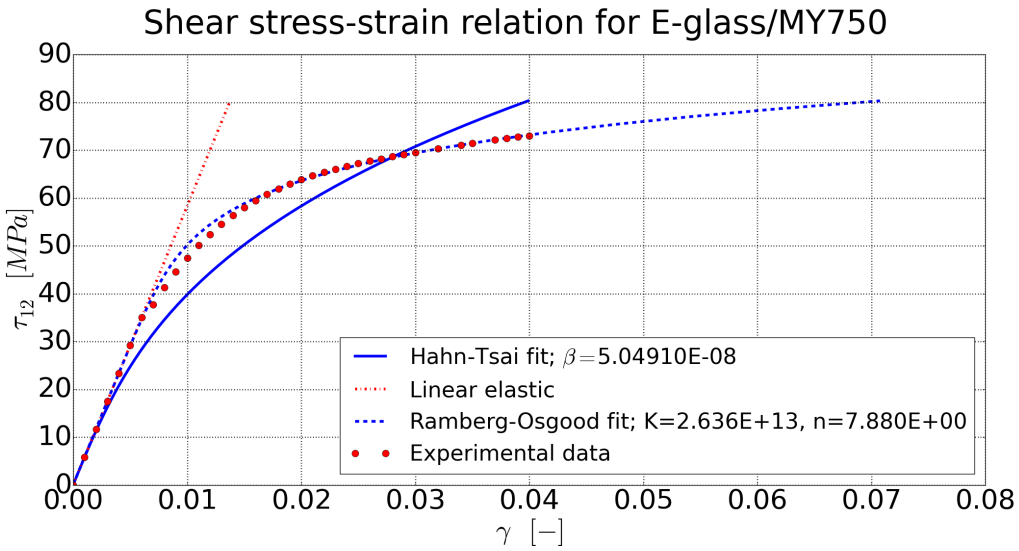

Figure B.2: A plot of the Hahn-Tsai shear model, linear elastic shear model and experimental data for a uni-directional E-glass/MY750 composite. The experimental data is obtained from Soden et al. [178].

glass/MY750, S-glass/Epoxy, AS/Epoxy and IM7/8551-7 are obtained from Pinho et al. [50] and is 0.082 for all cases. Therefore, it is assumed that for the other materials used for the UQSTCs are also equal to 0.082.

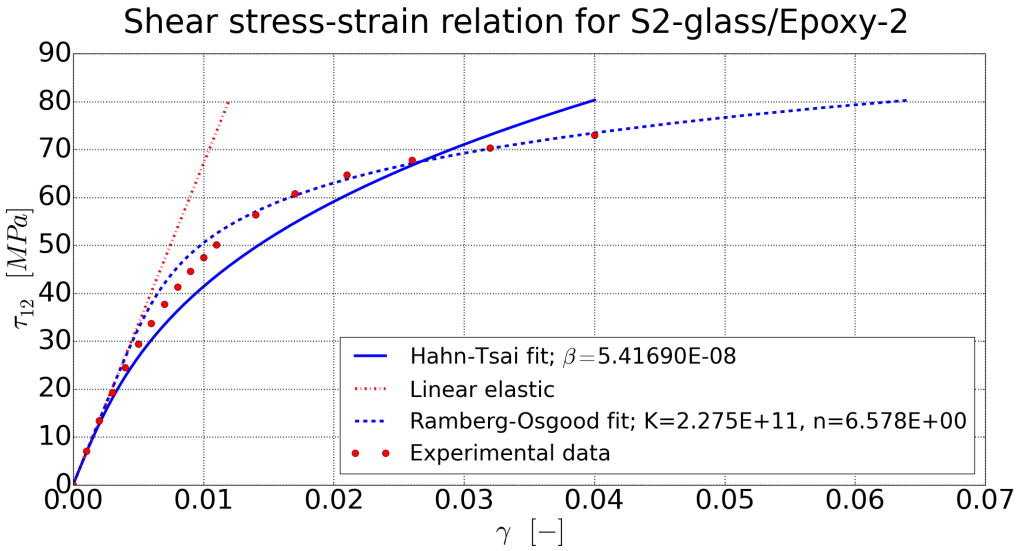

Figure B.3: A plot of the Hahn-Tsai shear model, linear elastic shear model and experimental data for a uni-directional S2-glass/Epoxy-2 composite. The experimental data is obtained from Kaddour and Hinton [179].

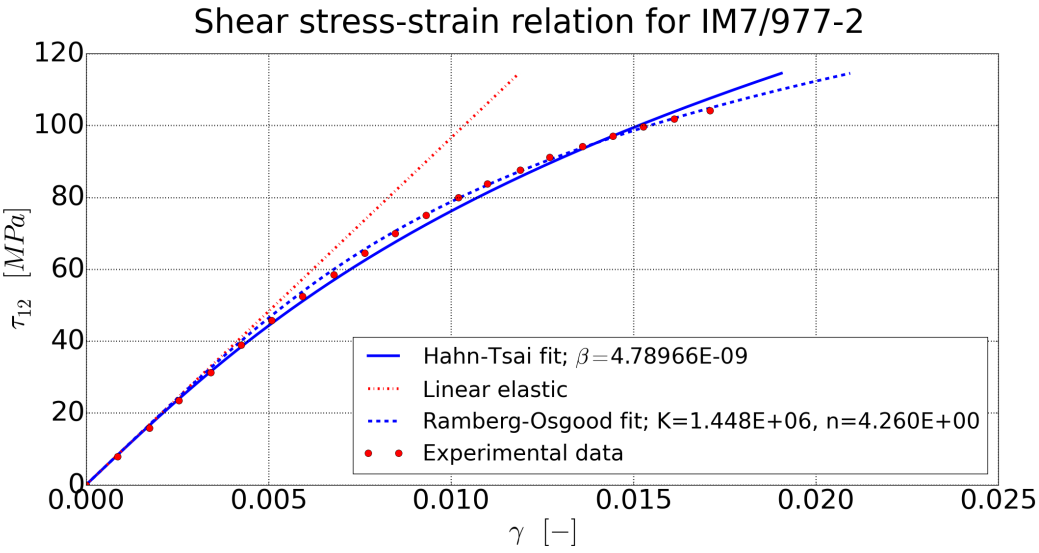

Figure B.4: A plot of the Hahn-Tsai shear model, linear elastic shear model and experimental data for a uni-directional IM7/977-2 composite. The experimental data is obtained from Goldberg [183].

B.4 In-situ strength

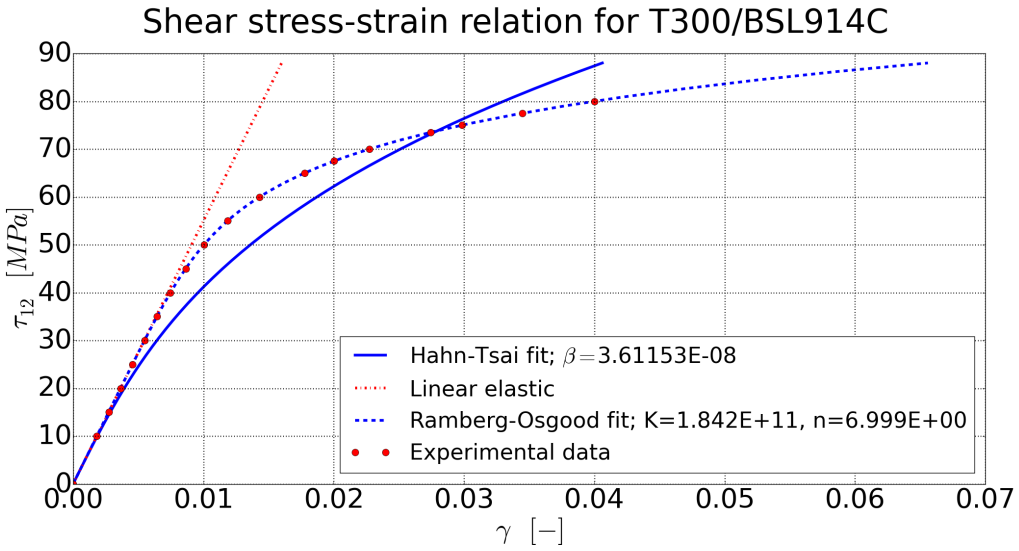

Figure B.5: A plot of the Hahn-Tsai shear model, linear elastic shear model and experimental data for a uni-directional T300/BSL914C composite. The experimental data is obtained from Soden et al. [178].

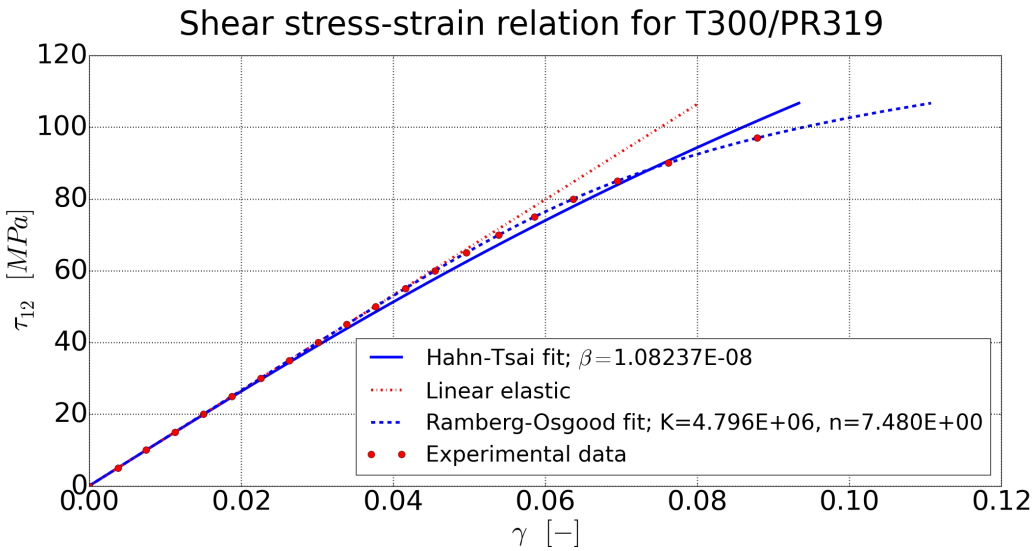

Figure B.6: A plot of the Hahn-Tsai shear model, linear elastic shear model and experimental data for a uni-directional T300/PR319 composite. The experimental data is obtained from Kaddour and Hinton [179].

Table B.3: LaRC-05 parameters used as inputs for the UQSTCs.

	E-glass LY556	**E-glass MY750**	**S2-glass Epoxy 2**	**IM7 977-2**	**T300 BSL914C**	**T300 PR319**	**AS Epoxy 1**
α_0 $[\circ]$	53.0	53.0	53.0	53.0	53.0	53.0	53.0
η_L $[-]$	0.082	0.082	0.082	0.082	0.082	0.082	0.082

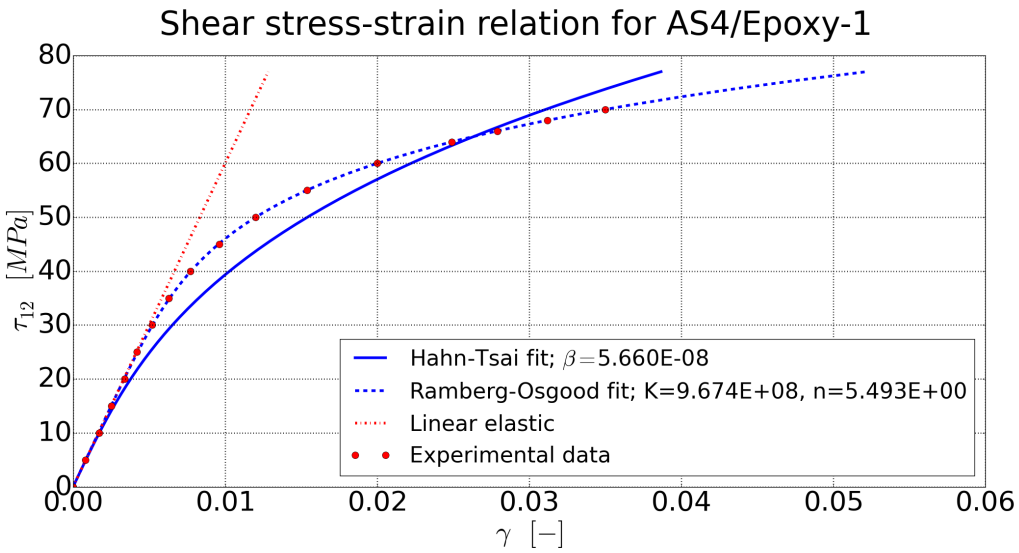

Figure B.7: A plot of the Hahn-Tsai shear model, linear elastic shear model and experimental data for a uni-directional AS/Epoxy-1 composite. The experimental data is obtained from Kaddour and Hinton [179].

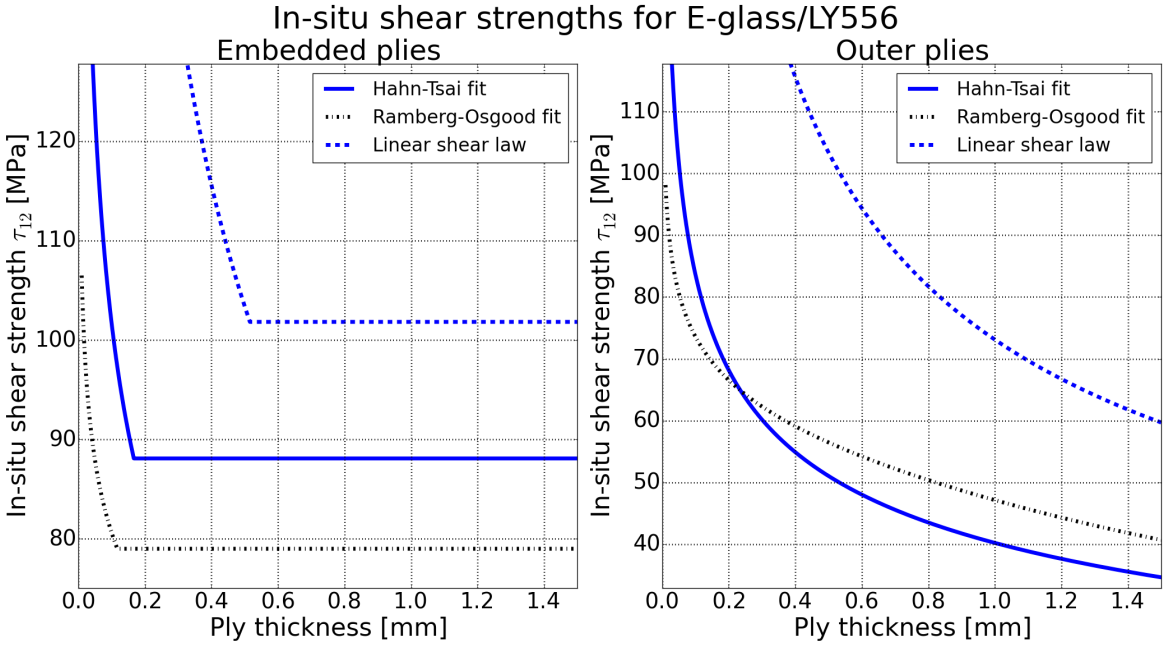

Figure B.8: The in-situ shear strengths for an unidirectional E-glass/LY556 FRP for a linear, Hahn-Tsai and Ramberg-Osgood shear relation. $\tau_{12}^{u} = 72\ MPa$

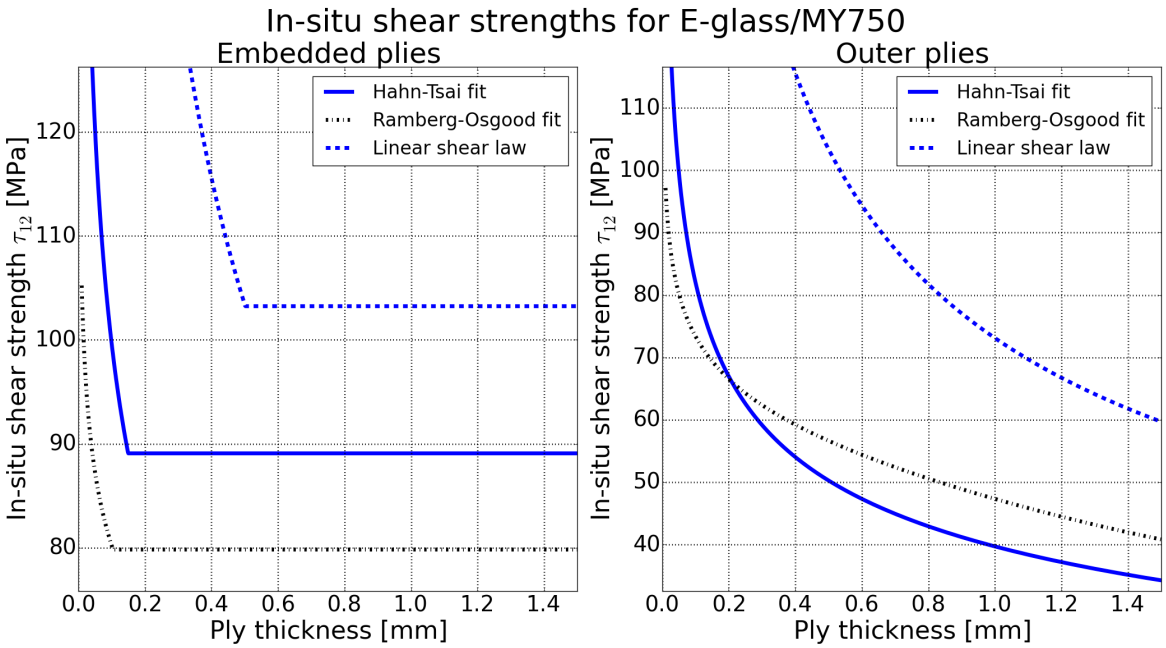

Figure B.9: The in-situ shear strengths for an unidirectional E-glass/MY750 FRP for a linear, Hahn-Tsai and Ramberg-Osgood shear relation. $\tau_{12}^u = 73\ MPa$

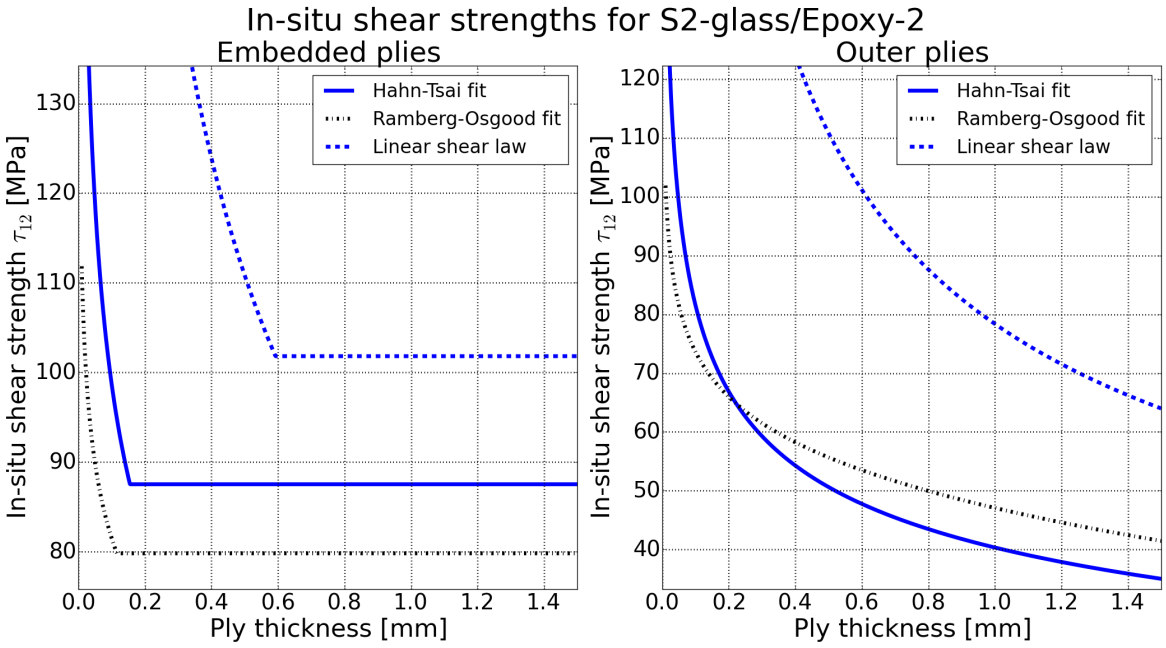

Figure B.10: The in-situ shear strengths for an unidirectional S2-glass/Epoxy-2 FRP for a linear, Hahn-Tsai and Ramberg-Osgood shear relation. $\tau_{12}^u = 72\ MPa$

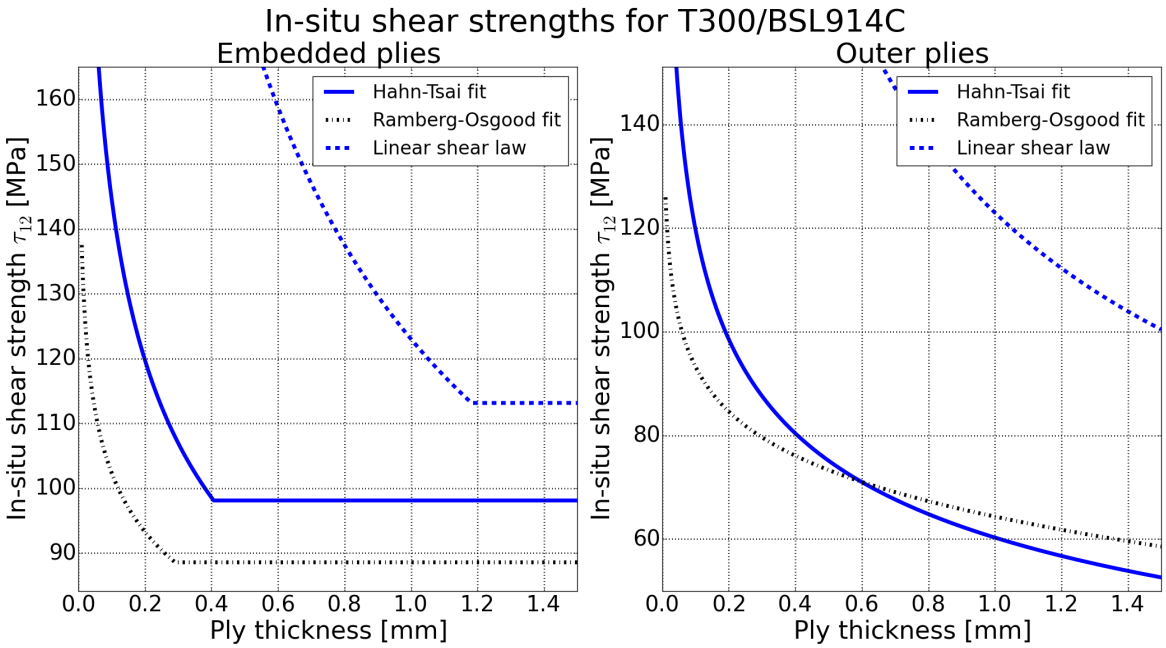

Figure B.11: The in-situ shear strengths for an unidirectional T300/BSL914C FRP for a linear, Hahn-Tsai and Ramberg-Osgood shear relation. $\tau_{12}^{u} = 80\ MPa$

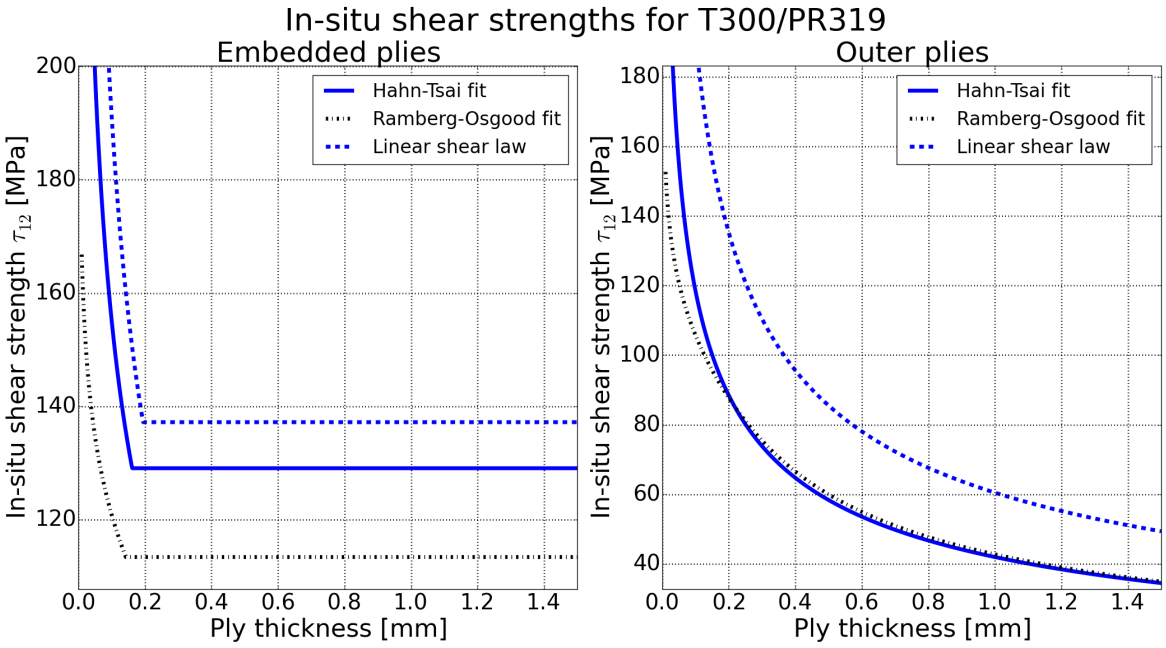

Figure B.12: The in-situ shear strengths for an unidirectional T300/PR319 FRP for a linear, Hahn-Tsai and Ramberg-Osgood shear relation. $\tau_{12}^{u} = 97\ MPa$

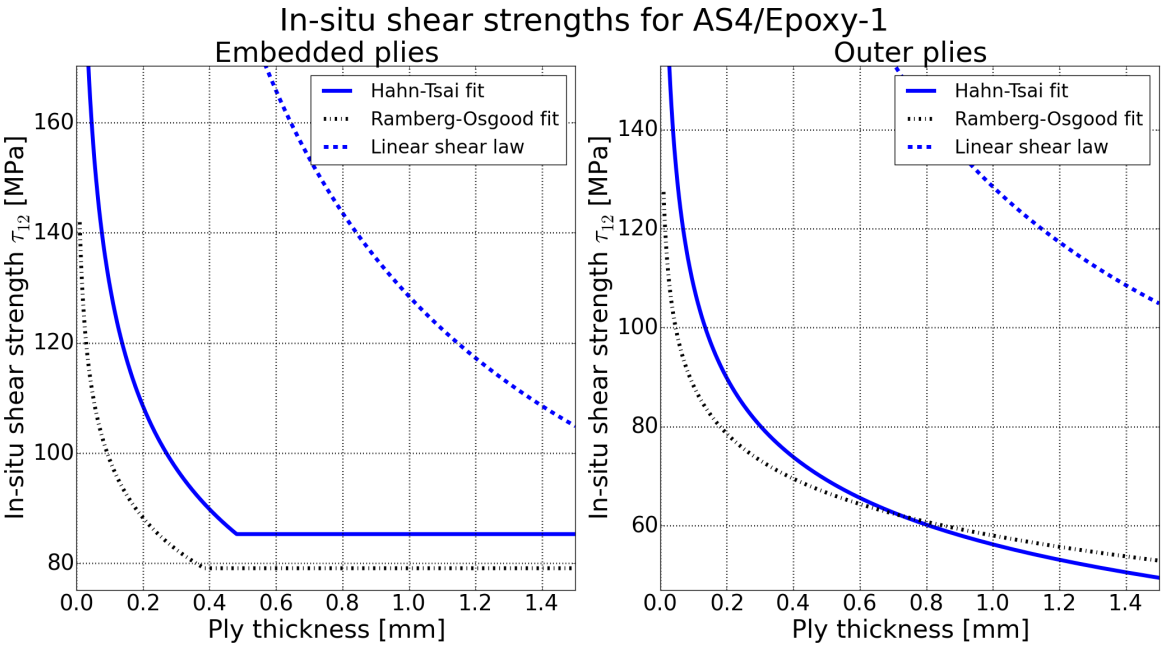

Figure B.13: The in-situ shear strengths for an unidirectional AS4/Epoxy-1 FRP for a linear, Hahn-Tsai and Ramberg-Osgood shear law. $\tau_{12}^{u} = 70\ MPa$

Appendix C

Continuum Damage Model (CDM): Additional information

This appendix provides additional information regarding the Continuum Damage Model (CDM) used in this report. The LaRC-05 damage initiation criterion is discussed in Section C.1; and the bilinear damage progression criterion is discussed in Section C.2.

C.1 LaRC-05

As motivated in Section 3.5.1, the LaRC-05 criterion is chosen to characterise damage initiation for the CDM. In Section C.1.1, the LaRC-05 criterion is introduced. An evaluation of the LaRC-05 criterion and an investigation on the influence of the estimated friction parameter η_L is provided in Section C.1.2. However, it should be noted that the scope of Section C.1.2 is limited to a few load cases and unidirectional laminates.

C.1.1 Criterion

The LaRC-05 criterion requires the ultimate strengths of the material and three experimentally determined parameters (α_0, η_L and η_T) as input. The parameter α_0 is the fracture angle of the material under pure compressive loading. For Glass Fibre Reinforced Polymers (GFRPs) and Carbon Fibre Reinforced Polymers (CFRPs), the value of α_0 is typically in the range of 50° and 55°. [29, 50, 55, 184] Therefore, in case of lack of data, the value of α_0 can be estimated to be 53° for GFRPs and CFRPs. The parameters η_L and η_T are friction coefficients that take into account the effect of pressure on the failure response. The parameter η_T can be determined with Equation C.1. [26] The parameter η_L should be determined experimentally. Various authors (such as van Dongen [6], Pinho et al. [26], Davila et al. [95, 185] and Lopes et al. [186]) use the relation provided by Equation C.2 to estimate η_L in the absence of biaxial test data. However, as will be shown in Section C.1.2, in case of triaxial compression, the approximated value gives poor results. Lastly, note that the transverse shear strength of a material is difficult to measure experimentally. [95] However, the

transverse shear strength can be computed from the transverse compressive strength and α_0 as is shown in Equation C.3. [26, 95]

$$\eta_T = -\frac{1}{\tan(2\alpha_0)} \tag{C.1}$$

$$\eta_L = -\frac{S_{12}\cos(2\alpha_0)}{\sigma^u_{22,c}\cos^2(\alpha_0)} \tag{C.2}$$

$$\tau^u_{23} = \sigma^u_{22,c}\cos(\alpha_0)[\sin(\alpha_0) + \frac{\cos(\alpha_0)}{\tan(2\alpha_0)}] \tag{C.3}$$

For Matrix Failure (MF) consider the material volume sketched in Figure C.1. A multitude of fracture planes can be defined depending on the fracture angle α. When failure occurs, the fracture plane will correspond to the fracture angle α which causes the most severe situation for fracture. In case of matrix failure, the failure criteria for both Tensile Matrix Failure (MFT) and Compressive Matrix Failure (MFC) is determined by a single inequality, as shown in Equation C.4, where failure occurs if the inequality evaluates to true. To accommodate for both MFT and MFC, the Macauley brackets are used for which $< x >_+ = max(0, x)$. The traction components τ_T, τ_L and σ_N (see Figure C.1) are a function of the fracture angle α and are given by Equation C.5. Due to the dependency on the fracture angle α, the expression in Equation C.4 should be maximised for α, where $0° \leq \alpha \leq 180°$. Maimi et al. [13] argue that the upper bound of the fracture angle α is equal to α_0. Therefore, the interval of α can be reduced to $0° \leq \alpha \leq \alpha_0$ which reduces the computational cost of evaluating Equation C.4.

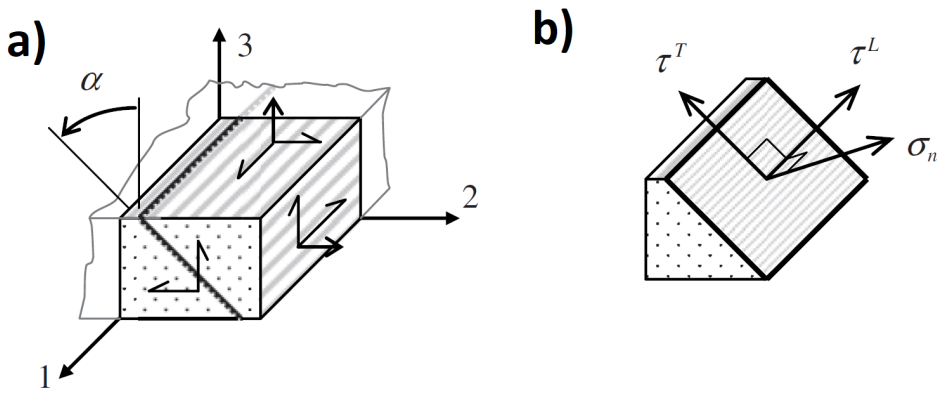

Figure C.1: The matrix fracture plane: a) material volume, with the principal axes and fracture plane angle α indicated; b) the traction components acting at the fracture plane. Copied from Pinho et al. [50].

$$FI_{MF} = \max_{\alpha}\left(\frac{\tau_T(\alpha)}{\tau^u_{23} - \eta_T\sigma_N(\alpha)}\right)^2 + \left(\frac{\tau_L(\alpha)}{\tau^u_{12} - \eta_L\sigma_N(\alpha)}\right)^2 + \left(\frac{< \sigma_N(\alpha) >_+}{\sigma^u_{22,t}}\right)^2 > 1 \tag{C.4}$$

$$\begin{cases} \tau_T = -\frac{\sigma_{22}-\sigma_{33}}{2}\sin(2\alpha) + \tau_{23}\cos(2\alpha) \\ \tau_L = \tau_{12}\cos(\alpha) + \tau_{31}\sin(\alpha) \\ \sigma_N = \frac{\sigma_{22}+\sigma_{33}}{2} + \frac{\sigma_{22}-\sigma_{33}}{2}\cos(2\alpha) + \tau_{23}\sin(2\alpha) \end{cases} \tag{C.5}$$

For Tensile Fibre Failure (FFT) the criterion given by Equation C.6 is used. Even though the FFT criterion is very simple, the criterion agrees well with experimental data. [50, 187] This can be expected as for a pure tensile loading in the direction of the fibres, the fibres carry the load and failure will occur when fibres start to fail.

$$FI_{FFT} = \frac{< \sigma_{11} >_+}{\sigma^u_{11,t}} > 1 \tag{C.6}$$

For Compressive Fibre Failure (FFC), the LaRC-05 considers two types of failure mechanisms: matrix splitting and fibre kinking. From experiments it is observed that matrix splitting occurs in between the fibres due to high shear stresses. The matrix splitting accommodates the bending of fibres which leads to more matrix splitting. Eventually, the fibres will break due to a combination of bending and compressive stresses, this results in a kink band. [50] Based on experiments, Pinho et al. [50], suggest that fibre kinking only occurs for an absolute value of longitudinal compression greater than $\frac{\sigma^u_{11,c}}{2}$. In case of longitudinal compression in combination with transverse tension, it is observed that no kink bands are formed for any longitudinal compression lower than $\sigma^u_{11,c}$; and hence the failure will occur due to matrix failure. The criteria for both fibre kinking and matrix splitting, are accommodated in a single expression as is shown by Equation C.7. The subscript m indicates the misalignment frame which is the coordinate system that is aligned with the misaligned fibres. The misalignment is caused by shear stresses caused by the stress-state during loading (i.e. applied shear loading and/or shear stresses caused by failure in neighbouring material) and due to localised shear stresses caused by manufacturing defects (such as fibre misalignment). The angle Ψ is the kink band angle and defines the plane in which fibres will kink. The angle Ψ is in the range of $0° - 180°$ and has to be determined iteratively by finding the highest failure index value of all possible Ψ.

$$FI_{kink} = FI_{split} = \max_{\Psi}\left(\frac{\tau^m_{23}(\Psi)}{\tau^u_{23} - \eta_T \sigma^m_{22}(\Psi)}\right)^2 + \left(\frac{\tau^m_{12}(\Psi)}{\tau^u_{12} - \eta_L \sigma^m_{22}(\Psi)}\right)^2 + \left(\frac{< \sigma^m_2(\Psi) >_+}{\sigma^u_{22,t}}\right)^2 > 1 \tag{C.7}$$

The expressions for σ^m_{22}, τ^m_{12} and τ^m_{23} are provided by Equation C.8. The expressions for σ^Ψ_{22}, τ^Ψ_{12}, τ^Ψ_{23} and τ^Ψ_{13} are given by Equation C.9.

$$\begin{cases} \sigma^m_{22} = \sigma_{11}\sin^2(\theta) + \sigma^\Psi_{22}\cos^2(\theta) - 2\sin(\theta)\cos(\theta)\tau^\Psi_{12} \\ \tau^m_{12} = -\sigma_{11}\sin(\theta)\cos(\theta) + \sigma^\Psi_{22}\sin(\theta)\cos(\theta) + \tau^\Psi_{12}(\cos^2(\theta) - \sin^2(\theta)) \\ \tau^m_{23} = \tau^\Psi_{23}\cos(\theta) - \tau^\Psi_{31}\sin(\theta) \end{cases} \tag{C.8}$$

$$\begin{cases} \sigma^\Psi_{22} = \sigma_{22}\cos^2(\Psi) + \sigma_{33}\sin^2(\Psi) + 2\tau_{23}\sin(\Psi)\cos(\Psi) \\ \tau^\Psi_{12} = \tau_{12}\cos(\Psi) + \tau_{31}\sin(\Psi) \\ \tau^\Psi_{23} = -\sigma_{22}\sin(\Psi)\cos(\Psi) + \sigma_{33}\sin(\Psi)\cos(\Psi) + \tau_{23}(\cos^2(\Psi) - \sin^2(\Psi)) \\ \tau^\Psi_{31} = \tau_{31}\cos(\Psi) - \tau_{12}\sin(\Psi) \end{cases} \tag{C.9}$$

The misalignment angle θ is assumed to consist of the initial misalignment angle θ_0 and the shear strain present in the coordinate system aligned with the manufacturing defect γ_m. The misalignment angle is then given by Equation C.10.

$$\theta = sign(\tau_{12}^{\Psi})\theta_0 + \gamma_m \tag{C.10}$$

Before deriving expressions for θ_0 and γ_m, consider the misalignment angle θ_c which is the misalignment angle at failure for pure compression. The angle θ_c is the sum of the initial misalignment and the rotation due to compressive loading. Davila and Camanho [185] derived an expression for θ_c as is shown in Equation C.11.

$$\theta_c = \arctan\left(\frac{1 - \sqrt{1 - 4(\frac{\tau_{12}^u}{\sigma_{11,c}^u} + \eta_L)\frac{\tau_{12}^u}{\sigma_{11,c}^u}}}{2(\frac{\tau_{12}^u}{\sigma_{11,c}^u} + \eta_L)}\right) \tag{C.11}$$

The initial misalignment angle θ_0 can be calculated by subtracting the shear strain at failure γ_{mc} from θ_c as is shown in Equation C.12.

$$\theta_0 = \theta_c - \gamma_{mc} \tag{C.12}$$

In order to obtain the shear strain at failure consider Equation C.13 which shows the general relation between the shear stress and the shear strain. The function f can be any function that describes the shear-strain relation.

$$\tau = f(\gamma) \tag{C.13}$$

At failure due to pure compression it is known that the shear stress angle at an angle θ_c is given by Equation C.14. [184] Hence, the angle γ_{mc} is given by Equation C.15, where f^{-1} is the inverse of the function f and not the reciprocal.

$$\tau_{mc} = \frac{1}{2}\sin(2\theta_c)\sigma_{11,c}^u \tag{C.14}$$

$$\gamma_{mc} = f^{-1}\left(\frac{1}{2}\sin(2\theta_c)\sigma_{11,c}^u\right) \tag{C.15}$$

For a highly non-linear shear behaviour/relation it might be required to solve γ_{mc} iteratively. However, when considering a linear shear law and assuming small angles then γ_{mc} is given by Equation C.16. [185]

$$\gamma_{mc} = \frac{\theta_c \sigma_{11,c}^u}{G_{12}} \tag{C.16}$$

In order to solve for τ_m, Equation C.17 has to be solved. [184] Solving Equation C.17 can be difficult, especially when $f(\gamma_m)$ is non-linear. Pinho et al. [184] argue that for most practical cases, Equation C.17 can be simplified as shown in Equation C.18 without losing too much accuracy. Solving Equation C.18 for a linear shear law results in Equation C.19. In case of a non-linear shear law a different expression has to be derive for γ_m, however this might not be possible and an iterative approach for solving Equation C.17 or C.18 has to be used.

$$\tau_m = f(\gamma_m) = -\frac{\sigma_{11} - \sigma_{22}}{2}\sin(2(\theta_0 + \gamma_m)) + |\tau_{12}|\cos(2(\theta_0 + \gamma_m)) \tag{C.17}$$

$$f(\gamma_m) \approx (\theta_0 + \gamma_m)(-\sigma_{11} + \sigma_{22}) + |\tau_{12}| \tag{C.18}$$

$$\gamma_m = \frac{\theta_0 G_{12} + |\tau_{12}|}{G_{12} + \sigma_{11} - \sigma_{22}} - \theta_0 \tag{C.19}$$

The procedures to determine the failure indices FI_{MFT}, FI_{MFC}, FI_{FFT}, FI_{split} and FI_{kink} have been discussed. These failure indices form the set to determine the failure indices FI_{MFT}, FI_{MFC}, FI_{FFT} and FI_{FFC}. The failure indices FI_{MFT} and FI_{MFC} are different than those provided by Equation C.4 as the matrix splitting failure mode has also to be taken into account. The failure indices of the LaRC-05 criterion for FI_{MFT}, FI_{MFC}, FI_{FFT} and FI_{FFC} are given in Equations C.20, C.21, C.22 and C.23, respectively. If any of these failure indices are equal or larger than 1, the material fails with the corresponding failure mode.

$$FI_{MFT} = max\left(\left[\begin{cases} 0 & \text{if } \sigma_{22} < 0 \\ FI_{MF} & \text{if } \sigma_{22} \geq 0 \end{cases}\right], \left[\begin{cases} FI_{split} & \text{if } \sigma_{11} \leq 0 \text{ and} \\ & \sigma_{11} > -\frac{\sigma^u_{11,c}}{2} \text{ and} \\ & \sigma_{22} \geq 0 \\ 0 & \text{otherwise} \end{cases}\right]\right) \tag{C.20}$$

$$FI_{MFC} = max\left(\left[\begin{cases} 0 & \text{if } \sigma_{22} > 0 \\ FI_{MF} & \text{if } \sigma_{22} \leq 0 \end{cases}\right], \left[\begin{cases} FI_{split} & \text{if } \sigma_{11} \leq 0 \text{ and} \\ & \sigma_{11} > -\frac{\sigma^u_{11,c}}{2} \text{ and} \\ & \sigma_{22} \leq 0 \\ 0 & \text{otherwise} \end{cases}\right]\right) \tag{C.21}$$

$$FI_{FFT} = \begin{cases} 0 & \text{if } \sigma_{11} < 0 \\ FI_{FFT} & \text{if } \sigma_{11} \geq 0 \end{cases} \tag{C.22}$$

$$FI_{FFC} = \begin{cases} 0 & \text{if } \sigma_{11} > -\frac{\sigma^u_{11,c}}{2} \\ FI_{kink} & \text{if } \sigma_{11} \leq -\frac{\sigma^u_{11,c}}{2} \end{cases} \tag{C.23}$$

For the implementation of the LaRC-05 criterion a linear shear behaviour was assumed. For a non-linear shear behaviour an additional failure mode occurs. [184] This additional failure mode competes with the matrix cracking failure mode. In case the shear behaviour is non-linear in the misalignment frame it is possible that there is no equilibrium point for the non-linear shear behaviour. When this phenomenon occurs, the material will fail due to instability instead of matrix cracking. In case of a linear shear law this is not possible.

Even if linear shear behaviour is assumed for the LaRC-05 criterion, the shear stress τ_{12} can still follow a non-linear shear behaviour. The shear stress τ_{12} is an input to the LaRC-05 criterion. Based on the results of the Unidirectional Quasi-Static Test Cases (UQSTCs) the linear shear assumption provides acceptable results, especially when considering the material scatter of the UQSTC data sets. Furthermore, the implementation of non-linear shear behaviour requires to solve Equation C.17 iteratively which will lead to increased computational

effort. Therefore, it is decided to assume linear shear behaviour for the LaRC-05 criterion. However, it is of interest for future work to investigate the effect of non-linear shear behaviour on the predictivity of the LaRC-05 model.

C.1.2 LaRC-05 performance evaluation

The present section will provide an initial evaluation of the performance of the LaRC-05 criterion. The evaluation is limited to a few load cases and for UniDirectional (UD) Fibre-Reinforced Polymer (FRP) laminates. Failure envelopes have been generated for the first seven UQSTC test cases shown in Figures C.2 through C.8. Pinho et al. [50] use different values for η_L than obtained from Equation C.2. The difference in the failure prediction between using the value for η_L from Pinho et al. [50] ('referenced' η_L) and the value from Equation C.2 ('approximated' η_L) is evaluated. The values for the 'referenced η_L' are provided in Appendix B.3.

For UQSTC-1 (Figure C.2) and UQSTC-3 (Figure C.4) the results of the LaRC-05 are in good correspondence with the experimental data and only a slight deviation in the compressive region exists between the two failure envelopes.

For UQSTC-2 (Figure C.3) and UQSTC-6 (Figure C.7), there is a significant deviation between the two failure envelopes. For UQSTC-2 the results of both failure envelopes are still in good correspondence with the experimental data. The failure envelope with the approximated η_L is less conservative in this region. Considering, the scatter of the experimental data, it is not possible to determine which envelope provides the best results. However, from UQSTC-6 it is clear that Equation C.2 does not hold and causes a significant deviation from the experimental data. This can be explained due to the combination of transverse compression and shear. For matrix failure and the current stress-state, the second term in Equation C.4 becomes $(\frac{\tau_{12}\cos(\alpha)}{\tau_{12}^u - \eta_L \sigma_{22}})^2$ Clearly, when $\alpha = 0$ this term is maximised and a higher value for η_L increases the denominator. As the predicted value from Equation C.2 is much higher than the η_L from Appendix B.3, the predicted failure occurs at higher stresses.

For UQSTC-4 (Figure C.5) the failure envelopes are similar and both are not able to capture the failure in the lower right region. From all of the considered failure criteria by van Dongen [6] only the Cuntze criterion (statistically-based criterion) was able to predict a curving behaviour in that region, however the Cuntze criterion still overpredicted the strength of the material in that region. This implies that in the lower region a failure mechanism/phenomenon occurs that current damage initiation criteria are not able to capture accurately yet.

For UQSTC-5 (Figure C.6) the failure envelopes coincide. The envelopes correspond well to the experimental data with the exception of the datapoints in the region $(-1000 < \sigma_{33} < -800)$. This is due to a relieving effect on the failure index due to the triaxial compression. This results in an open failure envelope as shown in Figure C.6. In reality, the material will be crushed eventually and hence the relieving effect should be up to the point of crushing of the material. The LaRC-05 is not able to capture this effect. The datapoints between $-1000 < \sigma_{33} < -800$ most likely indicate the region where failure will occur.

For UQSTC-7 (Figure C.8) the failure envelopes deviate in the compressive region. Both envelopes fit well with the experimental data. The failure envelope with the approximated η_L

is in this case better in correspondence with the experimental results than the other failure envelope.

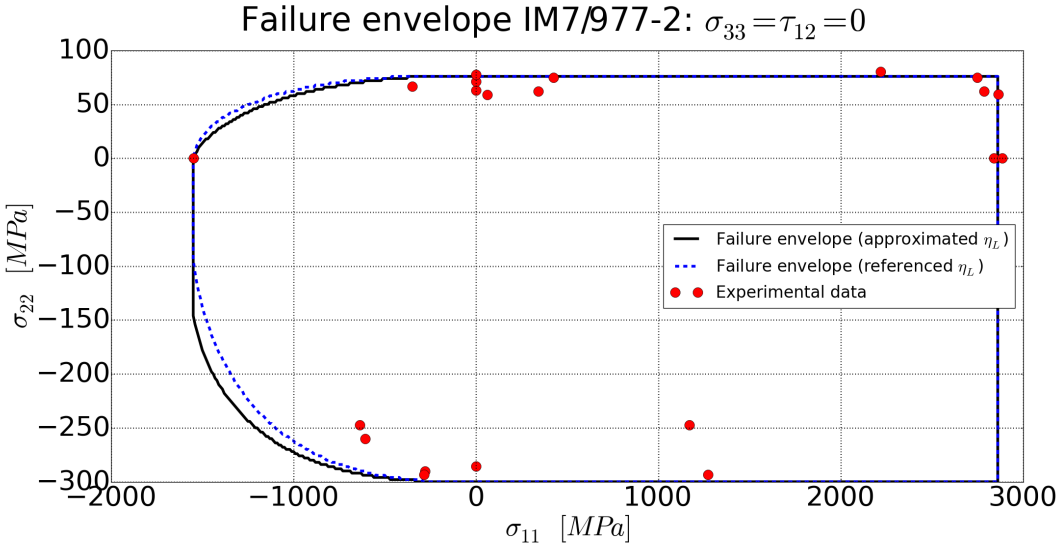

Figure C.2: The predicted failure envelopes for UQSTC-1. The experimental data is obtained from Welsh et al. [31].

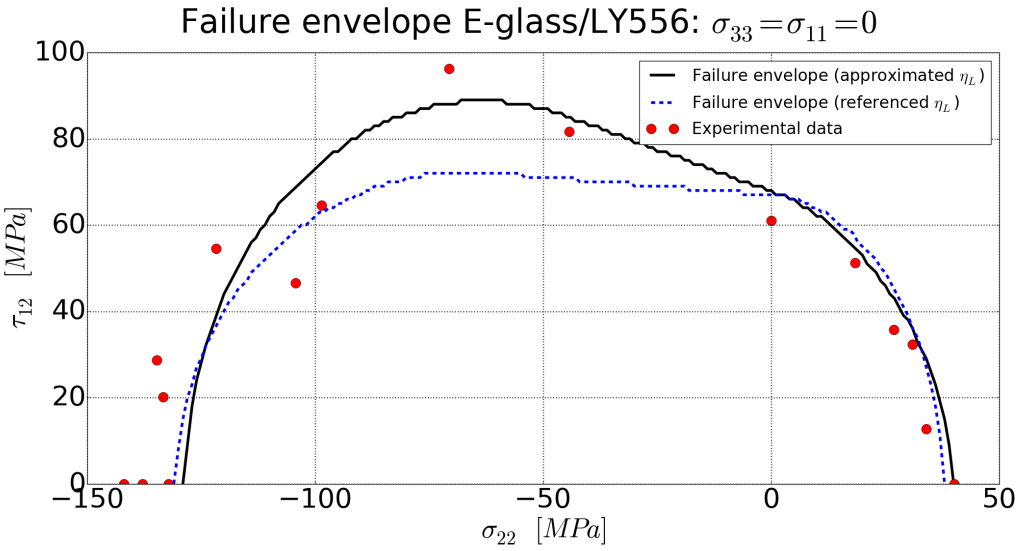

Figure C.3: The predicted failure envelopes for UQSTC-2. The experimental data is obtained from van Dongen [6] and Puck and Schurmann [29].

Based on the UQSTCs it is not possible to prefer the η_L value proposed by Pinho et al. [50] or the η_L value approximated by Equation C.2. Only for the case of triaxial compression and shear, the η_L value proposed by Pinho et al. [50] shows considerably better correlation to the experimental data. However, for UQSTC-7 this value for η_L produces overly conservative predictions in the compressive region. Therefore, it is decided to use the value of η_L approx-

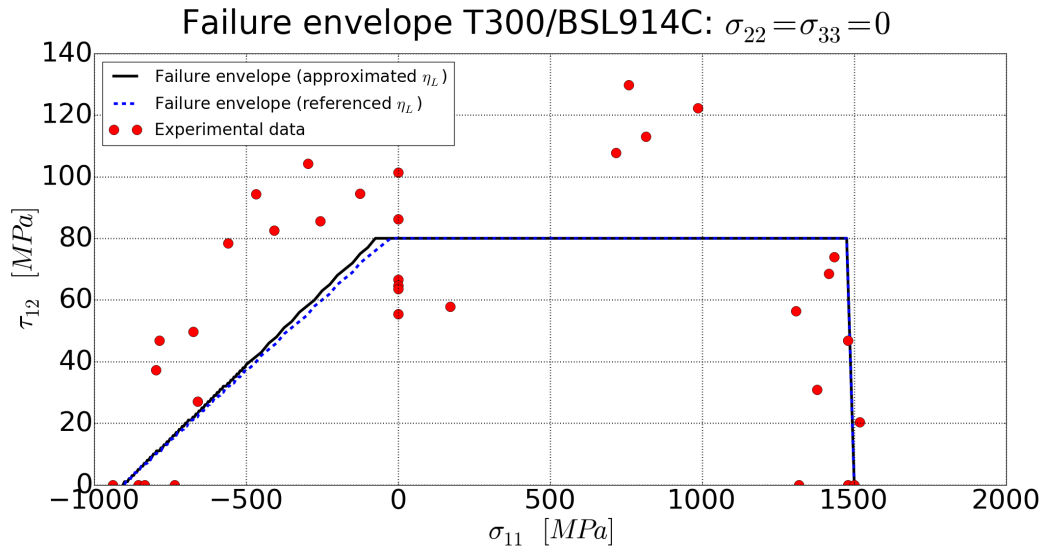

Figure C.4: The predicted failure envelopes for UQSTC-3. The experimental data is obtained from van Dongen [6] and Puck and Schurmann [29].

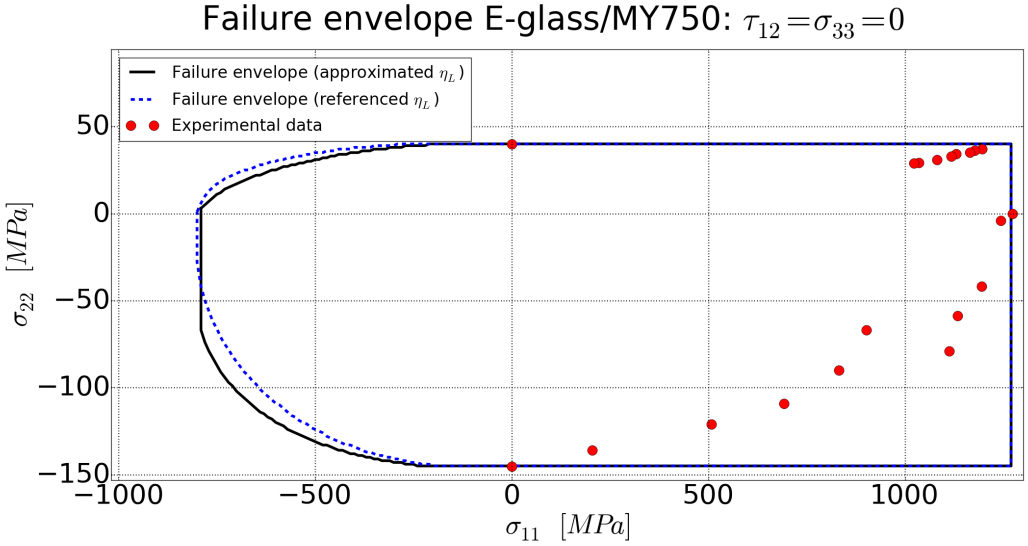

Figure C.5: The predicted failure envelopes for UQSTC-4. The experimental data is obtained from van Dongen [6] and Puck and Schurmann [29].

imated by Equation C.2 as the η_L value follows from other inputs and does not have to be inserted as an additional input. It is recommended to investigate the influence of η_L further and re-evaluate Equation C.2 for triaxial compression.

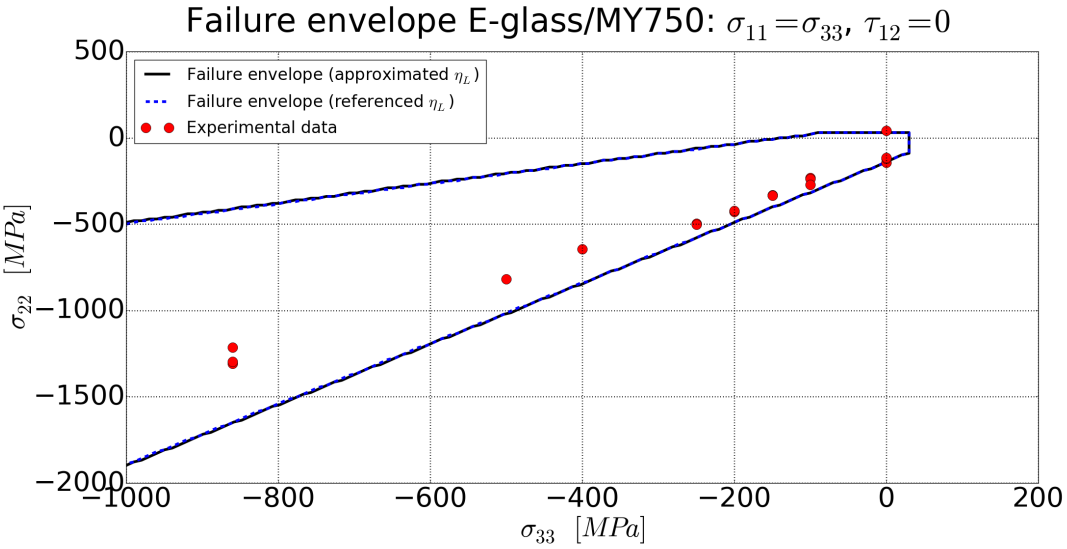

Figure C.6: The predicted failure envelopes for UQSTC-5. The experimental data is obtained from Hinton and Kaddour [30].

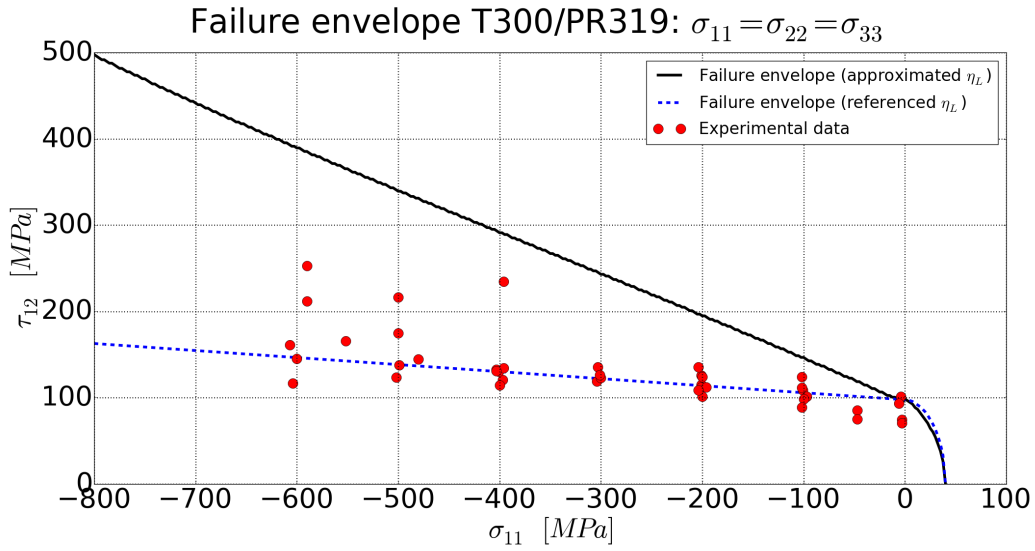

Figure C.7: The predicted failure envelopes for UQSTC-6. The experimental data is obtained from Hinton and Kaddour [30].

C.2 Bilinear softening

For the damage progression component of the CDM it has been decided to use the bilinear softening model (see Section 3.6.1. This section will briefly discuss this method and illuminate the main concept.

For the bilinear softening model, an equivalent stress ϵ_{eq} and strain σ_{eq} are introduced. Furthermore, based on the Hashin criteria a distinction is made between the FFT, FFC, MFT

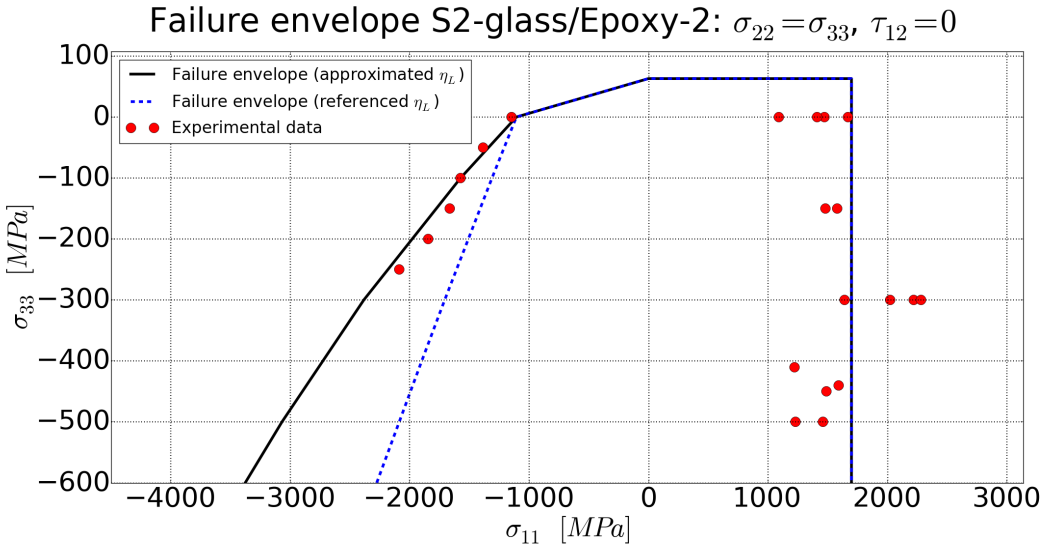

Figure C.8: The predicted failure envelopes for UQSTC-7. The experimental data is obtained from Hinton and Kaddour [30].

and MFC failure modes. In order to soften the material, a linear behaviour between ($\epsilon_{eq,0}$, $\sigma_{eq,0}$) and ($\epsilon_{eq,f}$, $\sigma_{eq,f}$) is modelled. The values of $\epsilon_{eq,0}$ and $\sigma_{eq,0}$ are known as they correspond to the point of damage initiation. In order to relieve the mesh dependency the crack band method introduced by Bazant and Oh [188] is used. A characteristic element is introduced and the value of $\epsilon_{eq,f}$ can be calculated with Equation C.24 [6]. This approach has also been used by Pinho et al. [26, 50].

$$\epsilon_{eq,i,f} = 2\frac{G_{i,c}}{\sigma_{eq,0}L} \tag{C.24}$$

In Equation C.24, $G_{i,c}$ is the intralaminar fracture toughness and the value of G_c depends on the failure mode i; and as such for each material four fracture toughnesses have to be determined for: G^+_{mc} (MFT), G^-_{mc} (MFC), G^+_{fc} (FFT) and G^-_{fc} (FFC). As stated by Camanho et al. [182], the transverse tensile fracture toughness, G^+_{mc}, is determined with a Double Cantilever Beam (DCB) test. The transverse compressive fracture toughness, G^-_{mc}, with a Four-point bending End Notched Flexure (4-ENF) test. Furthermore, the longitudinal tensile fracture toughness, G^+_{fc}, is determined from Compact Tension (CT) tests; and the longitudinal compressive fracture toughness, G^-_{fc}, is obtained with Compact Compression (CC) tests. [113, 116, 182] Furthermore, the characteristic length L is calculated with Equation C.25, where ω is the angle of the mesh lines with respect to the crack direction. [13] If the latter is unknown, the characteristic length can be approximated with Equation C.26. [13]

$$L = \frac{\sqrt{A}}{cos(\omega)} \tag{C.25}$$

$$L = 1.12\sqrt{A} \tag{C.26}$$

The damage parameter for each failure mode can be calculated by Equation C.27. [6] The influence of damage is incorporated in the coefficients of the constitutive model as shown in Equation C.28. This is based on the approach proposed by Matzenmiller et al. [189]. The coefficients d_f and d_m are the damage variables related to fibre and matrix failure, respectively.

$$d = \max_{time} < min(1, \epsilon_f \frac{\epsilon - \epsilon_0}{\epsilon_f - \epsilon_0}) >_+ \tag{C.27}$$

$$D_{ij} = \begin{cases} D_{11} = \left(E_{11} \frac{1-\nu_{23}\nu_{32}(1-d_m)}{\nu}\right)(1-d_f) \\ D_{12} = \left(E_{11} \frac{\nu_{21}+\nu_{31}\nu_{32}}{\nu}\right)(1-d_f)(1-d_m) \\ D_{13} = \left(E_{11} \frac{\nu_{31}+\nu_{21}\nu_{32}(1-d_m)}{\nu}\right)(1-d_f) \\ D_{22} = \left(E_{22} \frac{1-\nu_{13}\nu_{31}\left(1-d_f\right)}{\nu}\right)(1-d_m) \\ D_{23} = \left(E_{22} \frac{\nu_{32}+\nu_{12}\nu_{31}\left(1-d_f\right)}{\nu}\right)(1-d_m) \\ D_{33} = E_{33} \frac{1-\nu_{12}\nu_{21}\left(1-d_f\right)(1-d_m)}{\nu} \\ D_{44} = G_{12}(1-d_f)(1-d_m) \\ D_{55} = G_{31}(1-d_f) \\ D_{66} = G_{23}(1-d_m) \\ \nu = 1 - \nu_{12}\nu_{21}(1-d_f)(1-d_m) - \nu_{23}\nu_{32}(1-d_m) \\ -\nu_{13}\nu_{31}(1-d_f) - 2\nu_{32}\nu_{21}\nu_{13}(1-d_f)(1-d_m) \end{cases} \tag{C.28}$$

Appendix D

Cohesive Zone Model (CZM): Additional information

This appendix is concerned with providing more information and references concerning Cohesive Zone Models (CZMs). Furthermore, a more elaborate discussion on the validity of choosing a bilinear traction-separation relation is provided. This appendix will not focus on the advantages and shortcomings of the CZMs which can be found in Section 3.4. First of all, the general methodology of CZMs is discussed in Section D.1. The traction-separation relation is dicussed in Section D.2. Lastly, a brief review is provided regarding fatigue CZMs found in literature, in Section D.3.

D.1 Methodology

CZMs have been developed as an alternative for Virtual Crack Closure Techniques (VCCTs). The main drivers for the development of this alternative were the drawbacks of the VCCTs. The main drawbacks are (see for example, Abrate et al. [190]):

- A very fine mesh near the crack tip is required
- An existing crack with given shape and size is required
- In order to advance the crack front, complex moving mesh techniques are required.

To mitigate these drawbacks CZMs have been developed. Pascoe et al. [5], Camanho et al. [47], Hutchinson and Evans [191], Shet and Chandra [192] and Kuna [193], provide an overview of the early development of CZMs. As described by Abrate et al. [190], with CZMs it is assumed that ahead of the crack tip there is a thin layer separating two solids. In this thin layer damage mechanisms leading to failure are localised. The layer is referred to as the fracture (or cohesive) process zone. In Figure D.1, a sketch of a propagating crack between two laminae is shown. Furthermore, an arbitrary linear one-dimensional effective displacement-based traction separation model with exponential softening is shown in Figure D.1, where t is the traction and δ is the separation. The traction-separation relation defines a relation between

the boundary tractions and the separation of the interfaces (the distance between the crack faces). [193] Three regions can be distinguished in the sketch of the crack of Figure D.1: the undamaged cohesive zone, the cohesive process zone and the cracked zone. The undamaged cohesive zone corresponds to the material that has not failed yet. In the traction-separation relation this corresponds to the linear-elastic region. The region around the crack tip is the cohesive process zone. This corresponds to the non-linear region of the traction-separation relation. Lastly, the cracked zone is the region where the material has failed due to the crack. This corresponds to the failed cohesive zone part in the traction-separation relation.

D.2 Cohesive traction-separation relations

As introduced in Section D.1, CZMs use a cohesive traction relation to describe the separation of the interfaces due to the tractions on the boundary of the interfaces. CZMs used for mixed-mode fracture problems commonly use one-dimensional effective displacement-based models, such as by Pinho et al. [108], Harper and Hallett [153, 163] and Abrate et al. [190]. The one-dimensional effective displacement-based models introduce an effective displacement and traction which results in a straightforward formulation. The relative simple formulation is the major advantage of such models. This is especially advantageous for mixed-mode fracture problems as the cohesive law can be formulated within one framework. [112]

Due to the success of one-dimensional effective displacement-based models for crack-growth (and delaminations) this type of model is also used in this report for this purpose. However, there are some limitations for these type of models and it is important to be aware of such limitations. The limitations of one-dimensional effective displacement-based models are (see Park and Paulinho [112]):

- It is possible that the cohesive traction increases while separation increases (material becomes stiffer while separation increases), this is generally not the case and undesirable behaviour
- The fracture energy is constant regardless of the fracture mode which is not the case for most materials
- The models cannot distinguish between positive and negative normal separation.

In literature different one-dimensional cohesive models can be found such as bilinear, exponential, linear, exponential, trapezoidal and polynomial cohesive laws. All of these different cohesive models can generally be separated into intrinsic and extrinsic cohesive models. [7,190] Intrinsic cohesive models have an elastic slope initially, where extrinsic cohesive models are initially rigid. The traction-cohesive relation shown in Figure D.1 is of the intrinsic type. The main issue with extrinsic models is that the implementation requires updating the mesh; and intrinsic models are limited to problems where the fracture plane is known a priori. [7]

As stated before, in literature different types of one-dimensional cohesive models can be found. Shet and Chandra [194] argue that the energetics of the fracture process is not only dependent on the constitutive equation of the bounding material, but also on the choice of the traction-separation relation. The shape of the relation represent the net effect of the micromechanisms

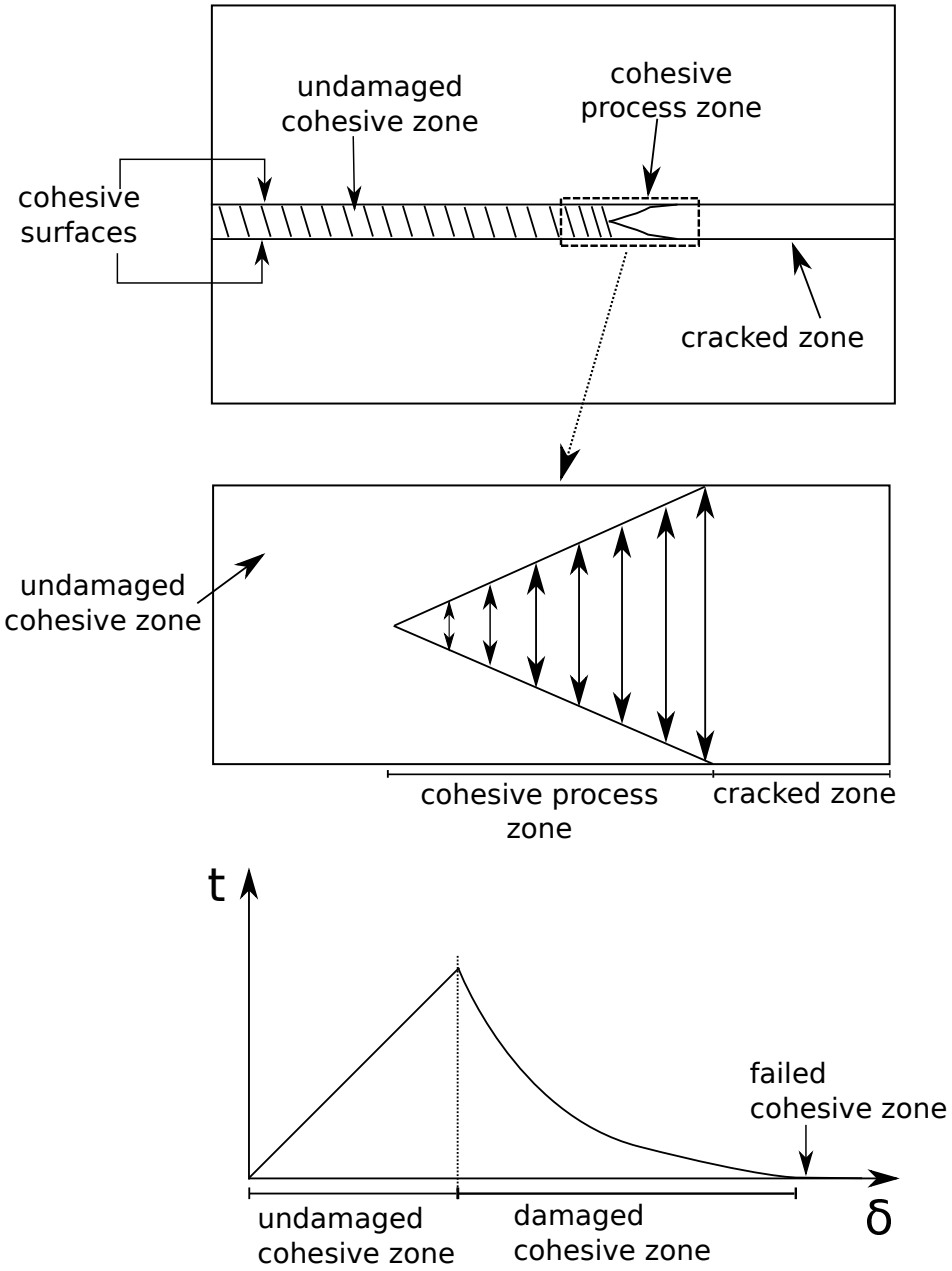

Figure D.1: Sketch of an interface of two materials connected by a cohesive zone. A crack is propagating through the cohesive zone. The separation of the cohesive surfaces is described by a cohesive traction $(\tau - \delta)$ model.

during crack growth. As these micromechanics are fundamental material characteristics, the shape of the traction-separation relation depends on the material. However, based on observations from experiments, Yang and Cox [195] argue that the crack growth characteristics are insensitive to the shape of the cohesive traction-separation relation in case there is only a single mechanism present. Furthermore, Yang and Cox [195] argue that for most fracture characteristics of engineering interests this is the case, provided that the correct maximum stress and fracture toughness are used for the cohesive traction-separation relation. [153] This

is supported by analytical solutions obtained by Williams and Hadavinia [196]. Therefore, if only a global analysis of the structure's response is required, the results are insensitive to the shape of the cohesive traction-separation relation. [153] However, in case more than one cohesive mechanism is active (e.g. long-range friction effects), the cohesive traction-separation relation should reflect this. [195]

D.3 Review of fatigue models in literature

The modelling of delamination growth due to fatigue by using CZMs has gained traction in recent years and has been explored by a variety of researchers, such as Nixon-Pearson et al. [11], Robinson et al. [14], Turon et al. [15], Bak et al. [81], Amiri-Rad and Mashayekhi [109], Tao et al. [149], May et al. [197] and Roth et al. [198]. All of these models use the load envelope approach discussed in Section 2.2.3.3. Following, the classification of Bak et al. [199], there is also another group of models called the loading-unloading hysteresis damage models. Such models irrecoverably reduce the stiffness of the CZM by some specified relation. The loading-unloading hysteresis damage models have been developed by, amongst others, Roe and Sigmund [200] and Abdul-Baqi et al. [201]. The loading-unloading hysteresis damage models are not considered any further, because it undermines the concept of a general high-fidelity tool for the following reasons:

- Parameters of the loading-unloading hysteresis damage models have to be obtained iteratively be comparing simulation results with experiments
- The influence of the load ratio has to be taken into account with a similar approach.

The load envelope models use a total damage rate consisting of a static (d_s) and fatigue contribution (d_f). The damage parameter has a value of zero when there is no damage and a value of one when total decohesion has occurred. The damage parameter is updated as a function of the number of cycle by defining a damage parameter rate, as is shown in Equation D.1. The damage parameter is then updated with a scheme such as shown in Equation D.2. Note that a higher-order integration scheme can also be used.

$$\frac{\partial d}{\partial N} = \frac{\partial d_s}{\partial N} + \frac{\partial d_f}{\partial N} \tag{D.1}$$

$$d_{N+\Delta N} = d_N + \frac{\partial d}{\partial N}\Delta N \tag{D.2}$$

In order to determine the damage rate shown in Equation D.1, a Paris-like relation is often used. However, from a physical point-of-view it is questionable whether a one-dimensional representation (crack growth rate) can be used to model a two-dimensional fracture problem (fracture surface). Nonetheless, a general format of the damage rate is provided in Equation D.3.

$$\frac{\partial d}{\partial N} = f\frac{\partial a}{\partial N} \tag{D.3}$$

The damage parameter can be formulated defined in various ways. First of all, in terms of area s shown in Equation D.4, where A^* is the damaged area and A is the pristine area. Secondly, in terms of strength as shown in Equation D.5, where S^* is the maximum strength of the cohesive zone in the damaged state and S the maximum strength in the pristine state. Furthermore, the damage parameter can be defined in terms of energy as shown in Equation D.6, where $G^*_{eq,c}$ is the equivalent critical Strain Energy Release Rate (SERR) in the damaged state and $G_{eq,c}$ the equivalent critical SERR in the pristine state. Lastly, the damage parameter can be expressed in terms of stiffness as shown in Equation D.7, where k^* is the stiffness in the damaged state and k is the stiffness in the pristine state. Note that the stiffness refers to the slope of the traction-separation relation.

$$d_A = \frac{A^*}{A} \tag{D.4}$$

$$d_S = \frac{S^*}{S} \tag{D.5}$$

$$d_G = \frac{G^*_{eq,c}}{G_{eq,c}} \tag{D.6}$$

$$d_K = \frac{k^*}{k} \tag{D.7}$$

The current state-of-the-art fatigue models have been developed by Kawashita and Hallett [16] and Bak et al. [81]. Kawashita and Hallett [16] argue that instead of using the instantaneous maximum SERR the maximum SERR at failure has to be used. In order to determine the maximum SERR at failure, a non-local algorithm is used to find neighbouring failed elements and use the value of the maximum SERR at failure between the consecutive cohesive elements. Furthermore, the method proposes the use of an algorithm to determine the characteristic element length l_e which depends on the non-local behaviour of the delamination front. The fatigue damage is inversely proportional to l_e; and l_e can vary for element with the same dimensions. Advantages of this method are:

- The notion of crack length a for delaminations makes more sense. This length is defined as the distance from the element front of elements damaged by fatigue to the next front of elements to which the delamination front is advancing
- Bak et al. [202] showed by comparison that the model is one of the more accurate models in literature. However, the validity of this advantage is based on the limited comparison by Bak et al. [202]
- The model is not influenced by parameters not directly linked to the damage rate. [202]

Shortcomings of this method, not considering the shortcomings of the principle of CZMs and the use of Paris-like relations, are:

- In order to obtain accurate results a very fine mesh is required

- It is not clear how to initiate a delamination without having a pre-crack or a pre-failed element. The proposed non-local algorithm to find the maximum SERR at failure cannot work when there has not been prior failure.

The model by Bak et al. [81] uses an energy-based approach, where the total amount of work and already dissipated energy are used to determine the damage-state of the cohesive zone. The damage rate is then derived based on energy considerations. The advantages of this model are:

- An energy-based approach is deemed to have a more physical-basis. However, in order to relate the rate of total energy dissipation to the delamination, a crack length is used instead of a fracture surface
- For self-similar cracks it requires a coarser mesh than other methods and still be able to obtain equally accurate results [202]
- Just as for the model of Kawashita and Hallett [16], the model is not influenced by parameters that are not directly linked to the damage rate.

However, the model by Bak et al. [81] has one shortcoming when excluding the shortcomings of the principle of CZMs and the use of Paris-like relations, the shortcoming of the model is:

- For non-self similar cracks a finer mesh is required, dissipating the advantage listed previously. Bak et al. [81] do propose an adaptive cycle integration with a predictor-corrector approach. This approach aims to compensate for non-self similar crack growth. However, in order to ensure Finite Element Analysis (FEA) convergence, the method requires an iterative approach to determine the number of cycles to skip ΔN which increases the computational effort.

To some extent the methodologies of the models by Bak et al. [81] and Kawashita and Hallett [16] show merit, however some of the shortcomings have to be addressed before they can be used for a general high-fidelity tool. Furthermore, the methods have been formulated within a load envelope approach which is of the joint implementation type. The proposed framework in this thesis is of the disjoint type and converting the formulations from one type to another is in this case not straightforward for the reasons provided in Section 4.1.2.2.